Remote Sensing Techniques for Nitrogen Stable Isotope Detection in Plant Matter

Sonja K. Capelle
Gordonsville, Virginia

Bachelor of Science, James Madison University, 2005
Master of Science, James Madison University, 2006

A Dissertation presented to the Graduate Faculty
of the University of Virginia in Candidacy for the Degree of
Doctor of Philosophy

Department of Environmental Sciences

University of Virginia
May, 2017

Abstract

Research was conducted to develop the foundations of a new method, infrared nitrogen stable isotope (INSI) ratio, for calculating nitrogen stable isotope ratios using infrared data in plant matter. Laboratory plant growth experiments, using buckwheat and ^{15}nitrogen enrichment, showed diagnostic wavelength shifts in the infrared. Data was collected at multiple frequencies that are associated with nitrogen functional group compounds. Computational modelling of common plant nitrogen compounds validate the spectral shifts and was used to identify ammonium as a unique compound for spectral data based ratio development. Field data was collected at locations using organic fertilizer, inorganic fertilizer and along known nitrogen impaired waterways in the Shenandoah Valley of the Chesapeake Bay watershed. The calculated INSI ratio values showed values consistent with expected levels of enrichment. The INSI ratio method developed in this research establishes the foundation for researchers to continue development of this new approach. In the future, infrared field based sensors could be developed that are tuned to the frequencies of ^{15}N wavelength shifts identified in this research. This will provide researchers with faster and cheaper isotope ratio measurements covering broader areas and eventually be translated for use with airborne or space-based instruments.

Acknowledgements

I would like to thank my adviser, Stephen Macko, for his continued guidance and vision to tackle this interesting research topic. His helpful mentorship and encouragement truly enabled my research. I would also like to thank my committee, Hank Shugart, John Porter and Fred Damon, for their support, advice and interesting office conversations during my research and time at the University. Thanks also to Declan McCarthy for his knowledge and efforts working with me on the Double Hoo Research Grant from the Office of Undergraduate Excellence. This dissertation could not have been completed without financial support and funding provided by the Department of Environmental Sciences, the Virginia Space Grant Consortium and the Department of the Army and for that I am truly grateful.

Table of Contents

List of Figures

List of Tables

Chapter 1 – Introduction and Background

Introduction

This research investigates the process by which a new method using spectral infrared data can measure nitrogen stable isotope ratios instead of traditional mass spectrometry. Traditional isotope ratios using mass spectrometry is limited to the laboratory, is expensive to maintain and measures data from one sample at a time. Conversely, spectral infrared data has the potential to bring the measurement of stable isotopes out into the field with either ground based, handheld, airborne or even space-based satellites that can measure data over larger areas. The foundations of this new method are described in this dissertation and include the identification of spectral regions where nitrogen compounds can be detected and specifically where the two nitrogen isotopes, the naturally abundant ^{14}N and low natural abundance ^{15}N, can be discriminated. This allows for the calculation of an infrared nitrogen stable isotope (INSI) ratio that can be compared to the traditional isotope ratio mass spectrometer (IRMS) measured data.

This new method development, called an INSI ratio, is important because stable isotopes are highly useful for indicating origins of materials, such as the origins of nitrogen based fertilizers. Fertilizers are a significant polluter in waterways because they provide an enrichment of nitrogen nutrient above normal levels. The method developed herein can be used to remotely identify fields along waterways where an overabundance of nitrogen based fertilizers have been applied. This can lead to better decision making by environmental scientists for specific location-based implementation of water

improvement techniques, like riparian buffers, to have a maximum impact on overall water quality. This will enable scientists to better manage their available funding for emplacing improvements where it matters most.

Background

Access to clean bodies of water for human use is an important safeguard that the Environmental Protection Agency seeks to continue through the Clean Water Act (CWA). When the CWA was established in 1976, there were many significant water quality issues to address. Although there has been much improvement, there are still hurdles to overcome. One of these is to identify nonpoint source pollution (NPS) in agricultural areas (Babin *et al*., 2016). This is a complex problem but one that continues to plague our nation's waterways and estuaries such as the Chesapeake Bay (Tango & Batiuk, 2013) and, to a greater extent, the Mississippi River Watershed (Ouyang *et al.*, 2015). As an example of water resource importance, the Bay produced $107.2 billion in goods in 2009 (*2014 State of the Bay*, 2014) and is the largest North American estuary (Malone, 1991). Even greater than the Bay, the Mississippi River accounts for $473 billion in revenue and over 1.7 million jobs in the surrounding counties (Black *et al.*, 2004; Grassi, 2016). Not only are these natural resources important to the U.S economy, but they include important intangibles such has the intrinsic value for recreation, enjoyment and being a habitat to a wealth of flora and fauna.

Agricultural NPS runoff is the largest pollution source impacting the Chesapeake Bay (*2014 State of the Bay,* 2014). There are many farms within the Bay watershed as agriculture is the second-largest land use category in the region (*2014 State of the Bay,*

2014). This can complicate restoration efforts as they are nearly all located on private lands. On an even larger scale, the NPS impacting the Mississippi River overloads the waters with nutrients causing devastating effects in the River Delta and the Gulf. The excessive nutrients and resulting algal blooms that eventually die off create anoxic or hypoxic dead zones preventing many marine species from flourishing in these areas. The pollution in these watersheds luckily is something that can be controlled. Most causes are anthropogenic, like the over application of fertilizers, where a small percentage absorbs into the soil and the remaining runs off during rain events and travels into the nearby waterways ultimately condensing in the Bay, Delta or Gulf. Besides sediments, nutrients, both phosphorus and nitrogen, are the largest contributor to NPS pollution (VA DEQ) and of that the largest nutrient contributor is runoff from agricultural operations (National Water Quality Index). This is a tough problem to solve. Even though the Clean Water Blueprint for the Chesapeake Bay has been implemented for the past six years, there have only been small improvements to agricultural-based NPS pollution. The complexity and large scale of agricultural NPS pollution make it an important topic to research for remote sensing applications. This dissertation outlines a new path forward aimed at mitigating and identifying possible agricultural based nitrogen NPS pollution from a new perspective.

The issue of mitigating NPS pollution and identifying priority watersheds for remediation efforts is often researched (Babin *et al.*, 2016). A direct measurement capability over large areas to assess NPS pollution related criteria is not yet available. To date many assessments require loads of field work, sample over small areas, are time

consuming and likely will not answer this multi-state water quality problem. This is where the interplay between geochemistry and remote sensing has advantages.

Stable Isotopes

The study of stable isotopes in the environment has many applications. Assessing the nitrogen stable isotope composition of components within a studied watershed can identify source materials (Macko & Ostrom, 1994). Isotopes are atoms with a different amount of neutrons but the same amount of protons and electrons. Those isotopes that are energetically stable interact with the environment in interesting ways and their varying signals can be used for comparative analysis. A stable isotope with an additional neutron interacts with physical and chemical processes differently than an atom with a lower atomic mass. The heavier atoms typically react slowly and require more energy to break the molecular bonds (Fry, 2006). Nitrogen has two stable isotopes, ^{14}N and ^{15}N. The stable isotope ^{15}N is rare, only occurring in the atmosphere 0.365% with the remaining nitrogen composition due to ^{14}N (Sulzman, 2007). When nitrogen interacts with the environment the byproducts of reactions are typically depleted and the substrates are enriched in ^{15}N (Shearer & Kohl, 1986). An analysis of amount of enrichment or depletion is calculated using an isotope ratio comparing the amount each isotope in a sample compared to a standard. In the case of nitrogen the standard is atmospheric nitrogen. Regarding agriculture based NPS, this approach can indicate whether the pollution comes from inorganic chemical fertilizers or organic fertilizers and manure (Townsend *et al.*, 2004; Yun *et al.*, 2006). When the source nitrogen comes from the organic fertilizers, the nitrogen

isotope signal is more enriched in ^{15}N in comparison to Haber process inorganic nitrogen where the source is atmospheric nitrogen.

Typically this analysis is performed with an isotope-ratio mass spectrometer (IRMS). The IRMS is a laboratory based instrument requiring manual inputs, long calibration times and only measures samples from one field sampling point at a time. This methodology produces highly accurate results but is limited by sample throughput when measuring large field areas such as those where agriculture NPS is an issue. Much research has been conducted to identify ways to measure ^{15}N signals over larger spatial extents using satellite imagery, hyperspectral reflectance and absorption spectroscopy (Changwen *et al*., 2009; Eiler *et al*., 2014; Elmore & Craine, 2011a; Kleinebecker *et al.*, 2009; Lorentz, 2013; Sun *et al*., 2012; Wang *et al*., 2010; Wang *et al.* , 2007).

The highly variable natural abundances in most stable isotopes in contrast to their standard elemental concentrations make their analysis particularly useful in many applications including environmental, ecological agricultural and archaeological problems. This information can be used like a fingerprint or signature of a material under study to indicate origins and history of the element in the material. Stable isotope ratios are calculated comparing the heavier rare isotope in a sample to the more abundant lighter isotope and are described as a delta or $\delta^{15}N$ value according to the following equation:

$$\delta^{15}\mathrm{N} = 1000 \left\lfloor \frac{\mathrm{Ratio}_{Sample} - \mathrm{Ratio}_{Standard}}{\mathrm{Ratio}_{Standard}} \right\rfloor \qquad \text{Equation 1}$$

The standard for nitrogen stable isotope ratio calculations is atmospheric nitrogen that has an isotope ratio of 0.3613.

Stable isotope ratio analysis is a commonly used tool among researchers owing to its unique ability to characterize samples that other techniques cannot. In plant matter, the stable isotope ratio of nitrogen can be used to understand the nitrogen cycle. Nitrogen fertilizer sources can be identified in plant matter and the surrounding soils as organic manure based fertilizers are more enriched in ^{15}N versus Haber process inorganic fertilizers (Yun *et al*. 2006). Also, in areas with high levels of nitrogen availability and increased rates of nitrogen leaching there is ^{15}N enrichment (Shearer & Kohl, 1986). This ability to determine fertilizer sources is important in understanding nutrient loads and origins, as anthropogenic impacts are often hard to quantify in the environment. Isotope analysis, when linked with water samples in nearby streams and rivers, enables researchers to better differentiate agricultural fields that have been applied with organic fertilizers and possibly better identify nonpoint source pollution in waterways.

Concentrations of the different isotope abundances, reported as ratios of the different forms of the element, are typically measured with an isotope ratio mass spectrometer (IRMS). Single sample laboratory-based analyses are generally very high in precision; however, sample run times and instrument calibrations are time consuming, costly and represent data from a single location on the Earth's surface at a particular time. This research aims to be a proof-of-concept that could eventually be used to develop techniques that will enable field-based measurements of stable isotope ratios in plant matter. This research aims to identify diagnostic wavelength shifts that are caused by the isotope and are able to be observed by the field based or spectral sensor. This would provide researchers with faster and cheaper measurements that could cover broader areas and

eventually be translated to use with airborne or space-based instruments. Specifically, this research produces the foundational information needed for the development of a field-based method for stable nitrogen isotope analysis. This fundamental research in stable isotope spectroscopy could be used for the development of future remote sensors and help provide biogeochemical understanding at larger spatial scales.

Most researchers still rely heavily on the IRMS for stable isotope analysis but some are investigating alternative methods such as using handheld spectrometers (Wang *et al*. 2010). There is a general consensus among the stable isotope community that a larger spatial scale, including regional analysis of isotope concentrations would be beneficial. Spectroscopic analysis and remote sensing capabilities for stable isotopes is currently being suggested and the possibility researched (Elmore & Craine, 2011; Kleinebecker *et al*. 2009 and Wang *et al*. 2007). Stable isotopes inherently have different masses that cause them to behave distinctly within the electromagnetic (EM) continuum. Specifically they generate isotope effects in their bonds with other elements where a bond with a heavier isotope will vibrate differently when analyzed spectrally (Hoefs, 2009). The spectral absorption regions (bands) identified directly relate to the specific elemental bonds present in the sample. The mid-wave infrared (MWIR) is considered to be the fingerprint region of spectroscopy where compound analysis can be performed. Each compound has a specific combination of bending, stretching and wagging bonds between the elements that enables researchers to specifically identify the compound being analyzed. This combination is as unique as a fingerprint. In this research the focus is less on compound analysis and more on which bonds with known vibrations are being shifted due to increased resistance from the

presence of the heavier isotope. Pure 99.99% ^{15}N labels were measured with Fourier Transform Infrared (FTIR) attenuated total reflectance (ATR) (FTIR-ATR) laboratory instrumentation and demonstrate this phenomenon. The shortwave infrared (SWIR) contains overtone vibrations of these MWIR bonds therefore the SWIR analysis is more complicated as specific compound analysis cannot be performed. However, large family groups of compounds can be identified. With advanced processing techniques small differences in the overtones can be amplified, specifically when using derivatives in the spectra, peak separation and peak fitting. Others have used apparent differences in the visible to near infrared (VNIR) region of the data as proxies for predicting isotope concentrations with some success (Wang *et al*, 2011). Proxies in the VNIR is a less rigorous approach than focusing on the SWIR region. The VNIR absorbs and emits radiation that is less impacted by material composition and more on material color, which can be good in some cases such as chlorophyll content (chlorophyll emits in the green region) or vegetation health analysis in the NIR. This is the basis for a spectroscopic analysis capability for stable isotopes detection.

Bulk nitrogen (not isotope) quantification in plants with spectral instruments is well-known (Belanger *et al*., 2007). Vegetation indices have been developed and the methods are in practice (Myneni *et al*., 1995). In addition, nitrogen concentration monitoring is practiced from remote sensors on cropland to evaluate fertilizer application rates in order to ensure a bountiful crop (Anderson, 2014). In precision agriculture, tractors even incorporate automated suggested nitrogen application rates for their fields with a GPS unit linked to satellites that calculate nitrogen demand in real-time (Lan *et al*. 2010). The

key to this research is to leverage the past successes, methodologies and indices in order to quantify nitrogen isotope abundances in plant matter across whole fields. The present enrichment experiment confirmed that the nitrogen compounds detected by the Nicolet spectrometer were contained in the amine groups, since family groups can be easily identified in the MWIR and absorb between 3,500-3,300 cm^{-1}, which is consistent with the data collected during the experiment. The other observed absorptions and wavelength shifts also need to be further understood as to their cause which is currently thought to be overtone absorptions stemming from the stronger amine group N-H bonds.

Continued corroboration between the field and lab instruments will need to be performed. This research shows specific absorption features that are identified and that can be used to for quantification of the isotope. The values, once compared to the high precision IRMS data is a methodology that can then be applied in practice. Field plant and water samples can be collected, measured and corroborated with IRMS measurements in order to understand the origin on the fertilizers contributing to nonpoint source pollution. This information can then help identify the specific fields where excess nitrogen originate and efforts can be made to cooperate with land owners and policy makers to potentially mitigate nutrient pollution through different management strategies.

Hyperspectral Remote Sensing

Remote sensing is the field of study concerned with extracting information about an object without coming into direct contact with a sample (Schott, 2007). Hyperspectral remote sensing is the combination of traditional spectrometry with imaging cameras and in some cases non-imaging sensors (Eismann, 2012). Hyperspectral sensors utilize many,

typically hundreds of, distinct bands of data to parse the energy from a material into a resulting data cube that can produce a spectral signature or spectrum. Multispectral data however, utilizes tens or less of bands of information. Ground based research sensors are most often hyperspectral instruments whereas most NOAA and NASA satellites are multispectral. Ground sensors are used initially by researchers to develop and outline the bands of energy for a specific purpose that future satellites can employ.

Energy can be sensed all along the electromagnetic spectrum, 0.4 µm to 14 µm, and is broken into five distinct regions: visible (VIS), near-infrared (NIR), short-wave infrared (SWIR), mid-wave infrared (MWIR), and long-wave infrared (LWIR). These regions are based on differing fundamental properties occurring therein.

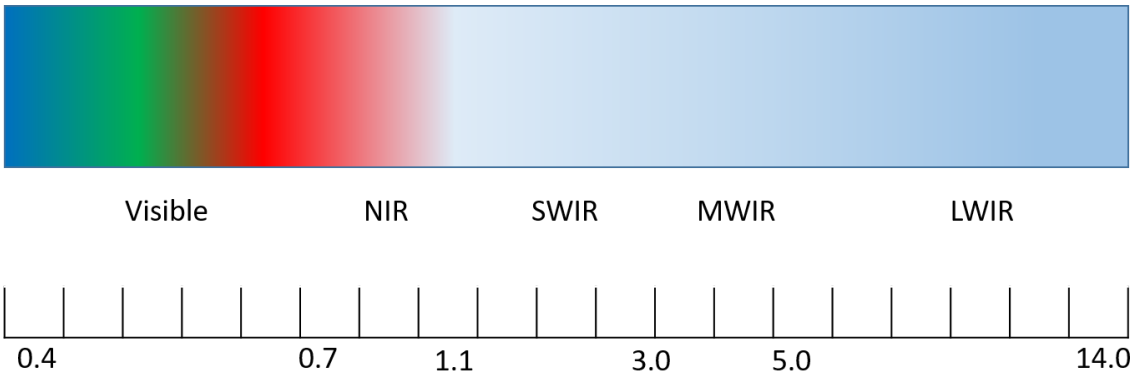

Figure 1 Representation of the electromagnetic spectrum defining the five region: visible, near-infrared, short-wave infrared, mid-wave infrared and long-wave infrared.

The VIS region, 0.4-0.7 µm, is that part of the spectrum humans can see. The energy above and below is not observable by human eyes and requires instrumentation and specific detectors to read this energy. The NIR region, 0.7-1.1 µm, is typically associated with vegetation reflectance response. The SWIR region, 1.1-3.0 µm is dominated by physical and chemical properties of materials. More specifically this region

is associated with vibrational overtones from the MWIR, 3-5μm. The MWIR is where the energy being observed begins to switch from reflected sunlight to thermal emission. The MWIR is also the typical portion of the spectrum in traditional spectroscopy where chemical function groups can be assigned. Thermal emission is observed in the LWIR, 5-14 μm, making it possible to observe hot objects like fires and sense temperatures of objects and the Earth.

The study of spectroscopy of materials provides the physical basis of hyperspectral remote sensing. The electromagnetic spectrum interacts with materials at the atomic and molecular level. Materials absorb, emit, or reflect energy that is measured by spectral sensors to produce a spectrum of the response across the wavelengths being observed. The peaks and valleys in the resulting spectrum indicate the properties of the material under observation. This spectrum is unique to the material and is termed a signature. Non-imaging spectral instruments capture this data or signature and it is plotted as a graph where the x-axis is the wavelength and the y-axis is the resulting energy value. Imaging sensors perform this measurement across a surface, effectively mapping out the spectral signature of each material along the surface being imaged. An image is constructed and is called a datacube that has three dimensions, where x and y are the positions within the image and z is the signature of the material across the wavelengths (x) of the sensor. Imaging sensors have the advantage of being able to make spectral measurements over large areas simultaneously.

Spectral instruments characterize the material under observation. This capability has been used by Wang *et al*. (2010; 2007) to suggest specific wavelengths in the

reflectance data leaves that are significantly linked to the IRMS measured ^{15}N signals of the same leaves. They showed strong correlations at both leaf and canopy levels. Seventeen significant regions were identified throughout the reflectance response of the utilized sensor in their research, specifically bands in the near infrared (NIR) around 600 and 700 nanometers (nm) are well correlated. Research by Lorentz (2013) confirms the ability to use reflectance data to predict ^{15}N concentration in evergreen needles. The results showed correlations from R^2=0.49 to 0.84 for different hyperspectral indices and previously reported wavelengths of interest throughout the 0.35-2.5 μm region. The strongest relationships were reported in the visible region. The visible and red-edge region, where the reflectance sharply rises for healthy vegetation, are well known regions where chlorophyll and other nitrogen containing compounds react with incident sunlight or radiation (Eismann, 2012). The SWIR region includes additional responses from vegetation where C-H, N-H and O-H bonds vibrate (Shenk *et al*., 2001). This makes it a specifically interesting region to study. Kleinebecker *et al*. (2009) developed a partial least-squares calibration model using hyperspectral reflectance values from the entire 1,250-2,350 nm region to predict the ^{15}N signals in various bog plant species with R^2 = 0.993. Instead of the entire SWIR region, Elmore and Craine (2011b) used the reflectance at the previously reported (Kokaly, 2001) 2,100 nm feature for bulk nitrogen measurement, but found it to be loosely correlated to ^{15}N content.

Imaging spectral data has also been researched for this application. Wang *et al*. (2011) utilized multispectral satellite data reflectance data indices to link to ^{15}N in various vegetation covered environments in the Everglades National Park. They

employed both the normalized difference vegetation index (NDVI) and the normalized difference water index (NDWI) computed from SPOT-4 satellite imagery data to determine their correlation to ^{15}N concentrations previously measured at the same locations. Their results varied between the different techniques (R^2 = 0.31-0.83) due to different ground sample locations, the index used and whether or not the image data was corrected for atmospheric interactions in the reflectance data.

There are many types of spectral instruments, each developed to meet a specific purpose. The reflectance data discussed above were collected by ground based hand held spectroradiometers. It measures the reflectance, calibrated to a known reference standard, of samples either in direct contact or remotely with a lens and tripod. Similar reflectance measurements can be made with FTIR spectrometers attached to ATR sample port. These types of instruments are most commonly used in the laboratory, but a few have been developed to be handheld and field portable. Instead of reflectance, the data is reported as absorbance as more energy is absorbed by materials in this region than reflected on average. These instruments generally operate in the MWIR or LWIR regions and therefore can measure reflectance at specific bond energies and types. Changwen *et al.* (2009) used this technique to measure $^{15}NO_3$-N and $^{14}NO_3$-N concentrations in soils and soil pastes at natural abundances.

Stable Isotopes and Spectroscopy

The ability to measure light energy and understand the chemical properties of the material under study can also be used to understand the structure (Coates, 2000). When energy is incident upon a material, the atomic bonds flex and rotate in characteristic

ways. Vibrational spectroscopy utilizes this principle to map certain elemental bond energies into functional groups across the spectrum. Since bond energies are being observed, most analyses are performed in frequency space, not wavelength space. The two domains are inversely related and describe the wave energy in different ways. Wavelength measures the distance for a single wave as a unit of distance in microns (μm) or nanometers (nm). Frequency measures the number of wave occurring per unit distance in wavenumbers or inverse centimeters (cm^{-1}). Most remote sensing spectroscopy research focuses on wavelength where chemistry spectroscopy focuses on wavenumbers. Wavenumbers are a linear representation of the electromagnetic spectrum whereas wavelength is not. The challenge of remote sensing scientists and chemists is to be able to understand and read each designator interchangeably.

The bonds vibrate differently for different isotopes. The heavier mass in the isotope changes the vibrational mode of all of the atoms in the molecule and create a downshift in frequency from the observed frequency in the lower mass molecule (Quillard *et al.*, 1997). These changes require instrumentation with high frequency or spectral resolution to measure these shifts. Changwen *et al*. (2009) conducted their research on the known 1,350 cm^{-1} response region (7,407 nm) for nitrate. This region allows for a level of specific information which can be interpreted in infrared data (Stuart, 2004). Changwen *et al*. (2009) observed the wavelength shift in the nitrate band for each species. There was an observed 35 cm^{-1} downshift in response from the lighter to the heavier isotope nitrate species. Using the FTIR data at the two regions identified for

each species they were able to estimate concentration with a determination error around 8 or 6.5 mg N for aqueous solutions and soil pastes respectively.

Research Objectives

The field of research investigating spectral based nitrogen isotope ratio measurements varies in methodology and results. There is a fundamental scientific basis that has given credence to the field. This dissertation presents hyperspectral technologies that can be used for nitrogen isotope analysis. In many cases, the prior research results are simply proxy measurements of the actual physics occurring. The change in a vegetation index or the change in reflectance values are in fact due to the wavelength shifts occurring in the nitrogen bonds in compounds that are reacting with energy in different ways due to the presence of the isotope. The research objectives are as follows:

1. To determine where isotope induced shifts occur along the VIS, NIR, SWIR, MWIR and LWIR regions. Hypothesis: By enriching a fertilizer supplied to plants with labeled ^{15}N far above natural abundance levels, spectral instruments will be able to identify absorption regions specific to the heavier isotope when compared to a control.
2. To investigate what bonds or compounds are being observed at the identified wavelengths through infrared interpretation and compound modeling. Hypothesis: Qualification of the data in the band absorption regions identified will be possible through computational chemistry.

3. To develop a model for predicting ^{15}N ratios in plant matter. Hypothesis: The development of a spectral algorithm will be able to quantify the amount of ^{15}N that will compare to traditional $\delta^{15}N$ from IRMS measurements.
4. To apply the technique to field acquired vegetation samples in different fields and along or within nitrogen impaired waterways. Hypothesis: Spectral instrumentation can be used to measure natural abundance nitrogen isotope ratios to identify the origins of nitrogen nutrients in runoff and contributing nearby waterways.

The above objectives will be discussed in subsequent chapters.

References

2014 State of the Bay. (2014). Chesapeake Bay Foundation.

Anderson, C. (2014) Agricultural Drones: Relatively cheap drones with advances sensors and imaging capabilities are giving farmers new ways to increase yields and reduce crop damage. *MIT Technology Review*. May/June 2014.

Babin, N., Mullendore, N. D., & Prokopy, L. S. (2016). Using social criteria to select watersheds for non-point source agricultural pollution abatement projects. *Land use Policy, 55*, 327-333.

Belanger, M.C., A.A. Viau, G. Samson & Chamberland M. (2007). Comparison of reflectance and fluorescence spectroscopy for the detection of nitrogen deficiency in potato plants. *Canadian Journal of Remote Sensing*, 33 (2), 69-80.

Black, R., Hutchison, S., & Warshaw, C. (2004). *Economic profile of the lower mississippi River region.* Cambridge, MA: Industrial Economics Incorporated.

Changwen, D., Linker, R., Shaviv, A., & Jianmin, Z. (2009). In situ evaluation of net nitrification rate in terra rossa soil using a fourier transform infrared attenuated total reflection 15N tracing technique. *Applied Spectroscopy, 63*(10), 1168-1173.

Coates, J. (2000). In Meyers R. A. (Ed.), *Interpretation of infrared spectra, a practical approach*. England: John Wiley & Sons Ltd. Print.

Eiler, J. M., Bergquist, B., Bourg, I., Cartigny, P., Farquhar, J., Gagnon, A., Stolper, D. (2014). Frontiers of stable isotope geoscience. *Chemical Geology, 372*(0), 119-143.

Eismann, M. T. (2012). *Hyperspectral remote sensing*. Bellingham, Washington: SPIE.

Elmore, A. J., & Craine, J. M. (2011a). Spectroscopic analysis of canopy nitrogen and nitrogen isotopes in managed pastures and hay land. *Ieee Transactions on Geoscience and Remote Sensing, 49*(7), 2491-2498.

Elmore, A. J., & Craine, J. M. (2011b). Spectroscopic analysis of canopy nitrogen and nitrogen isotopes in managed pastures and hay land. *IEEE Transactions on Geoscience and Remote Sensing, 49*(7), 2491-2498.

Fry, B. (2006). *Stable isotope ecology*. New York: Springer. Print.

Grassi, J. (2016). Upper Mississippi river basin: A vital resource for regional economic prosperity. Retrieved from http://www.umrba.org/umr-econ-profile.pdf

Kleinebecker, T., Schmidt, S. R., Fritz, C., Smolders, A. J. P., & Hölzel, N. (2009). Prediction of ^{13}C and ^{15}N in plant tissues with near-infrared reflectance spectroscopy. *New Phytologist, 184*(3), 732-739.

Kokaly, R. F. (2001). Investigating a physical basis for spectroscopic estimates of leaf nitrogen concentration. *Remote Sensing of Environment, 75*(2), 153.

Lorentz, L. J. (2013). *Hyperspectral reflectance and stable isotopic nitrogen: Tools to assess forest ecosystem nitrogen cycling.* (Unpublished Master of Science). Virginia Polytechnic Institute and State University,

Macko, S. A., & Ostrom, N. E. (1994). Pollution studies using stable isotopes. In K. Lajtha, & R. Michener (Eds.), *Stable isotopes in ecology* (pp. 42-65). United Kingdom: Blackwell Scientific.

Malone, T. C. (1991). *River flow, phytoplankton production and oxygen depletion in Chesapeake Bay. Modern and ancient continental shelf anoxia.* Geological Society Special Publication, 1991, 58, 83-93.

Myneni, R.B., F.G. Hall, P.J. Sellers, & A.L. Marshak (1995). The interpretation of spectral vegetation indexes. *IEEE Transaction on Geoscience and Remote Sensing*, 33, 481-486.

Ouyang, Y., Leininger, T. D., & Moran, M. (2015). Estimating effects of reforestation on nitrogen and phosphorus load reductions in the lower Yazoo river watershed, Mississippi. *Ecological Engineering, 75*, 449-456.

Quillard, S., Louam, G., Buisson, J. P., Boyer, M., Lapkowski, M., Pron, A., & Lefrant, S. (1997). Vibrational spectroscopic studies of the isotope effects in polyaniline. *Synthetic Metals, 84*(1–3), 805-806.

Schott, J. R. (2007). *Remote sensing, the image chain approach* (Second ed.). Oxford, New York: Oxford University Press. Print.

Shearer, G., & Kohl, D. H. (1986). N_2-fixation in field settings: Estimations based on natural ^{15}N abundance. *Functional Plant Biology, 13*, 699-756.

Shenk, J., Workman Jr, J., & Westerhaus, M. (2001). Application of NIR spectroscopy to agricultural products. *Handbook of near-infrared analysis, second edition* CRC Press. Print.

Stuart, B. (2004). *Infrared spectroscopy: Fundamentals and applications*. England: John Wiley & Sons Ltd. Print.

Sulzman, E. W. (2007). Stable isotope chemistry and measurement: A primer. In R. Michner, & K. Lajtha (Eds.), *Stable isotopes in ecology and environmental science* (pp. 1-21). Malden: Blackwell.

Sun, S., Guo, B., Wei, Y., & Fan, M. (2012). Classification of geographical origins and prediction of $\delta^{13}C$ and $\delta^{15}N$ values of lamb meat by near infrared reflectance spectroscopy. *Food Chemistry, 135*(2), 508-514.

Tango, P. J., & Batiuk, R. A. (2013). Deriving Chesapeake Bay water quality standards. *Journal of the American Water Resources Association, 49*(5), 1007-1024.

Townsend, M. A., Young, D. P., & Macko, S. A. (2004). Kansas case study applications of nitrogen-15 natural abundance method for identification of nitrate sources. *Journal of Hazardous Substance Research, 4*, 1-22.

Wang, L., Okin, G. S., & Macko, S. A. (2010). Remote sensing of nitrogen and carbon isotope compostions in terrestrial ecosystems. In J. West, G. J. Bowen, T. Dawson & K. P. Tu (Eds.), *Isoscapes* (pp. 51-70). Dordrecht Heidelberg London New York: Springer.

Wang, L., Okin, G. S., Wang, J., Epstein, H., & Macko, S. A. (2007). Predicting leaf and canopy ^{15}N compositions from reflectance spectra. *Geophysical Research Letters, 34*(2).

Wang, X., Fuller, D. O., Sternberg, L., & Miralles-Wilhelm, F. (2011). Foliar nutrient and water content in subtropical tree islands: A new chemohydrodynamic link between satellite vegetation indices and foliar delta^{15}N values. *Remote Sensing of Environment, 115*(3), 923-930.

Yun, S. I., Ro, H. M., Choi, W. J., & Chang, S. X. (2006). Interactive effects of N fertilizer source and timing of fertilization leave specific N isotopic signatures in Chinese cabbage and soil. *Soil Biology and Biochemistry, 38*, 1682-1689.

Chapter 2 – Finding the Spectral Signature of ^{15}Nitrogen Isotopes in Plants by Hyperspectral Techniques

Published in the Journal of Remote Sensing Technology, 2016, Vol. 4 Iss. 1, PP. 115-120

Abstract

Expensive laboratory based instrumentation is typically used to perform stable isotope analysis, making sample run times lengthy and costly. Research was conducted to identify novel approaches to stable isotope analysis using infrared spectroscopy techniques in both laboratory and field based instrumentation. Buckwheat plants were grown in aeroponic conditions at three nitrogen concentration levels (0.32%, 0.20%, and 0.10%) of 95% ^{15}N-labelled fertilizer solutions and compared to a control with natural abundance (0.0036%) nitrogen based fertilizer. Infrared instrumentation was used to measure the buckwheat leaves and show diagnostic wavelength shifts are correlated to their fertilizer concentration, occur at multiple infrared frequencies, and are associated with nitrogen functional group compounds present in the buckwheat. These measurements confirm that with remote sensing techniques, nitrogen isotopes are detectible in the infrared region. The ability to remotely sense nitrogen isotopes with either field or airborne sensors will enable faster analysis and wider spatial coverage than current techniques.

Keywords

Stable Isotopes; FTIR; Infrared Spectroscopy; Nitrogen

Introduction

In contrast to its standard concentrations, the highly variable natural abundances in the most stable isotopes of an element make their analysis particularly useful in many applications, including environmental, ecological, agricultural and archaeological problems (Hoefs, 2009). This information can be used as a fingerprint or signature of a material under study to indicate the element's origins and history in the material. In the laboratory, isotope-ratio mass spectrometry (IRMS) is the primary analytical tool of choice in order to obtain accurate nitrogen stable isotope data for a sample of organic matter. IRMS is very accurate, however, sample run times and instrument calibrations are time consuming, costly, can only be performed in a laboratory, and represent data from a single location on the Earth's surface at a particular time.

This problem can be helped by a new technique for isotope ratio measurements utilizing the infrared portion of the electromagnetic spectrum. In the infrared, elemental composition can be analyzed based on the elemental structure of the supplied sample (Coates, 2000). Molecules flex and rotate in characteristic ways when they are bound together. These movements vibrate at specific and known frequency locations in the infrared. Isotope effects can alter these characteristic frequency locations due to the heavier mass of the isotope. Heavier masses change the vibrational modes of the bonds in the molecules and create a downshift in frequency from the one expected in the lower mass isotope molecule (Quillard *et al*., 1997). These changes require instrumentation with high frequency or spectral resolution of hundreds of bands of information to measure these shifts, often termed hyperspectral. This study shows that by utilizing hyperspectral

instrumentation that operates in the infrared, the effects of these isotopes are observable. This can provide researchers with faster and cheaper measurements that could cover broad areas of the Earth's surface. In the future, in order to provide biogeochemical understanding at larger spatial extents, this technology can be translated for use with airborne or space-based instruments since it is not possible using current instrumentation and techniques.

Ultimately, for agricultural and environmental analysis, hyperspectral remote-sensing techniques that focus on the fundamental spectral data gathered from field and laboratory based Fourier Transform Infrared (FTIR) and dispersive spectrometers could be applied. Nitrogen fertilizer sources can be identified in plant matter and the surrounding soils as organic manure based fertilizers since they are more enriched in the heavier ^{15}N isotope in comparison to Haber process inorganic urea fertilizers (Townsend *et al*., 2004; Yun *et al.*, 2006). As anthropogenic impacts are often hard to quantify in the environment, determining fertilizer sources is important in understanding nutrient loads and origins (Townsend *et al*., 2004). Nitrogen based nutrient loads are still identified as an improvement area in United States' current Environmental Protection Agency's assessment on the Chesapeake Bay, Eastern United States (*2014 state of the bay*.2014). Our research shows application for remote detection of improvement areas within watersheds, such as the Bay, and may enable municipalities to meet their Bay Initiative improvement goals more effectively. By linking these remote sensing techniques with water samples, spatial analysis could be used to help identify non-point source polluters within the Chesapeake Bay watershed.

Background

A nitrogen stable isotope (^{15}N) labeled fertilizer plant growth enrichment experiment was conducted in order to identify the isotope induced frequency/wavelength shifts in plant matter, as well as to determine if they are detectible by current FTIR and dispersive spectroscopy techniques, rather than mass spectrometry. The isotope was supplied in liquid fertilizer solutions to buckwheat plants growing in separate aeroponic systems. Compared to a control containing no labeled fertilizer, different concentration levels were chosen to assess quantity of nitrogen uptake and to observe plants under these different conditions. After 21 days of growth, the infrared reflectance of the plant leaves was measured by lab and field grade spectrometers when the buckwheat reached maturity. Both fresh and dried leaves were measured in order to simulate different times of year when sample measurements could be conducted.

Plants incorporate nitrogen because it is a required macronutrient for their growth and metabolic processes, such as photosynthesis. In plants, amino acids, proteins, and molecules, such as chlorophyll contain nitrogen (Jones *et al,* 2013). Chlorophyll has known characteristics across the electromagnetic spectrum, but its isotope influences have yet to be reported (Vernon & Seely, 1966).

Materials

Plant Growth and Fertilizers

Aeroponic plant growing systems, shown in Fig. 2, were used to concentrate the uptake of nitrogen isotopes and grow plants under controlled conditions. Aeroponics is a system of misters that spray the plant's root systems with nutrients. The systems spray the

plants every hour for a 30-minute duration. The systems are housed within a seed-starting cart that has a humidity tent and wide-spectrum fluorescent lighting, which illuminates the plants for 16 hours over a 24 hour period. This accurately simulates summer environment in which buckwheat thrives. Buckwheat is a quick growing summer annual that is well suited for this study.

Figure 2 Buckwheat is growing in an aeroponic unit. Four units were used one each for the control and three experimental trials

Instrumentation

Three analytical spectroscopy instruments were used in this research. Each of them has specialties within the infrared spectrum and is measured in terms of frequency in chemistry applications, and wavelength in remote sensing applications. The infrared spectrum spans the region from 1.1 – 10+ microns (9,090 - 1,000 cm^{-1}) and can be further broken down into specific regions. The 1.1 – 2.5 micron (9,090 - 4,000 cm^{-1}) region is the short-wave infrared and is dominated by vibrational overtones from the mid-wave infrared. The mid-wave infrared spans the 2 – 5 micron (5000 - 2000 cm^{-1}) region; this is the region

where functional groups can be assigned. The long-wave infrared is above five microns (2000 cm^{-1}). Specific compounds can be identified in the fingerprint region of the infrared spectrum between 6.6 – 20 microns (1,500 - 500 cm^{-1}).

These spectrum regions are best analyzed by specific instrumentation and for different field or lab applications. The Analytical Spectral Devices Inc. (ASD) Field Spec Pro (*FieldSpec(R) pro user's guide.* 2002)is a dispersive spectrometer. It was used to measure plant reflectance from the visible to the overtone vibrations region up to 2.5 microns. It has a spectral resolution of up to ten nanometers in the short-wave infrared. The Agilent 4100 Exoscan (*Agilent 4100 exoscan FTIR operation manual.* 2013) is a FTIR spectrometer that measures from 2.5 – 15 microns (4000 – 650 cm^{-1}) with a frequency resolution of up to 4 cm^{-1}. It can also be used for field measurements. The Thermo Scientific Nicolet 6700 (*Nicolet (TM) FT-IR user's guide.* 2004) is a laboratory bench top FTIR spectrometer that measures the entire infrared spectrum and was set up for 4 cm^{-1} frequency resolution.

Methods

For four weeks, buckwheat plants were grown in simulated summer conditions at which point leaves from each trial were harvested for instrumental analysis. Fresh and dried whole leaves were measured to determine the likelihood of remote or field based sensors to detect any isotope effects. The three analytical instruments described above were used to measure the front and back of the leaves, as well as the ground leaves. All instruments were operated under vendor specifications for collection of reflectance or absorption spectra. The instruments measured the data from the fresh, dried, and ground

leaves through direct contact with the leaf surface or powder. Over a few seconds, each instrument collects a series of either 30 or 60 spectra and averages them together in one resulting spectra. From each trial, three spectra were measured of each of the ten collected leaves.

The software package ENVI 4.7 (Environment for Visualizing Information, Excelis, Inc.) compared and analyzed the resulting spectra. This experimental design is often used (Slonecker, Haack, & Price, 2009) and allows for observation of ^{15}N uptake to occur in the spectrum across multiple instruments, and consequently different regions of the electromagnetic spectrum. For validation of collection practices, spectra from the instrumentation are imported and compared against library spectra. Chemical functional groups can be identified from infrared spectral interpretation algorithms supplied by vendor software. The isotope induced shifts along the spectrum and their known functional groups are then assessed.

Results

The only variable in this experiment was the amount of ^{15}N available to the buckwheat. Spectral wavelength shifts were observed when compared to the control in all three trials and measured leaf conditions (fresh, dried, front, back, ground). As expected, fresh leaf spectra contained water features throughout the spectrum. Dried leaf conditions presented the best results for wavelength shift analysis. Across all samples, the results of the dried leaf front, back, and ground samples were consistent. Samples from the three ^{15}N abundance levels did show an uptake of ^{15}N that were measurable by the spectrometers.

Due to changes in the molecular bonds and vibrational modes, the addition of the heavier isotope does in fact create downward frequency shifts. Both lab and field grade FTIR and dispersive spectrometers can measure these shifts. The primary area of isotope shifting was observed to be in the region of the infrared spectrum associated with the chlorophyll molecule. Additional shifts were observed in amine/amide/imine and other chemical functional group absorption regions.

Laboratory Based Instrumentation

The Nicolet data showed major shifts occurring in the 3350 -3180 cm^{-1} region where primary aliphatic amine NH bonds are stretching. In Fig. 3, a 102-wavenumber shift was observed by the Nicolet spectrometer where the control peak centered at 3,296 cm^{-1} and the isotope-induced spectrum centered at 3,194 cm^{-1}.

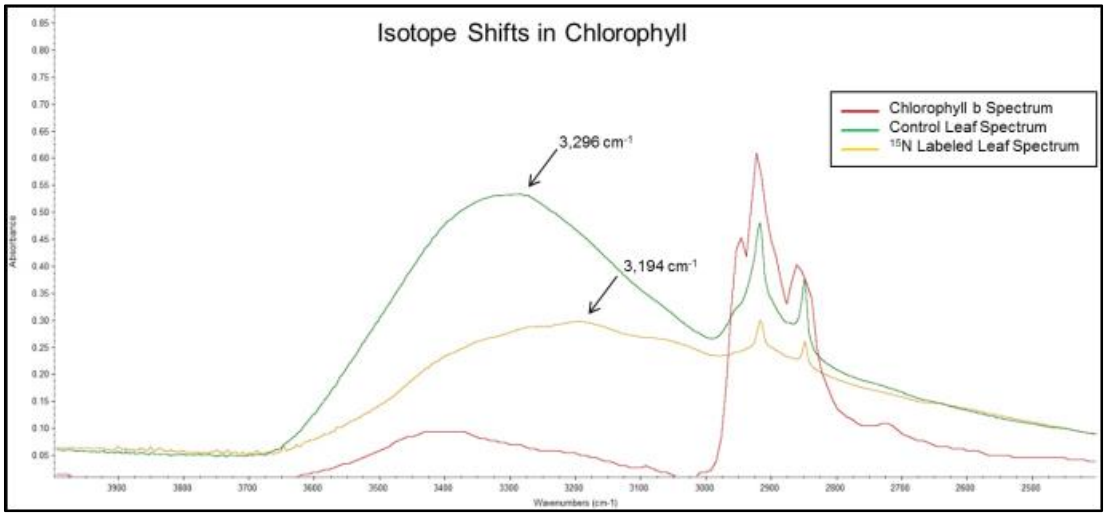

Figure 3 Nicolet Measured Spectra of Dried Buckwheat Leaves (Control and Trial 3) Compared to Thermo Scientific FTIR Library Spectra of Chlorophyll Showing a 102 Wavenumber Downshift

Both primary amide II NH2 bonds and imine C-N bonds vibrate in the 1,600 cm-1 region. Primary amide II bonds vibrate between 1,650 cm^{-1} and 1,620 cm^{-1}, and imines vibrate between 1,690 cm^{-1} and 1,640 cm^{-1}.

As shown in Fig. 4, a 15-wavenumber downshift was observed from 1,634 cm^{-1} to 1,619 cm^{-1} in the Nicolet data. Notably, these CN bond vibrations can be directly attributed to the chlorophyll structure, suggesting that the ^{15}N labeled nitrogen is being introduced into the chlorophyll molecule.

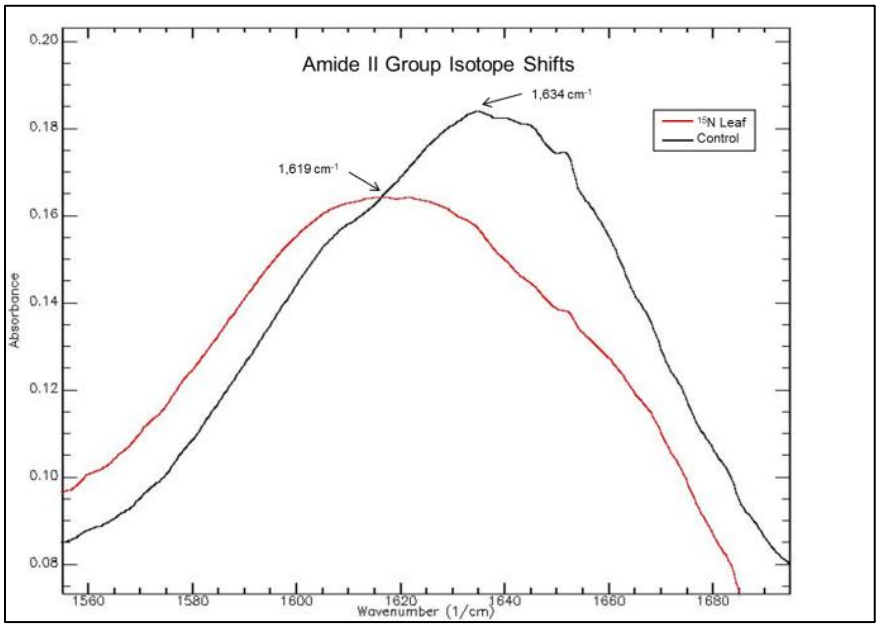

Figure 4 Nicolet Measured Spectra of Buckwheat Leaves (Control and Trial 3), in 1,600 cm^{-1} Region, Showing a 15 Wavenumber Downshift

Field Based Instrumentation

In addition to the laboratory instrumentation described earlier, the field instrumentation was able to detect the wavelength shifts that occur by adding the heavier

^{15}N isotope. As shown in Fig. 4, the Exoscan showed a nine wavenumber shift in the 2,300 cm^{-1} region from 2,372 cm^{-1} to 2,363 cm^{-1} that is associated with NH bonds.

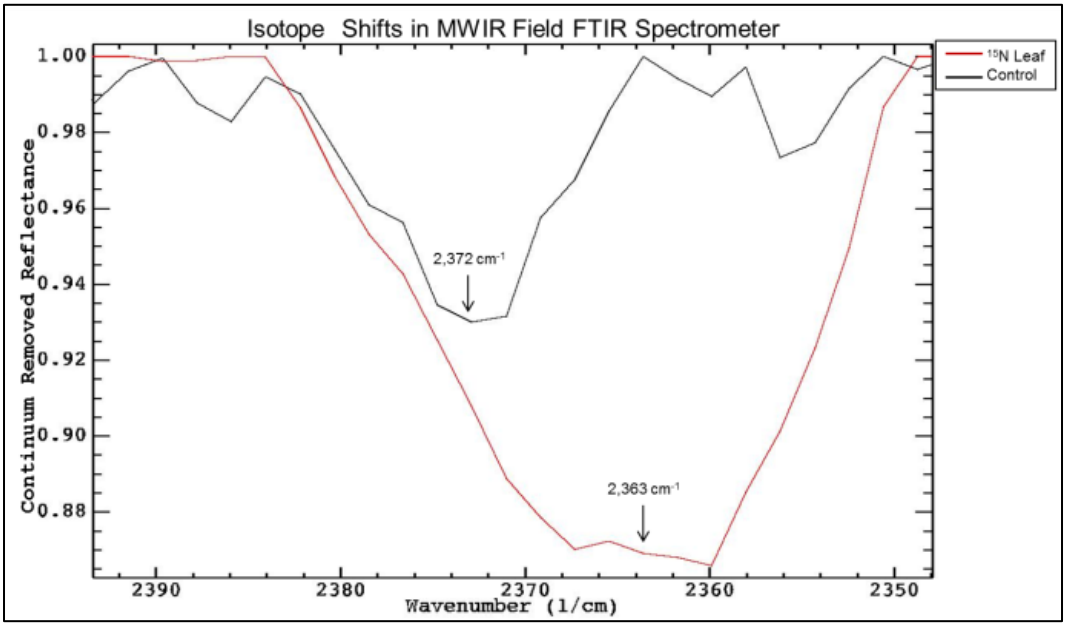

Figure 5 Exoscan Measured Spectra of Buckwheat Leaves (Control and Trial 3) Showing a 9 Wavenumber Downshift

This result is especially interesting as it was measured by the field grade FTIR spectrometer, the Exoscan, which showed potential field applications of this method. Continuum removal was used in ENVI to normalize the spectra to a common baseline. This technique aids in the analysis of specific absorption features. Compared with those in the laboratory, field grade instrumentals typically have lower sensitivity and thereby somewhat limited capabilities. In this case however, these results show promise for the ability to detect stable isotopes in the field.

The field based dispersive spectrometer, or ASD, also showed a shift in Fig. 6, but not in the functional group overtone region. To accentuate the differences between the experimental trials and the control, the data was analyzed in the 1st derivative. The 16

nanometer (nm) shift was observed in the near infrared (NIR) region where the control had a 1st derivative peak of 719 nm and the isotope induced shift peaked at 703 nm. The chemical origin of this shift is associated to the mesophyll plant cells that absorb or transmit light energy in the NIR (Elvidge & Chen, 1995).

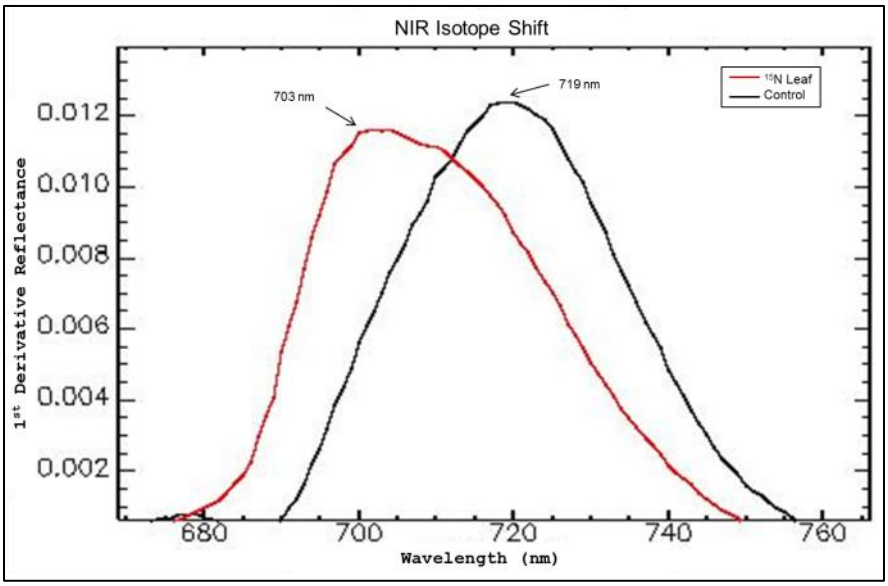

Figure 6 ASD Measured Spectra of Buckwheat Leaves (Control and Trial 3) Showing a 16 Nanometer Downshift

Discussion

The frequency shifts represented here are not the only ones observed by all the instrumentation, only strong examples, or those that have direct functional group assignments. Due to its high concentration in the measured samples, chlorophyll was easily identified in the plant spectra. These spectra represent the bulk nitrogen contained in the plants with an increased amount of ^{15}N, thereby creating spectral downshifts. Future work could include analysis of chemical extractions of plant molecules, which could illuminate specific compounds that are being observed.

The increased isotope abundance in the fertilizer trials did not appear to correlate to the concentration in the plant. This could possibly be due to the limiting factors in some cases preventing ^{15}N uptake, or to the duration exposure to the isotope fertilizer. Adding the ammonium nitrate isotope to the fertilizer solution decreases the pH as well as the exposure of deionized water to atmospheric carbon dioxide. The availability of nitrogen for plant uptake decreased as the pH of the liquid fertilizer solution decreased. In some cases, the large amount of nitrogen created nitrogen burn, stunting the plants growth, and therefore restricting the ease of leaf measurement. Additionally, the homemade fertilizer mixture only supplied N-P-K to the plants during their growth and it is suspected that other missing micronutrients should be considered in future experiments.

No difference was observed in the fresh versus dried samples of the plant leaves with the instruments that measured the mid-wave infrared region, as water is highly transparent in this region. However, the dried samples measured by the ASD did yield better results. The short-wave infrared region of the ASD data is highly prone to water absorption bands, either in the atmosphere or in this case of the leaf samples. No functional group overtone shifts were observed by the ASD in the shortwave infrared. This is most likely due to the complex chemical nature of the plant leaf and the multiple compounds interacting with light energy in this region. Shifts were identified in the first derivative of the spectra in the NIR, where healthy vegetation is reflective and is not associated with chlorophyll absorptions. No isotope shifts were shown by the ASD data in visible regions that are associated with chlorophyll absorptions (0.4-0.7 microns).

Additionally, the ASD data showed a decrease in wavelength, and since it is inversely related to wavenumber, it would represent an increase in frequency, which is not an expected isotope effect. The infrared region is the most indicative portion of the spectrum for identifying isotope effects. Based on the results of this experiment, there is reason to believe that amine/imine groups and chlorophyll molecules are the main cause.

Although quantification of the isotope abundance was not possible by this three level calibration experiment, it should be addressed in future work. The spectral data from the Nicolet or Exoscan did not show an increase in absorption depth based on an increase in isotope concentration. In order for quantification to occur, the complex nature of plant structures and compounds needs to be further isolated.

Conclusions

With this study, in addition to traditional mass spectrometry, FTIR and dispersive spectroscopy are proven to be sensitive enough to measure isotope effects in plant matter. This research highlights the utility of lab and field based spectroscopy for stable isotope analysis of plant's spectral reflectance and absorbance values at the currently known ^{15}N response regions. The ease of use and sample preparation of spectroscopy methods is an added benefit over the traditional methods. Allowing the bringing of isotope ratio measurements into the field and outside of the lab would provide significant advancements in the field of geochemistry.

When coupled with water quality measurements, agricultural non-point source pollution areas can be identified more rapidly and over entire watersheds. Hyperspectral sensors can now be developed for the capability of remotely analyzing fertilizer sources

from their ^{15}N signals. This technique would greatly improve scientist's abilities to rapidly identify improvement areas within watersheds where degraded water quality occurs. With the advancement of sensor development, future airborne or space based sensors tuned to the frequencies of isotope absorptions could be fielded. This will provide researchers with greater biogeochemical understanding at larger spatial scales than are currently available.

There should be continued research on this topic. Specifically, further research of plant structures and nitrogen compounds would help to confirm and validate the experimental results achieved in this research. This would enable isolation of specific molecules that create the spectral shifts when they are exposed to nitrogen isotope fertilizers. Additionally, continued experiments and measurements will also help to confirm the wavenumber and wavelength locations of the isotope induced shifts and how quantification can occur. By saving time and money, this technique can help aid researchers by providing more rapid stable isotope analysis in the field, as well as by focusing efforts on specific areas for field sampling and subsequent analysis by traditional more accurate IRMS.

References

2014 state of the bay. (2014). ().Chesapeake Bay Foundation.

Agilent 4100 Exoscan FTIR operation manual. (2013). Unpublished manuscript.

Coates, J. (2000). In Meyers R. A. (Ed.), *Interpretation of infrared spectra, a practical approach*. England: John Wiley & Sons Ltd.

Elvidge, C. D., & Chen, Z. (1995). Comparison of broad-band and narrow-band red and near-infrared vegetation indices. *Remote Sensing of Environment, 54*(1), 38-48.

FieldSpec(R) pro user's guide. (2002). Unpublished manuscript.

Hoefs, J. (2009). *Stable isotope geochemistry* (6th Ed.). Berling Heidelberg: Springer-Verlag.

Jones, R., Ougham, H., Thomas, H., & Waalang, S. (2013). *The molecular life of plants*. New Jersey: Wiley-Blackwell.

Nicolet (TM) FT-IR user's guide. (2004). Unpublished manuscript.

Quillard, S., Louam, G., Buisson, J. P., Boyer, M., Lapkowski, M., Pron, A., & Lefrant, S. (1997). Vibrational spectroscopic studies of the isotope effects in polyaniline. *Synthetic Metals, 84*(1–3), 805-806.

Slonecker, T., Haack, B., & Price, S. (2009). Spectroscopic analysis of arsenic uptake in pteris ferns*. Remote Sensing, 1(4), 644-675.*

Townsend, M. A., Young, D. P., & Macko, S. A. (2004). Kansas case study applications of nitrogen-15 natural abundance method for identification of nitrate sources. *Journal of Hazardous Substance Research, 4*, 1-22.

Vernon, L., & Seely, G. (1966). *The chlorophylls*. New York: Academic Press Inc.

Yun, S. I., Ro, H. M., Choi, W. J., & Chang, S. X. (2006). Interactive effects of N fertilizer source and timing of fertilization leave specific N isotopic signatures in Chinese cabbage and soil. *Soil Biology and Biochemistry, 38*, 1682-1689.

Chapter 3 – Computational Chemistry as a Tool for the Identification of ^{15}Nitrogen Stable Isotope Induced Diagnostic Wavelength Shifts of Nitrogen Compounds in Plants

To Be Submitted

Abstract

To obtain laboratory based accurate nitrogen stable isotope data for a given portion of organic matter in the laboratory, isotope-ratio mass spectrometry (IRMS) is the analytical tool of choice. The IRMS data is very high in precision; however, sample run times and instrument calibrations are time consuming and costly. The samples collected for IRMS analysis represent data from a single location on the Earth's surface at a particular time. Additionally, IRMS is performed only in laboratory conditions. Isotope analysis by FTIR has many benefits over traditional IRMS. Field based FTIR spectroscopy can be performed in the field, rapidly, at a lower cost, and provide geospatially robust data. Wavelength shifts within the infrared spectrum that are caused by the presence of ^{15}N can be observed with FTIR spectrometers. A nontraditional computational approach is employed to validate the shifts observed experimentally and link specific vibrations to their nitrogen containing compounds in plants. The modeled data show that isotope induced shifts in ammonium are detected by FTIR spectrometers and spectral separation of nitrogen isotopes is possible. This will provide researchers with faster and cheaper isotope ratio measurements that could cover broader areas and eventually be translated to use with airborne or space-based instruments.

Keywords

Computational Chemistry; Stable Isotopes; FTIR; Infrared Spectroscopy; Nitrogen

Introduction

Stable isotope information can be used like a fingerprint or signature of a material under study to indicate origins and history of the element in the material (Engel *et al*., 1991). Stable isotope ratios are traditionally calculated using mass spectrometry. The ratios are calculated by comparing the heavier rare isotope in a sample to the more abundant lighter isotope and are described as a delta or δ^{15}N value according to the following equation:

$$\delta^{15}\mathrm{N} = 1000 \left[\frac{\mathrm{Ratio}_{Sample} - \mathrm{Ratio}_{Standard}}{\mathrm{Ratio}_{Standard}} \right] \qquad \text{Equation 1}$$

The standard for nitrogen stable isotope ratio calculations is atmospheric nitrogen with an isotope ratio of 0.3613. A new technique for isotope ratio measurements utilizing the infrared portion of the electromagnetic spectrum is being developed. In the infrared, material composition can be analyzed based on the elemental structure of the supplied sample (Coates, 2000). In molecules, bonds flex and rotate in characteristic ways. These movements vibrate at specific and known frequencies in the infrared. Isotope effects can alter these characteristic frequency locations due to the different masses of the molecule. A heavier mass modifies the vibrational modes of the bonds in the molecule and creates a downshift in the frequency response. (Quillard *et al*., 1997). Observation of these changes requires instrumentation with high frequency or spectral resolution to measure these shifts, termed hyperspectral.

The FTIR spectra represent isotope shifts in an additive way that makes specific identification of bonds complex as many responses overlap with each other. This requires additional analysis to separate individual molecular responses in FTIR data. Computational chemistry is a tool that can be used to address this problem. The independent compounds contribution to the FTIR data can be known through modeling of each compound and calculation of their IR vibrations. This is done with specialty software such as Gaussian (Priyangika *et al,* 2006). Once the specific compounds and their frequencies are identified in the FTIR spectrum, development of ^{15}N isotope ratios is possible. The novel methodology for isotope ratios can then be translated for use with airborne or space-based instruments in the future in order to provide biogeochemical understanding at larger spatial scales not possible by current IRMS instrumentation and techniques.

Nitrogen fertilizer sources can be identified in plant matter and the surrounding soils as organic manure based fertilizers are more enriched in the heavier ^{15}N isotope versus Haber process inorganic fertilizers (Yun *et al*., 2006). An ability to determine fertilizer sources is important in understanding nutrient loads and origins, as anthropogenic impacts are often difficult to quantify in the environment. Nitrogen based nutrient loads are identified as an improvement area in the assessment of the Chesapeake Bay water quality (*2016 State of the Bay*, 2016). This research herein shows the application for remote detection of improvement areas within watersheds, such as the Bay and may enable municipalities to better meet their improvement goals. An important area of improvement is the identification of non-point source polluters coming from the

agricultural sector. Spatial analysis linking the remote sensing techniques with water samples could then be used to help identify non-point source polluters within the impaired watersheds such as the Chesapeake Bay.

Background

A nitrogen stable isotope (^{15}N) labeled experiment was conducted on in order to identify the isotope induced frequency/wavelength shifts in plant matter. It was determined that they are detectible by current FTIR and dispersive spectroscopy techniques rather than mass spectrometry (Capelle & Macko, 2016). The FTIR instruments were used to identify shifts within three distinct regions of the electro-magnetic spectrum. The largest shift was linked to primary aliphatic amine NH bonds centered at 3,296 cm^{-1} and 3,194 cm^{-1} for the natural abundance control and the isotope-enriched spectrum, respectively. This region of the spectrum was shown to correspond to the chlorophyll molecule (Capelle & Macko, 2016). Additional shifts were observed in the 1,600 cm^{-1} region associated with amide (N-H) and imine (C-N) bonds. Other amide region shifts were also observed around 2,300 cm^{-1}. These results describe functional groups of compounds. Computational chemistry is a tool that can be used to model the infrared spectra of the nitrogen compounds in plants to aid in understanding the FTIR data.

There are many nitrogen containing compounds in plants (Coruzzi, 2003; Naik *et al*., 1982). Plants uptake nitrogen as it is a required macronutrient for their growth and metabolic processes. Nitrogen is found in plant amino acids, proteins and molecules such as chlorophyll and alkaloids (Jones *et al*., 2013). Six nitrogen containing plant amino

acids, proline, glutamine, glutamate, aspartate, aspartame, asparagine (Vernon & Seely, 1966), and ammonium were modeled using Gaussian software. Gaussian provides for chemical computational modeling under both natural and isotope enriched conditions. The software optimizes the structure and is able to calculate the vibrational modes of the bonds in order to produce the infrared spectra. These spectral results from the models are then able to be compared to the shifts observed from direct measurement of the labeled plants by spectral sensors (Capelle & Macko, 2016).

Materials

Previously collected FTIR experimental data (Capelle & Macko, 2016) from buckwheat plants is used in this research for comparison to newly collected IRMS data on the same samples. An IsoPrime IRMS was used to measure the actual isotope ratio of the control and experimental trials from Capelle and Macko. Control plants were grown at natural abundance levels of ^{15}N whereas each of three experimental trials were heavily enriched in the isotope. The FTIR data included ten spectra of each experimental group as well as the average. Each spectra represents 60 scans from each leaf measured. The computational chemical modeling of six amino acids and ammonia was performed using Gaussian 03 software on Rivanna, a high performance computing cluster at the University of Virginia.

Methods

Computational Modeling

The Hartree-Fock method and 6-31G basis set were used for all models in the Gaussian software. Two models were run for each of the eight nitrogen containing compounds common to plants, one as ^{14}N and the other as ^{15}N. Hartree-Fock Theory (also known as self-consistent field theory or SCF theory) provides an approximate solution to the Schrödinger equation; the energy calculated serves as an upper bound on the actual energy. Specifically, this method invokes variational theory to produce a set of equations which can be solved iteratively. It should be noted that computational times will scale according to the fourth power of the number of basis sets (N4) (Shuh, 2009), therefore the large chlorophyll molecule was not computed in this study. The Gaussian computational chemistry program produces theoretical results of compound structures, including their vibrational states and resulting infrared spectra of molecules.

Computational chemistry programs are capable of providing theoretical results of compound structures, including the vibrational spectra of molecules and their intensities in the infrared spectrum. Programs like Gaussian, Spartan, and NWChem all allow for the calculation of the vibrational modes of molecules. These programs allow users to select from a variety of potential computational methods that best fits the molecule under study. There are two major categories of methods; classical mechanics and quantum mechanical. The classical mechanics approach is more appropriate for systems like proteins with hundreds or thousands of atoms whereas quantum mechanical approaches are often applied to smaller molecules.

The calculations relevant to the work included herein are all quantum mechanical in nature; that is they approximate or solve the relevant Hamiltonian. While there are numerous quantum mechanical methods/theories for performing these calculations, only two relevant methods will be described here. Hartree-Fock Theory (also known as self-consistent field theory or SCF theory) provides an approximate solution to the Schrödinger equation; the energy calculated serves as an upper bound on the actual energy. Specifically this method invokes variational theory to produce a set of equations which can be solved iteratively. It should be noted that computational times will scale according to the fourth power of the number of basis sets (N^4) (Shuh, 2009).

Density Functional Theory (DFT) is a theory relies on the concept that the energy of the system can be approximated using the electron density. This method makes use of an exchange-correlation operator; this is typically separated into an exchange functional and correlation functional. Again, iterative methods are used to find the energy minima. Computational times will scale according to the cube of the number of basis sets (N^3). Density functional theory is widely regarded to be particularly efficient in calculations; the accuracy of calculations is similar to higher levels of theory like MP2, while keeping computational times shorter and closer to those of less accurate methods like Hartree-Fock. For this reason, DFT is very popular and lends itself to a wide variety of computational chemistry calculations (Shuh, 2009).

Molecular orbitals are constructed by a linear combination of atomic orbitals (LCAO). The selected basis set allows the user to choose the description of molecular orbitals. The most common types of atomic orbitals available are Slater Type Orbitals

(STO) and Gaussian Type Orbitals (GTO). Gaussian type orbitals compromise somewhat in their approximation of the orbital shape, but allow for more rapid calculations. Each atomic orbital is assigned at least one corresponding basis function. However, Pople split-valence basis sets add additional basis functions, which lead to an overall more accurate approximation; more basis functions allow for more accurate characterization of the molecular orbitals (Shuh, 2009).

FTIR-ATR Spectral Measurements

The Thermo Scientific Nicolet 6700 (*Nicolet (TM) FT-IR user's guide,* 2004) is a laboratory bench top FTIR spectrometer that measures the entire infrared spectrum and was set up for 4 cm^{-1} frequency resolution. The instrument was operated under vendor specifications for collection of absorption spectra. The instrument measures the spectral response from the sample through direct contact with the ATR diamond crystal. Over a few seconds, the instrument collects a series of 60 spectra and averages them together in one resulting spectra. The spectra are then able to be analyzed in the software package ENVI 4.7 (Environment for Visualizing Information, Excelis, Inc.).

Results

Modeled Spectra

The modeled nitrogen compounds show multiple peak shifts that occur at different wavenumbers. For each compound modeled, both the ^{14}N spectra and ^{15}N spectra are included. The shifts are easily identified (figures 7-24).

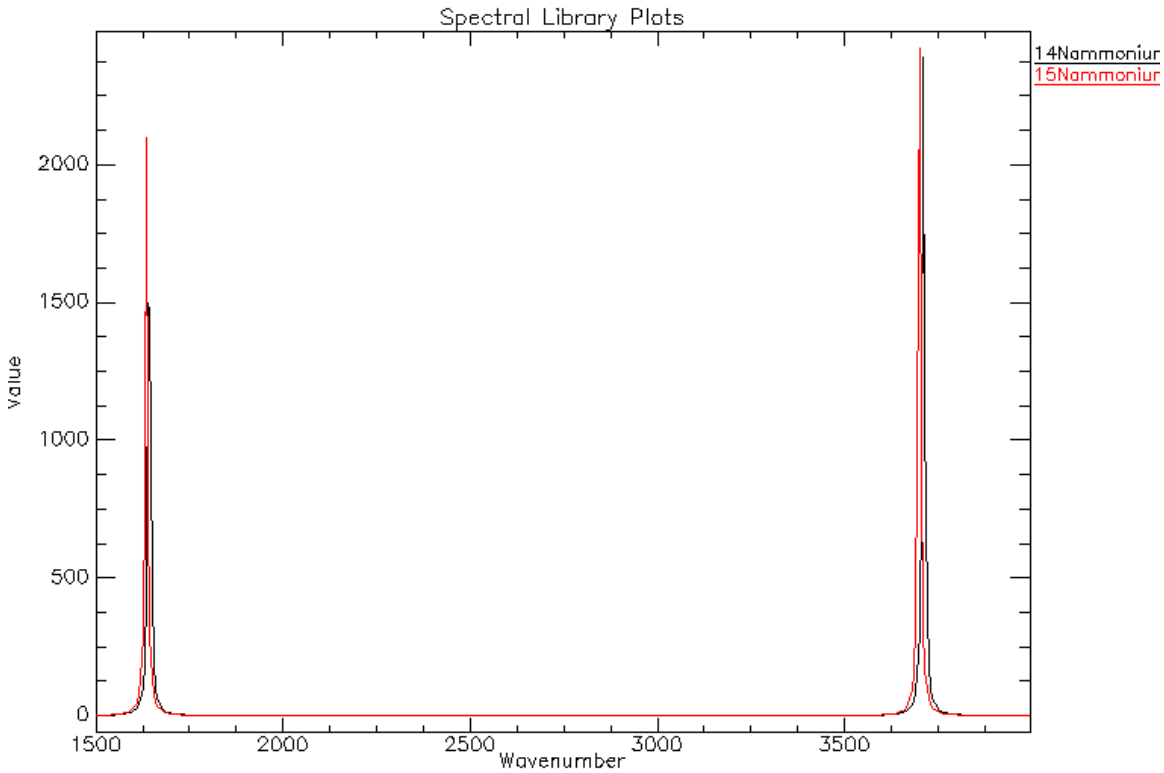

Figure 7 Modeled spectra of ammonium, ^{14}N (in black) and ^{15}N (in red) shown at full spectral resolution.

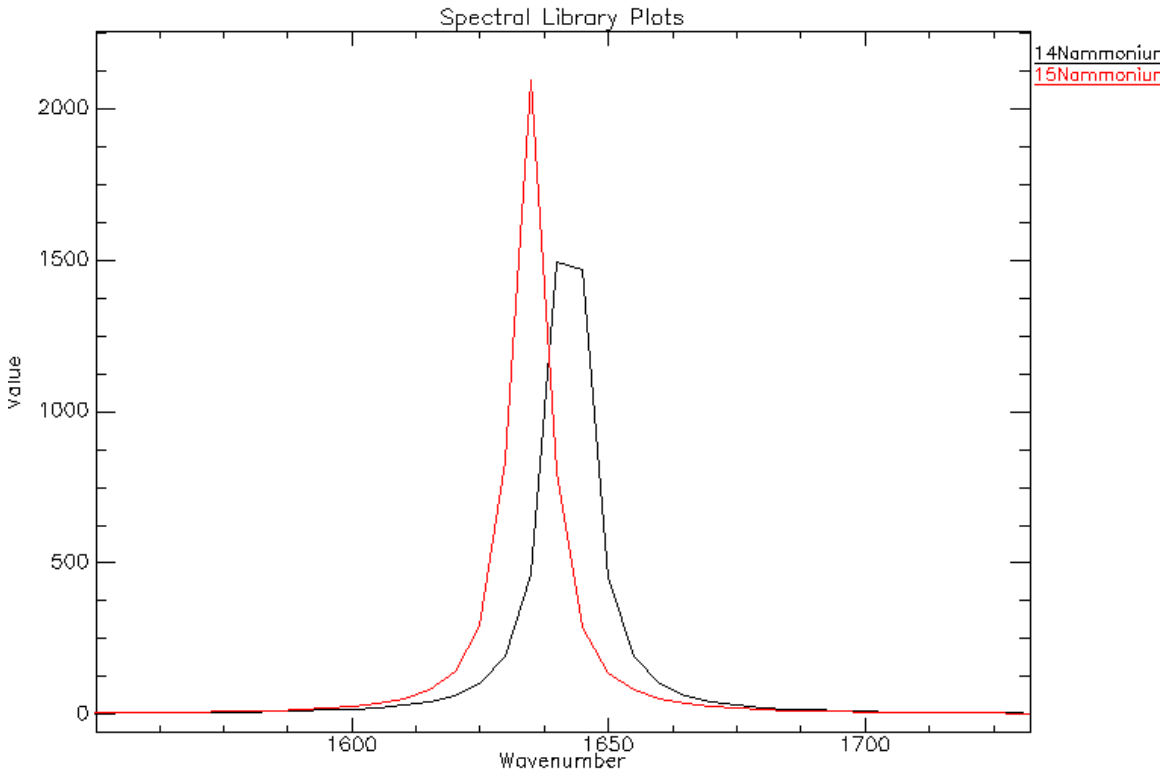

Figure 8 Shift occurring at 1,635 cm^{-1}, ^{14}N (in black) and ^{15}N (in red) in the ammonium modeled spectra.

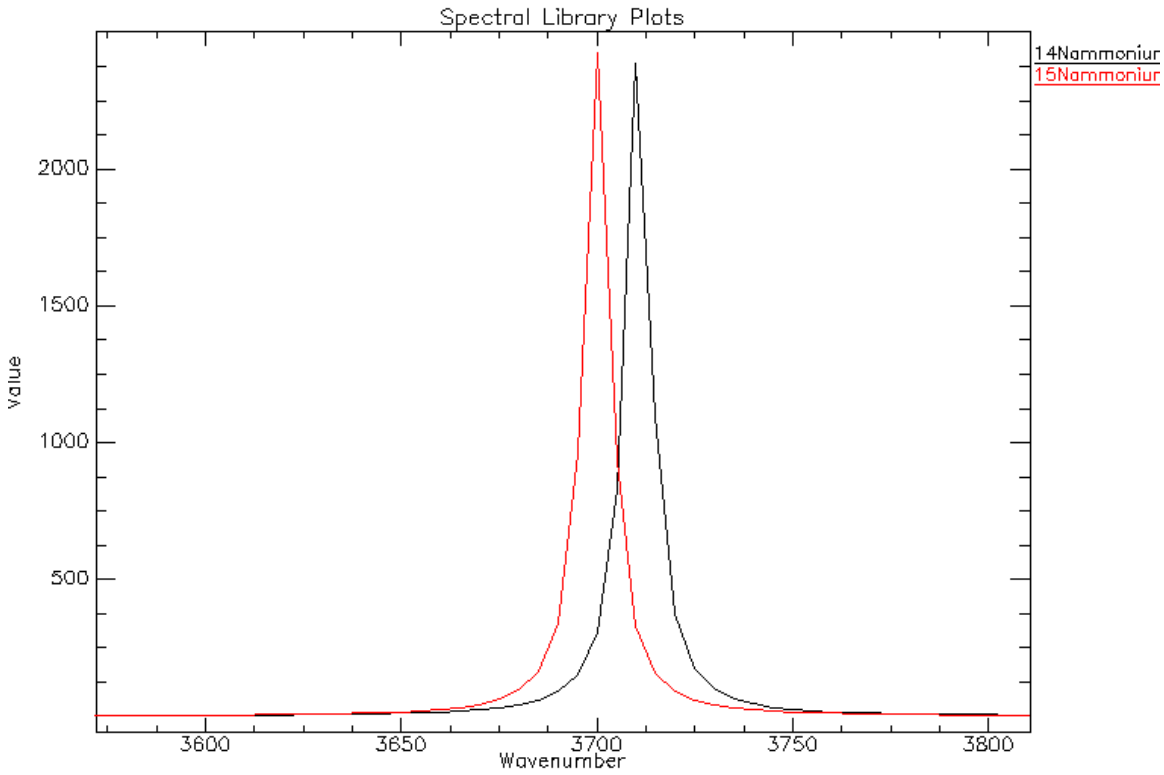

Figure 9 Shift occurring at 3,700 cm^{-1}, ^{14}N (in black) and ^{15}N (in red) in the ammonium modeled spectra

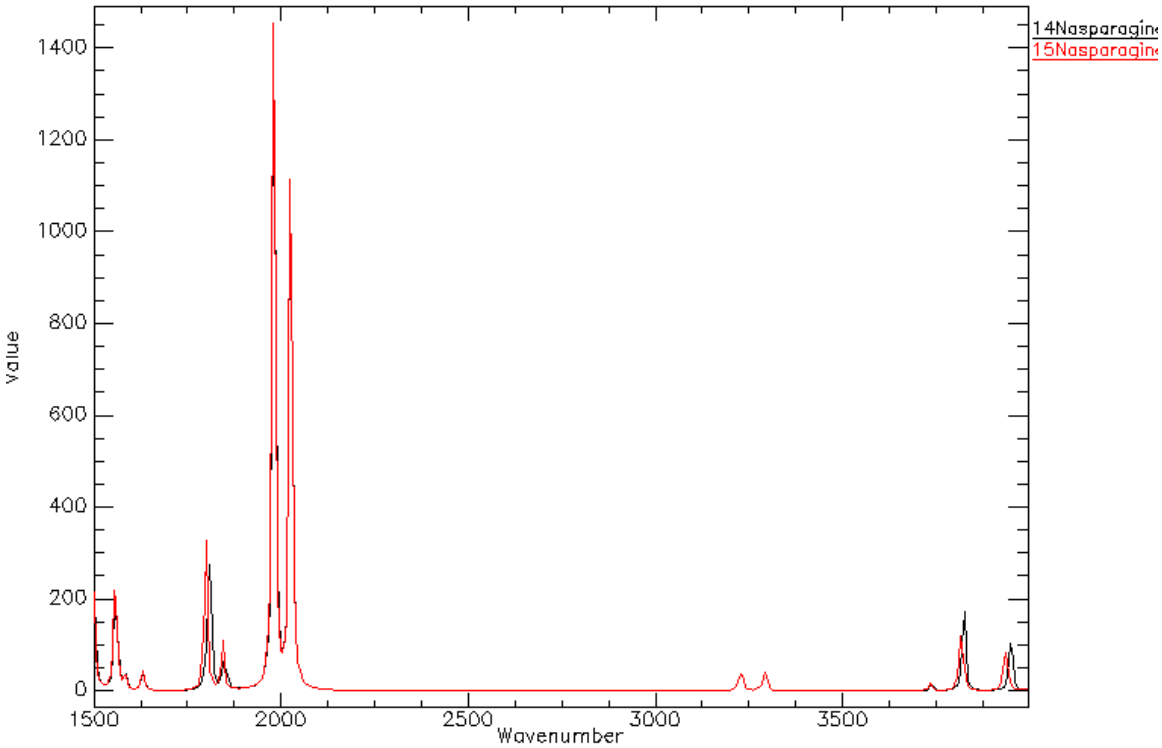

Figure 10 Modeled spectra of asparagine, ^{14}N (in black) and ^{15}N (in red) shown at full spectral resolution

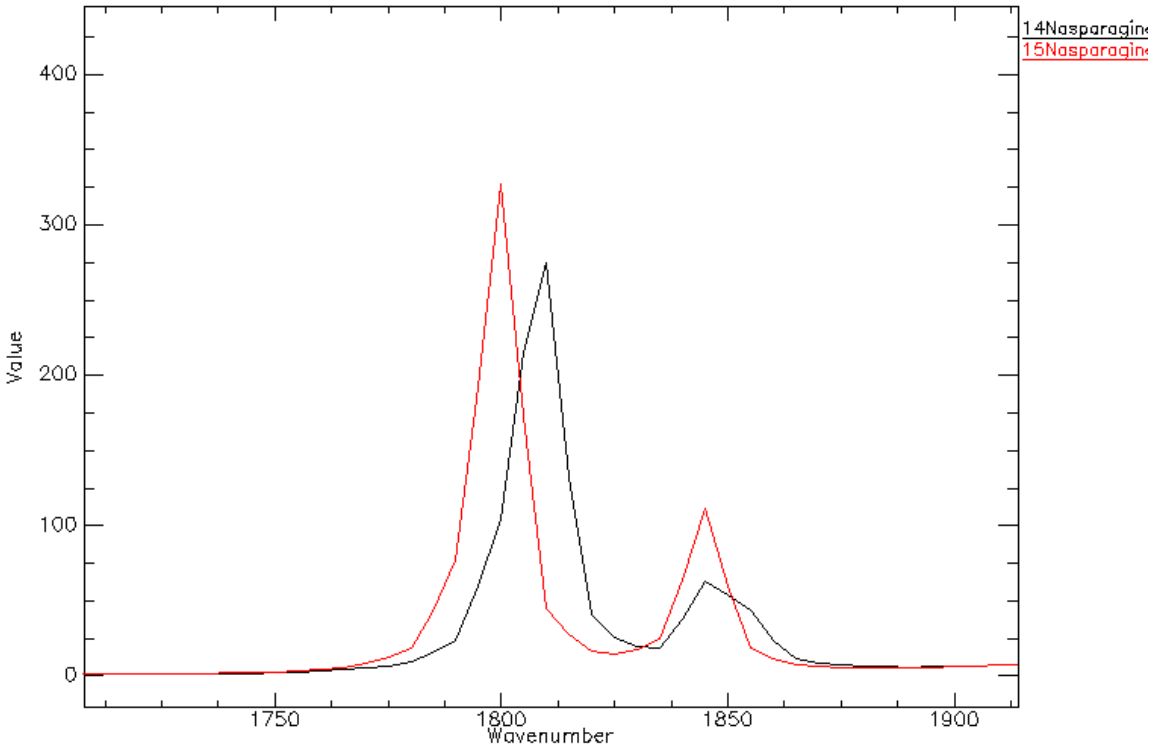

Figure 11 Shift occurring at 1,800 cm^{-1}, ^{14}N (in black) and ^{15}N (in red) in the asparagine modeled spectra

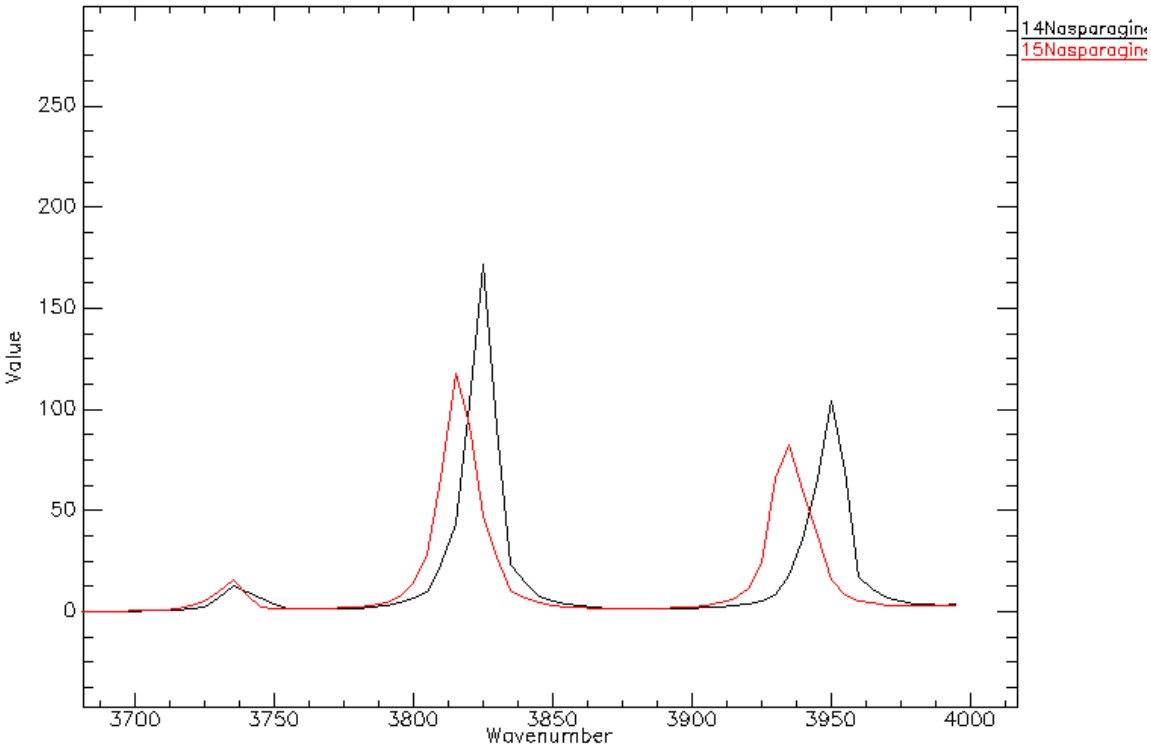

Figure 12 Shifts occurring at 3,735 cm^{-1}, 3,815 cm^{-1} and 3,935 cm^{-1}, ^{14}N (in black) and ^{15}N (in red) in the asparagine modeled spectra

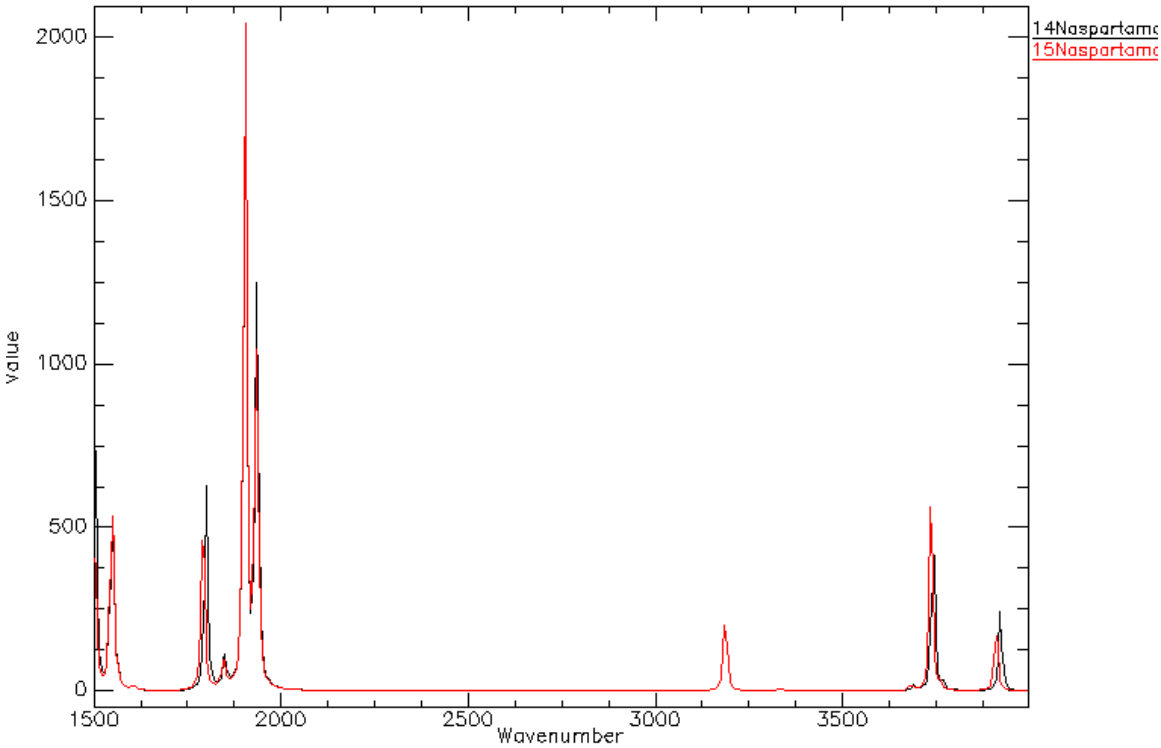

Figure 13 Modeled spectra of ^{14}N (in black) and ^{15}N (in red) aspartame shown at full spectral resolution

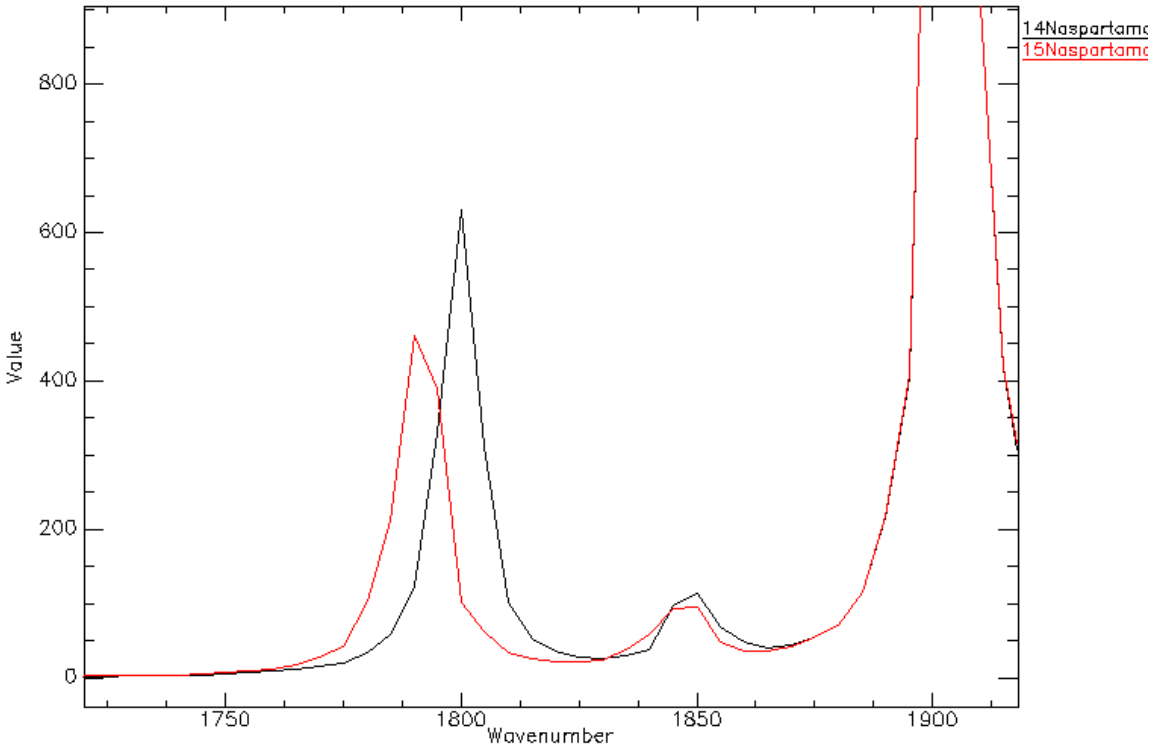

Figure 14 Shift occurring at 1,790 cm^{-1}, ^{14}N (in black) and ^{15}N (in red) in the aspartame modeled spectra

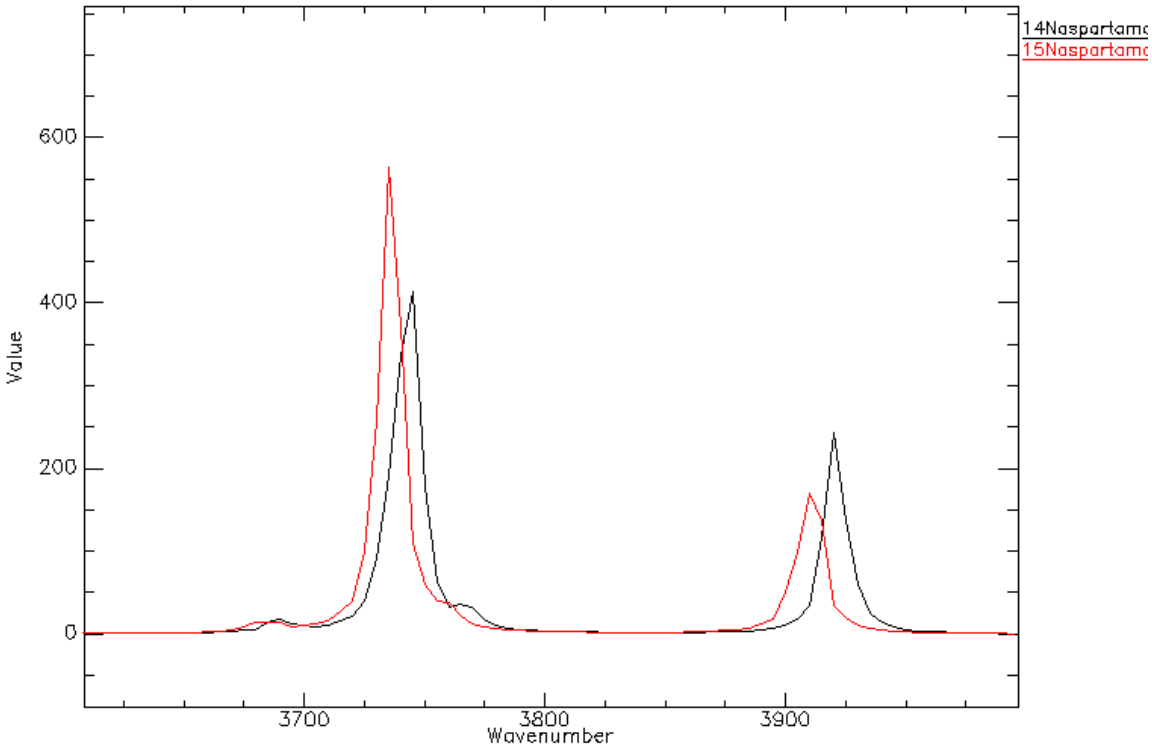

Figure 15 Shifts occurring at 3,735 cm^{-1} and 3,910 cm^{-1}, ^{14}N (in black) and ^{15}N (in red) in the aspartame modeled spectra

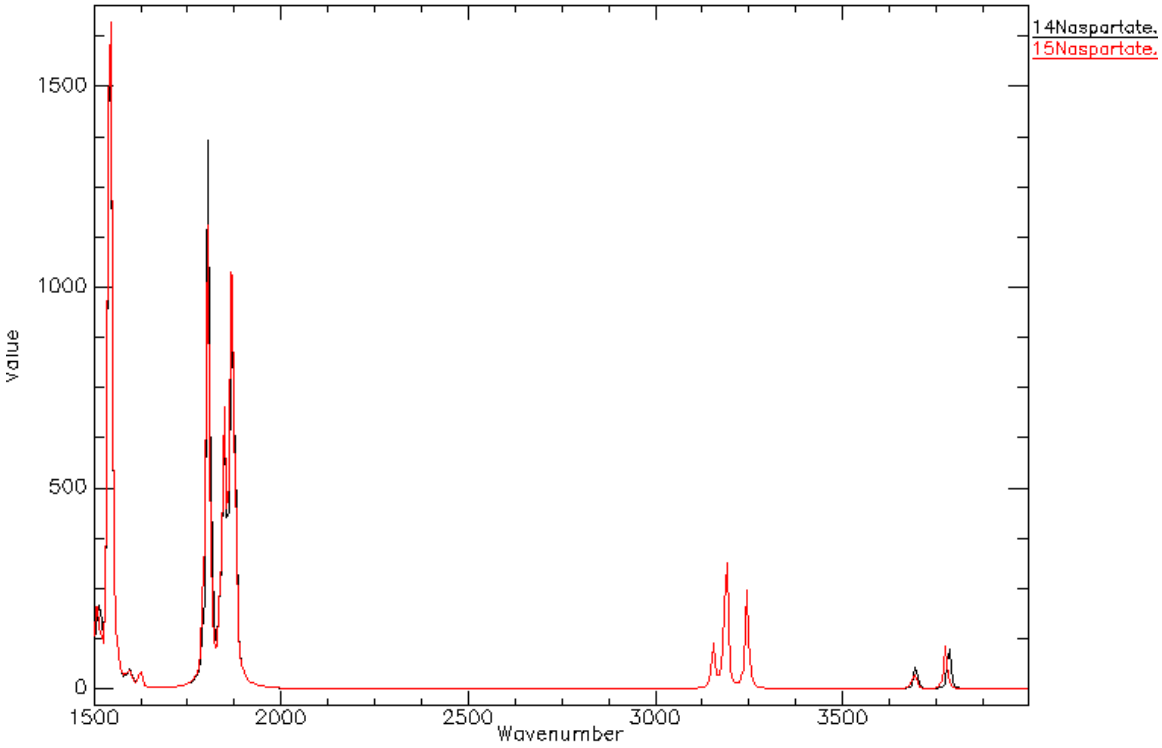

Figure 16 Modeled spectra of ^{14}N (in black) and ^{15}N (in red) aspartate shown in full spectral resolution.

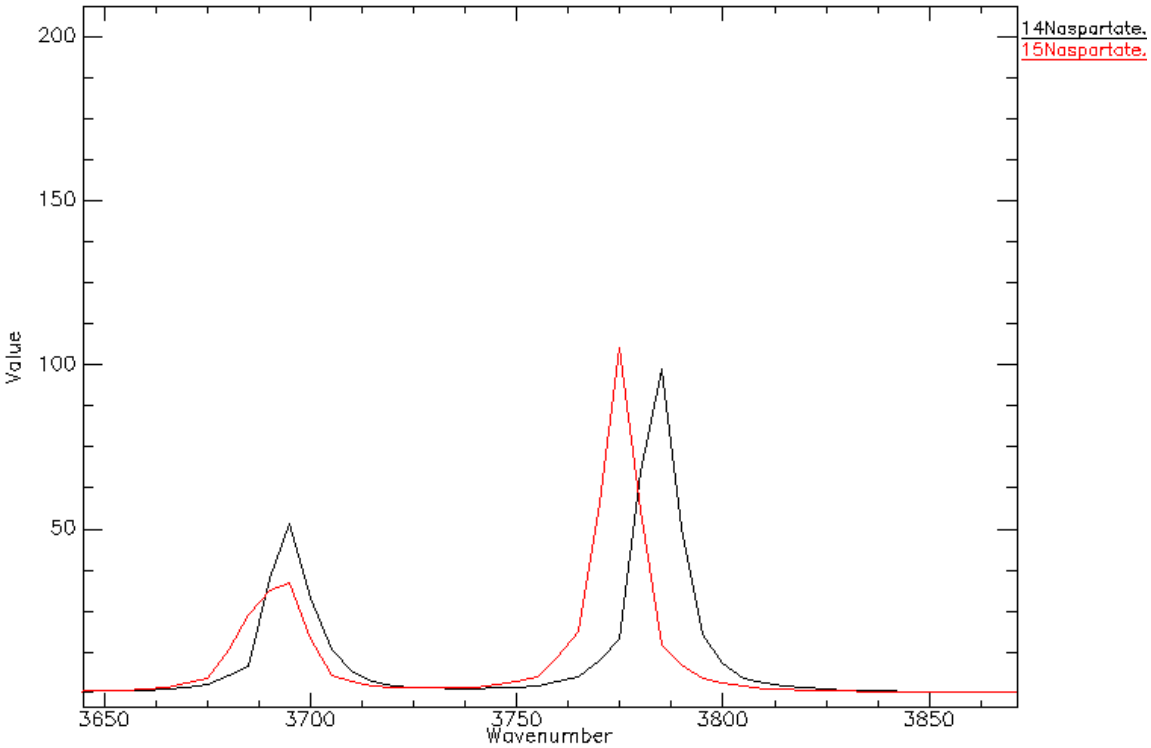

Figure 17 Shift occurring at 3,775 cm^{-1}, ^{14}N (in black) and ^{15}N (in red) in the aspartate modeled spectra

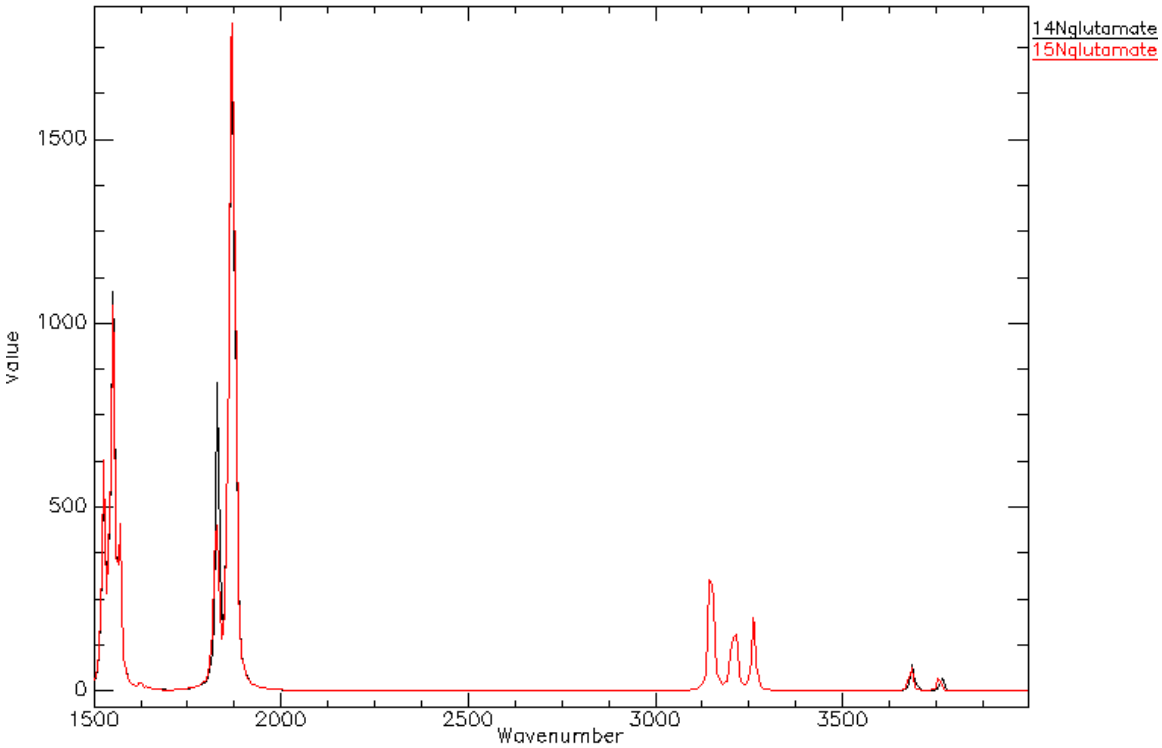

Figure 18 Modeled spectra of ^{14}N (in black) and ^{15}N (in red) glutamate shown at full spectral resolution

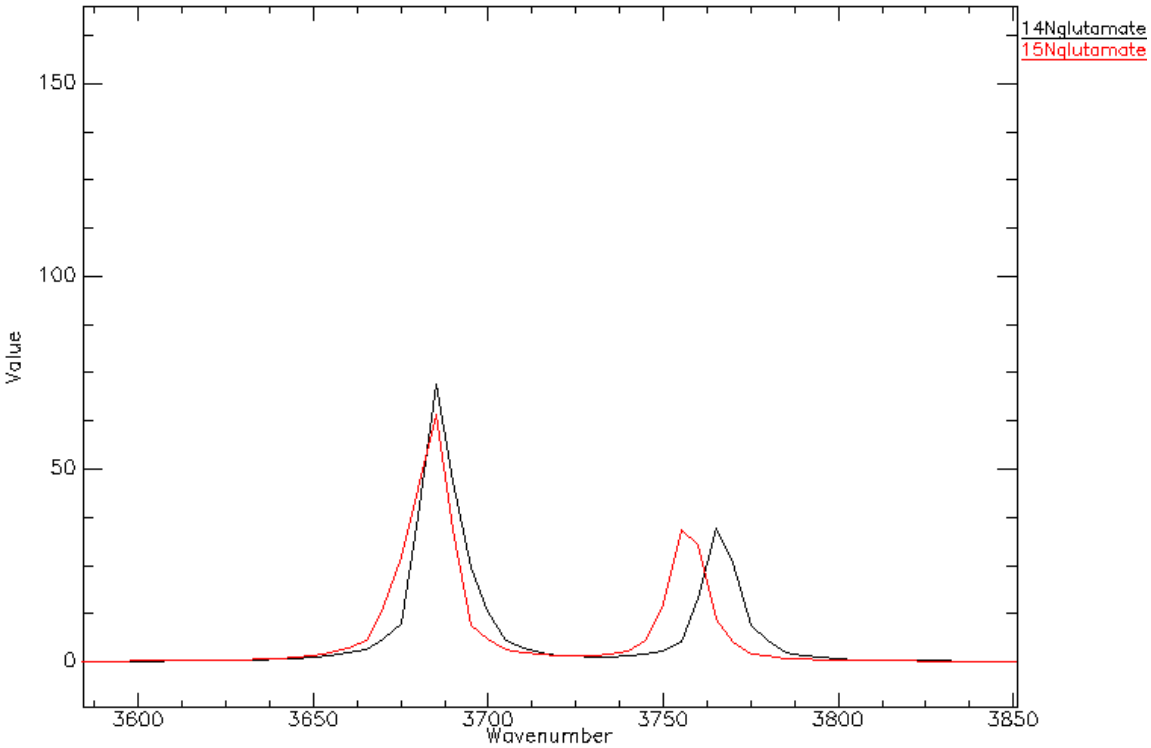

Figure 19 Shift occurring at 3,755 cm^{-1}, ^{14}N (in black) and ^{15}N (in red) in the glutamate modeled spectra.

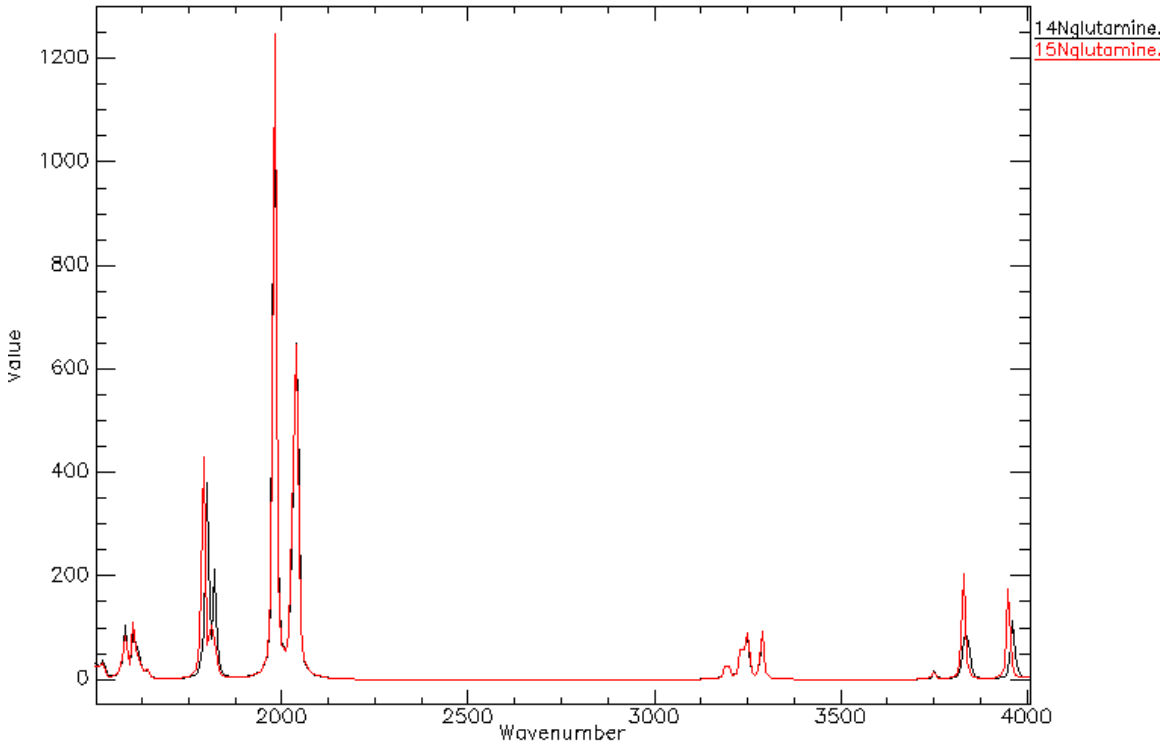

Figure 20 Modeled spectra of ^{14}N (in black) and ^{15}N (in red) glutamine shown at full spectral resolution.

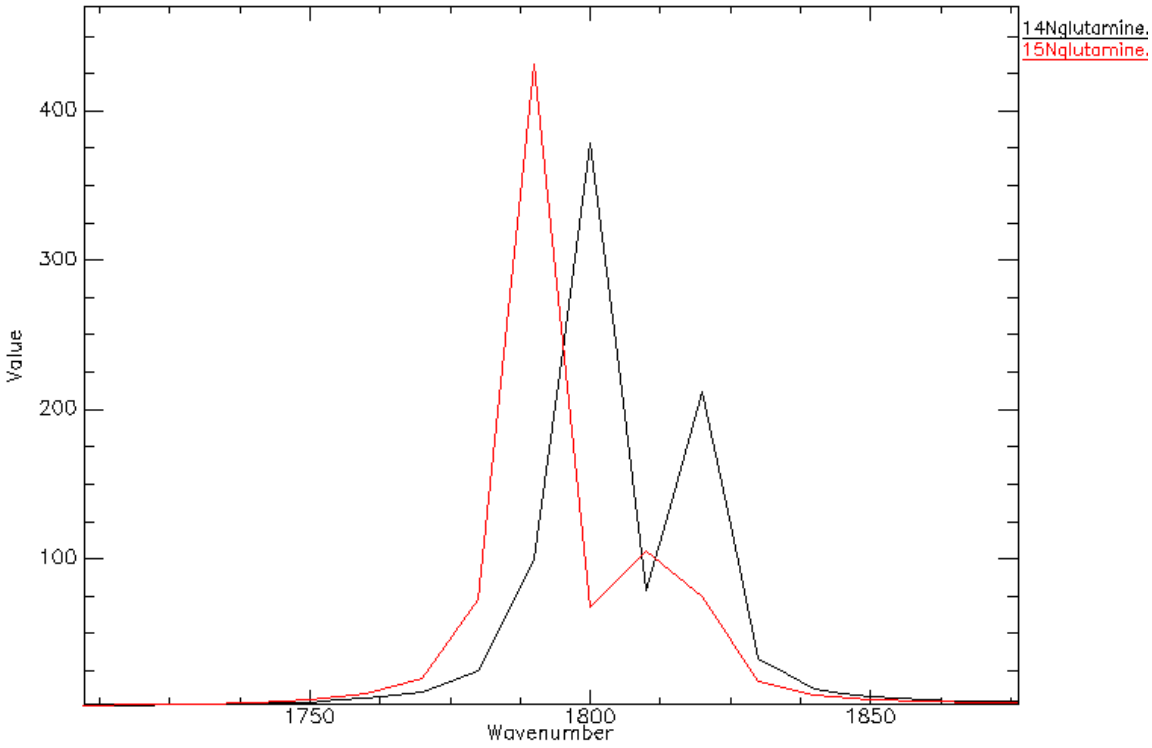

Figure 21 Shifts occurring at 1,790 $cm^{-1}$and 1,810 cm^{-1}, ^{14}N (in black) and ^{15}N (in red) in the glutamine modeled spectra

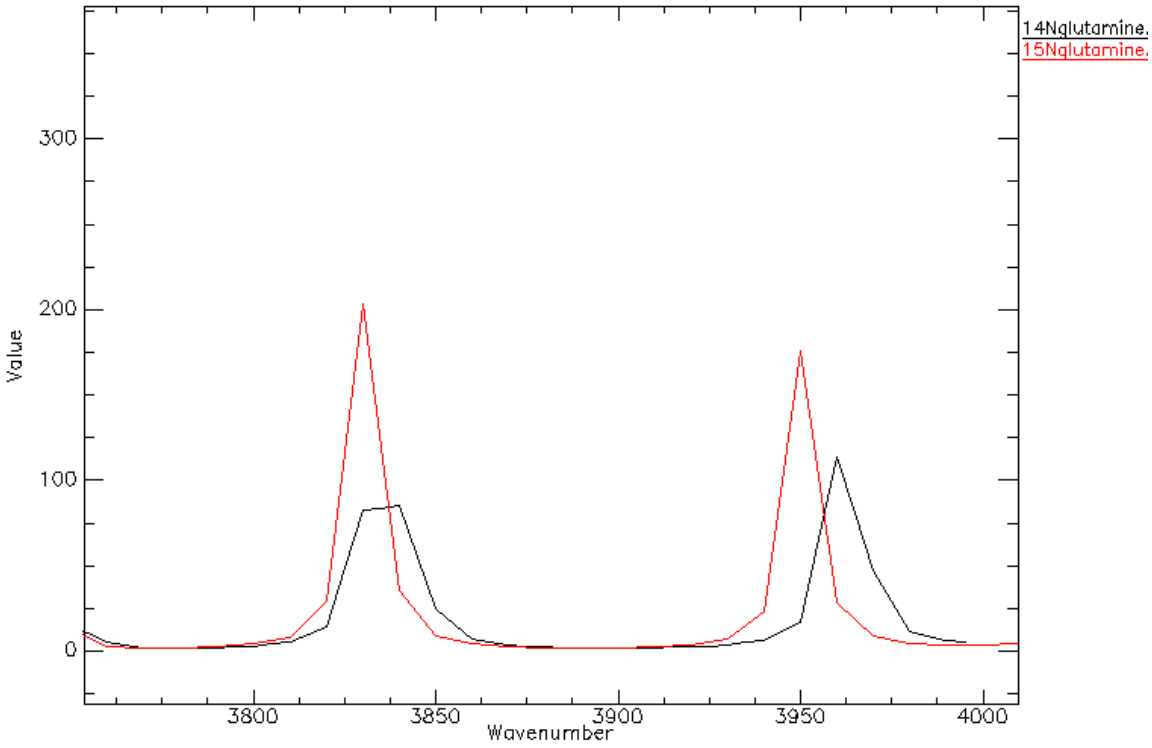

Figure 22 Shifts occurring at 3,830 cm^{-1} and 3,950 cm^{-1}, ^{14}N (in black) and ^{15}N (in red) in the glutamine modeled spectra

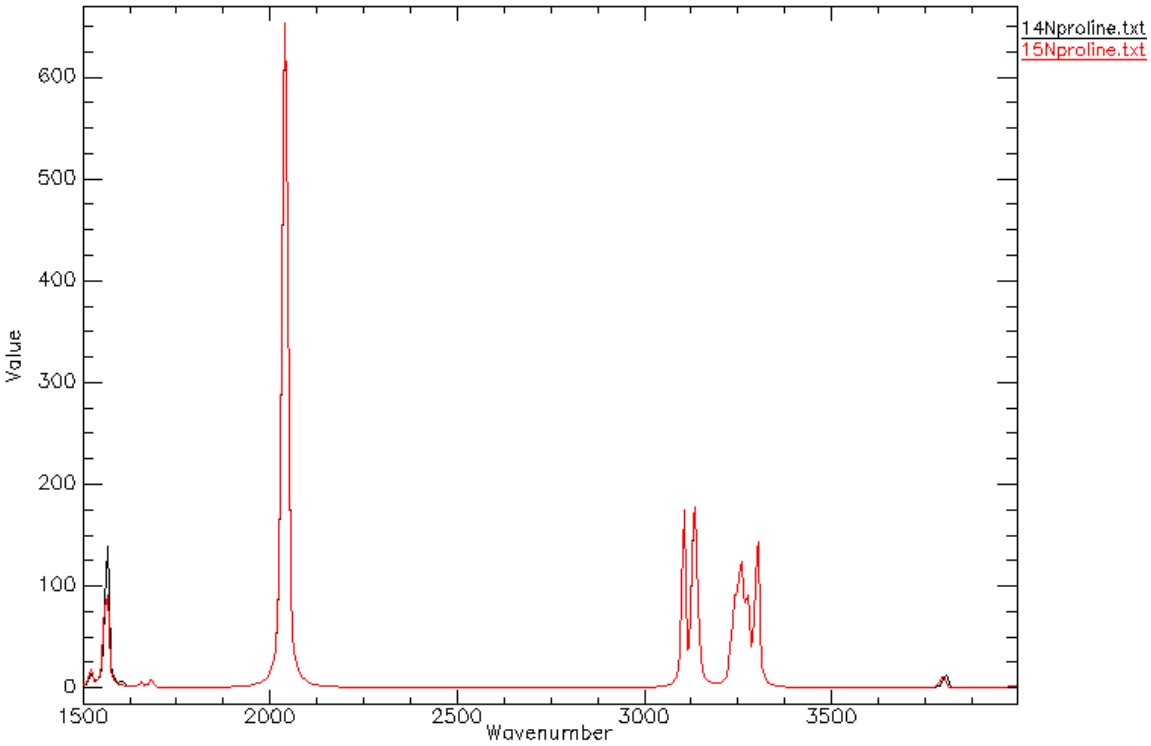

Figure 23 Modeled spectra of ^{14}N (in black) and ^{15}N (in red) proline shown at full spectral resolution.

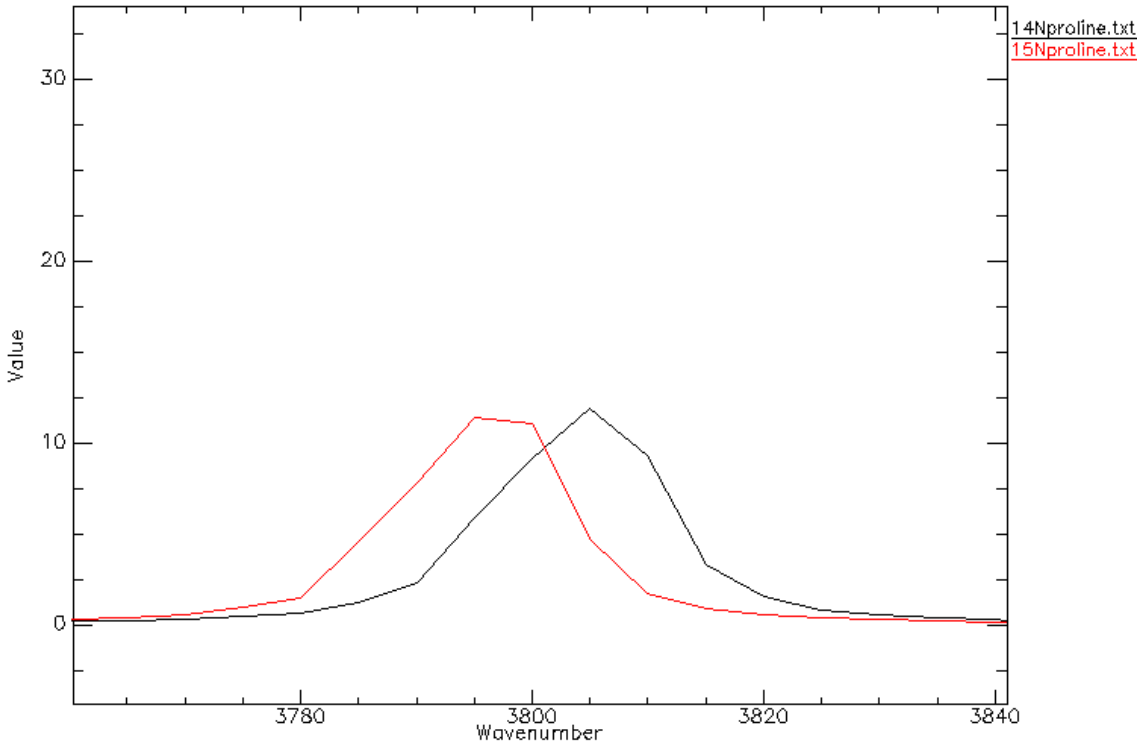

Figure 24 Shift occurring at 3,797 cm^{-1}, ^{14}N (in black) and ^{15}N (in red) in the proline modeled spectra

FTIR-ATR Spectra

The ammonium nitrate, sodium nitrate and glycine isotope labels that were used in the original enrichment experiments from Capelle and Macko (2016) were measured to identify potential wavelength shifts observable in the resulting spectra. For each, the natural abundance and the 99% ^{15}N labels of each compound were collected by the FTIR-ATR spectrometer and show clear separation of peaks and their wavenumber shifts along the spectrum (figures 25-38).

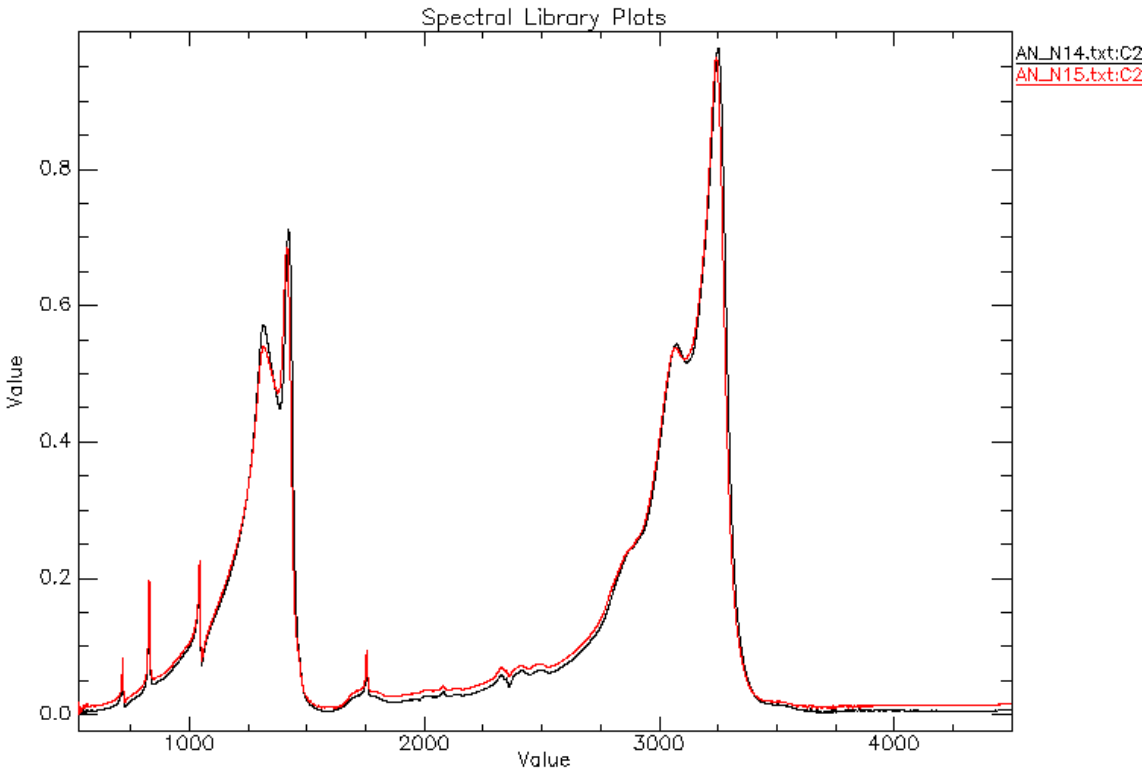

Figure 25 Natural abundance ammonium nitrate (in black) and 99% ^{15}N ammonium nitrate label (in red) shown in full FTIR-ATR spectral resolution.

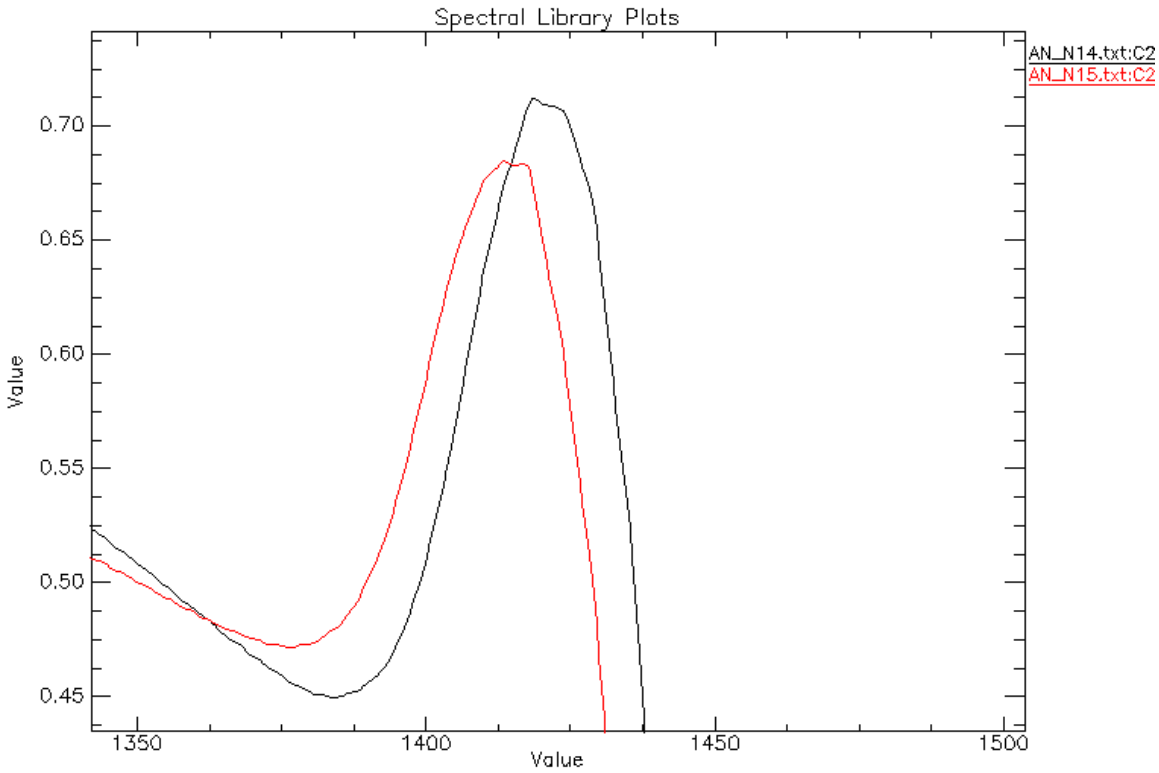

Figure 26 Shift occurring at 1,415 cm^{-1} between the natural abundance ammonium nitrate (in black) and the 99.99% ^{15}N label (in red).

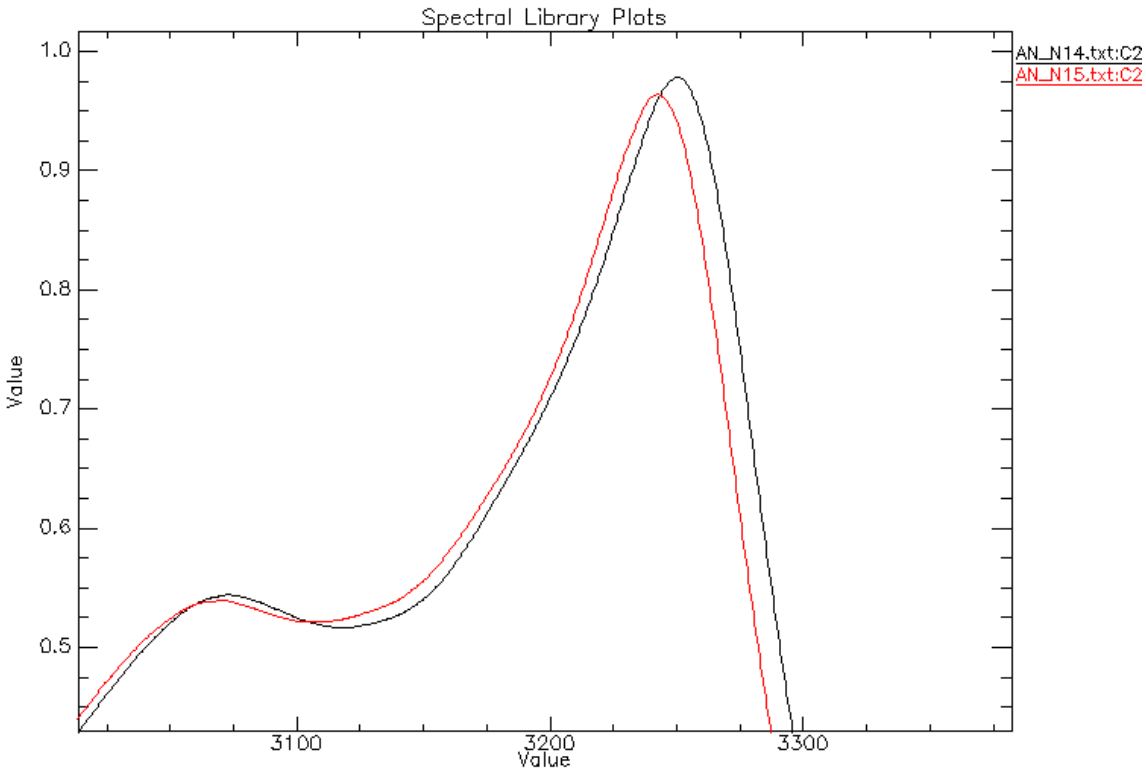

Figure 27 Shift occurring at 3,241 cm^{-1} between the natural abundance ammonium nitrate (in black) and the 99.99% ^{15}N label (in red).

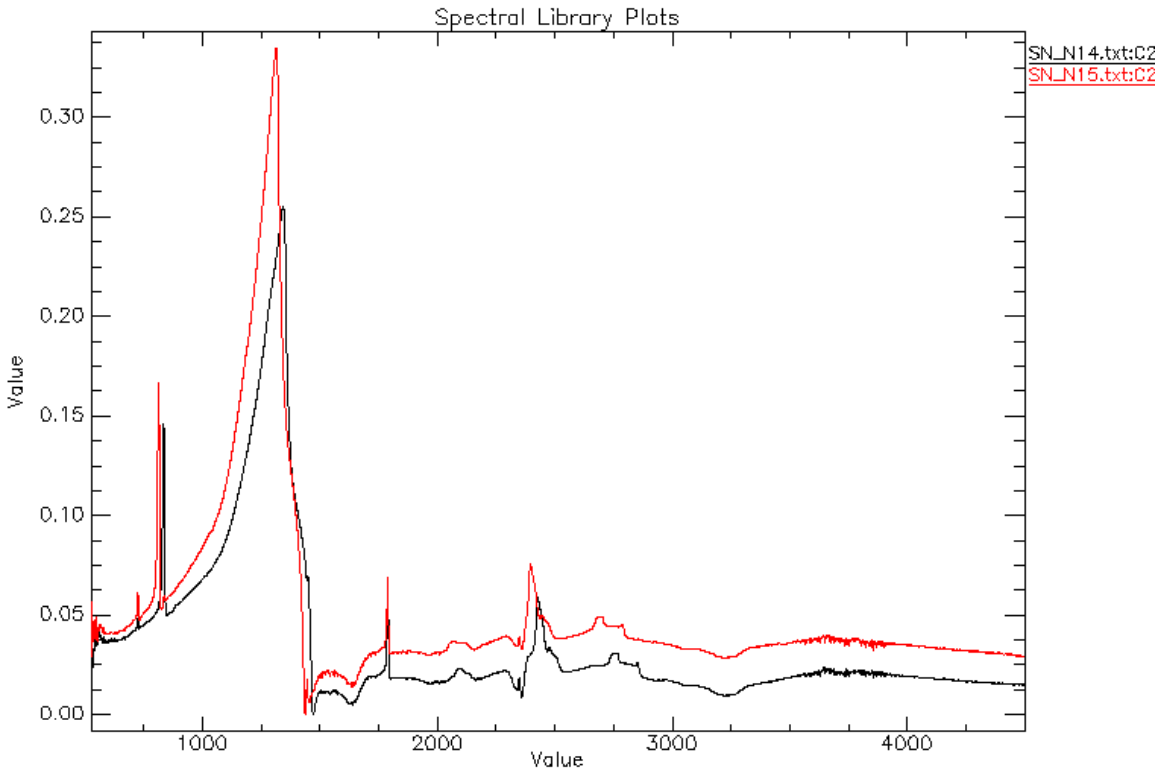

Figure 28 Natural abundance sodium nitrate (in black) and 99% ^{15}N sodium nitrate label (in red) shown at full FTIR-ATR spectral resolution.

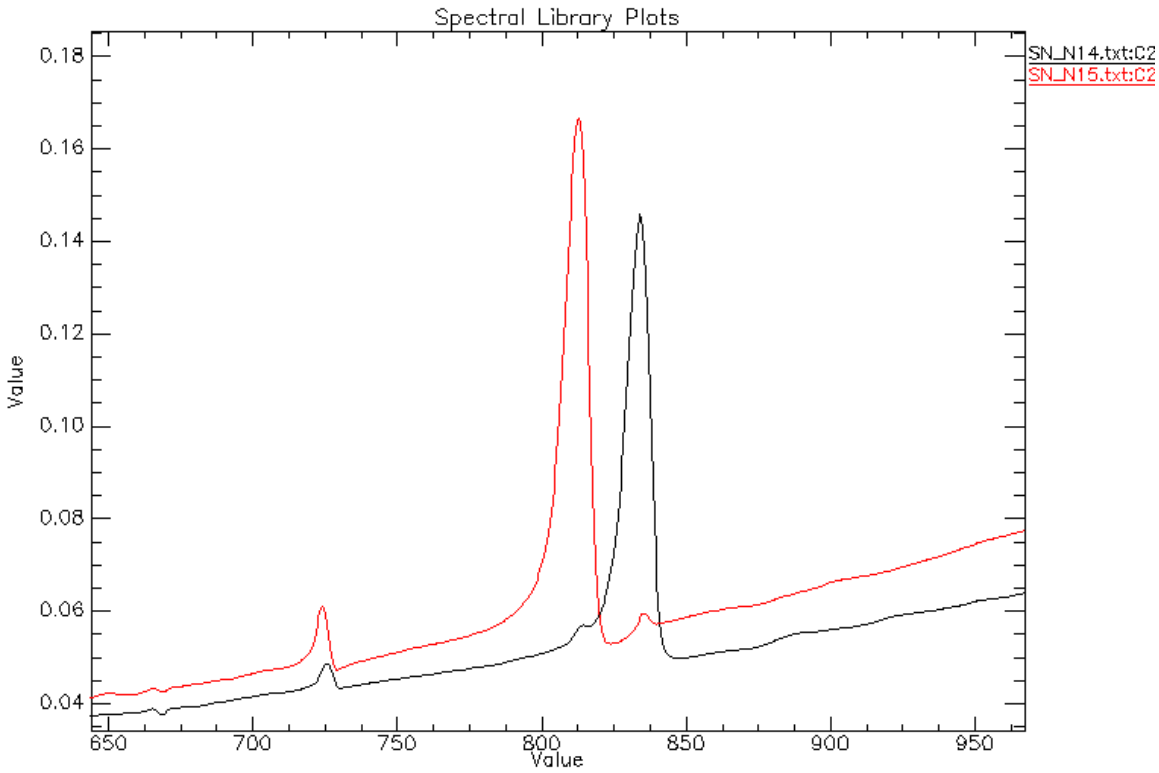

Figure 29 Shift occurring at 812 cm^{-1} between the natural abundance sodium nitrate (in black) and the 99.99% ^{15}N label (in red).

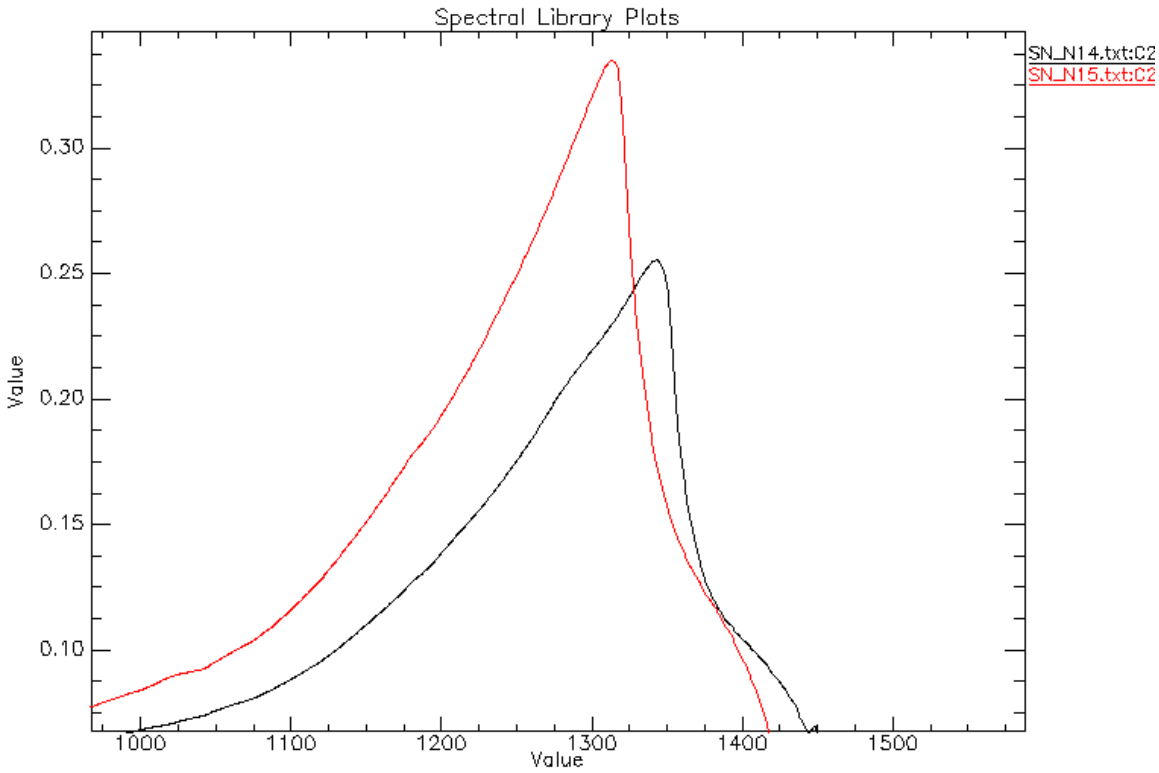

Figure 30 Shift occurring at 1,312 cm^{-1} between the natural abundance sodium nitrate (in black) and the 99.99% ^{15}N label (in red).

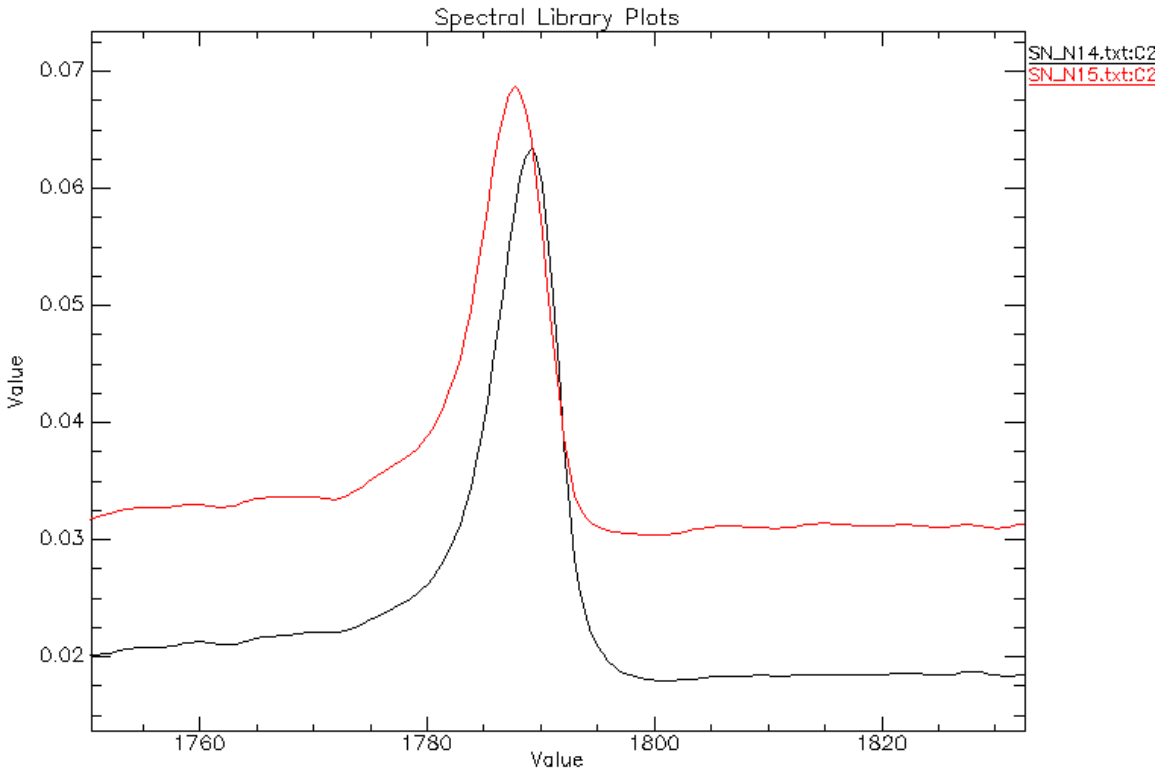

Figure 31 Shift occurring at 1,787 cm^{-1} between the natural abundance sodium nitrate (in black) and the 99.99% ^{15}N label (in red).

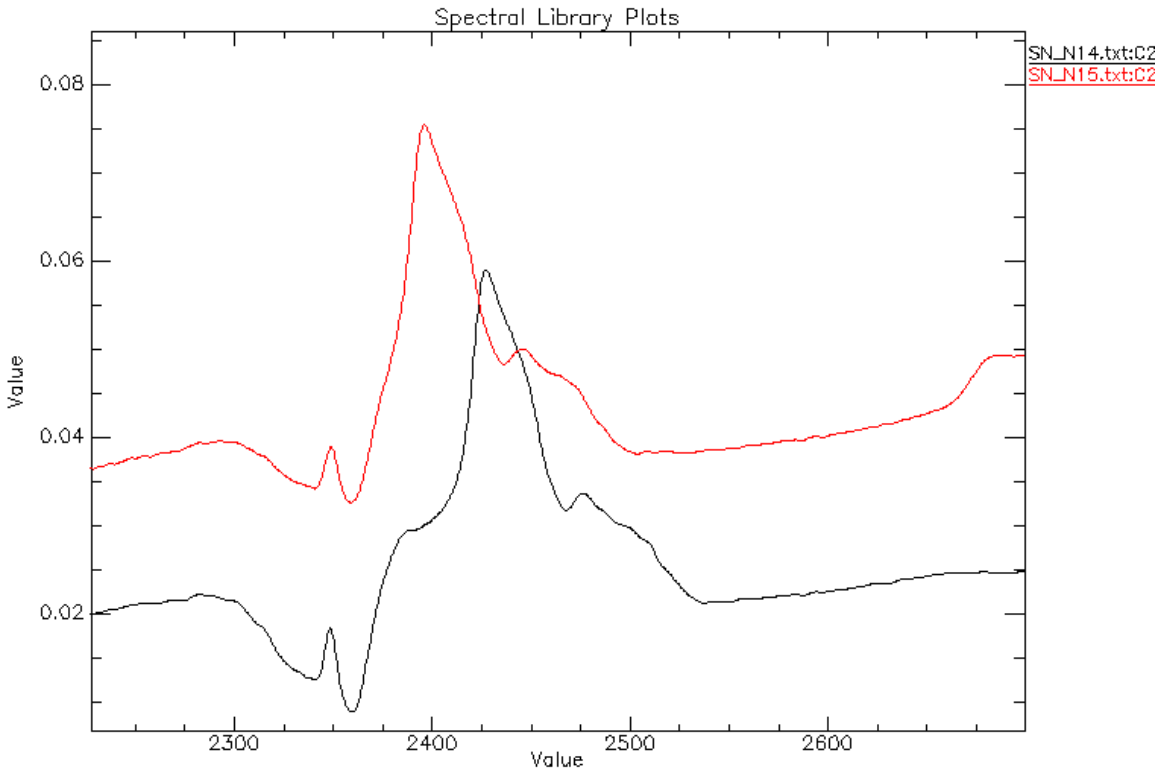

Figure 32 Shift occurring at 2,395 cm^{-1} between the natural abundance sodium nitrate (in black) and the 99.99% ^{15}N label (in red).

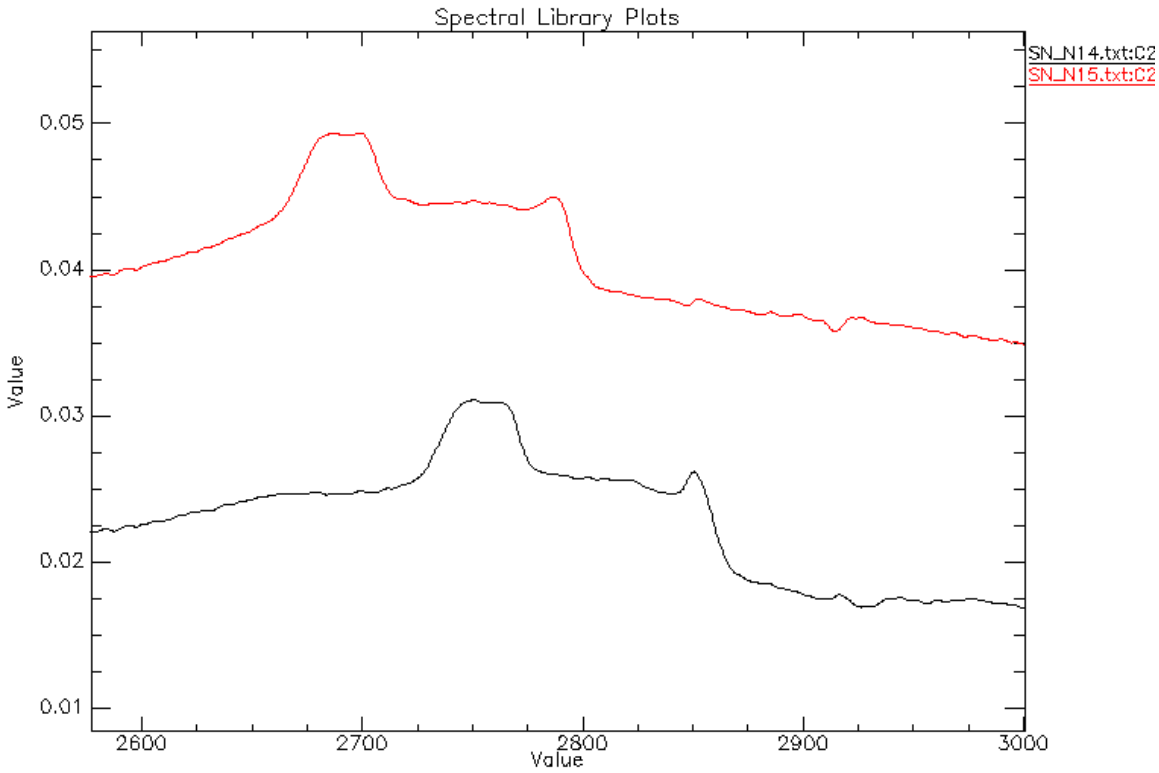

Figure 33 Shift occurring at 2,692 cm^{-1} and 2,788 cm^{-1} between the natural abundance sodium nitrate (in black) and the 99.99% ^{15}N label (in red).

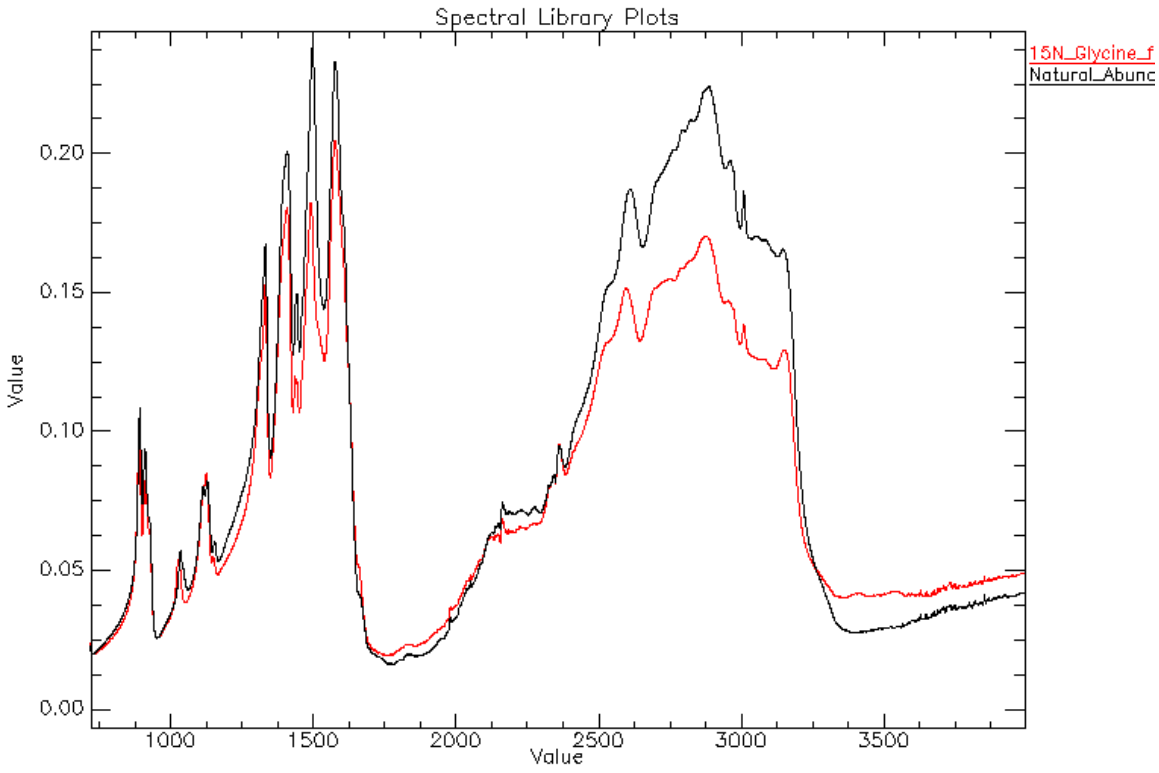

Figure 34 Glycine amino acid spectra with ^{15}N enrichment (in red) and natural abundance (in black) shown at full FTIR-ATR spectral resolution.

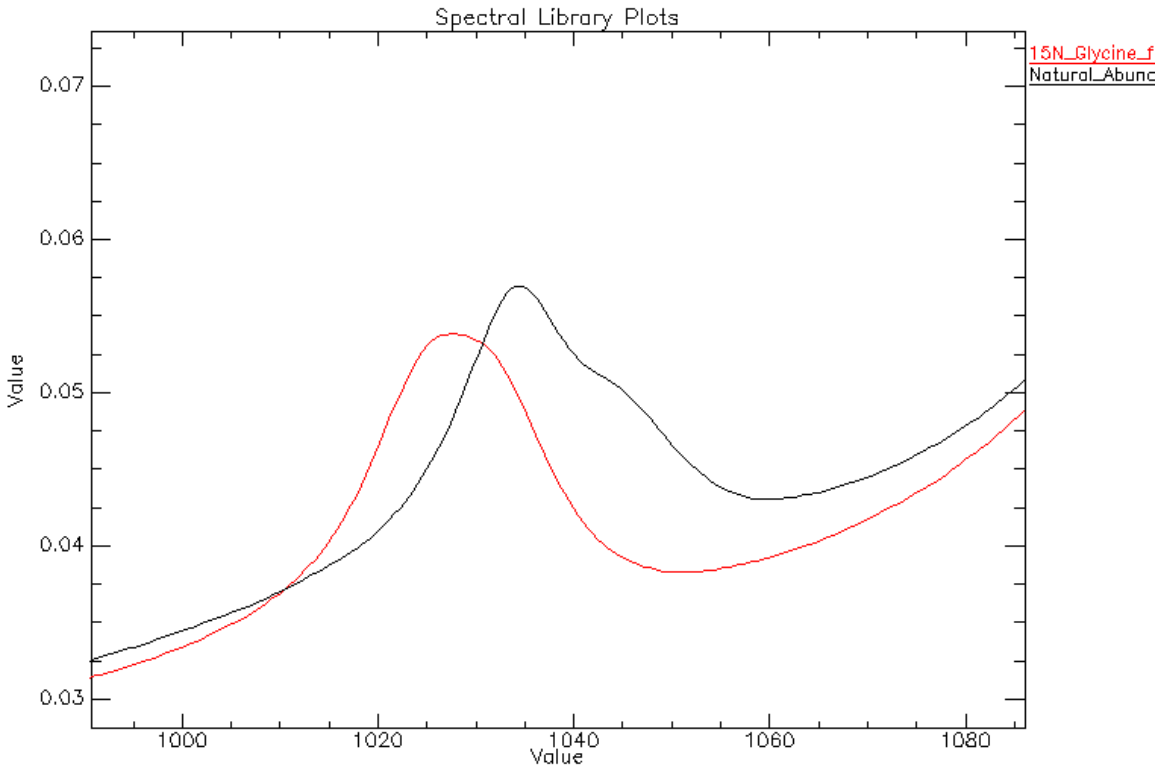

Figure 35 Shift occurring at 1,027 cm^{-1} between the natural abundance glycine (in black) and the 99.99% ^{15}N label (in red).

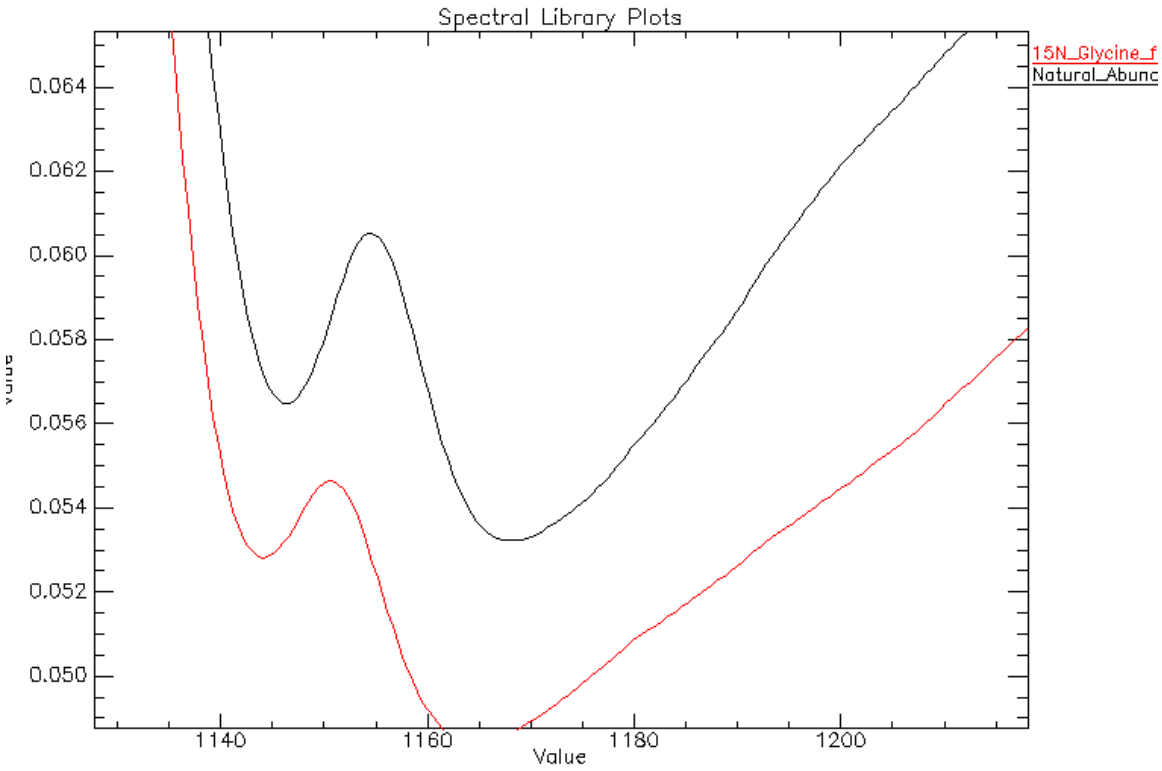

Figure 36 Shift occurring at 1,150 cm^{-1} between the natural abundance glycine (in black) and the 99.99% ^{15}N label (in red).

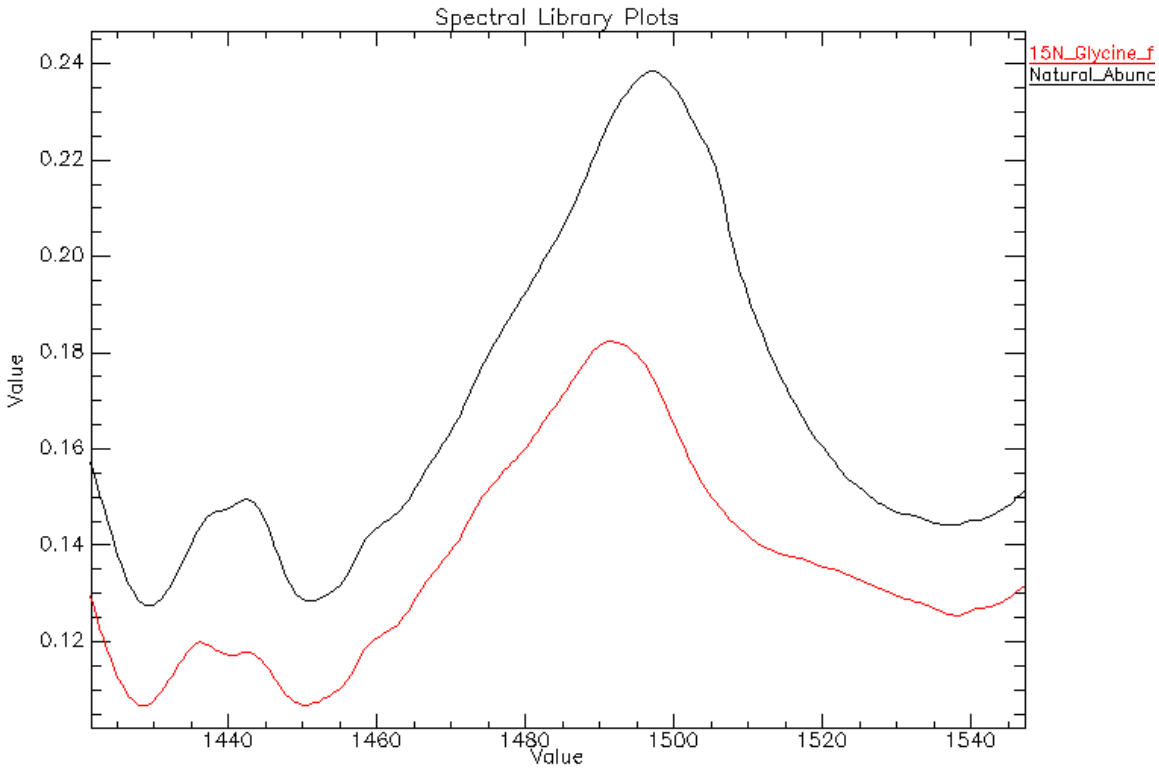

Figure 37 Shift occurring at 1,435 $cm^{-1}$and 1,492 cm^{-1} between the natural abundance glycine (in black) and the 99.99% ^{15}N label (in red).

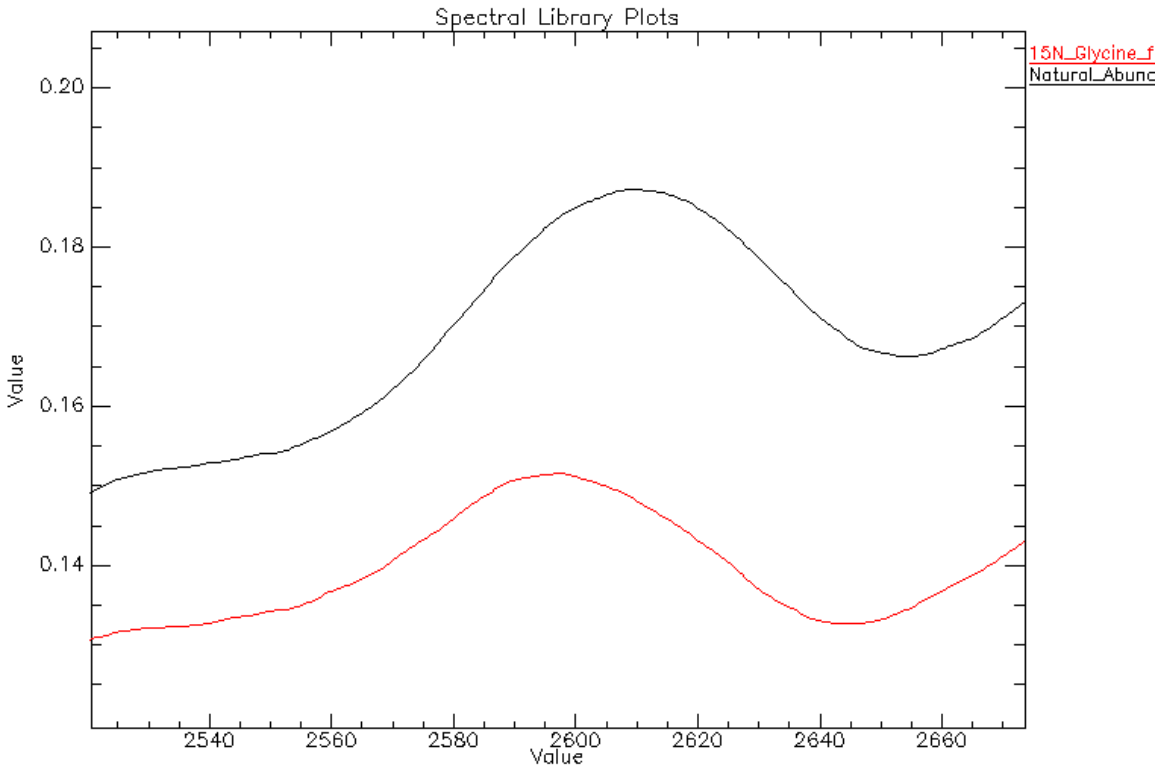

Figure 38 Shift occurring at 2,595 cm^{-1} between the natural abundance glycine (in black) and the 99.99% ^{15}N label (in red).

All modeled natural abundance and isotope edited nitrogen compounds along with the experimental trial averaged FTIR spectra of buckwheat are analyzed together for feature analysis (figure 39 and 40). Modeled data intensities and experimental data intensities have are scale independent and not correlated here. The positions of intensity, the wavenumber region, along the graph's x-axis are the important features to observe. The areas where the experimental data has a corresponding peak to the modeled data suggest that there is a greater abundance of the nitrogen containing plant compounds in the measured sample. Therefore the peak in the FTIR data is likely caused by that nitrogen containing compound identified in that region.

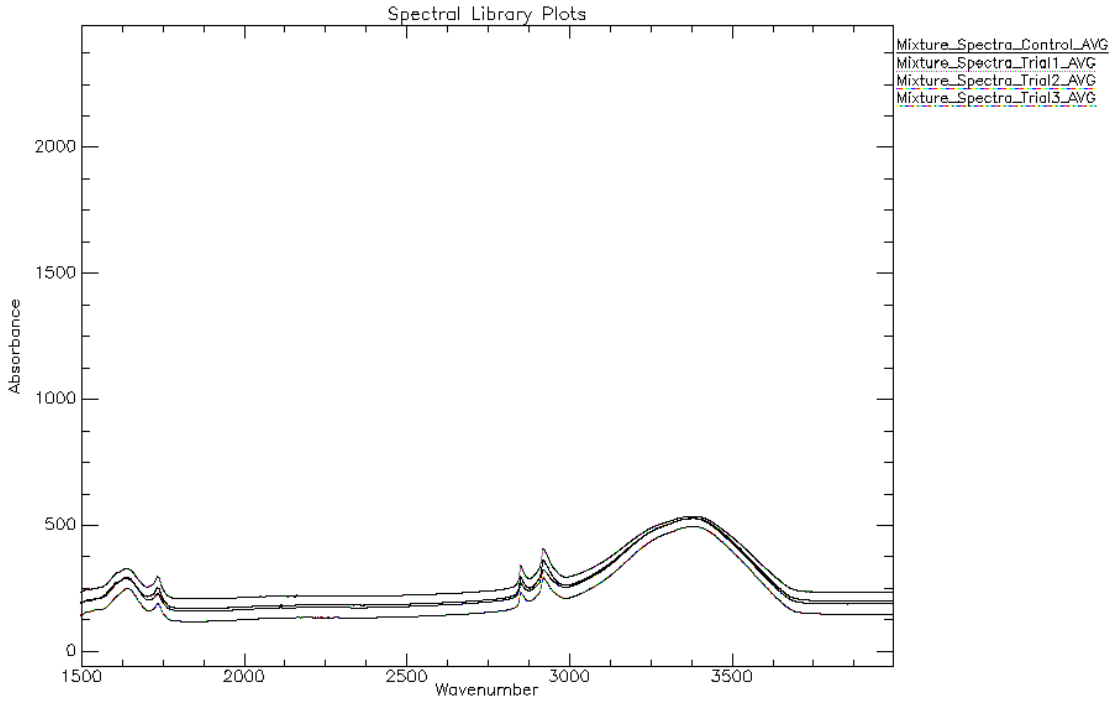

Figure 39 Part A: Nicolet FTIR-ATR Spectra of enriched buckwheat experiment that includes the spectra of the control and three experimental trials containing ^{15}N.

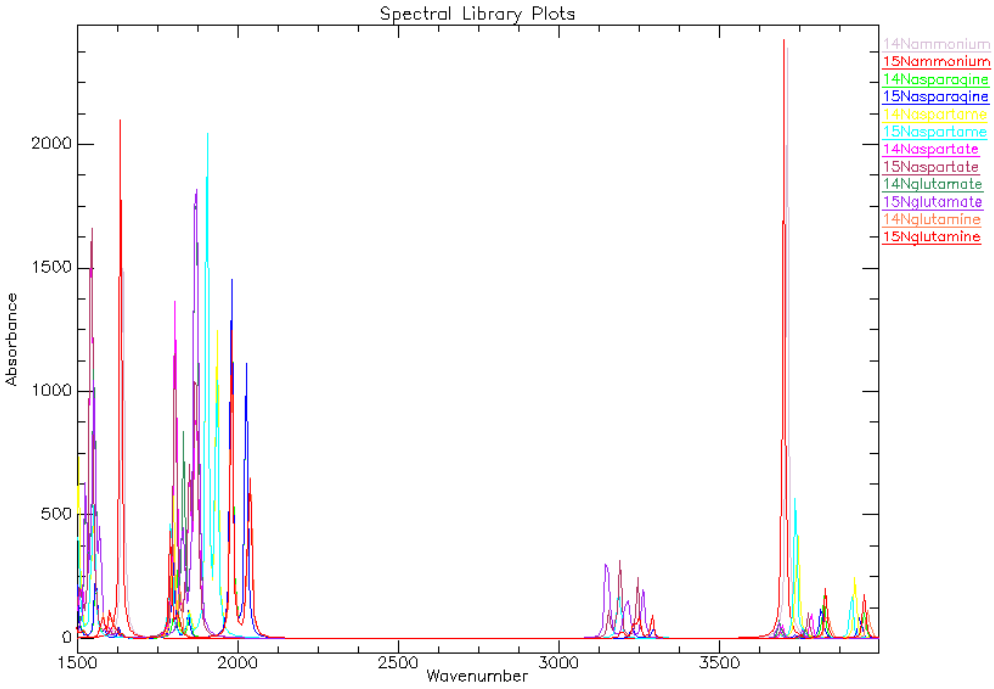

Part B: Spectra of seven nitrogen containing compounds in plants showing spectra of both ^{14}N and ^{15}N variations. Spectra were modeled using Gaussian software and plotted in ENVI for spectral signatures analysis.

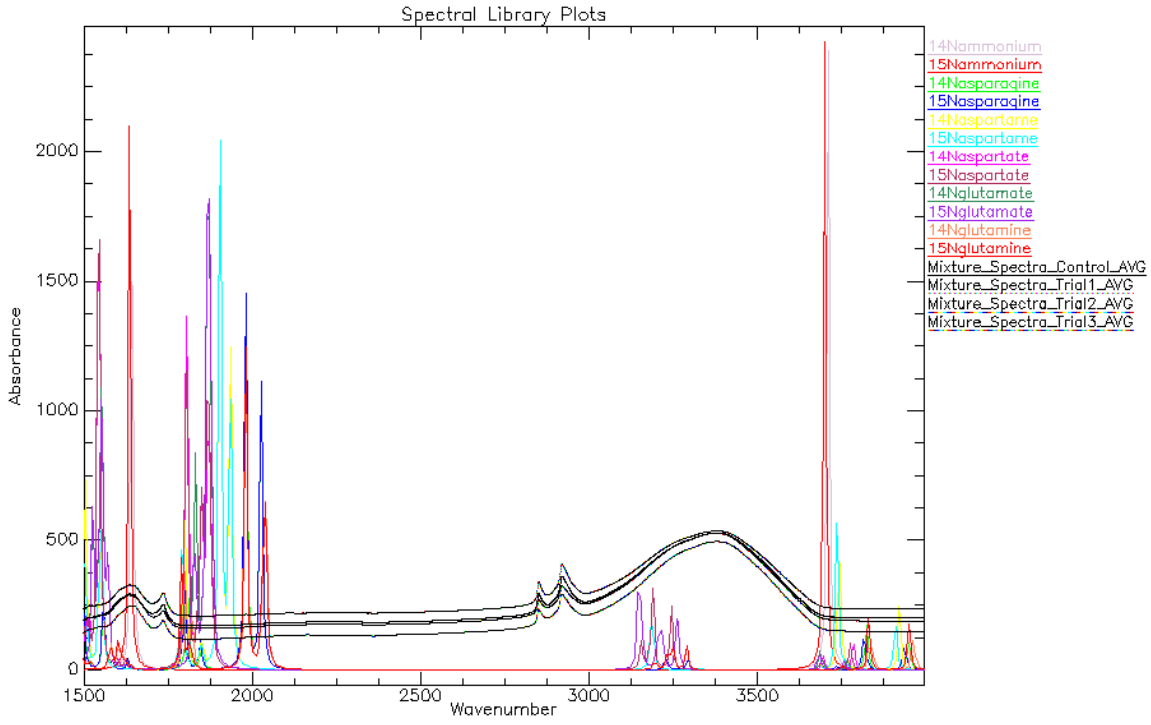

Figure 39 Part C: A plot of both the experimental FTIR-ATR spectra (in black in part a) and the modeled plant nitrogen compounds (in color in part b).

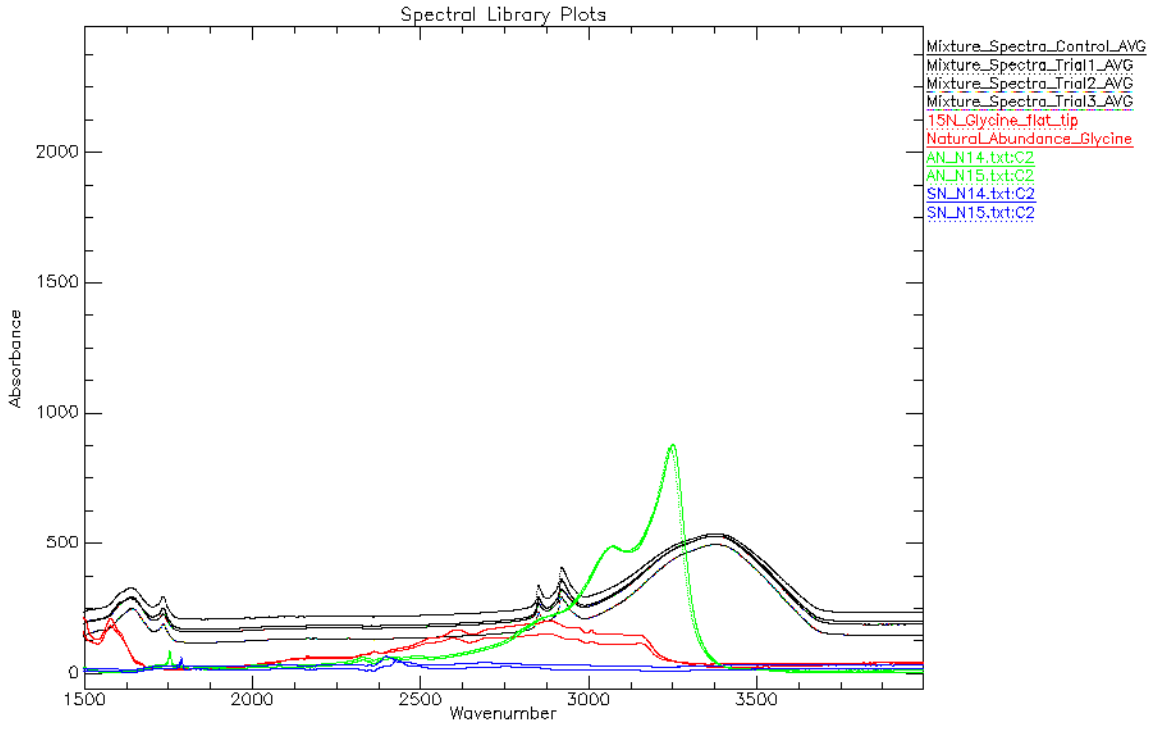

Figure 40 Overlay plot of the experimental FTIR-ATR spectra from enriched buckwheat plants (in black), glycine (in red), ammonium nitrate (in green) and sodium nitrate (in blue).

Spectral analysis of all the modeled and measured data show that only one peak position overlaps with the experimental FTIR data. This is the area centered near 1,630 cm^{-1} where there are corresponding peaks in the experimental and modeled data. The computational modeling can attribute this area to ammonium (figure 41) and confirm a frequency downshift from 1,643 cm^{-1} to 1,635 cm^{-1} when labeled with ^{15}N isotope.

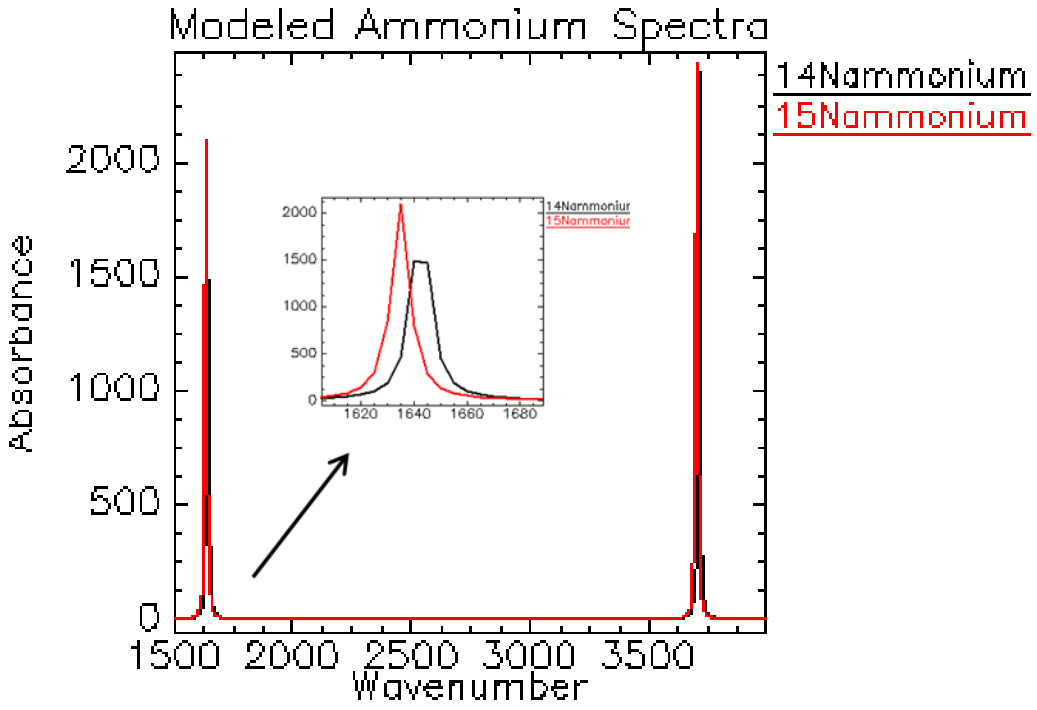

Figure 41 Gaussian modeled infrared spectra of ammonium with inset of matching wavenumber shift region occurring near 1,600 cm^{-1}

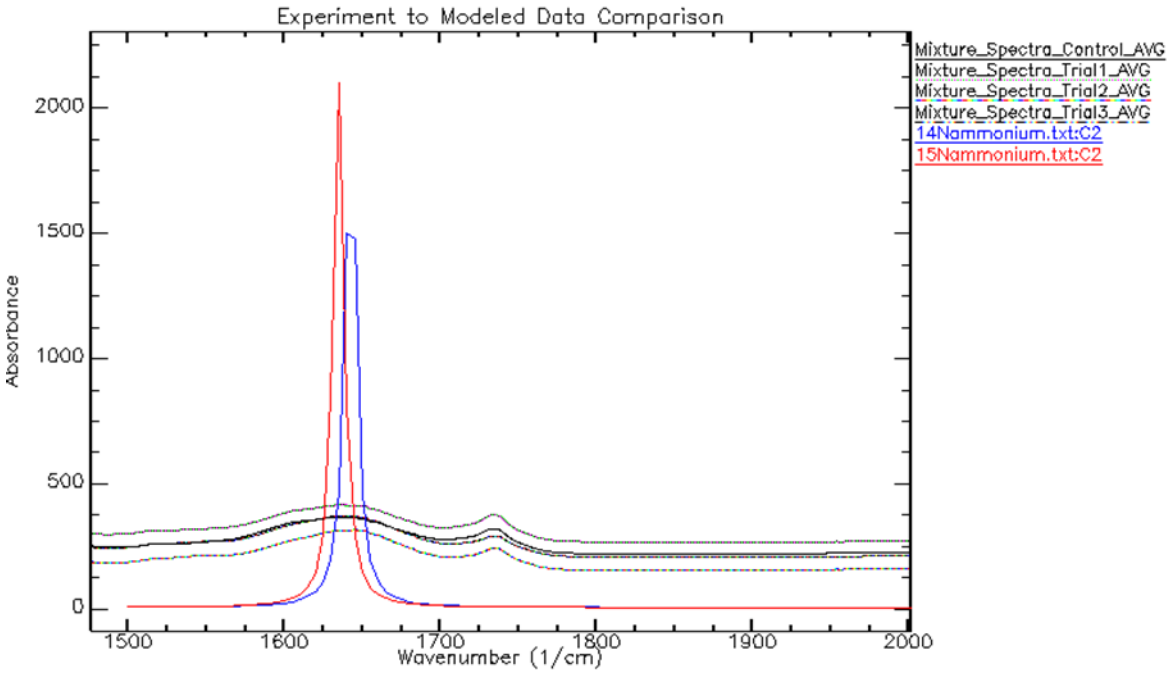

Figure 42 Modeled ^{15}N Ammonium Compound (in red) and ^{14}N (in black) overlaid with the FTIR Buckwheat Spectrum from Capelle and Macko (2016).

The region near 1,600 cm^{-1} is consistent with the amine/amide/imine chemical functional group absorption regions reported previously (Capelle & Macko, 2016). This ammonium isotope effect was observed in the Nicolet data causing a 15 wavenumber downshift from 1,634 cm^{-1} to 1,619 cm^{-1} (figure 43). This confirms and validates the isotope effect this region.

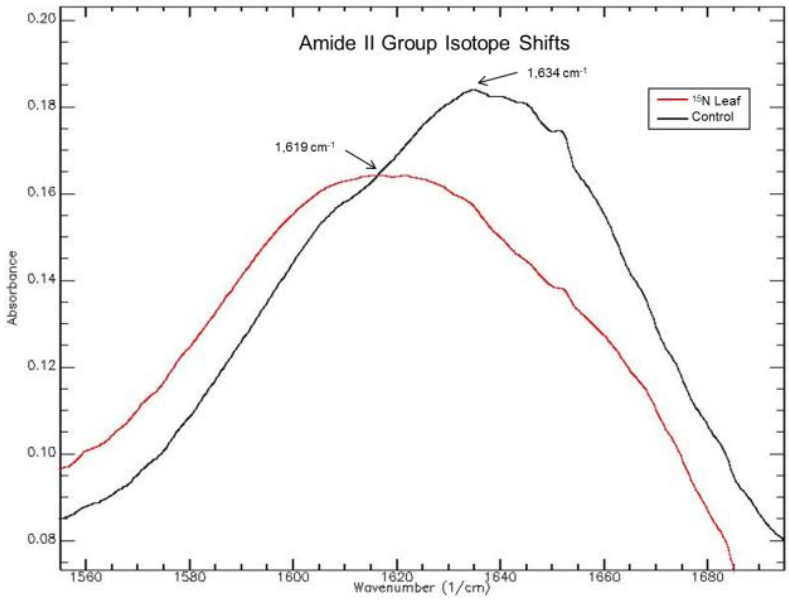

Figure 43 FTIR Measured Buckwheat Spectrum from Capelle and Macko, 2016. ^{15}N isotope labeled spectrum in red compared to natural abundance in black.

A one-tailed t-test was performed between the control and experimental trials as the shift was expected to shift in only one direction. Comparing the peak intensity value at the identified wavenumbers that corresponds to the ^{15}N and ^{14}N peaks it can be determined if the shift observed is significant (table 1). Interestingly, only the control when compared to the averaged spectra from trial two was significant.

Test	t Score	t Critical	Alpha
Control Average to Trial 1 Average	-19.91	1.65	0.05
Control Average to Trial 2 Average	22.42	1.65	0.05
Control Average to Trial 3 Average	0.63	1.65	0.05

Table 1 Ammonium region t- scores of the control and the three trials

The IRMS data from three samples of each experimental trial and the control is shown in table 2. Clearly all measured values are well above natural abundance and show contamination likely occurring from sample handling and preparation. Natural abundances for the control are 1-3 ‰, or delta ^{15}N. It is interesting to notice the other trials with higher values of %N were not statistically different. An abundance of factors can impact these results and range from IRMS contamination, FTIR instrument settings and instrument sensitivity or signal to noise.

Sample	Delta ^{15}N	%N
Control	178.1	3.29
Control	198.8	3.62
Control	164.9	3.94
Trial 1	129,238	5.53
Trial 1	119,995	6.09
Trial 1	138,210	6.34
Trial 2	76,421	7.04
Trial 2	71,546	6.97
Trial 2	71,750	6.87
Trial 3	91,650	8.75
Trial 3	94,810	8.28
Trial 3	89,784	8.22

Table 2 IRMS Results on Experimental Buckwheat Plants

Discussion

These frequency shifts represented here are not the only ones observed by all the instrumentation measured, but are strong examples or those that have direct functional group and amino acid assignments. Other nitrogen plant compounds like chlorophyll were not able to be modeled due to the complex structure and resulting computational time. The six modeled amino acids and ammonium contribute largely to peak broadening that is observed in the experimental data. Experimental data was measured directly on the

whole leaf thereby measuring all compounds within the leaf, resulting in mostly mixed vibrations that are inseparable at the instrument resolutions of 4 cm^{-1}. Ammonium vibrations however appear to be isolated to two regions, (figure 41), of which the region around 1,600 cm^{-1} is directly observed in the FTIR acquired data. The peak beyond 3,500 cm^{-1} is muted by other compounds that also vibrate at this region that are either in a greater quantity, have stronger vibrations or both. Particularly, chlorophyll was previously shown to be a dominant molecule in this region (Capelle & Macko, 2016) and likely masks the ammonium features. The fact that ammonium only vibrates in two locations within this region of the spectrum is important for quantification. The calculation complexity increases when more regions need to be analyzed. Ammonium is a small molecule and likely only has small interactions with other plant based molecules, unlike the more complex glutamine amino acid.

Performing continuum removal (figure 44), on the spectra of the FTIR experimental data in only the ammonium region (around 1,640 cm^{-1}) highlights the spectral features at 1,637 cm^{-1} and 1,642 cm^{-1} corresponding to the ammonium amino acid as validated from the computational modeling performed in this research. Two peaks can now be observed that otherwise are broadened into one wider peak using this technique. These two peaks are caused by the two variants of nitrogen, ^{14}N and ^{15}N available for plant uptake as confirmed by the modeled data. Additionally, the peaks in the FTIR data are somewhat offset from the peaks in the modeled data. The instrument resolution at 4 cm^{-1} indicates that the peak can shift within that narrow resolution window. Continuum removal not only breaks the broad peak (figure 43) into two dips or

troughs but also pinpoints the specific locations at 1637.7 cm^{-1} and 1642.5 cm^{-1} (figure 44). Note that the sensor noise is shown as the curves are not smooth.

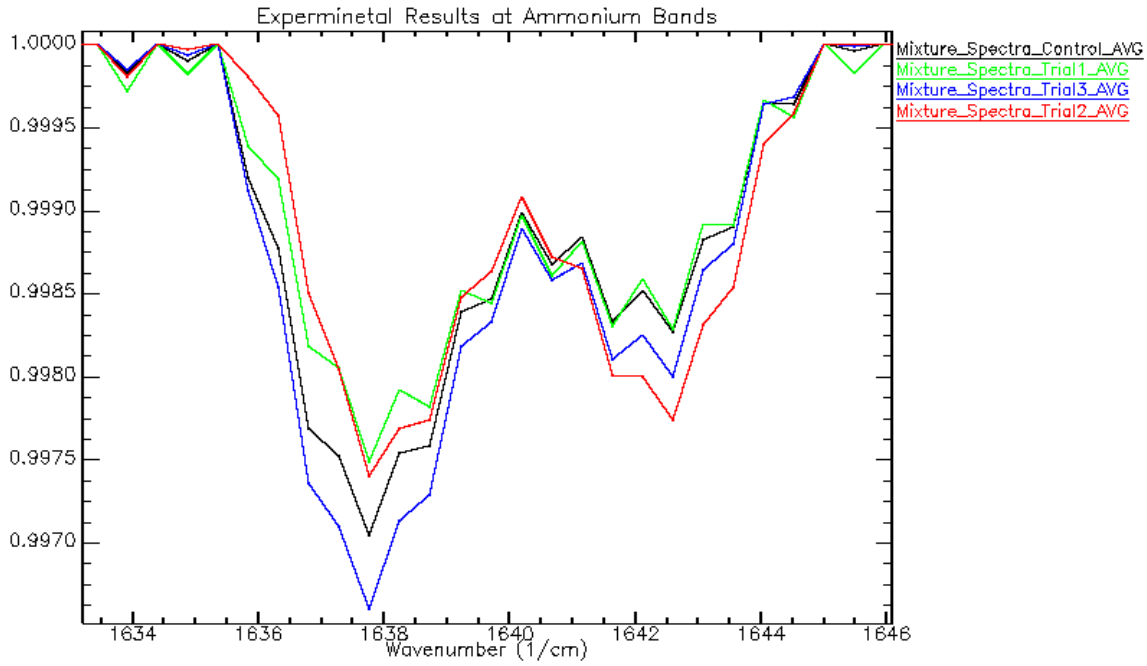

Figure 44 Continuum Removed FTIR Spectra in Ammonium Region

The data from trial three (in blue in figure 44) has a larger response in this region, indicated as a deeper trough in continuum removal. The spectral resolution of the spectrometer and scale of the graphic makes the data appear coarse. This signifies a need for increased resolution in order to more accurately detect and quantify nitrogen isotope ratios from lab based FTIR spectroscopy. With the lack of higher resolution data, the spectra can be smoothed mathematically and inverted to derive a peak value that is correlated to abundance or quantity (figure 45).

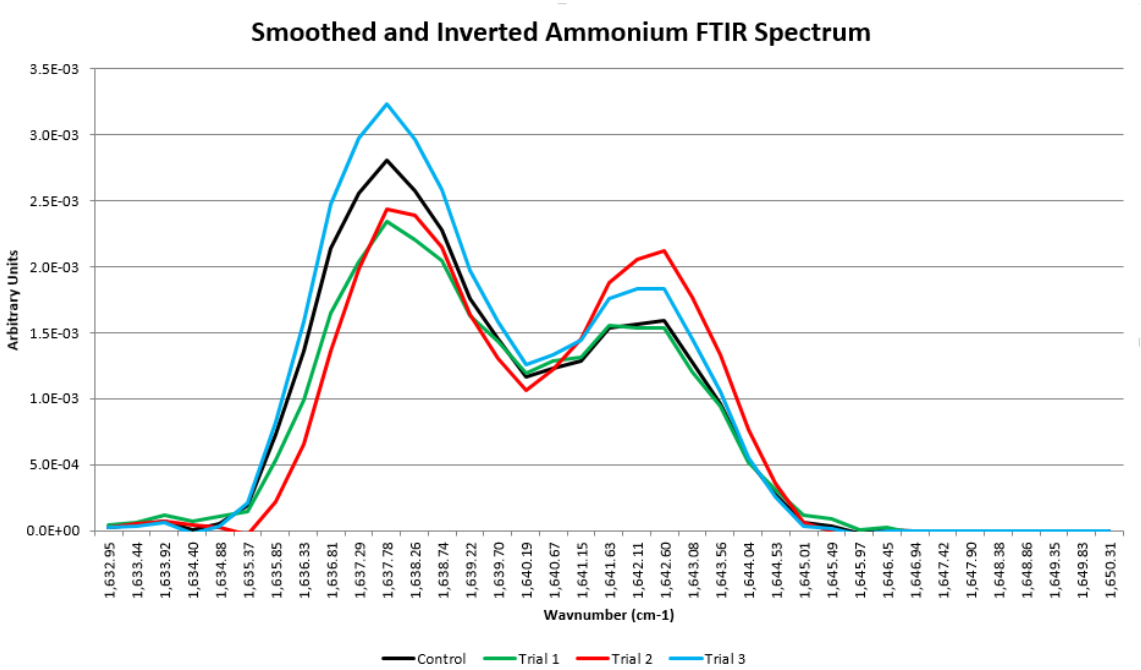

Figure 45 Smoothed and Inverted Ammonium FTIR Spectra from Capelle and Macko, 2016.

The abundance values of each nitrogen isotope are shown in table 3 along with the ratio of the FTIR value of ^{15}N to ^{14}N. This ratio cannot be compared to above IRMS measurements in table 2 without further research and measurement, specifically on samples at natural abundance levels and under conditions where no contamination has occurred.

	^{15}N Peak FTIR Value	^{14}N Peak FTIR Value	FTIR Ratio ($^{15}N/^{14}N$)
Control	0.002805429	0.001588952	0.765584486
Trial 1	0.002340095	0.001537	1.522508133
Trial 2	0.002439333	0.002118048	1.151689197
Trial 3	0.003235571	0.001836524	1.761790753

Table 3 Peak FTIR values and FTIR ratios

Conclusions

The FTIR instrumentation is proven to measure isotope effects in plant matter at large concentrations. Computational chemical modeling validated the shifts observed in experimental data specifically due to ammonium in the 1600 cm^{-1} region. The ratio of the peak values for each nitrogen variant in the ammonium region should continue to be investigated and determine its correlation to IRMS measurements. It is apparent that the current state of the art FTIR and dispersive spectrometers need advancement for detection and quantification at natural abundance levels. Refinement in signal to noise within this narrow band region would enable ultraspectral sampling of each isotope species in the infrared. Continued research and development in this topic area should occur to develop a fine tuned field based spectrometer centered on ammonium ^{15}N assimilation in plants.

Enabling isotope ratio measurements to be brought out into the field and outside of the lab would provide significant advancements in the field of geochemistry. A potential application where this technology could assist is in the research and mitigation of nitrogen based pollution in water ways. When coupled with water quality measurements, non-point source pollution areas can be identified sooner and over entire watersheds because organic based fertilizers, like manure, are more enriched in ^{15}N than traditional agricultural or Haber process fertilizers (Townsend *et al.*, 2004). As sensor development advances, future ground, airborne or space based sensors could be fielded that are tuned to the frequencies of isotope absorptions developed in this research.

References

Capelle, S. K., & Macko, S. A. (2016). Finding the spectral signature of ^{15}Nitrogen isotopes in plants by hyperspectral techniques. *Journal of Remote Sensing Technology, 4*(1), 115-120.

Coates, J. (2000). In Meyers R. A. (Ed.), *Interpretation of infrared spectra, a practical approach*. England: John Wiley & Sons Ltd.

Jones, R., Ougham, H., Thomas, H., & Waalang, S. (2013). *The molecular life of plants*. New Jersey: Wiley-Blackwell.

Quillard, S., Louam, G., Buisson, J. P., Boyer, M., Lapkowski, M., Pron, A., & Lefrant, S. (1997). Vibrational spectroscopic studies of the isotope effects in polyaniline. *Synthetic Metals, 84*(1–3), 805-806.

Shuh, H. W. (2009). Fundamentals of computational chemistry: A guide for organic chemists. Retrieved from https://www.princeton.edu/chemistry/macmillan/group-meetings/HWS_computational.pdf

Vernon, L., & Seely, G. (1966). *The chlorophylls*. New York: Academic Press Inc.

Yun, S. I., Ro, H. M., Choi, W. J., & Chang, S. X. (2006). Interactive effects of N fertilizer source and timing of fertilization leave specific N isotopic signatures in chinese cabbage and soil. *Soil Biology and Biochemistry, 38*, 1682-1689.

Chapter 4 – Development of the Infrared Nitrogen Stable Isotope Ratio

To Be Submitted

Abstract

The measurement of nitrogen stable isotope data in vegetation samples is possible through isotope-ratio mass spectrometry (IRMS). This technique is very high in accuracy and precision; however, sample preparation methods, run times and instrument calibrations are time consuming and costly. Additionally, IRMS measurements are only possible in the laboratory and sample measurements only represent data from a single location on the Earth's surface at a time. These limitations have created the desire for researchers to create an alternative method for IRMS measurements, particularly one capable of actively measuring samples in the field. This is possible through infrared spectral sensors. Isotope induced wavelength shifts are observable in lab and field based infrared spectrometers under artificially enriched nitrogen isotope conditions (Capelle & Macko, 2016). Two sets of field samples were acquired to observe the isotope induced shifts identified at natural abundance levels in grass for comparison to the shifts identified under enrichment. Data was collected on the field samples using a spectroradiometer and two FTIR spectrometers. Four isotope induced wavelength shift regions (703 nm, 1,619 cm^{-1}, 2,363 cm^{-1}, and 3,300 cm^{-1}) were analyzed in the data from the field samples and show trends that correlate to observations identified during isotope enrichment (Capelle & Macko, 2016). Furthermore, the field sample data was used to derive a stable isotope ratio using infrared data, called the infrared nitrogen stable isotope

(INSI) ratio, of ^{15}N in grass from the peak areas identified in two regions (1,600 cm^{-1} and 2,300 cm^{-1}) of the infrared data associated with each isotope. This was performed through peak separation and modeling of the FTIR-ATR data. The FTIR-ATR infrared data based nitrogen stable isotope (INSI) ratios calculated from the field samples were consistent with expected ^{15}N enrichment levels. This indicates a strong foundation for the continued development of this methodology. Based on this research, future sensors could be developed to enable the measurement of nitrogen stable isotope ratios in the field with handheld, airbased or spacebased infrared spectrometers.

Keywords

Stable Isotopes; FTIR; Infrared Spectroscopy; Nitrogen

Introduction

Stable isotope information can be used like a fingerprint or signature of a material under study to indicate origins and history of the element in the material (Townsend *et al., 2004)*. Nitrogen fertilizer sources can be identified in plant matter and the surrounding soils as organic manure based fertilizers are more enriched in the heavier ^{15}N isotope versus Haber process inorganic fertilizers (Townsend *et al*., 2004; Yun *et al*., 2006). An ability to determine fertilizer sources is important in understanding nutrient loads and origins, as anthropogenic impacts are often hard to quantify in the environment.

A new technique for isotope ratio measurements utilizing the infrared portion of the electromagnetic spectrum is developed (Capelle & Macko, 2016). In the infrared, elemental composition can be analyzed based on the elemental structure of the supplied sample (Coates, 2000). Molecular bonds flex and rotate in characteristic ways. These

movements vibrate at specific and known frequency locations in the infrared. The presence of an isotope can alter these characteristic frequency locations due to the heavier mass of the isotope. The heavier mass changes the vibrational modes of all the atoms in the labeled molecule and create a downshift in frequency from the expected frequency in the lighter isotope molecule (Quillard *et al.*, 1997). These changes require instrumentation with high frequency or spectral resolution to measure these shifts, often termed hyperspectral. By utilizing hyperspectral instrumentation that operates in the infrared these isotopes effects are observable at both enriched and natural abundance levels.

Background

A nitrogen stable isotope (^{15}N) labeled fertilizer plant growth enrichment experiment was conducted previously (Capelle & Macko, 2016) to identify isotope induced frequency or wavelength shifts in the measured spectral data from three spectrometers; the Analytical Spectral Devices Inc. (ASD) Field Spec Pro, the Agilent 4100 Exoscan and the Thermo Scientific Nicolet 6700 with an attenuated total reflectance (ATR) sample interface. High levels of ^{15}N was supplied to the plants using 99% ^{15}N-labelled fertilizer solutions. In comparison to a control plant containing natural abundance (0.0036%) levels of ^{15}N in traditional fertilizer, four regions of interest were identified in the instrument data. These regions can be associated with specific chemical functional groups or known plant behaviors (table 4).

Instrument	Identified Feature in Control Plant	Identified Feature in ^{15}N Labeled Plant	Functional Group or Behavior
ASD Spectroradiometer	719 nm	703 nm	Vegetation Red-Edge
Exoscan FTIR Spectrometer	2,372 cm^{-1}	2,363 cm^{-1}	NH Bonds
Nicolet FTIR-ATR Spectrometer	3,296 cm^{-1}	3,194 cm^{-1}	Primary aliphatic amine NH bonds / Chlorophyll
Nicolet FTIR-ATR Spectrometer	1,634 cm^{-1}	1,619 cm^{-1}	CN Bonds / Amide II

Table 4 Regions of interest where isotope induced wavelength / wavenumber shifts were observed in collected data from three different instruments during a ^{15}N isotope enrichment plant growth experiment

Materials

Field Samples

Two sets of field samples were collected, each with different expected ^{15}N signals to allow for the observation of the regions identified under enrichment to be observed at natural abundance levels. The first set of samples, termed herein as grass samples, contains three groups of samples and were collected in a Virginia hay field and within a poultry farm. The first group was collected where commercial inorganic Haber process fertilizer had been applied to the fields at least once per year for over 15 years. The expected ^{15}N signals in the grasses, termed herein as inorganic grass, are close to atmospheric levels, near zero permil or 0.0036 % ^{15}N abundance. The second group of samples were collected in an adjacent field where cattle have been grazing for the same time period, termed herein

as organic grass. The ^{15}N signals are expected to be more enriched due to the organic fecal matter under constant application in the field for nearly the same time period as the inorganic grass samples. The last group of field samples in this set were collected from grass growing within poultry cages at Timbercreek Farm in Charlottesville, Virginia. Timbercreek works with the University of Virginia's Environmental Science Department to enable scientific research of the biochemical processes that occur in the sustainably managed farm. The grass within the cages was exposed to a higher amount of poultry litter leading to an expected greater level of ^{15}N enrichment.

The second set of grass field samples, termed herein as stream bank samples and identified by their monitoring site number, were collected along six Virginia streams shown in figure 12; Toms Brook (NS05), Stoney Creek (NS14), Stanley (FP10), Muddy Creek (JR01), Pleasant Run (JR10) and Cooks Creek (JR07), with known elevated nitrate nitrogen content and in some cases with levels above the Virginia Department of Environmental Quality (DEQ) total maximum daily load (TMDL) of 10 ppm. The grass sample nitrogen values are assumed to be related to the streams with known elevated nitrate nitrogen levels in the water quality samples due to the common nitrogen source contained in the watershed runoff. Water sample data was acquired from the Friends of the Shenandoah River (FOSR) water quality monitoring program and website (Friends of the Shenandoah River). The Friends of the Shenandoah River (FOSR) is a 72 member volunteer group who sample tributaries and the Shenandoah four times per month and has a record of 23 years. The data is sent for laboratory analysis at Shenandoah University. The sites chosen represent nutrient loading from different sources with expected different

nitrogen isotope signals. Three of the impaired sites are downstream of known point source polluters. NS05 and FP10 are sites at wastewater treatment plants and NS14 is located at a chicken processing plant. Their June 2014 nitrate-nitrogen loads were 32.01, 6.48 and 6.86 ppm respectively. The remaining three are nonpoint source locations and include sites along Muddy Creek, Pleasant Run and Cooks Creek. Their most recent data collection for nitrate nitrogen was 6.52, 5.95, and 5.92 respectively. Each site has had data collections since 1997, 2001 or 2003 and a predominance of the data show impairment. It is hypothesized that the three point source sample origins are organic and will be enriched in ^{15}N.

Grass samples were acquired as close to each stream as possible and also from grass growing within the shallow areas of each stream. Samples collected that were growing within the stream are identified by the designator AQ following their monitoring site number. In two cases (FP01 and JR02), after sample preparation there was not enough usable material for measurement and the samples were then disregarded from the study.

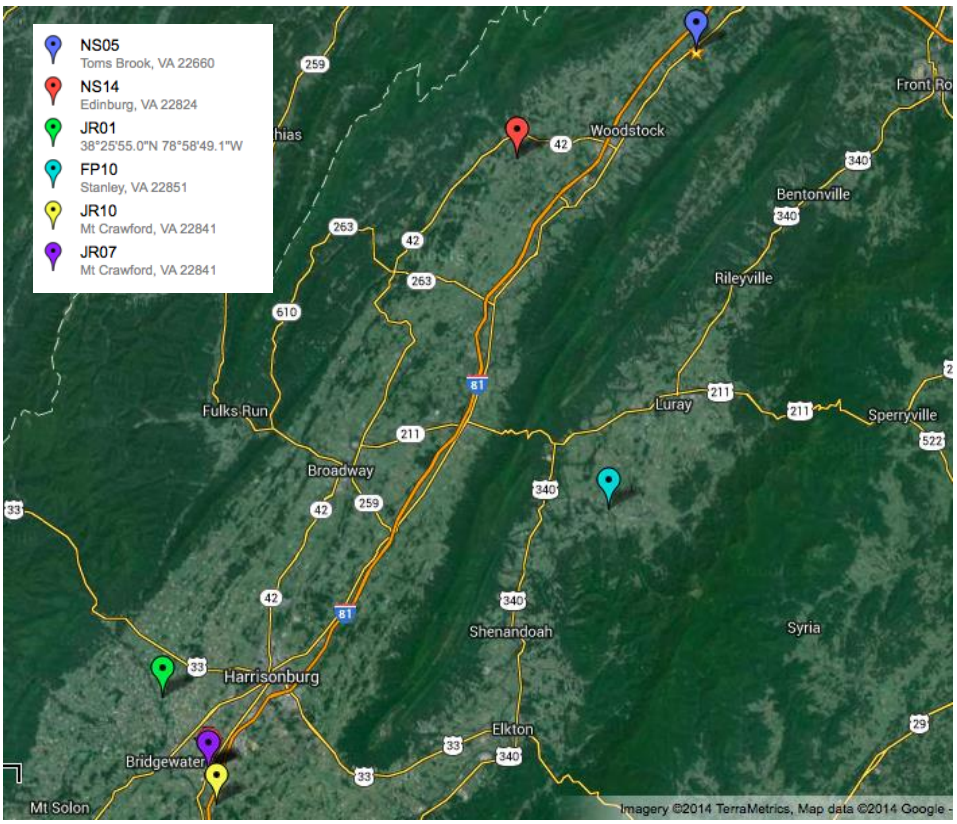

Figure 46 Six FOSR Monitoring sites where grass samples were collected along the stream banks

Sample Set	Sample Group	Sample
Grass Samples	Poultry	Poultry0
		Poultry1
		Poultry2
		Poultry3
		Poultry4
		Poultry5
		Poultry6
		Poultry7
		Poultry8
		Poultry9
	Organic	Organic0
		Organic1
		Organic2
		Organic3
		Organic4
		Organic5
		Organic6
		Organic7
		Organic8
		Organic9
	Inorganic	Inorganic0
		Inorganic1
		Inorganic2
		Inorganic3
		Inorganic4
		Inorganic5
		Inorganic6
		Inorganic7
		Inorganic8
		Inorganic9

Table 5 List of grass samples and sample groups of samples collected in fields utilizing different fertilizers; organic cow manure, inorganic Haber process and organic poultry manure.

Sample Set	Stream	Sample
Stream Bank Samples	Stanley Creek	FP10_01
		FP10_02
		FP10_AQ_01
		FP10_AQ_02
	Muddy Creek	JR01_01
		JR01_02
	Cook's Creek	JR07_01
		JR07_02
	Pleasant Run	JR10_01
		JR10_02
		JR10_AQ_01
		JR10_AQ_02
	Tom's Brook	NS05_01
		NS05_02
		NS05_AQ_01
		NS05_AQ_02
	Stoney Creek	NS14_01
		NS14_02
		NS14_AQ_01
		NS14_AQ_01

Table 6 List of field samples collected along stream banks in Virginia located within the Chesapeake Bay watershed and with historic poor water quality due to elevated levels of nitrate nitrogen; likely from agricultural runoff in these areas.

Instrumentation

The Analytical Spectral Devices Inc. (ASD) Field Spec Pro (*FieldSpec(R) pro user's guide,* 2002)) is a dispersive spectroradiometer. It was used to measure plant reflectance from the visible to the overtone vibrations region up to 2.5 microns. It has a spectral resolution of up to ten nanometers in the short-wave infrared. The Agilent 4100 Exoscan (*Agilent 4100 exoscan FTIR operation manual,* 2013) is a FTIR spectrometer that measures from 2.5 – 15 microns (4000 – 650 cm^{-1}) with a frequency resolution of up to 4 cm^{-1}. It can also be used for field measurements. The Thermo Scientific Nicolet 6700

(*Nicolet (TM) FT-IR user's guid,.* 2004) is a laboratory bench top FTIR spectrometer that measures the entire infrared spectrum and was set up for 4 cm^{-1} frequency resolution.

Software

Two software packages were used in this study; ENVI 4.7 and PeakFit 4.12. The software package ENVI (Environment for Visualizing Information, Excelis, Inc.) compared and analyzed the resulting spectra collected by each instrument. ENVI enables spectral libraries to be created for each sample grouping. PeakFit is a spectroscopy tool to identify peaks in spectral data through modeling and allows for peak areas to be measured.

Methods

Field Sampling and Measurement

All grass samples were dried to remove water content and measured across all three instruments according to vendor specifications for the collection of reflectance or absorption spectra. Over a few seconds, each instrument collects a series of either 30 or 60 sample scans and averages them together in one resulting spectra. For the grass sample set, both the ASD and Exoscan instruments resulted in ten spectra representative of ten different clippings of grass and in the case of the Nicolet three spectra were produce representing three different clippings. For the stream bank sample set, two spectra of each monitoring site were produced that each represent two different clippings in two different locations. The multiple spectra collected within each sample set were used to assess sample variability and determine consistency between results.

Peak Analysis

The instrument spectra were truncated to the desired analytical region (table 4). Data were then normalized to a range of 0-1, baseline corrected and smoothed with a Savitsky-Golay filter to remove instrument noise. Peak fitting was performed using the residuals method to achieve a peak fit with an r^2 value of at least 0.98. The model was then used to calculate the integrated peak area for each peak identified near the features listed in table 4.

Stable Isotope Ratio Calculation

Peak areas derived from the PeakFit model were used to calculate the stable isotope ratio and the resulting $\delta^{15}N$ value according to the following equation:

$$\delta^{15}\mathrm{N} = 1000 \left\lfloor \frac{\mathrm{Ratio}_{Sample} - \mathrm{Ratio}_{Standard}}{\mathrm{Ratio}_{Standard}} \right\rfloor \qquad \text{Equation 1}$$

The standard for nitrogen is atmospheric nitrogen with an isotope ratio of 0.3613.

Results

Each of the four regions identified in the table 4 were analyzed in the field sample data to compare to the ^{15}N enriched plant spectra, collected previously (Capelle & Macko, 2016). A spectral signature comparison was performed to look for the presence of the features identified during enrichment by Capelle and Macko (2016). In cases where the features were present in the natural abundance samples, the data was analyzed in PeakFit to derive a stable isotope ratio.

Grass Sample Spectral Analysis

Instrument	Functional Group or Behavior	Identified in Poultry Grass Sample	Identified in Inorganic Grass Sample	Identified in Organic Grass Sample
ASD Spectroradiometer	Vegetation Red-Edge	No	No	No
Exoscan FTIR Spectrometer	NH Bonds	Yes	Yes	Yes
Nicolet FTIR-ATR Spectrometer	Primary aliphatic amine NH bonds / Chlorophyll	No	No	No
Nicolet FTIR-ATR Spectrometer	CN Bonds / Amide II	Yes	Yes	Yes

Table 7 Results of analysis of the grass sample data from three spectrometers describing if the data shows a similar wavelength / wavenumber shift or feature to the ones identified during a plant isotope enrichment growth experiment

The measured data from the ASD spectroradiometer's vegetation red-edge feature (figures 47-49) in all samples (shown in black) have a trend consistent with the previously collected enriched buckwheat sample (shown in red). No samples show a feature consistent with the growth experiment control (shown in green). This is not an expected result as the buckwheat plants in the previously experiment were heavily enriched with ^{15}N. This eliminates this region from continued investigation as the field samples should not contain the same amount of the stable isotope as the plants in the experiment.

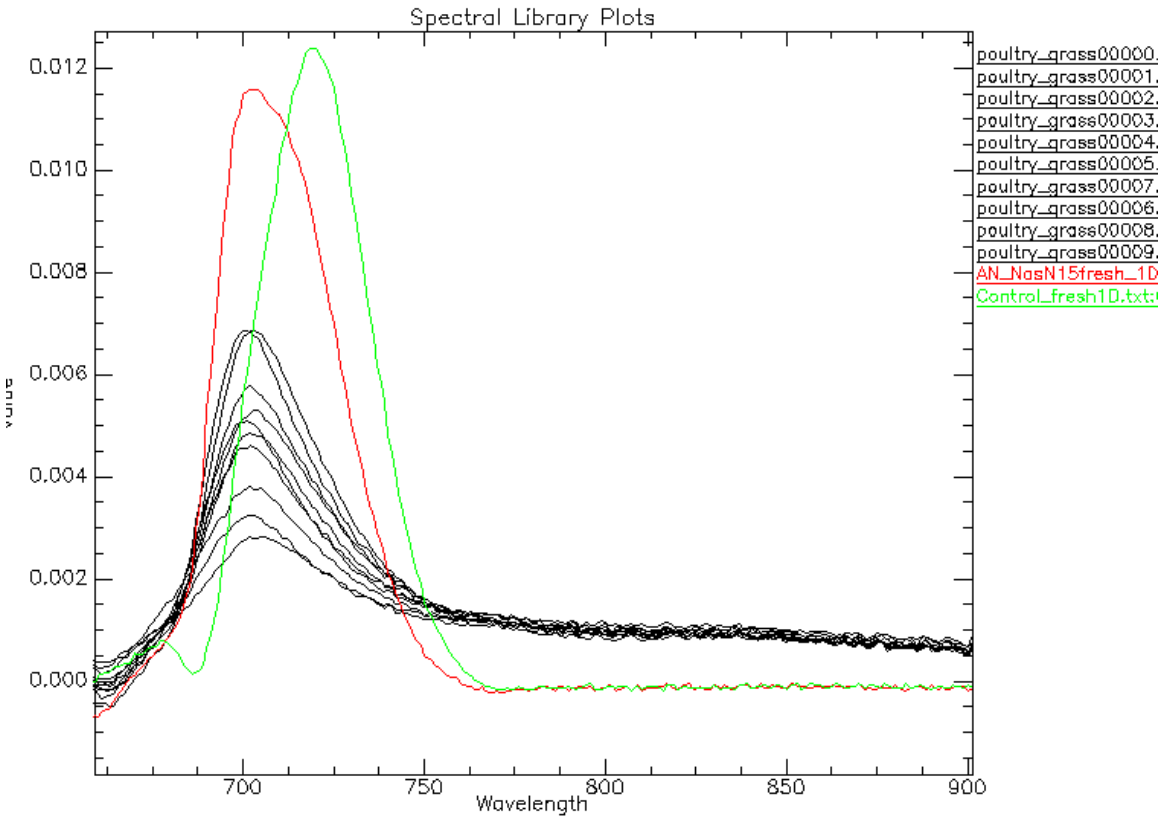

Figure 47 ASD spectra of ten grass samples growing under a poultry cage (in black) compared to the enriched buckwheat experiment data (in red) and the buckwheat control from the same experiment (in green).

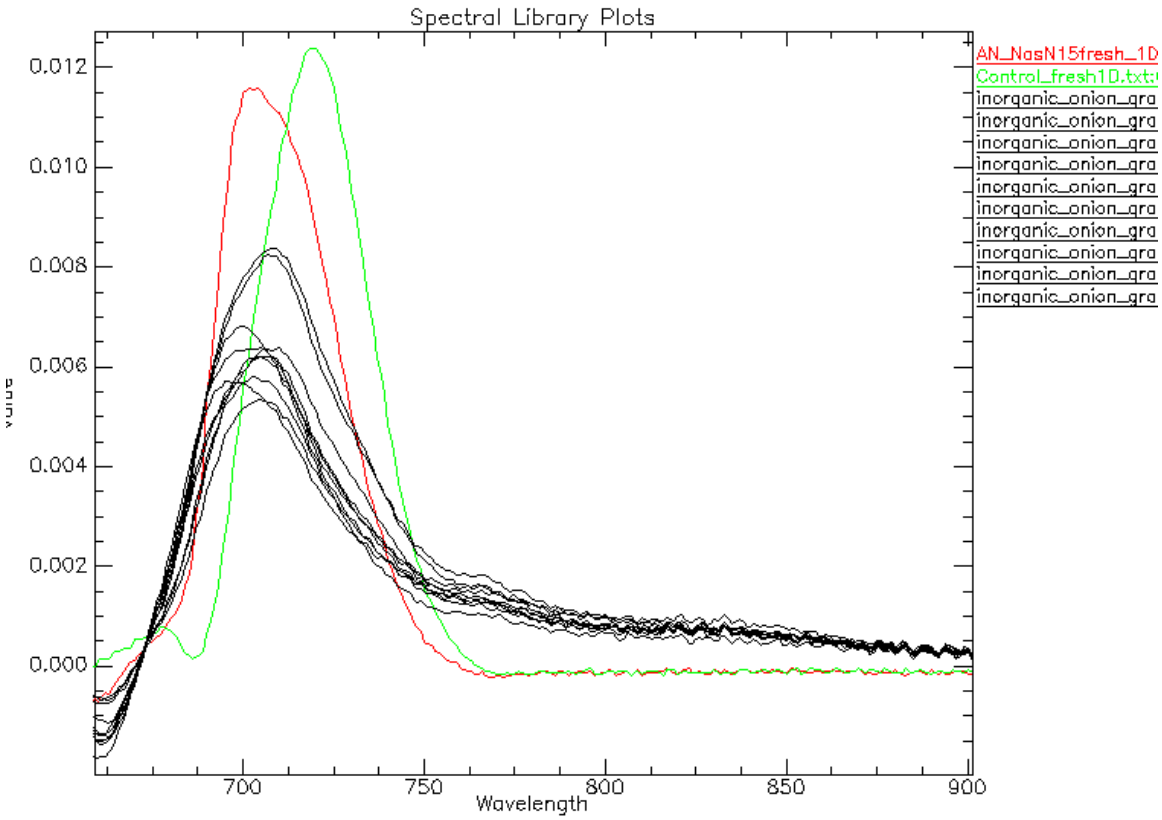

Figure 48 ASD spectra of ten grass samples growing in a field with regular application of agricultural grade inorganic fertilizer (in black) compared to the enriched buckwheat experiment data (in red) and the buckwheat control from the same experiment (in green).

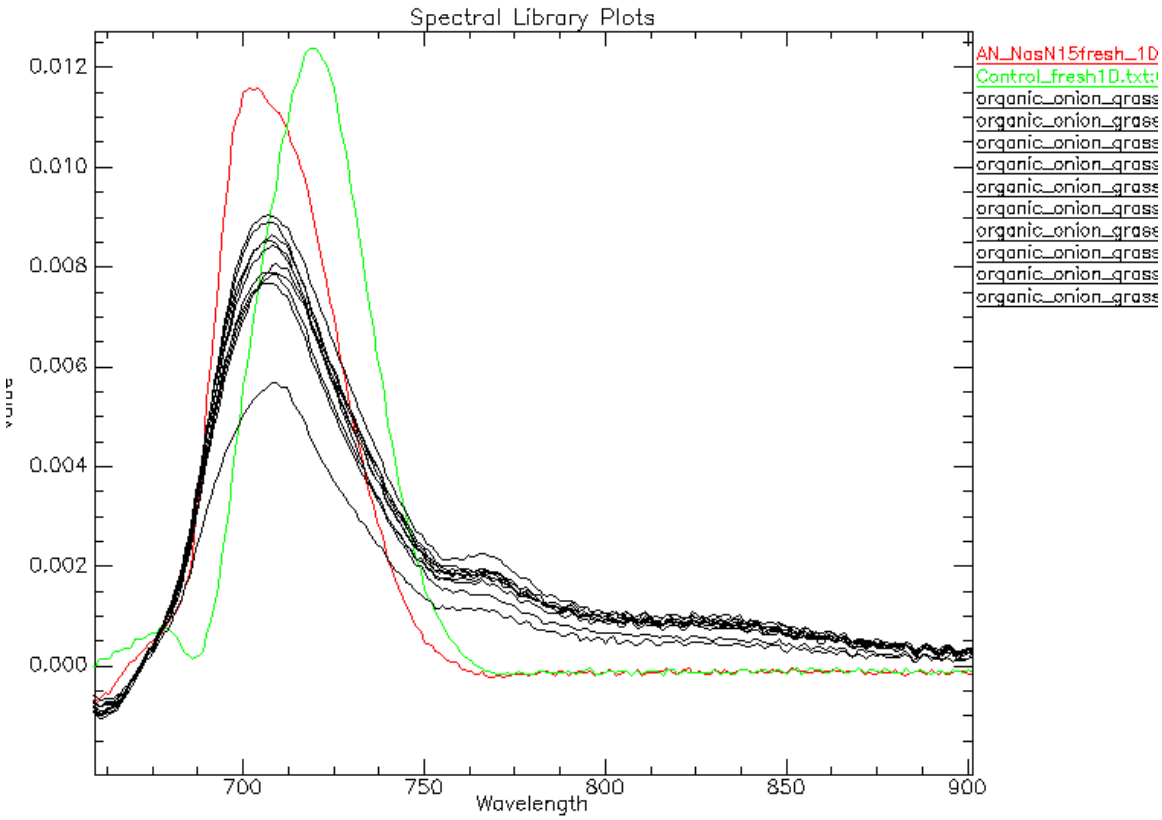

Figure 49 ASD spectra of ten grass samples growing in a cow field (in black) compared to the enriched buckwheat experiment data (in red) and the buckwheat control from the same experiment (in green).

The data from the Exoscan near the NH bond region shows the presence of the expected features (figures 50-52). The enriched buckwheat plants (in red) clearly show deeper features near 2,300 cm^{-1} that are both not observed in the control from the buckwheat growth experiment and are observed in the grass samples to a lesser degree. The Exoscan data in this region for these grass samples (poultry, inorganic and organic) were selected for peak analysis and infrared based isotope ratio calculations.

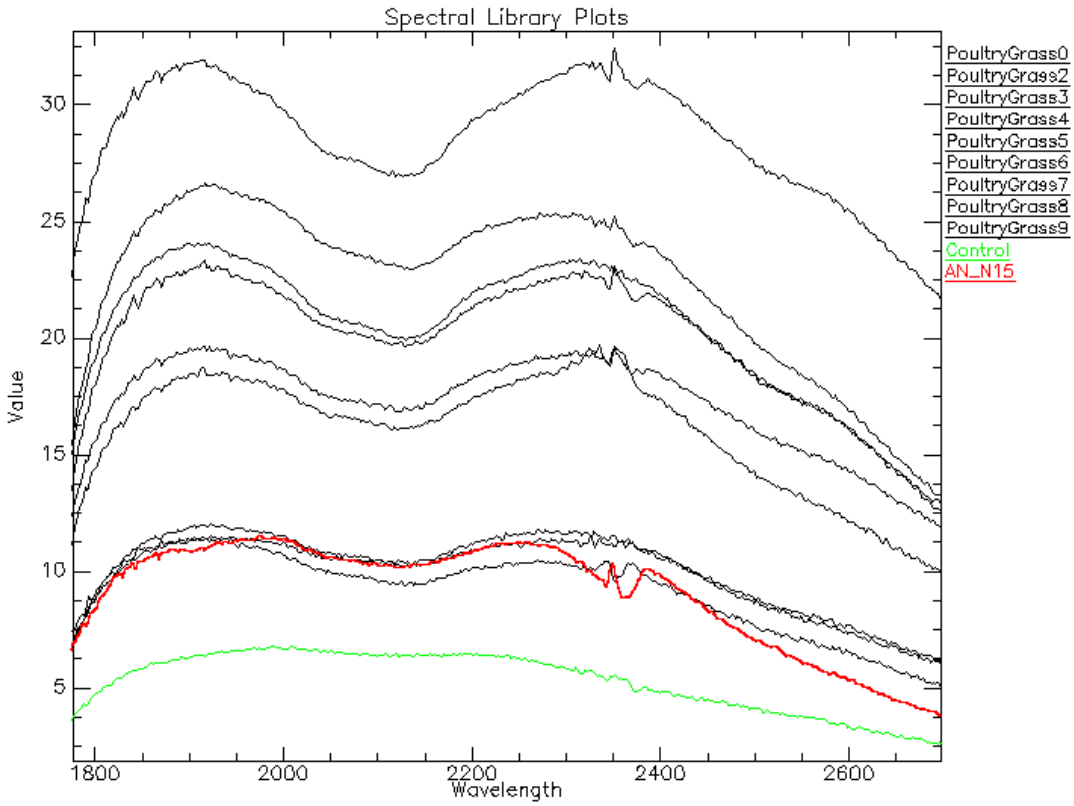

Figure 50 Exoscan spectra of ten grass samples growing under a poultry cage (in black) compared to the enriched buckwheat experiment data (in red) and the buckwheat control from the same experiment (in green).

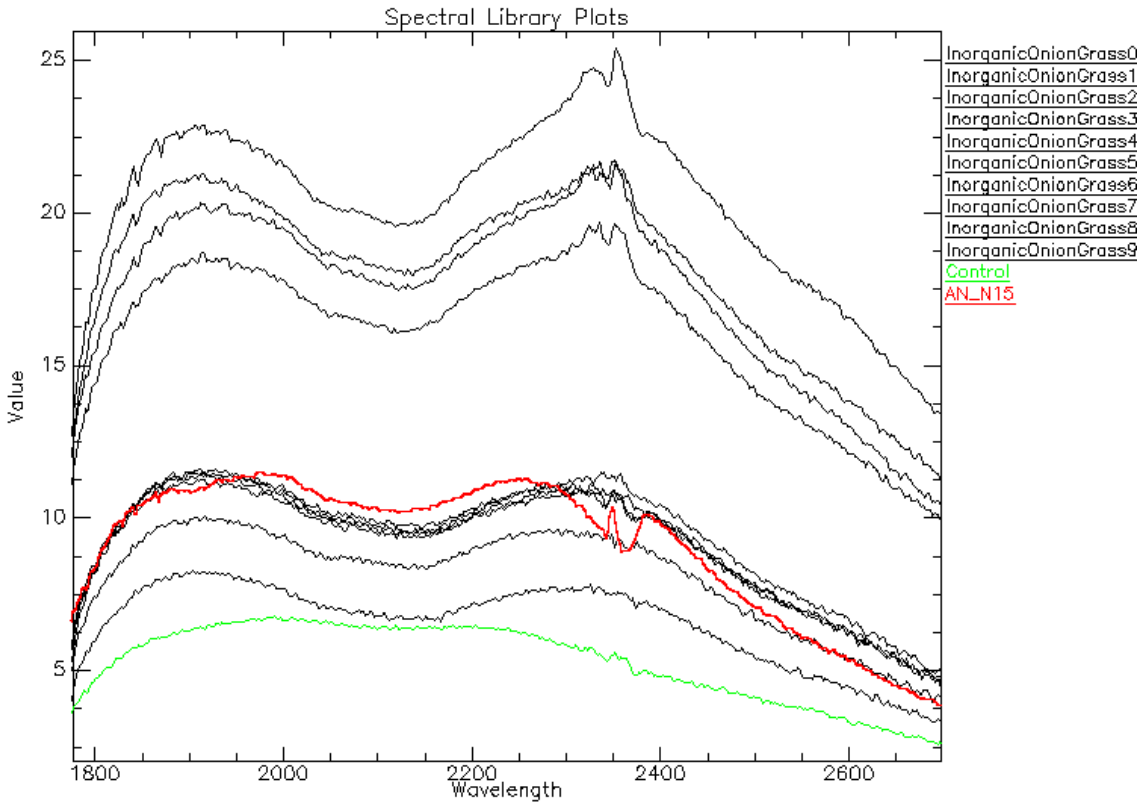

Figure 51 Exoscan spectra of ten grass samples growing in a field with regular application of agricultural grade inorganic fertilizer (in black) compared to the enriched buckwheat experiment data (in red) and the buckwheat control from the same experiment (in green).

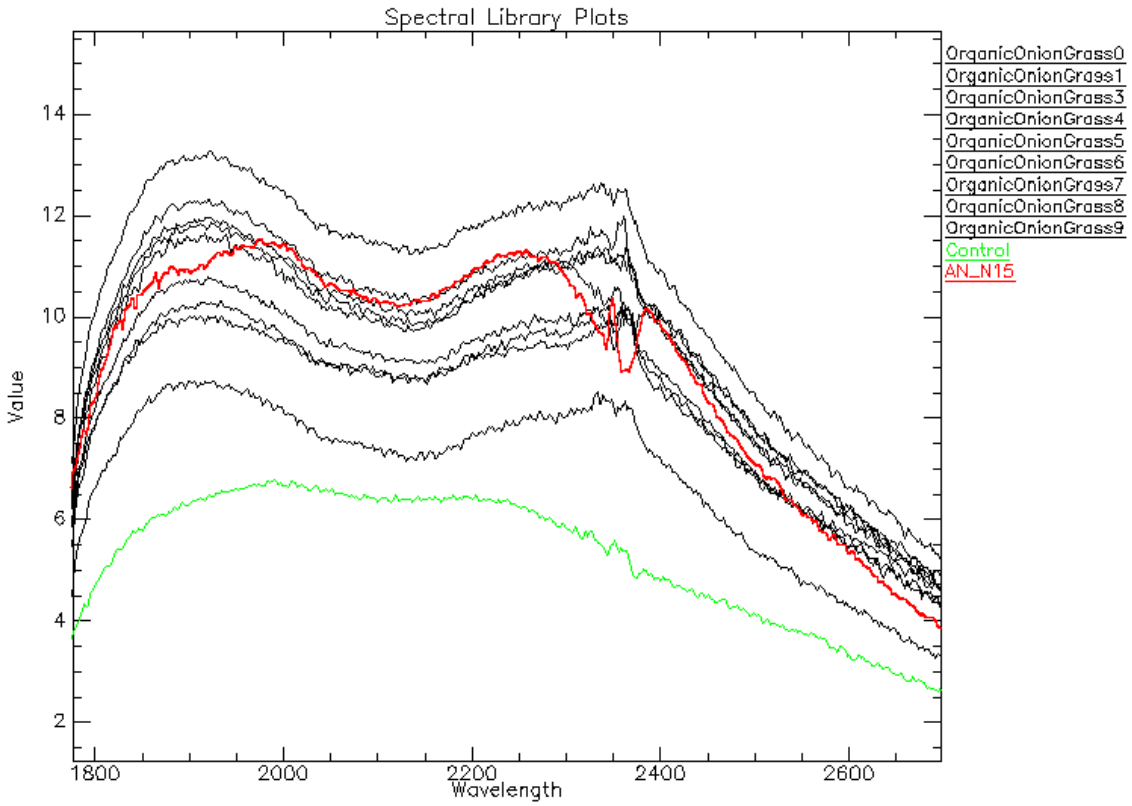

Figure 52 Exoscan spectra of nine grass samples growing in a cow field (in green) compared to the enriched buckwheat experiment data (in red) and the buckwheat control from the same experiment (in black).

The measured data from the Nicolet FTIR-ATR spectrometer is broken down into two different regions; the NH and CN bond regions. The NH bond region near 3,300 cm^{-1} shows one broad peak that spans over 600 wavenumbers (figure 53). The data does show a peak that has a frequency downshift in the poultry grass and organic grass, however peak separation over this broad span is complex and precludes this region from peak analysis with PeakFit. The broad shape means that the model has low confidence in the potential peaks assigned. Further research into the compounds and behaviors that occur within this region are required.

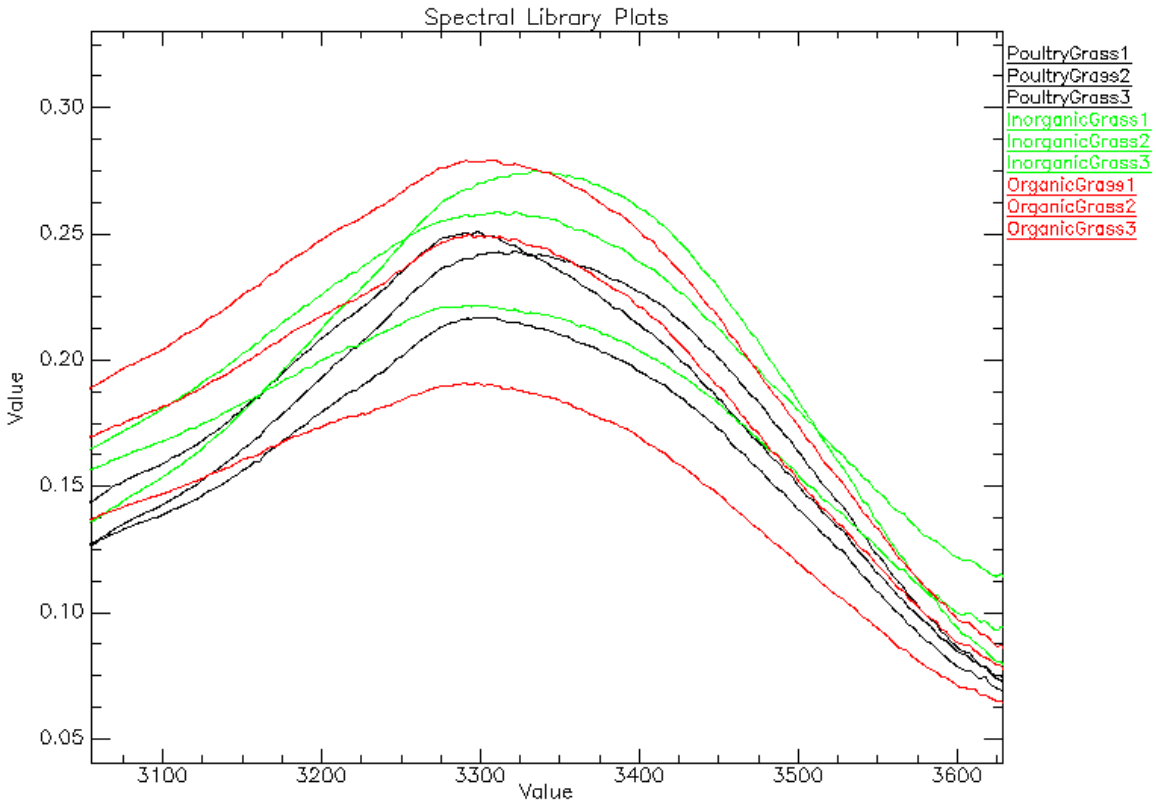

Figure 53 Nicolet FTIR-ATR spectra in the 3,300 cm^{-1} region of three grasses of each group; poultry (in black) where grass was growing in a poultry cage, inorganic (in green) from grass growing in a field with regular application of agricultural grade inorganic fertilizer, and organic (in red) where grass was growing in a cow field.

The FTIR-ATR spectrometer data in the CN bond region near 1,600 cm^{-1} show distinct wavenumber shifts between grass sample groups (figure 54). The three spectra from each sample group trend similarly within the group and also different between the groups. This is a good indicator for peak separation in this region where one peak is attributed to ^{15}N and the other to ^{14}N.

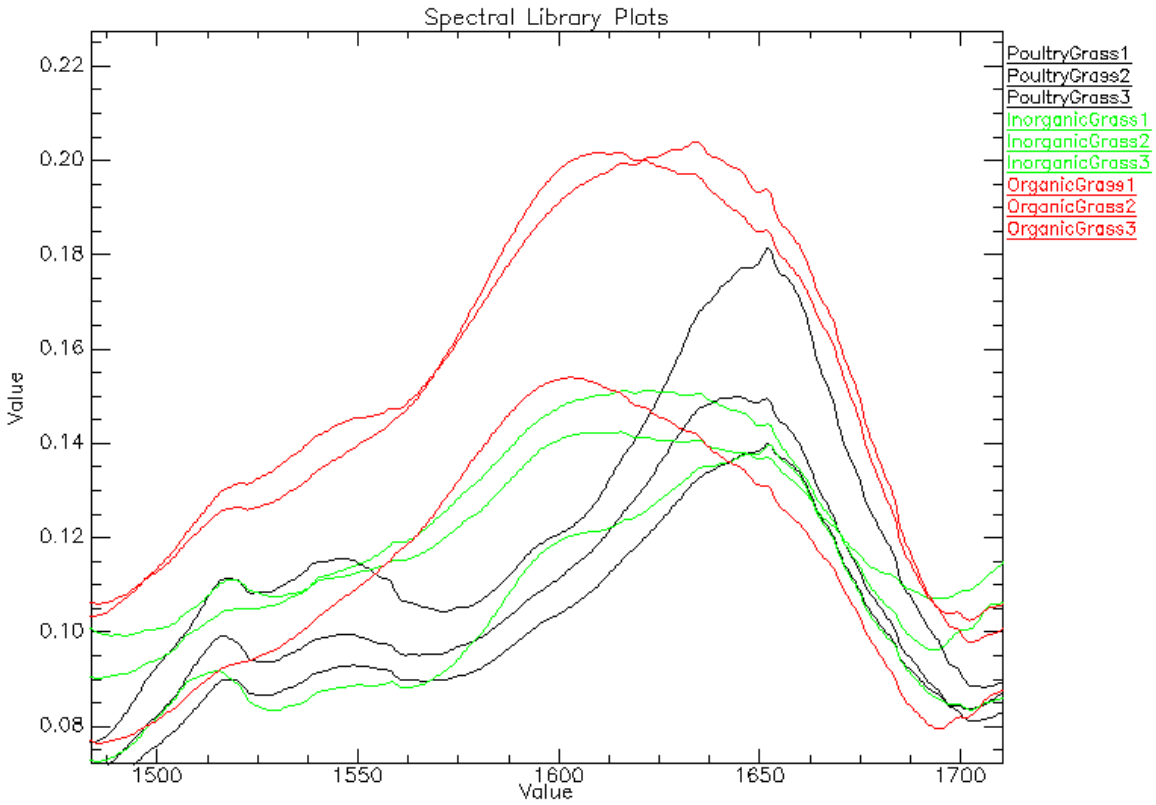

Figure 54 Nicolet FTIR-ATR spectra in the 1,600 cm^{-1} region of three grasses of each group; poultry (in black) where grass was growing in a poultry cage, inorganic (in green) from grass growing in a field with regular application of agricultural grade inorganic fertilizer, and organic (in red) where grass was growing in a cow field.

Stream Bank Sample Spectral Analysis

The ASD and Exoscan measurements were not able to be collected on the field sample data due to availability and instrument malfunctions. Additionally, the NH bond region around 3,300 cm^{-1} in the Nicolet FTIR-ATR data was not assessed based on the inconclusive results from the grass samples described above. All stream bank sample data

was analyzed in the CN bond region in the Nicolet FTIR-ATR data around 1,600 cm^{-1}.

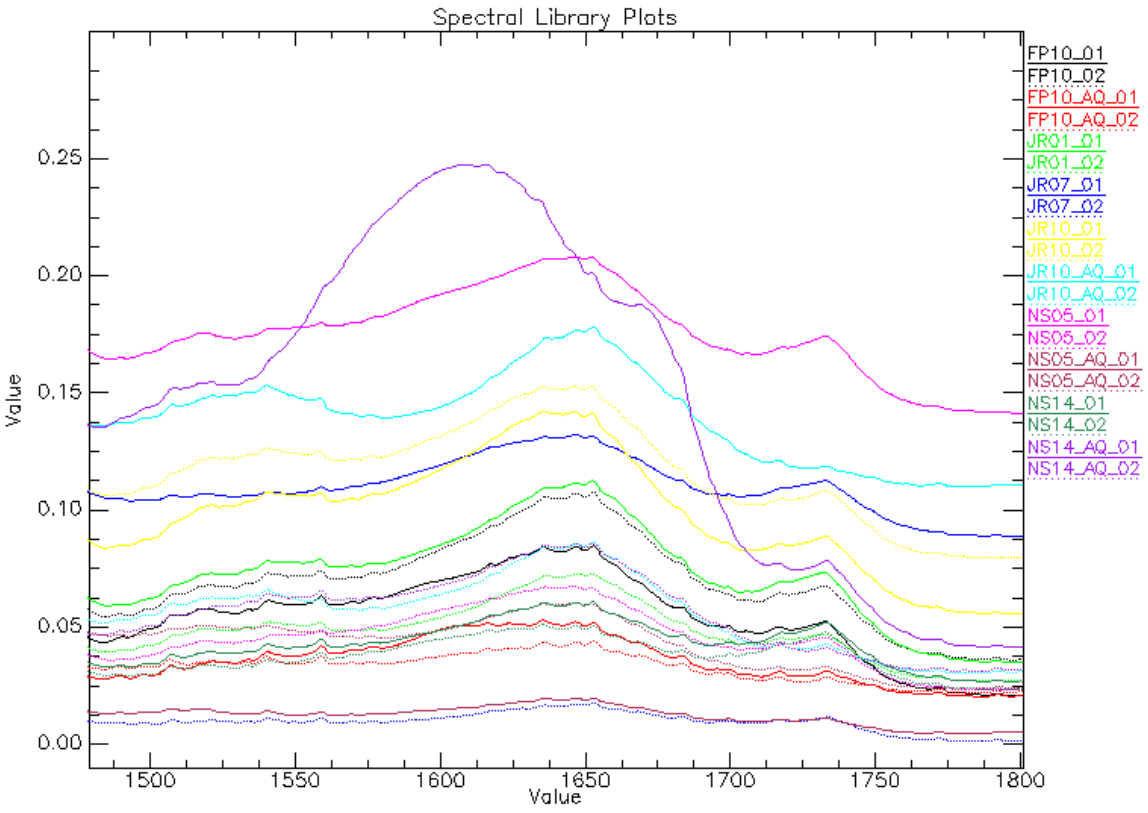

Figure 55 Nicolet FTIR-ATR measured data in the CN bond region near 1,600 cm^{-1} for grass collected along and within (designated AQ) six Virginia streams with known elevated nitrogen levels.

Peak Analysis

PeakFit models (figures 56 – 114) were computed for two different spectral regions based on observation of features in the spectral data. PeakFit models were computed of the Nicolet FTIR-ATR data near 1,300 cm^{-1} for both field grass samples and stream bank grass collected. Only the grass sample set enabled PeakFit models to be computed from the Exoscan collected data near 2,300 cm^{-1}. No models were created from the Nicolet FTIR-ATR collected data near 3,300 cm^{-1}. PeakFit models achieved a good fit with an r^2 of at least 0.98 and a low standard error. Peaks were chosen from the

models for stable isotope analysis that matched previous data collected during the isotope enriched buckwheat growing experiment or through computational chemistry modeling.

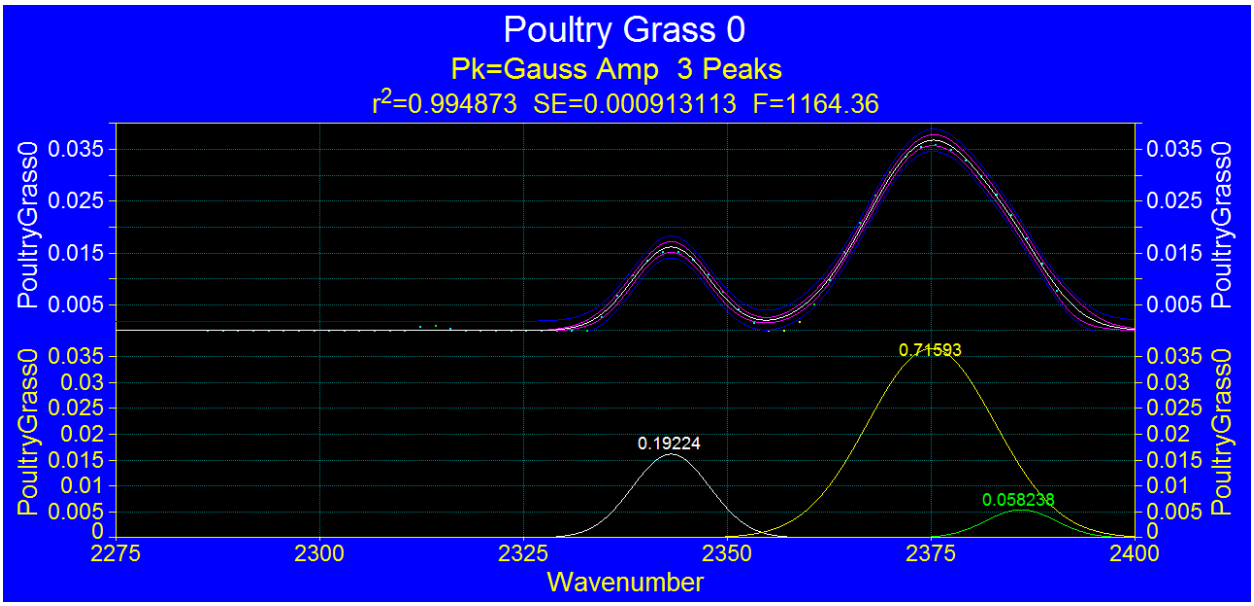

Figure 56 PeakFit model of poultry grass sample 0 from the Exoscan data in the 2,300 cm^{-1} region. Upper graph displays the input measured data in white with the 95% confidence interval of the model in pink that consists of the separated peaks shown in the bottom graph.

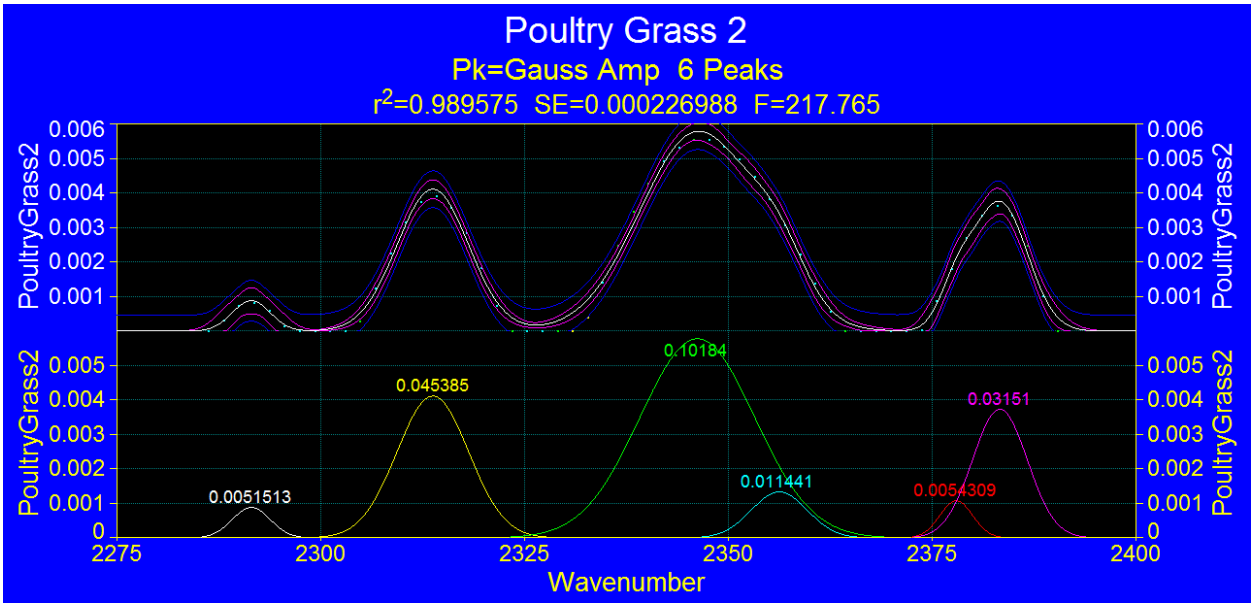

Figure 57 PeakFit model of poultry grass sample 2 from the Exoscan data in the 2,300 cm^{-1} region. Upper graph displays the input measured data in white with the 95% confidence interval of the model in pink that consists of the separated peaks shown in the bottom graph.

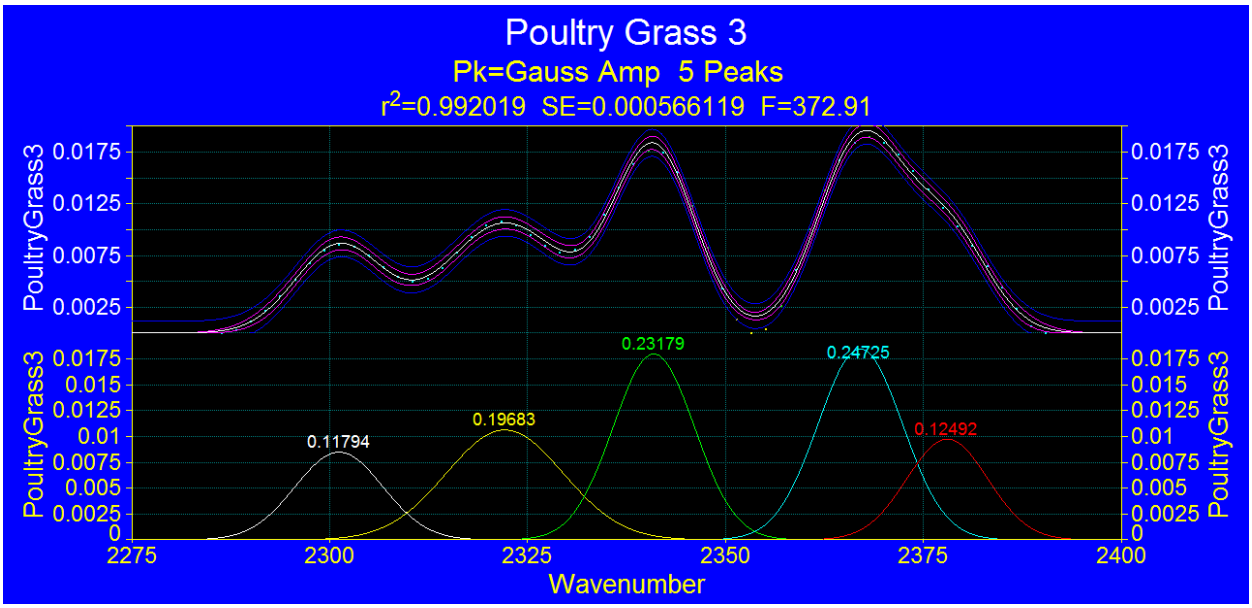

Figure 58 PeakFit model of poultry grass sample 3 from the Exoscan data in the 2,300 cm^{-1} region. Upper graph displays the input measured data in white with the 95% confidence interval of the model in pink that consists of the separated peaks shown in the bottom graph.

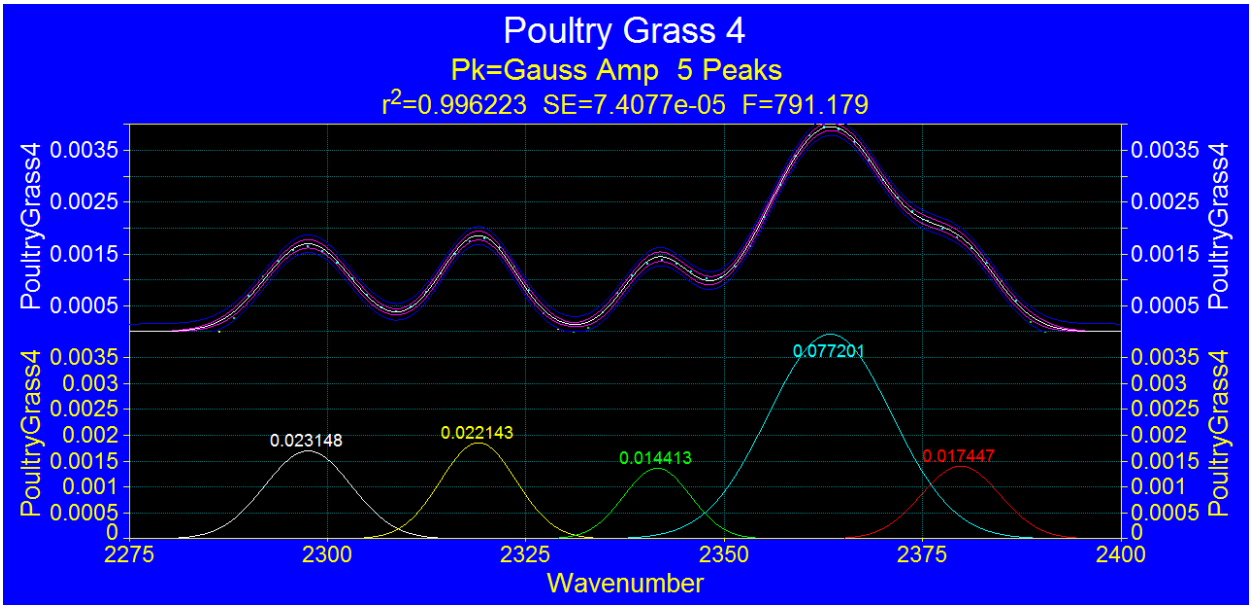

Figure 59 PeakFit model of poultry grass sample 4 from the Exoscan data in the 2,300 cm^{-1} region. Upper graph displays the input measured data in white with the 95% confidence interval of the model in pink that consists of the separated peaks shown in the bottom graph.

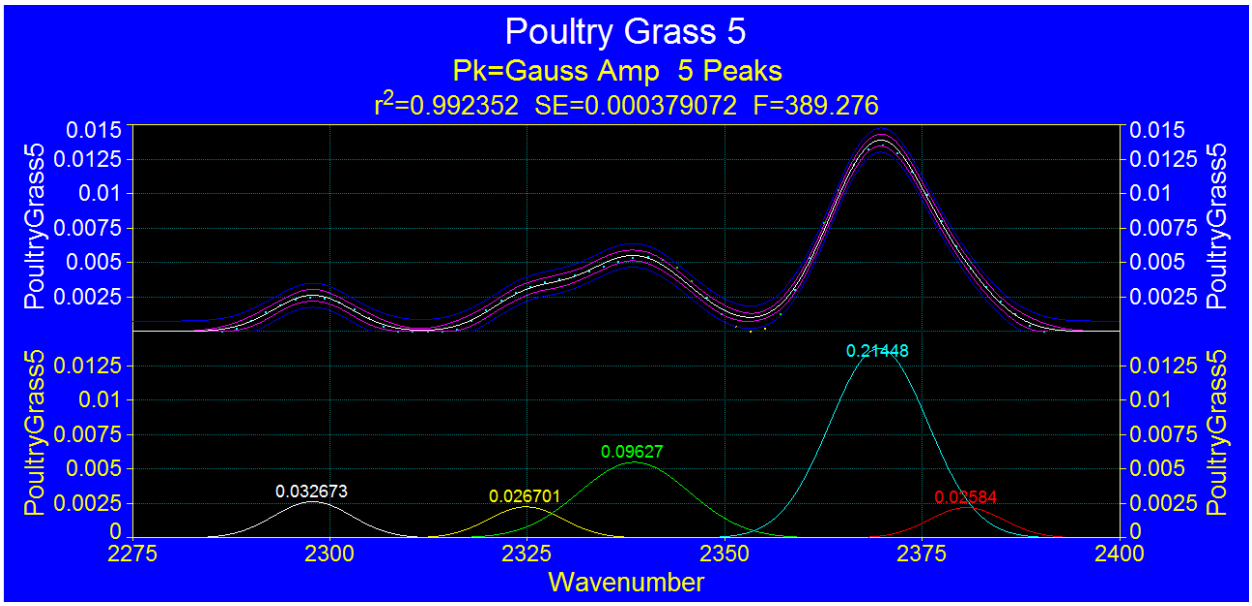

Figure 60 PeakFit model of poultry grass sample 5 from the Exoscan data in the 2,300 cm^{-1} region. Upper graph displays the input measured data in white with the 95% confidence interval of the model in pink that consists of the separated peaks shown in the bottom graph.

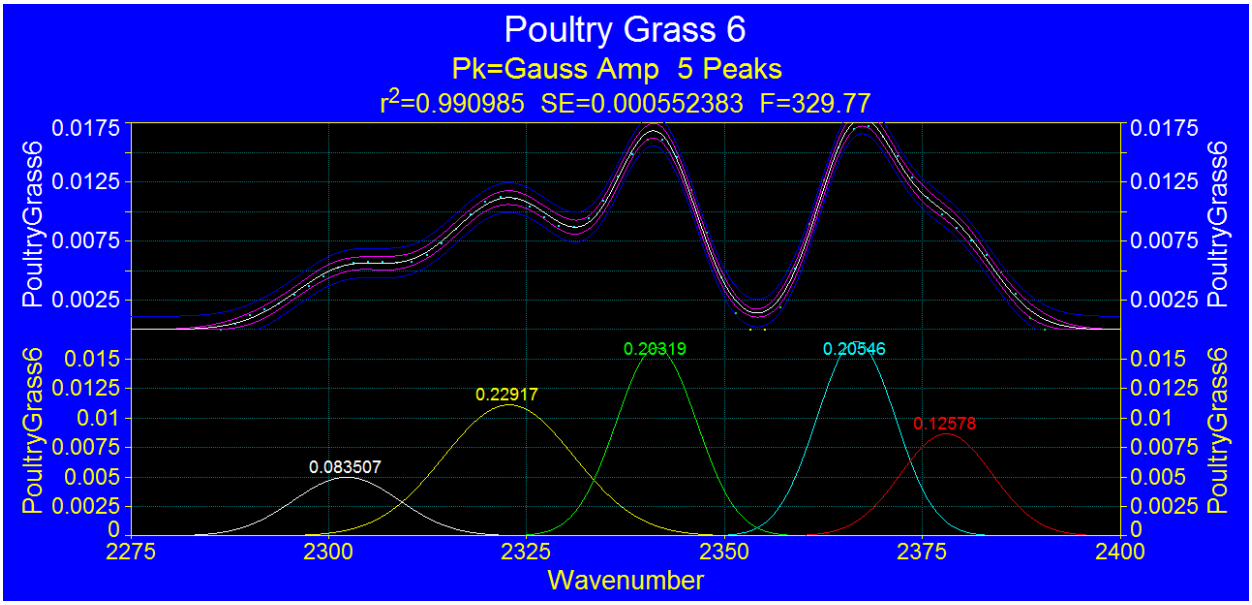

Figure 61 PeakFit model of poultry grass sample 6 from the Exoscan data in the 2,300 cm^{-1} region. Upper graph displays the input measured data in white with the 95% confidence interval of the model in pink that consists of the separated peaks shown in the bottom graph.

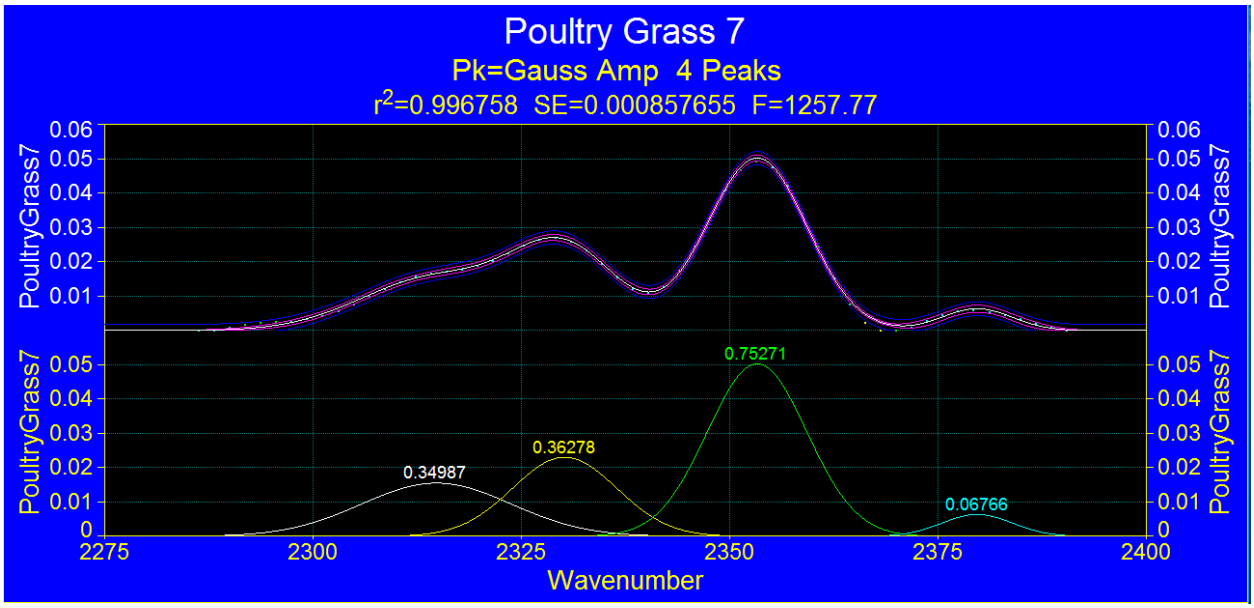

Figure 62 PeakFit model of poultry grass sample 7 from the Exoscan data in the 2,300 cm^{-1} region. Upper graph displays the input measured data in white with the 95% confidence interval of the model in pink that consists of the separated peaks shown in the bottom graph.

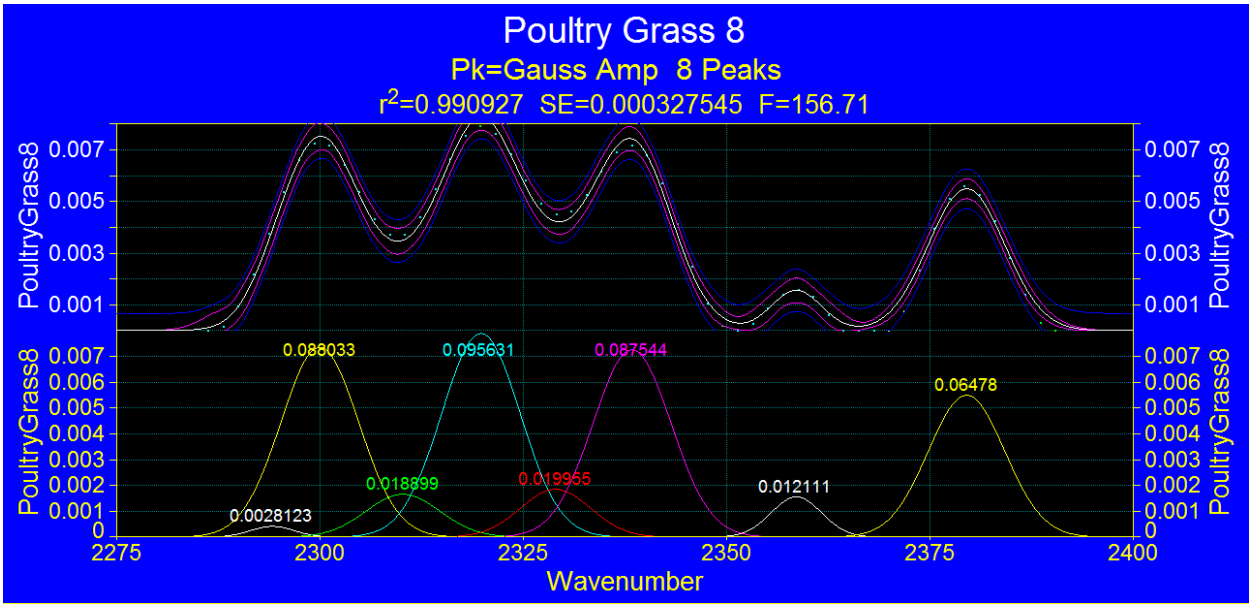

Figure 63 PeakFit model of poultry grass sample 8 from the Exoscan data in the 2,300 cm^{-1} region. Upper graph displays the input measured data in white with the 95% confidence interval of the model in pink that consists of the separated peaks shown in the bottom graph.

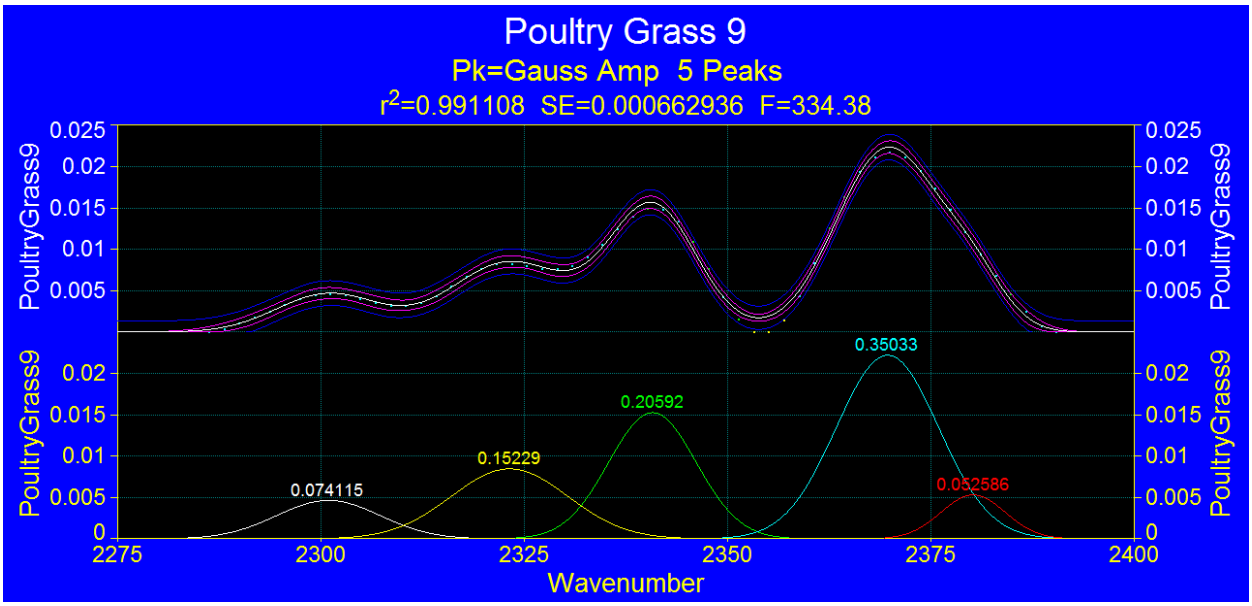

Figure 64 PeakFit model of poultry grass sample 9 from the Exoscan data in the 2,300 cm^{-1} region. Upper graph displays the input measured data in white with the 95% confidence interval of the model in pink that consists of the separated peaks shown in the bottom graph.

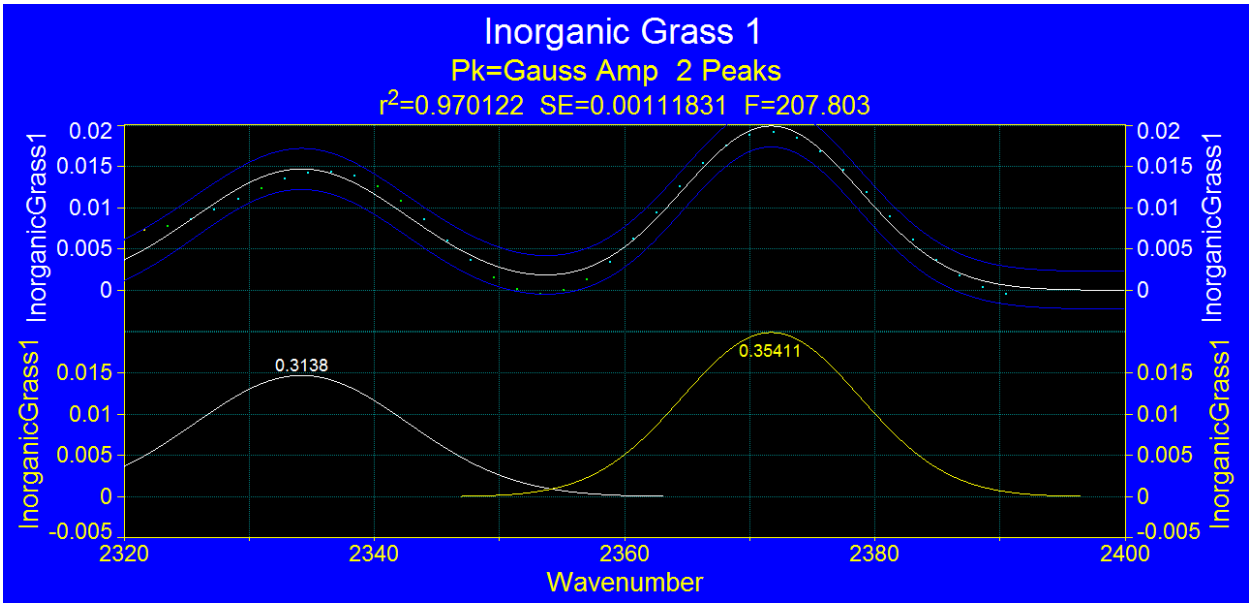

Figure 65 PeakFit model of inorganic grass sample 1 from the Exoscan data in the 2,300 cm^{-1} region. Upper graph displays the input measured data in white with the 95% confidence interval of the model in pink that consists of the separated peaks shown in the bottom graph.

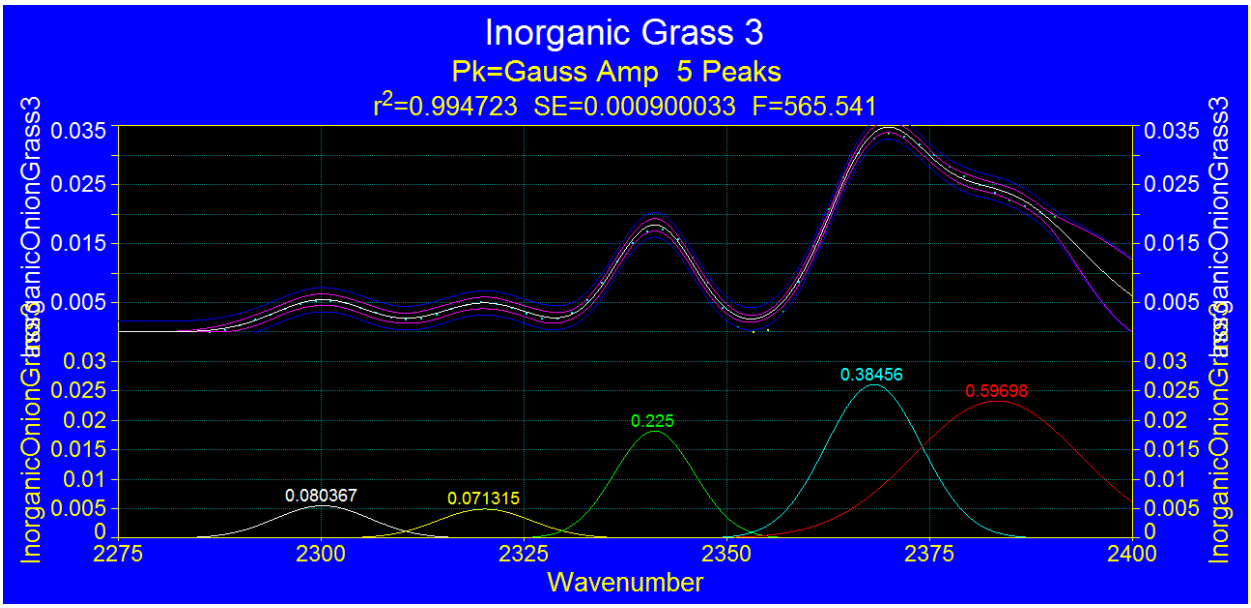

Figure 66 PeakFit model of inorganic grass sample 3 from the Exoscan data in the 2,300 cm^{-1} region. Upper graph displays the input measured data in white with the 95% confidence interval of the model in pink that consists of the separated peaks shown in the bottom graph.

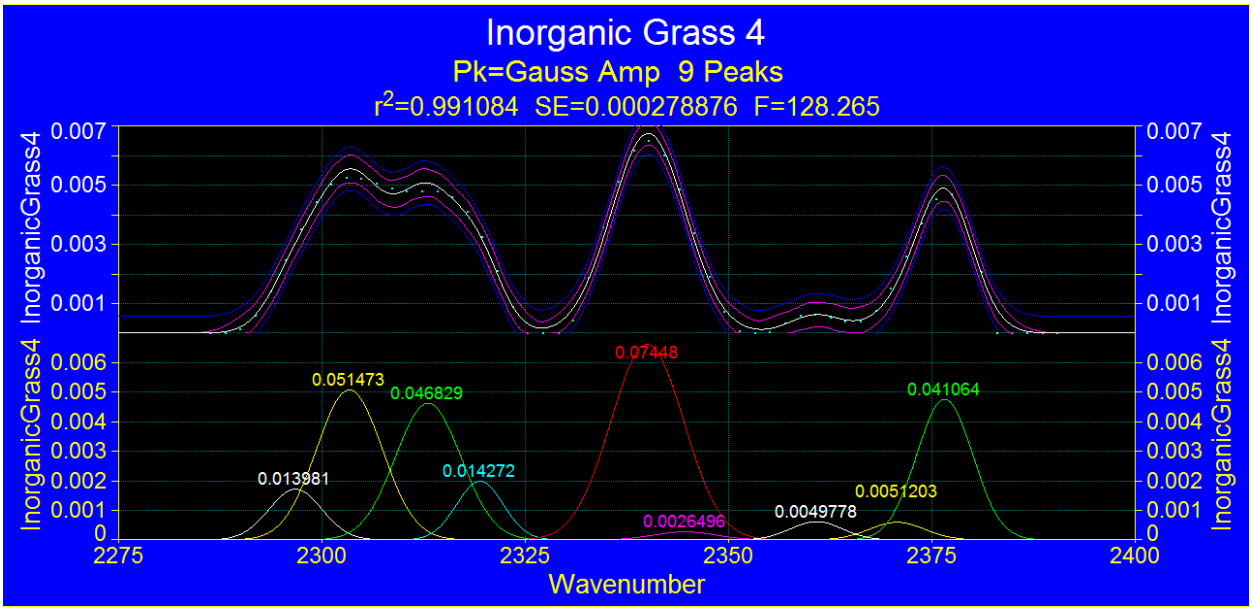

Figure 67 PeakFit model of inorganic grass sample 4 from the Exoscan data in the 2,300 cm^{-1} region. Upper graph displays the input measured data in white with the 95% confidence interval of the model in pink that consists of the separated peaks shown in the bottom graph.

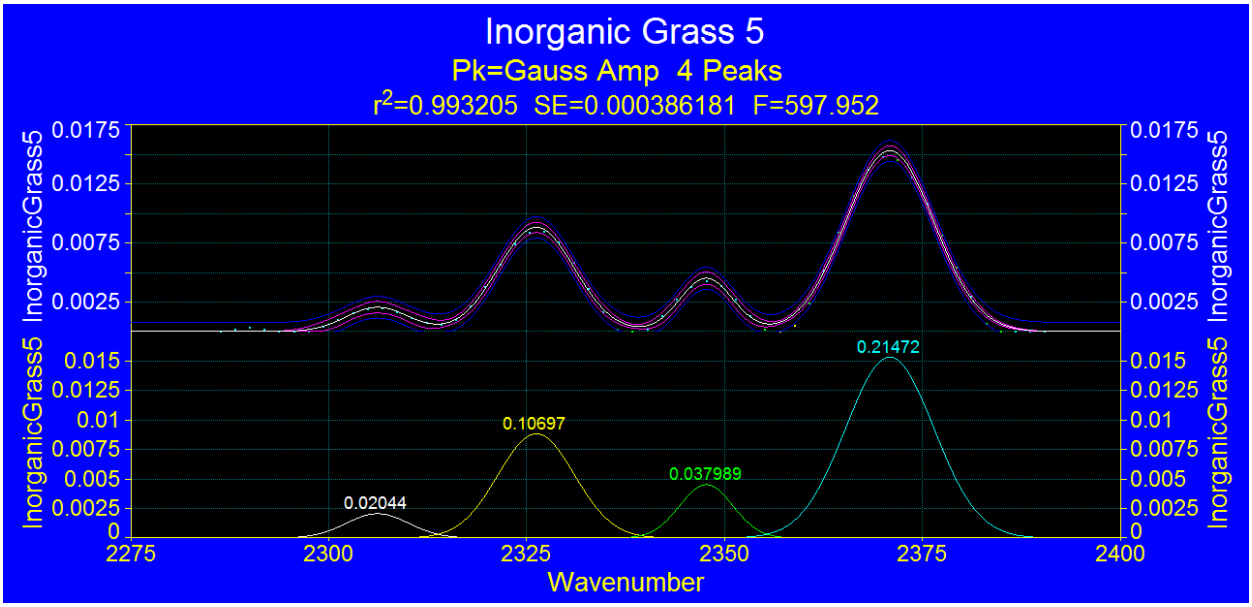

Figure 68 PeakFit model of inorganic grass sample 5 from the Exoscan data in the 2,300 cm^{-1} region. Upper graph displays the input measured data in white with the 95% confidence interval of the model in pink that consists of the separated peaks shown in the bottom graph.

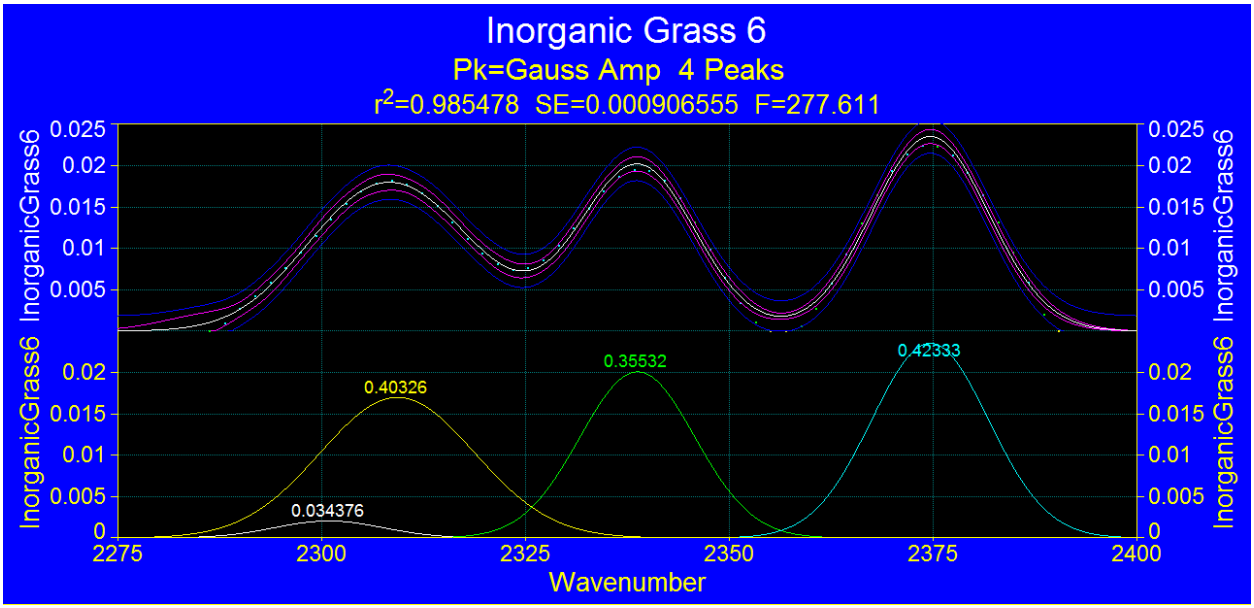

Figure 69 PeakFit model of inorganic grass sample 6 from the Exoscan data in the 2,300 cm^{-1} region. Upper graph displays the input measured data in white with the 95% confidence interval of the model in pink that consists of the separated peaks shown in the bottom graph.

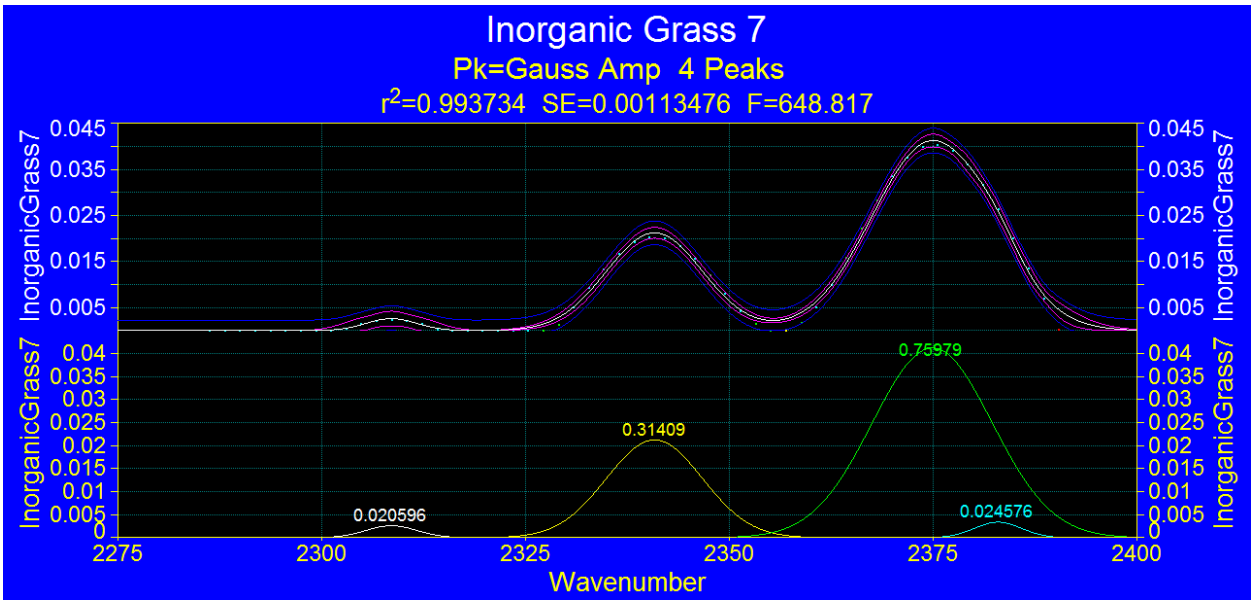

Figure 70 PeakFit model of inorganic grass sample 7 from the Exoscan data in the 2,300 cm^{-1} region. Upper graph displays the input measured data in white with the 95% confidence interval of the model in pink that consists of the separated peaks shown in the bottom graph.

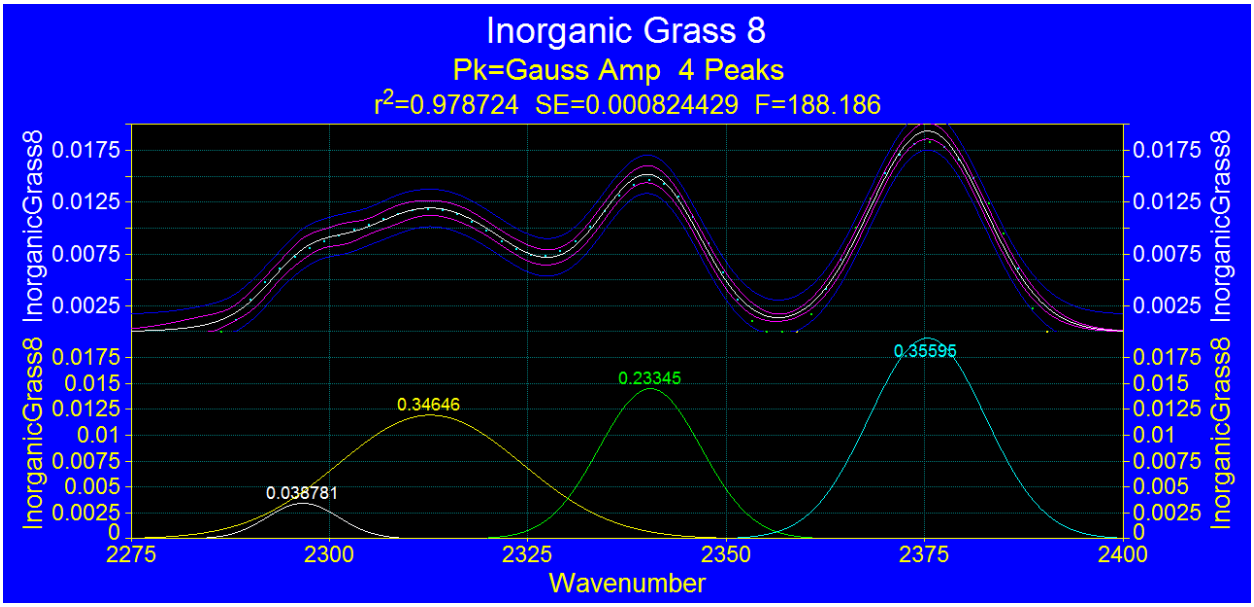

Figure 71 PeakFit model of inorganic grass sample 8 from the Exoscan data in the 2,300 cm^{-1} region. Upper graph displays the input measured data in white with the 95% confidence interval of the model in pink that consists of the separated peaks shown in the bottom graph.

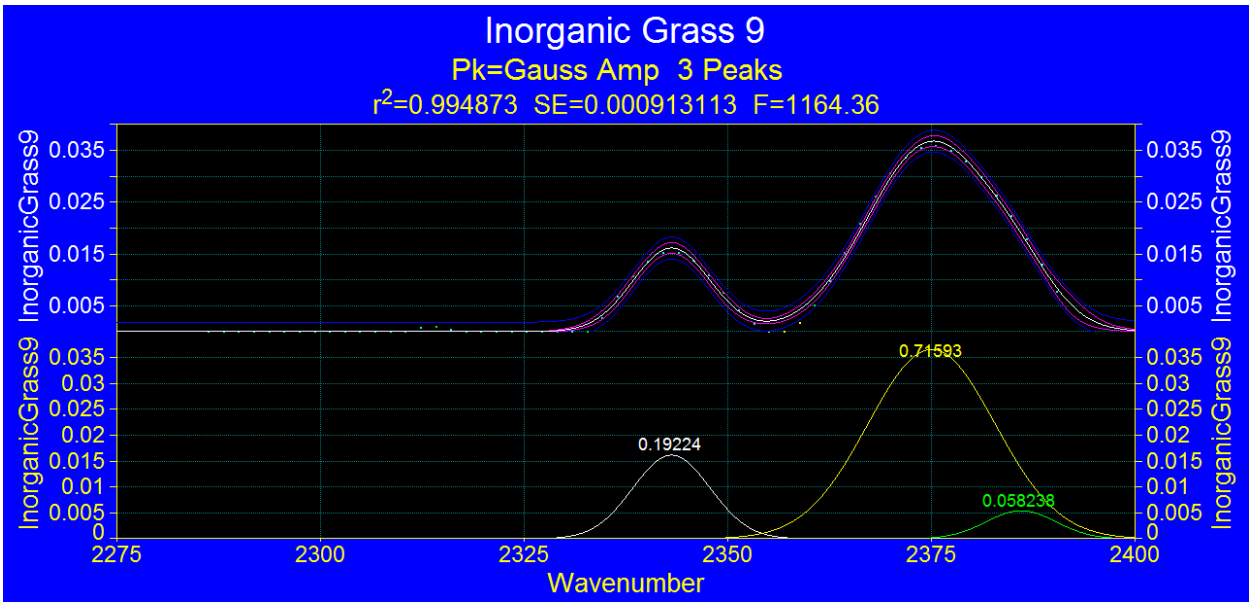

Figure 72 PeakFit model of inorganic grass sample 9 from the Exoscan data in the 2,300 cm^{-1} region. Upper graph displays the input measured data in white with the 95% confidence interval of the model in pink that consists of the separated peaks shown in the bottom graph.

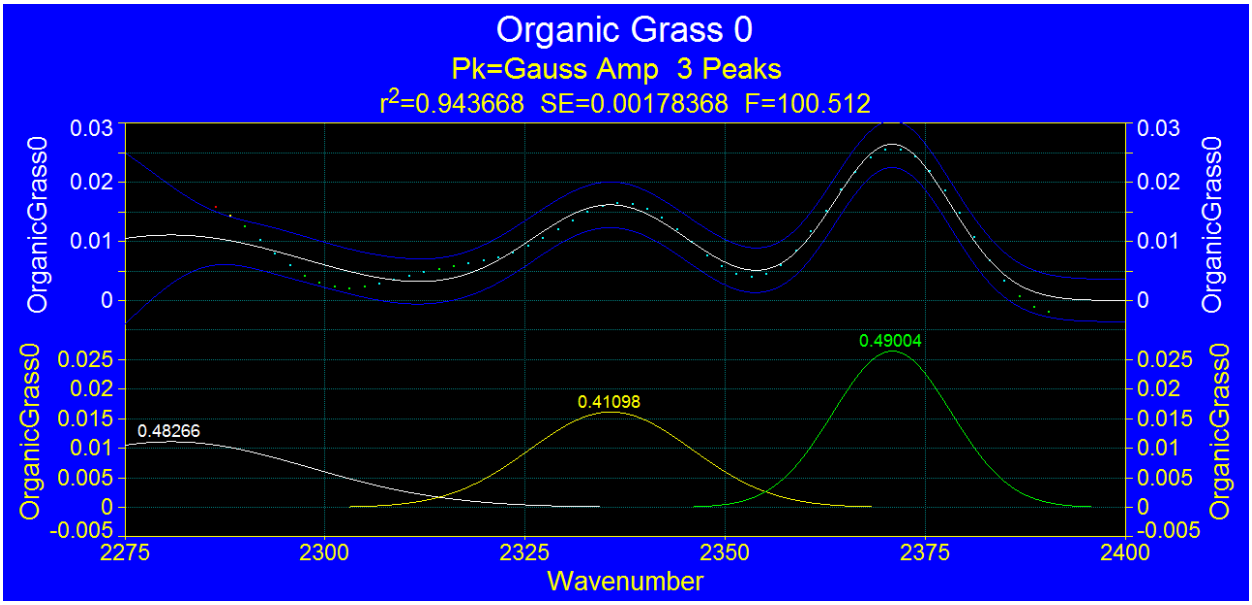

Figure 73 PeakFit model of organic grass sample 0 from the Exoscan data in the 2,300 cm^{-1} region. Upper graph displays the input measured data in white with the 95% confidence interval of the model in pink that consists of the separated peaks shown in the bottom graph.

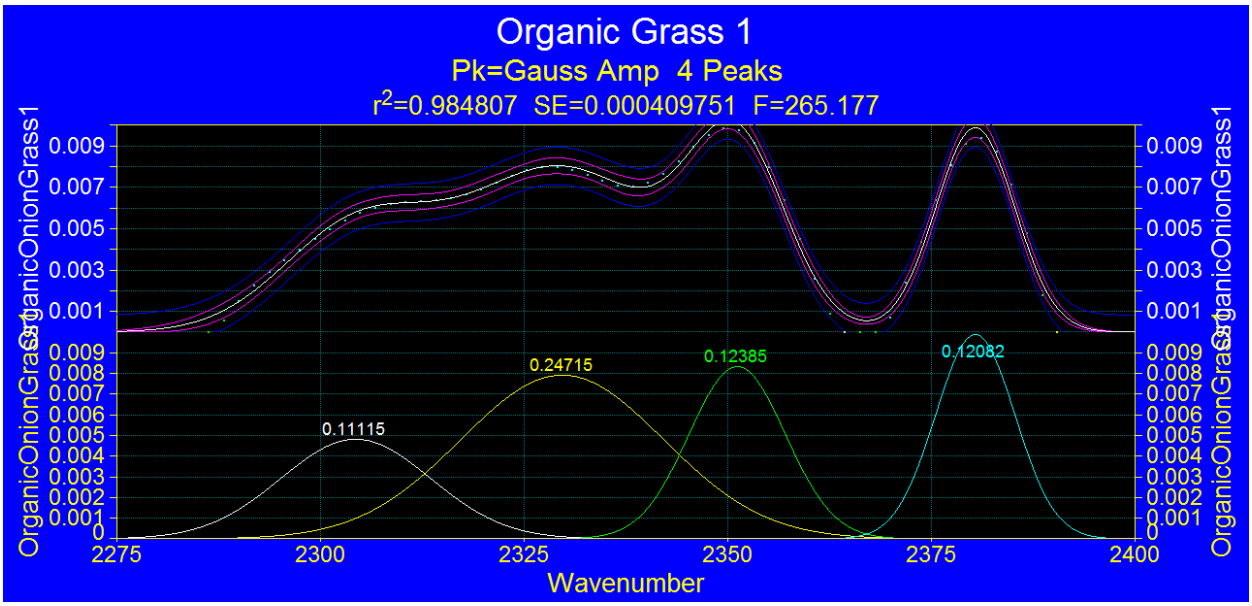

Figure 74 PeakFit model of organic grass sample 1 from the Exoscan data in the 2,300 cm^{-1} region. Upper graph displays the input measured data in white with the 95% confidence interval of the model in pink that consists of the separated peaks shown in the bottom graph.

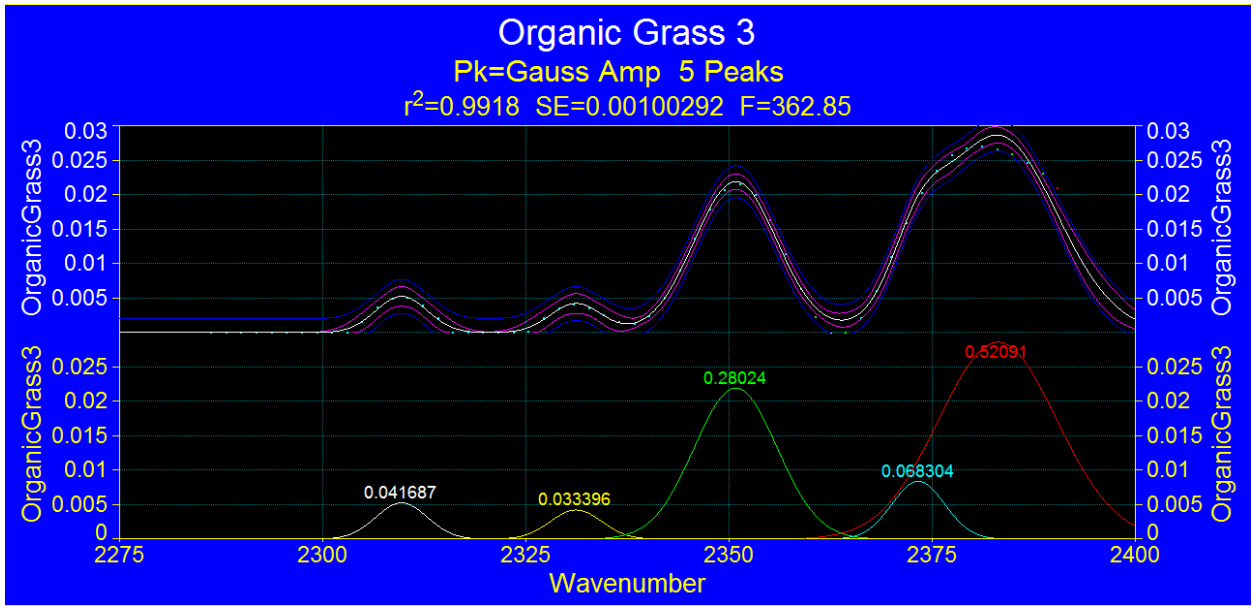

Figure 75 PeakFit model of organic grass sample 3 from the Exoscan data in the 2,300 cm^{-1} region. Upper graph displays the input measured data in white with the 95% confidence interval of the model in pink that consists of the separated peaks shown in the bottom graph.

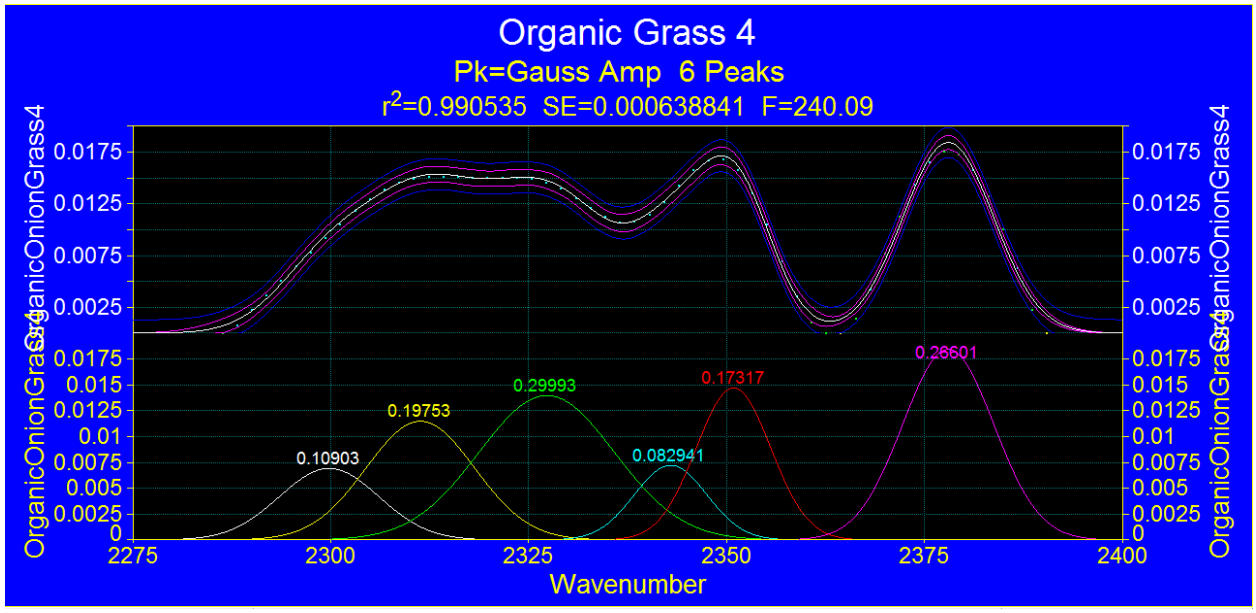

Figure 76 PeakFit model of organic grass sample 4 from the Exoscan data in the 2,300 cm^{-1} region. Upper graph displays the input measured data in white with the 95% confidence interval of the model in pink that consists of the separated peaks shown in the bottom graph.

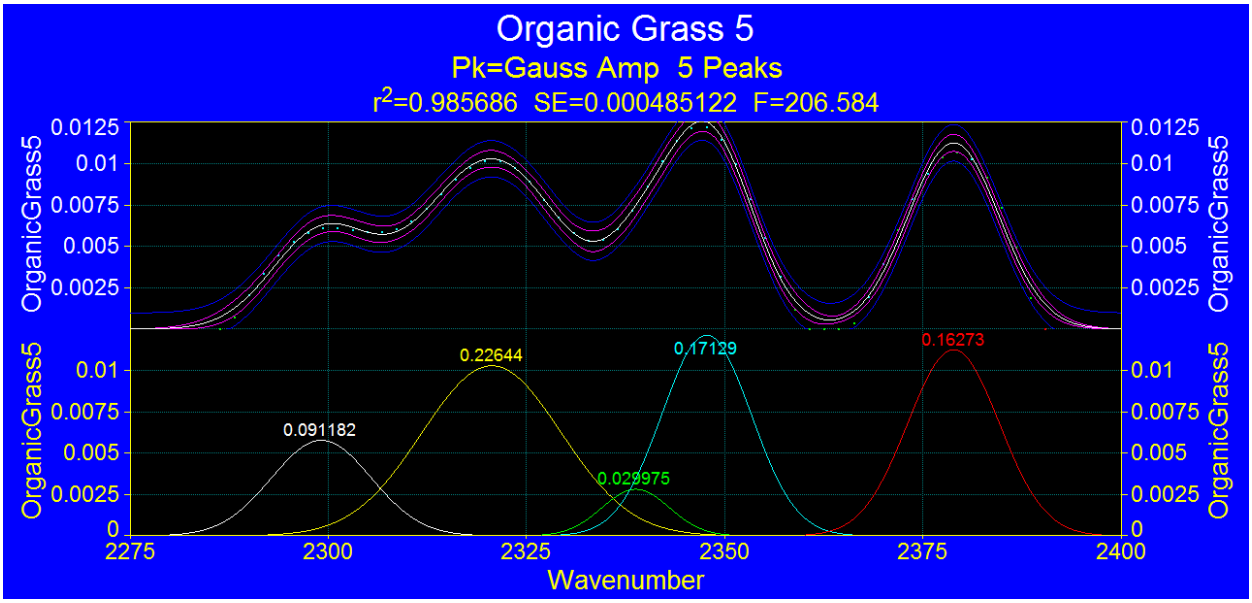

Figure 77 PeakFit model of organic grass sample 5 from the Exoscan data in the 2,300 cm^{-1} region. Upper graph displays the input measured data in white with the 95% confidence interval of the model in pink that consists of the separated peaks shown in the bottom graph.

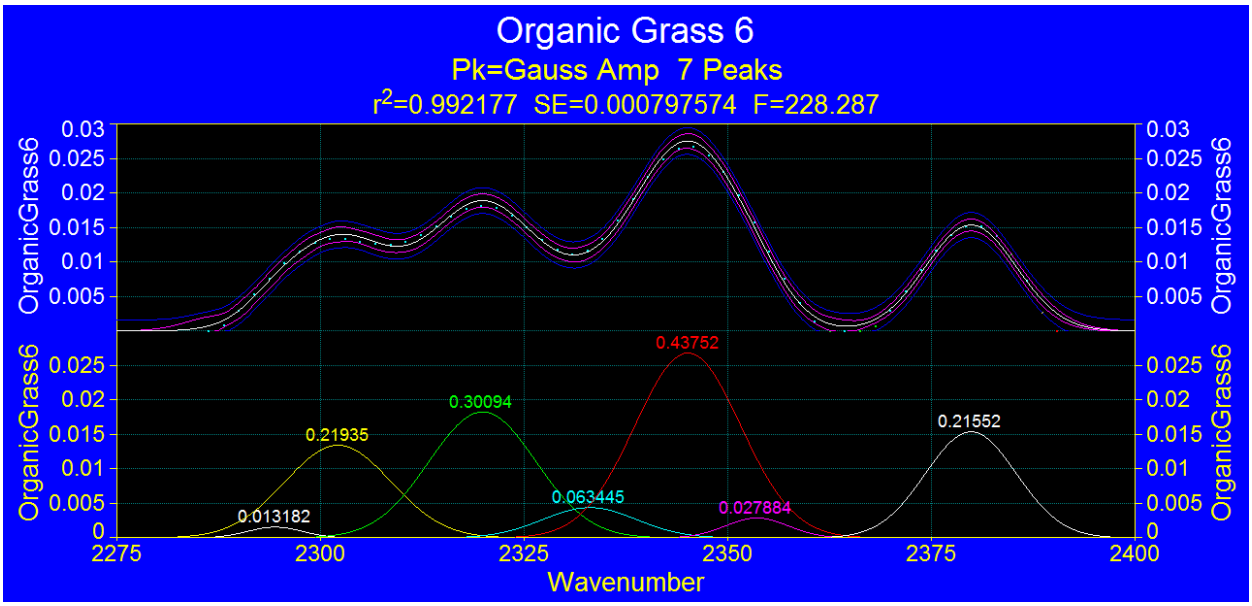

Figure 78 PeakFit model of organic grass sample 6 from the Exoscan data in the 2,300 cm^{-1} region. Upper graph displays the input measured data in white with the 95% confidence interval of the model in pink that consists of the separated peaks shown in the bottom graph.

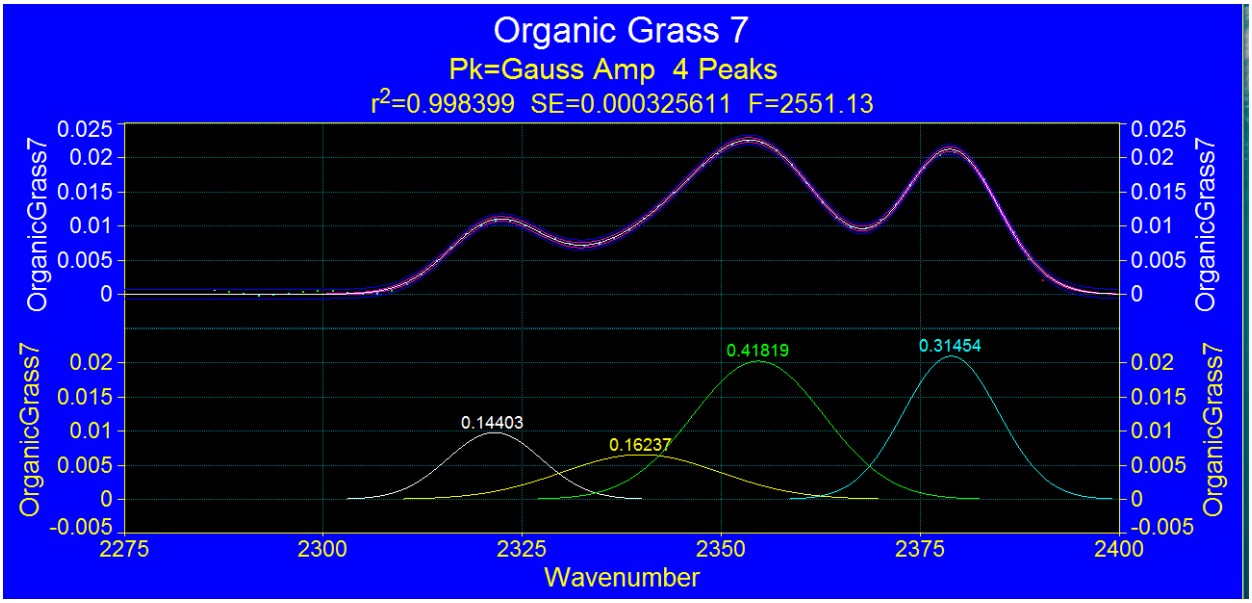

Figure 79 PeakFit model of organic grass sample 7 from the Exoscan data in the 2,300 cm^{-1} region. Upper graph displays the input measured data in white with the 95% confidence interval of the model in pink that consists of the separated peaks shown in the bottom graph.

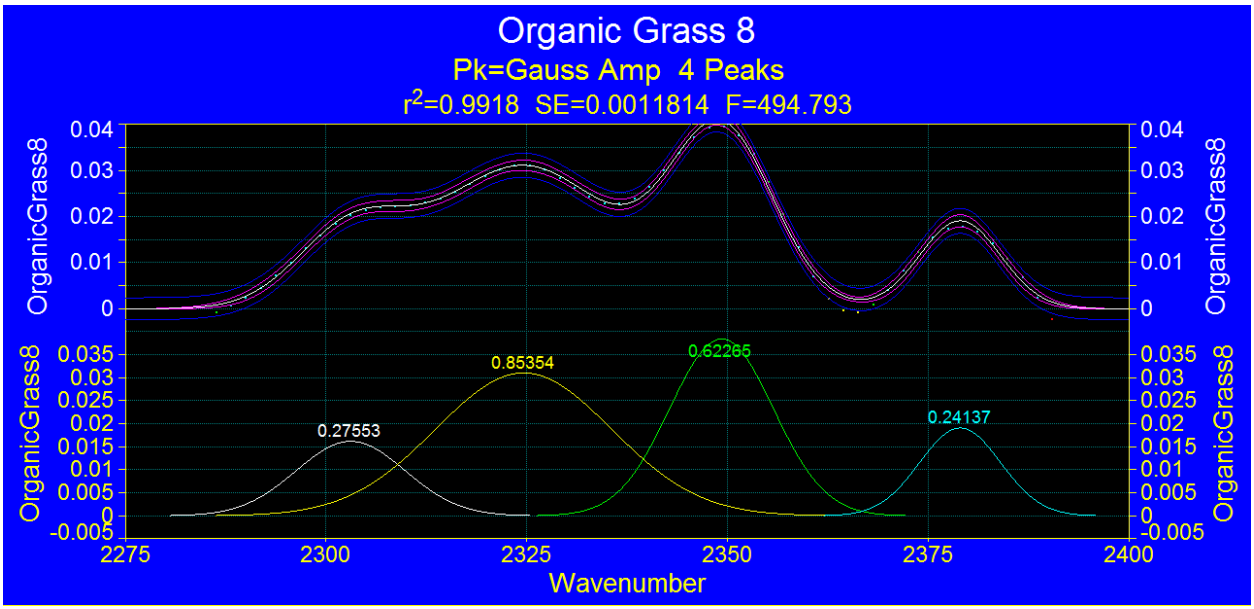

Figure 80 PeakFit model of organic grass sample 8 from the Exoscan data in the 2,300 cm^{-1} region. Upper graph displays the input measured data in white with the 95% confidence interval of the model in pink that consists of the separated peaks shown in the bottom graph.

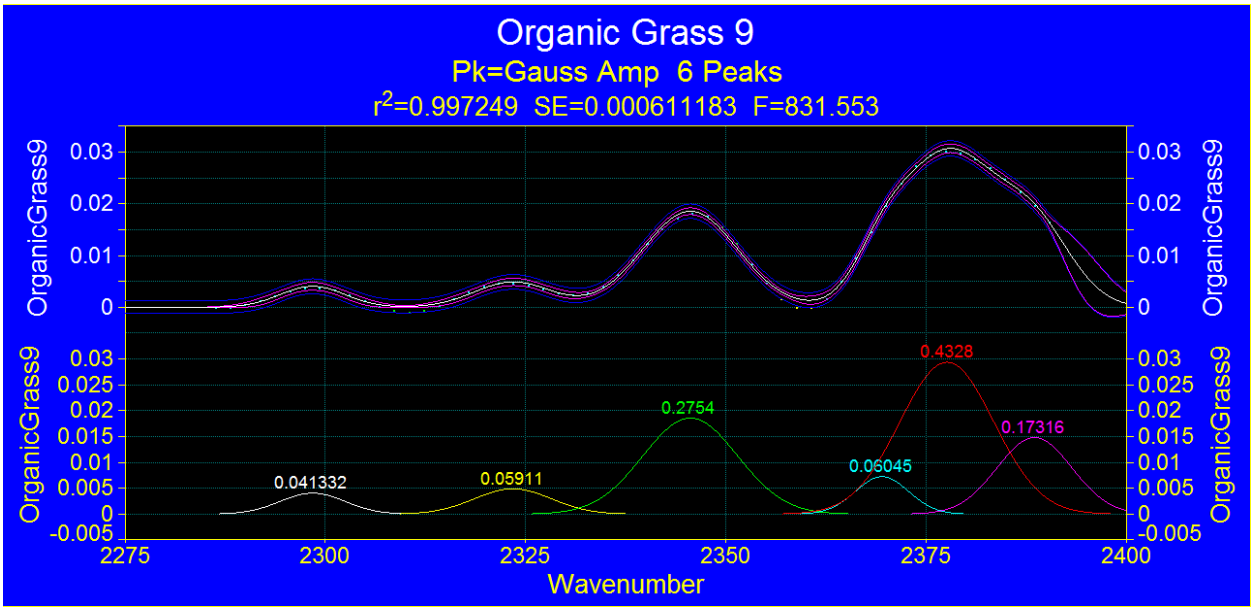

Figure 81 PeakFit model of organic grass sample 9 from the Exoscan data in the 2,300 cm^{-1} region. Upper graph displays the input measured data in white with the 95% confidence interval of the model in pink that consists of the separated peaks shown in the bottom graph.

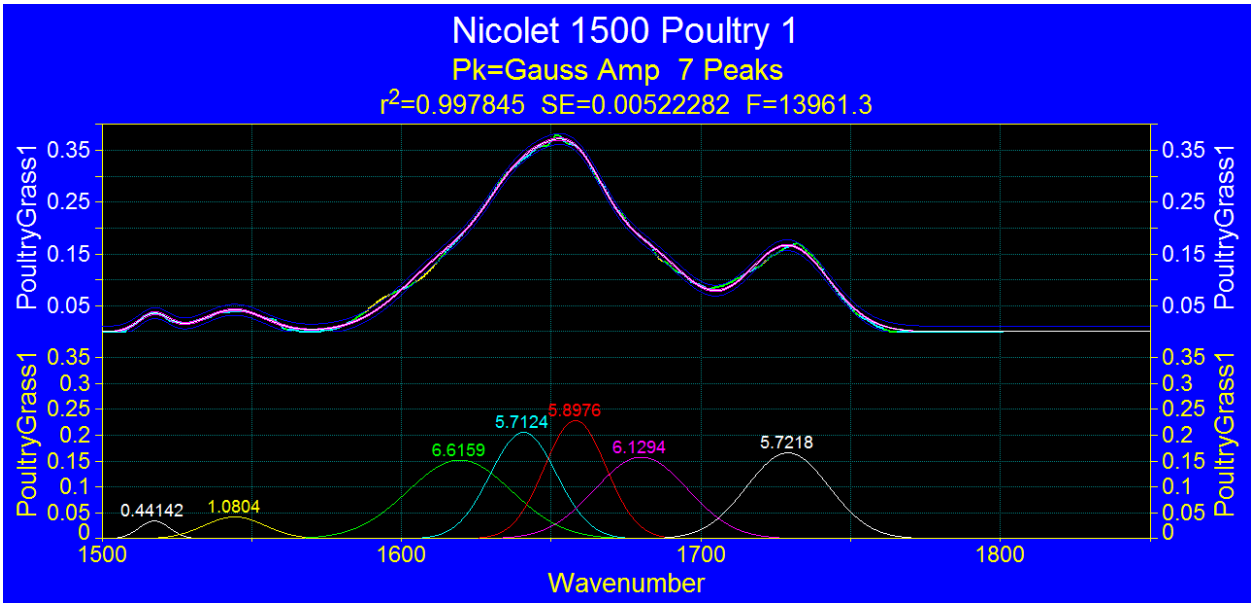

Figure 82 PeakFit model of poultry grass sample 1 from the Nicolet data in the 1,600 cm^{-1} region. Upper graph displays the input measured data in white with the 95% confidence interval of the model in pink that consists of the separated peaks shown in the bottom graph.

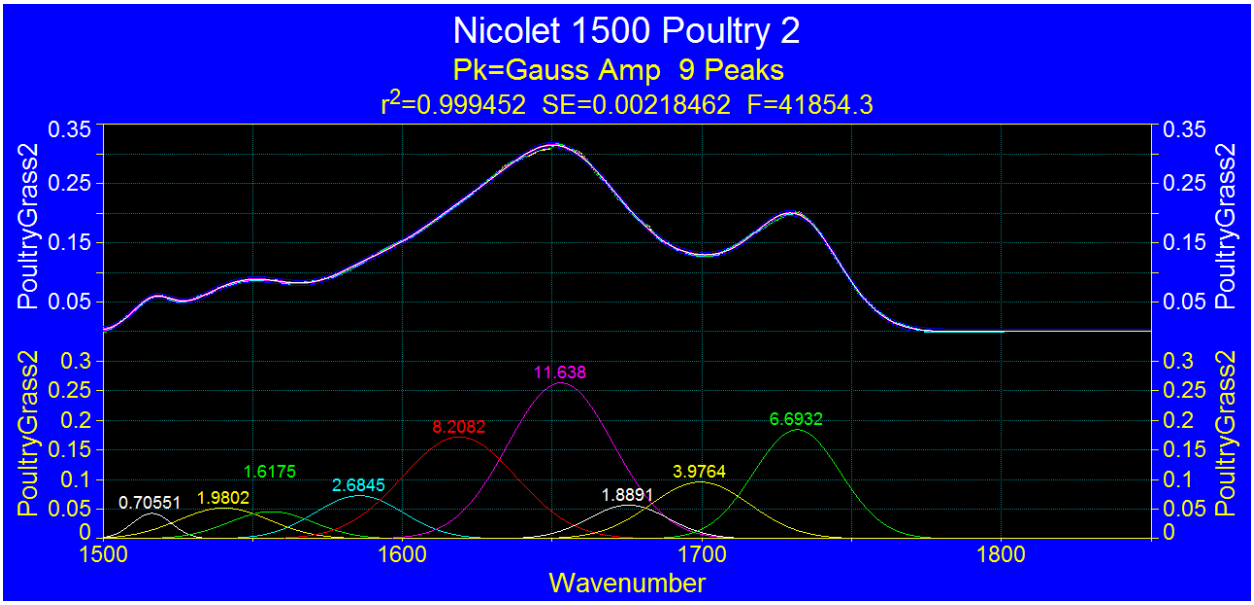

Figure 83 PeakFit model of poultry grass sample 2 from the Nicolet data in the 1,600 cm^{-1} region. Upper graph displays the input measured data in white with the 95% confidence interval of the model in pink that consists of the separated peaks shown in the bottom graph.

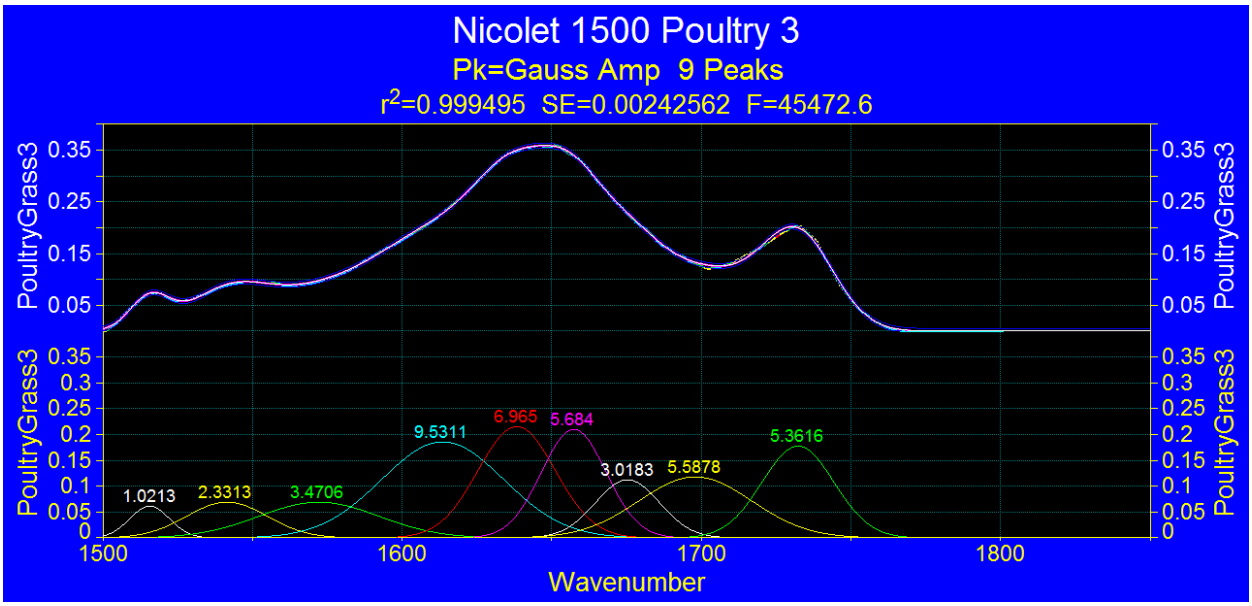

Figure 84 PeakFit model of poultry grass sample 3 from the Nicolet data in the 1,600 cm^{-1} region. Upper graph displays the input measured data in white with the 95% confidence interval of the model in pink that consists of the separated peaks shown in the bottom graph.

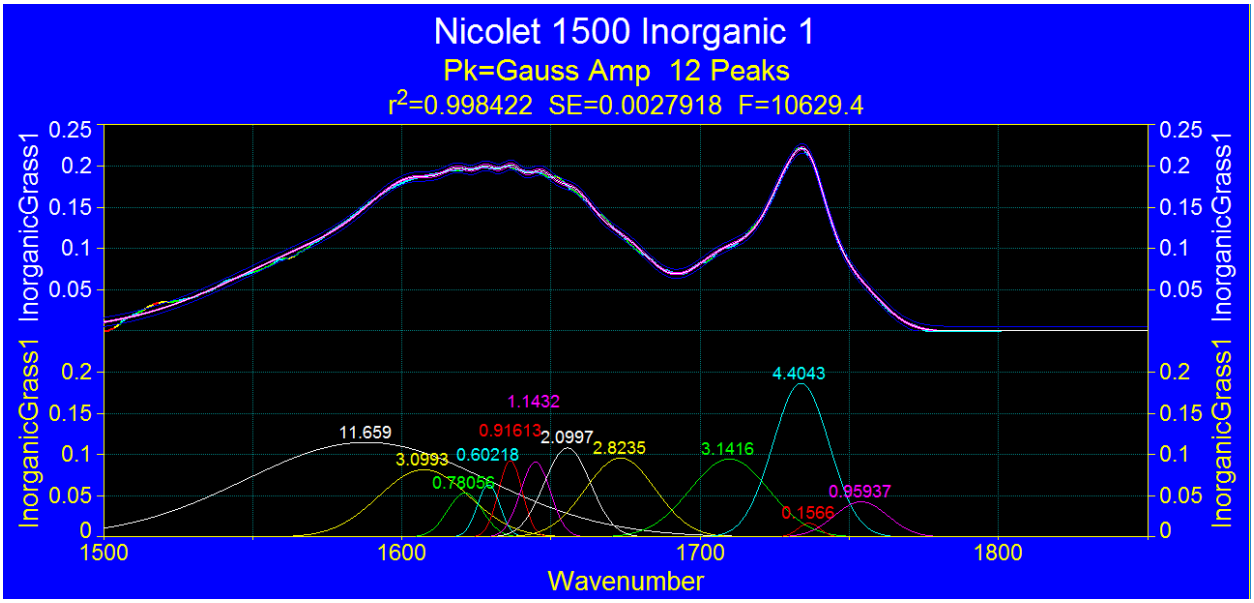

Figure 85 PeakFit model of inorganic grass sample 1 from the Nicolet data in the 1,600 cm^{-1} region. Upper graph displays the input measured data in white with the 95% confidence interval of the model in pink that consists of the separated peaks shown in the bottom graph.

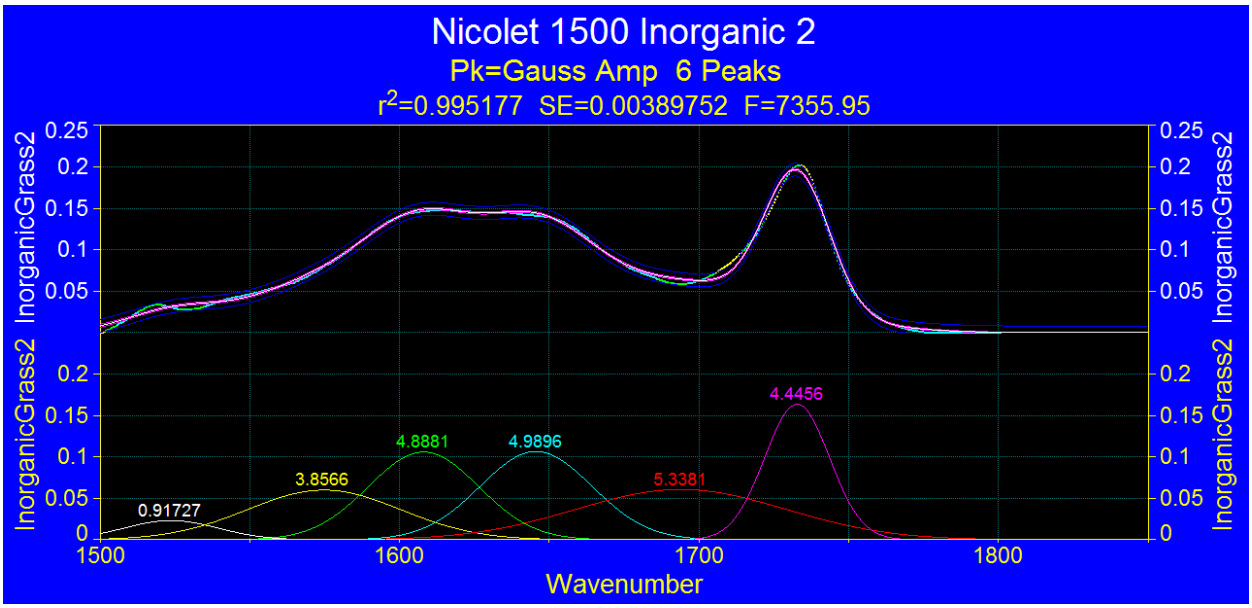

Figure 86 PeakFit model of inorganic grass sample 2 from the Nicolet data in the 1,600 cm^{-1} region. Upper graph displays the input measured data in white with the 95% confidence interval of the model in pink that consists of the separated peaks shown in the bottom graph.

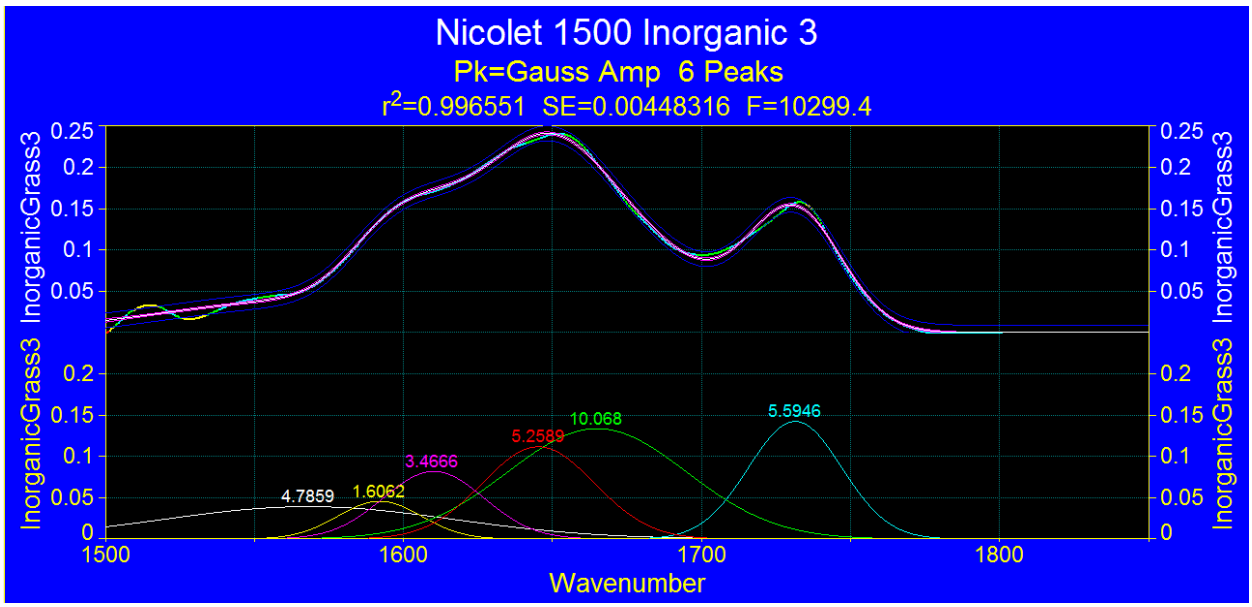

Figure 87 PeakFit model of inorganic grass sample 3 from the Nicolet data in the 1,600 cm^{-1} region. Upper graph displays the input measured data in white with the 95% confidence interval of the model in pink that consists of the separated peaks shown in the bottom graph.

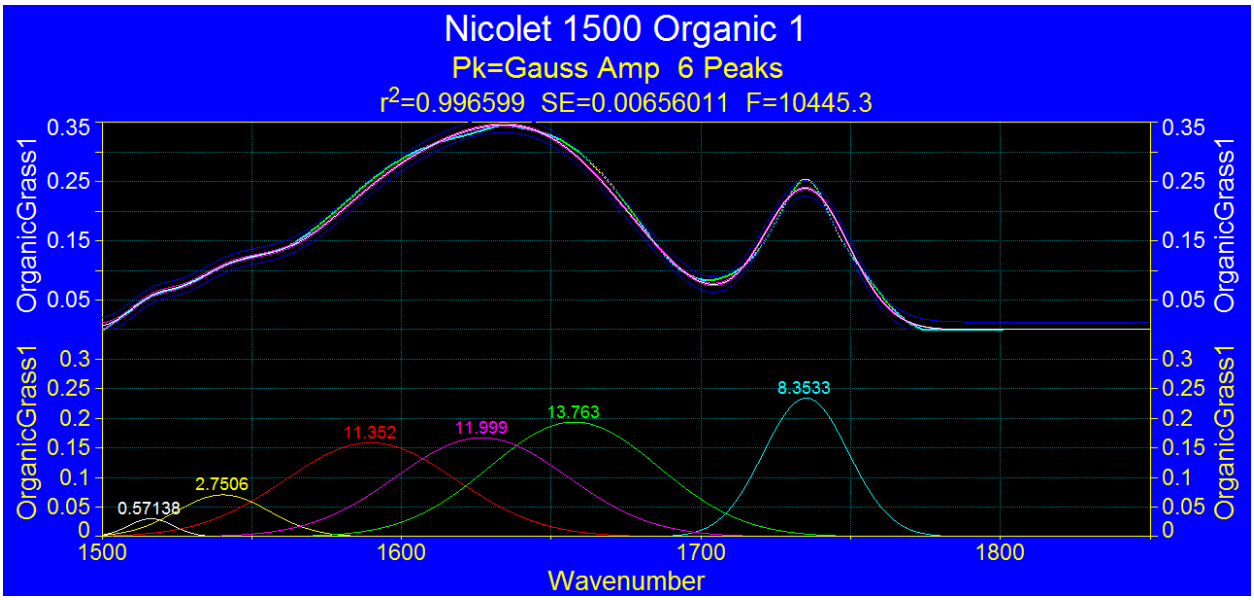

Figure 88 PeakFit model of organic grass sample 1 from the Nicolet data in the 1,600 cm^{-1} region. Upper graph displays the input measured data in white with the 95% confidence interval of the model in pink that consists of the separated peaks shown in the bottom graph.

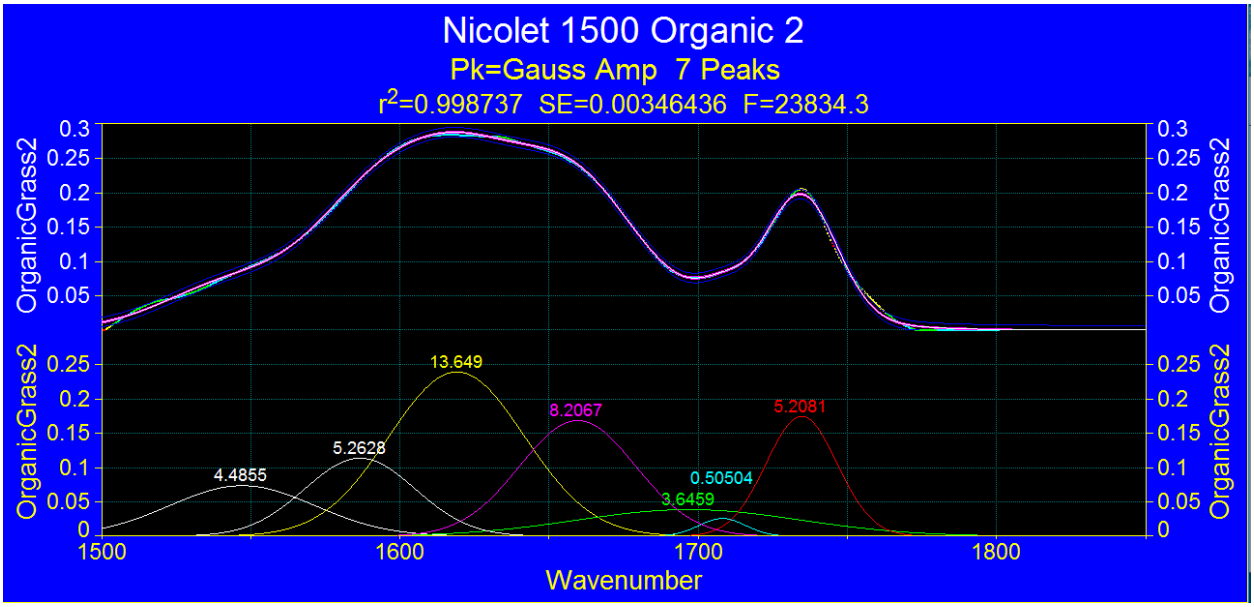

Figure 89 PeakFit model of organic grass sample 2 from the Nicolet data in the 1,600 cm^{-1} region. Upper graph displays the input measured data in white with the 95% confidence interval of the model in pink that consists of the separated peaks shown in the bottom graph.

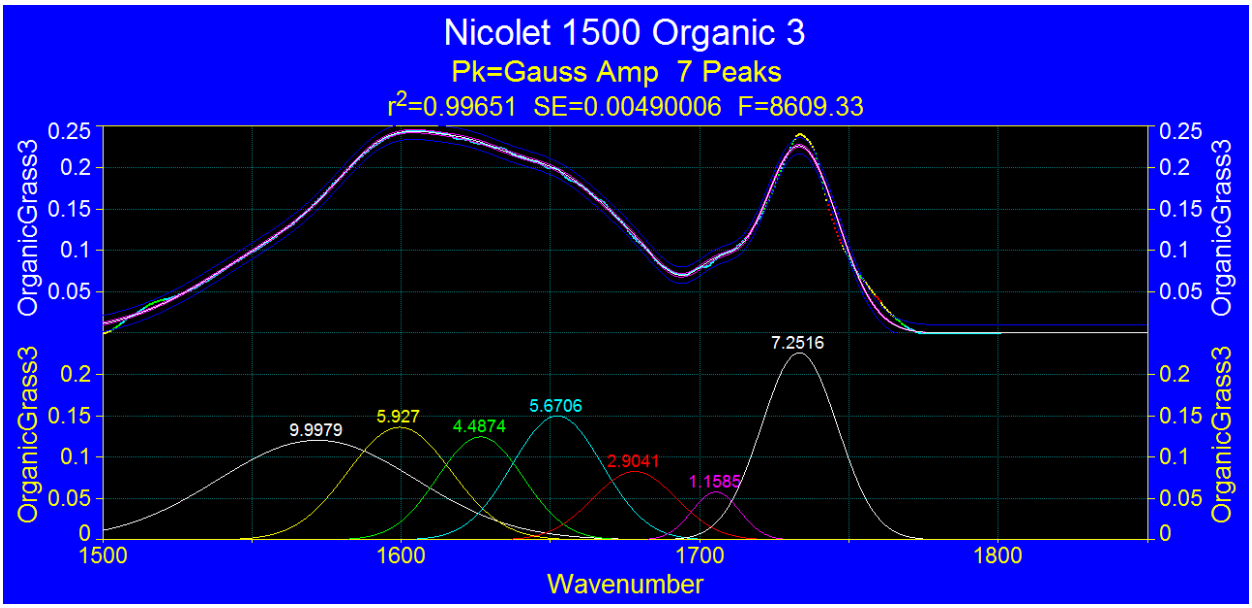

Figure 90 PeakFit model of organic grass sample 3 from the Nicolet data in the 1,600 cm^{-1} region. Upper graph displays the input measured data in white with the 95% confidence interval of the model in pink that consists of the separated peaks shown in the bottom graph.

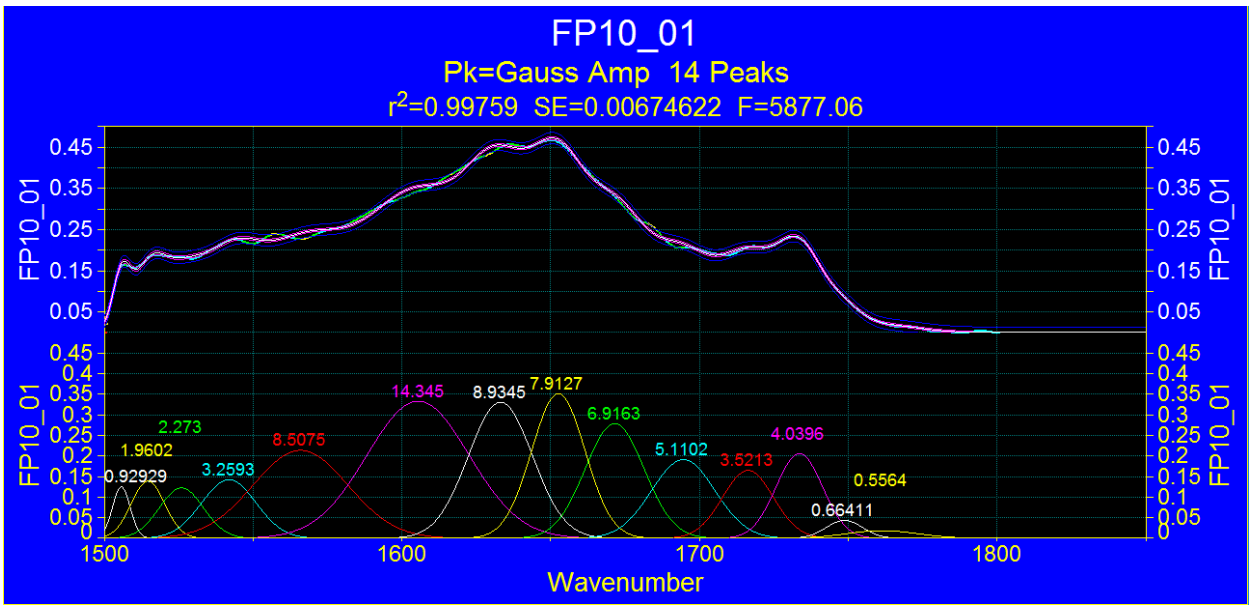

Figure 91 PeakFit model of stream bank grass sample FP10_01 from the Nicolet data in the 1,600 cm^{-1} region. Upper graph displays the input measured data in white with the 95% confidence interval of the model in pink that consists of the separated peaks shown in the bottom graph.

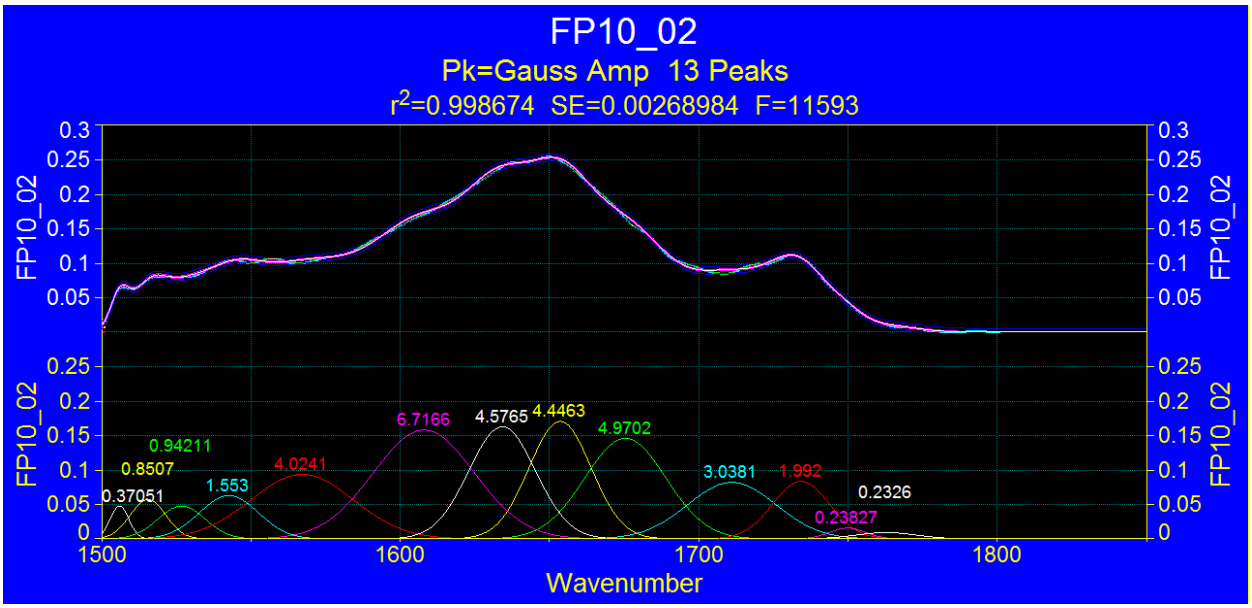

Figure 92 PeakFit model of stream bank grass sample FP10_02 from the Nicolet data in the 1,600 cm^{-1} region. Upper graph displays the input measured data in white with the 95% confidence interval of the model in pink that consists of the separated peaks shown in the bottom graph.

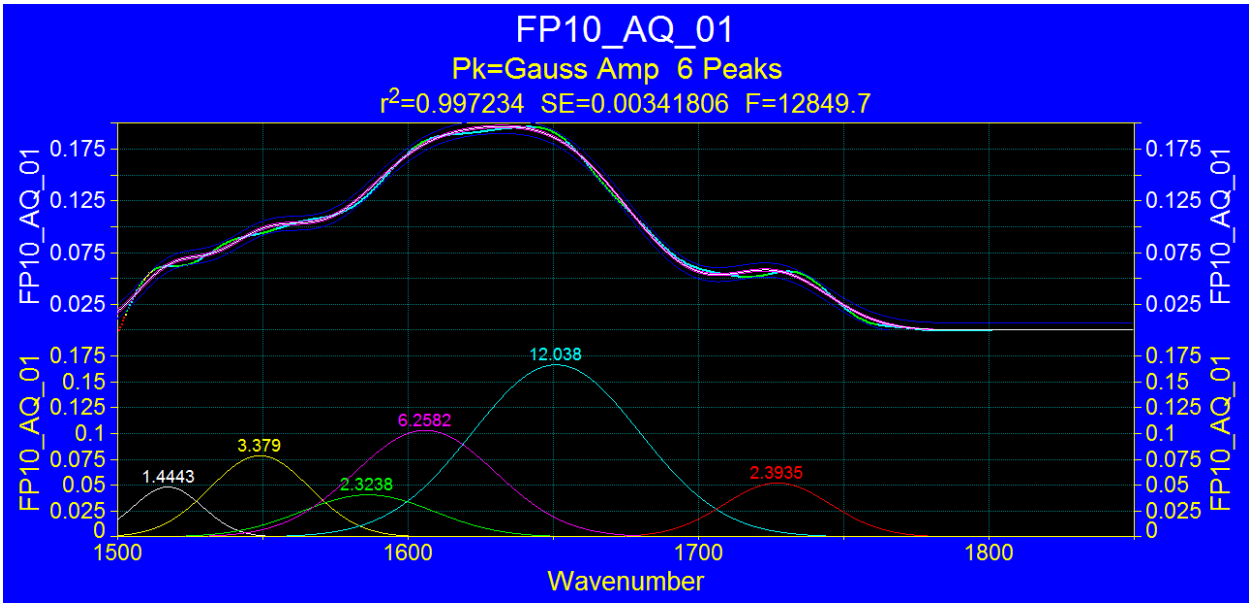

Figure 93 PeakFit model of stream bank grass sample FP10_AQ_01 from the Nicolet data in the 1,600 cm^{-1} region. Upper graph displays the input measured data in white with the 95% confidence interval of the model in pink that consists of the separated peaks shown in the bottom graph.

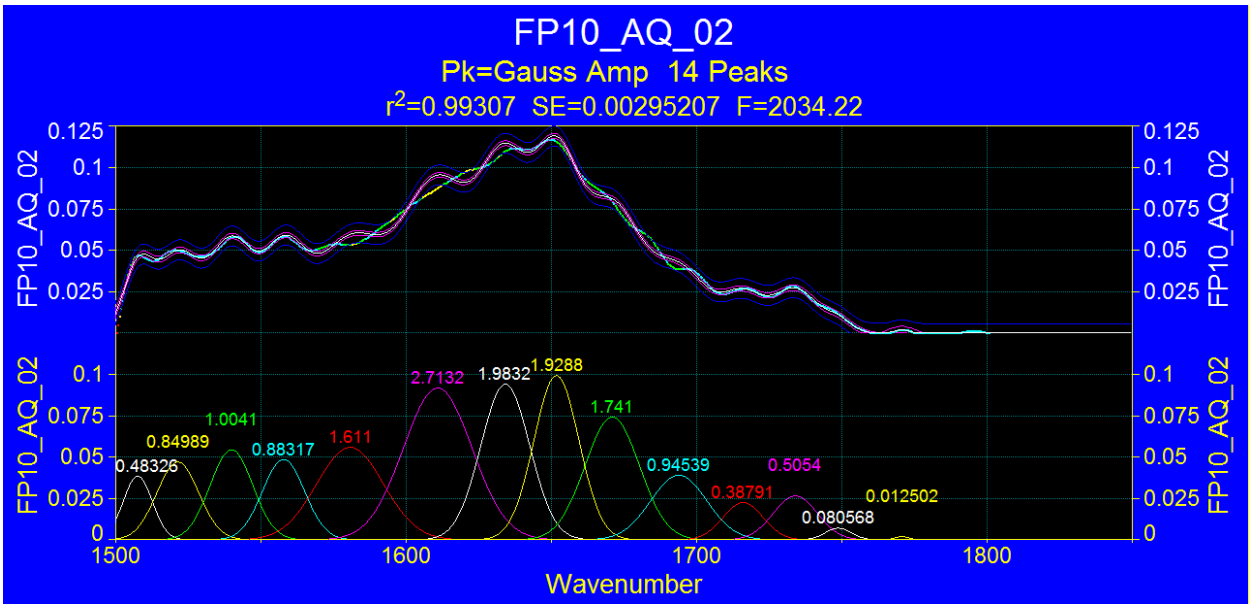

Figure 94 PeakFit model of stream bank grass sample FP10_AQ_02 from the Nicolet data in the 1,600 cm^{-1} region. Upper graph displays the input measured data in white with the 95% confidence interval of the model in pink that consists of the separated peaks shown in the bottom graph.

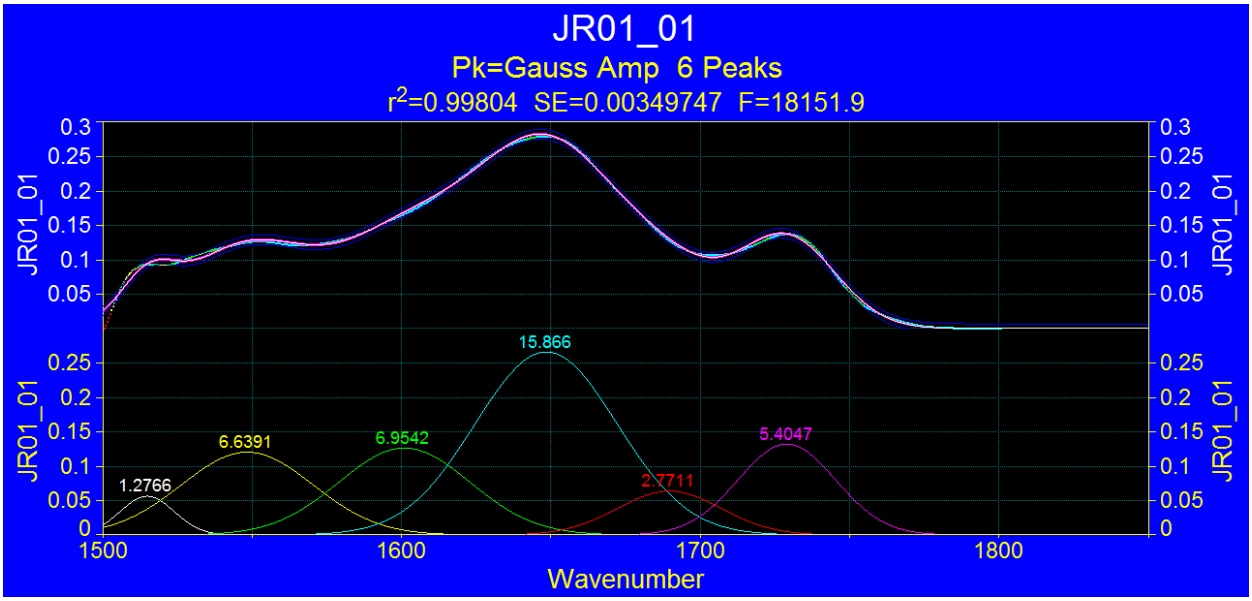

Figure 95 PeakFit model of stream bank grass sample JR01_01 from the Nicolet data in the 1,600 cm^{-1} region. Upper graph displays the input measured data in white with the 95% confidence interval of the model in pink that consists of the separated peaks shown in the bottom graph.

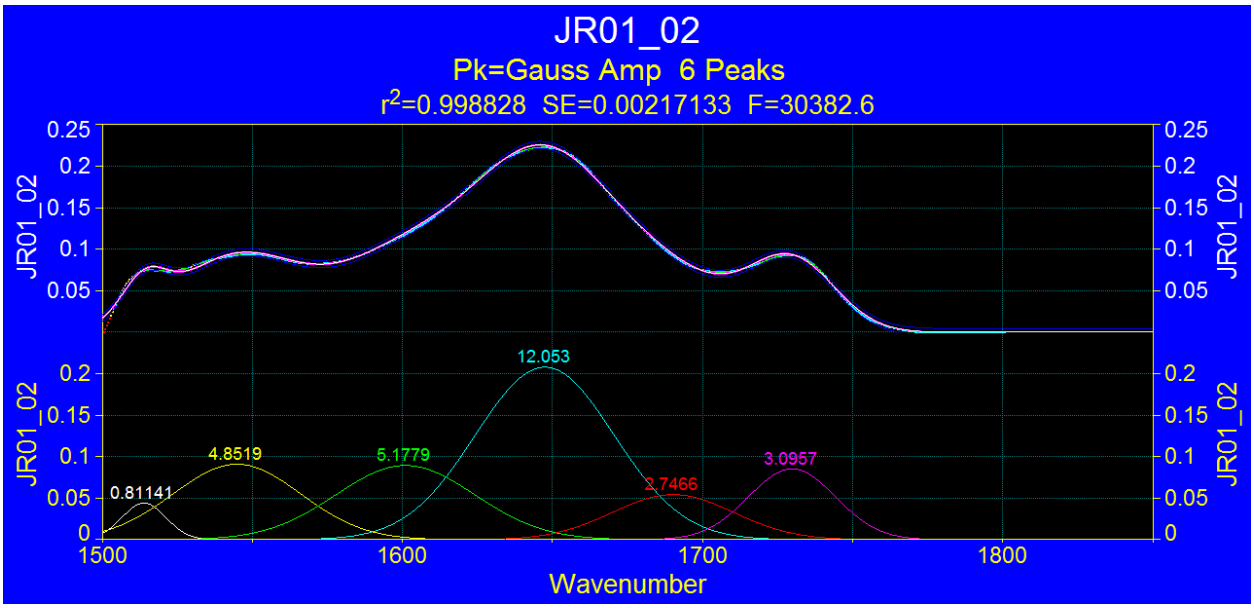

Figure 96 PeakFit model of stream bank grass sample JR01_02 from the Nicolet data in the 1,600 cm^{-1} region. Upper graph displays the input measured data in white with the 95% confidence interval of the model in pink that consists of the separated peaks shown in the bottom graph.

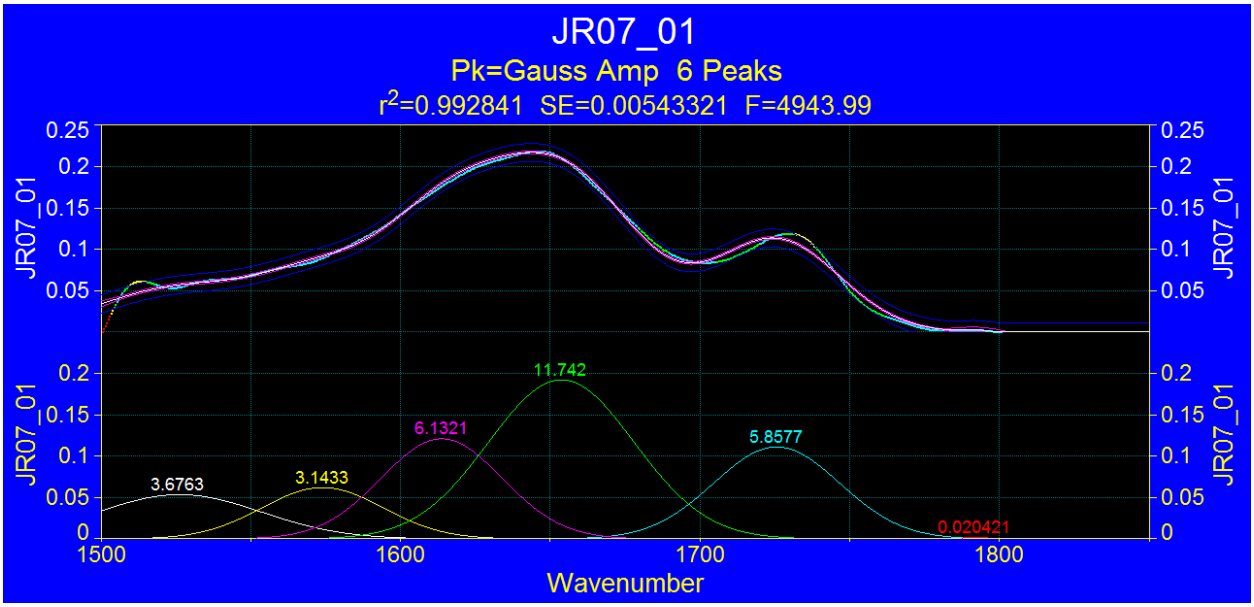

Figure 97 PeakFit model of stream bank grass sample JR07_01 from the Nicolet data in the 1,600 cm^{-1} region. Upper graph displays the input measured data in white with the 95% confidence interval of the model in pink that consists of the separated peaks shown in the bottom graph.

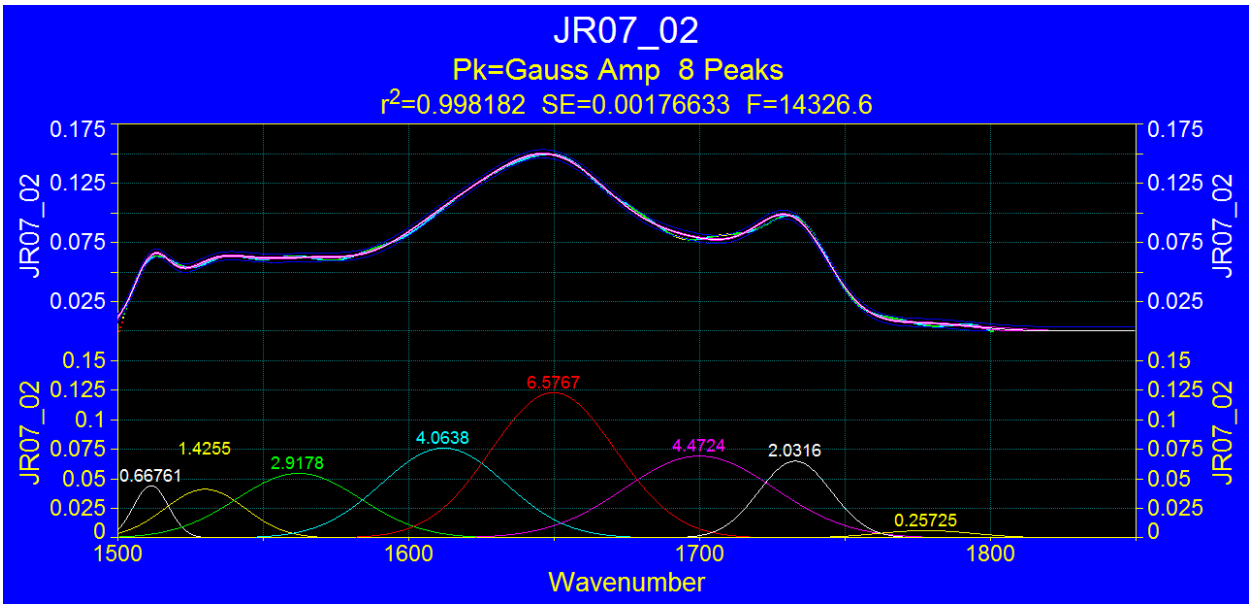

Figure 98 PeakFit model of stream bank grass sample JR07_02 from the Nicolet data in the 1,600 cm^{-1} region. Upper graph displays the input measured data in white with the 95% confidence interval of the model in pink that consists of the separated peaks shown in the bottom graph.

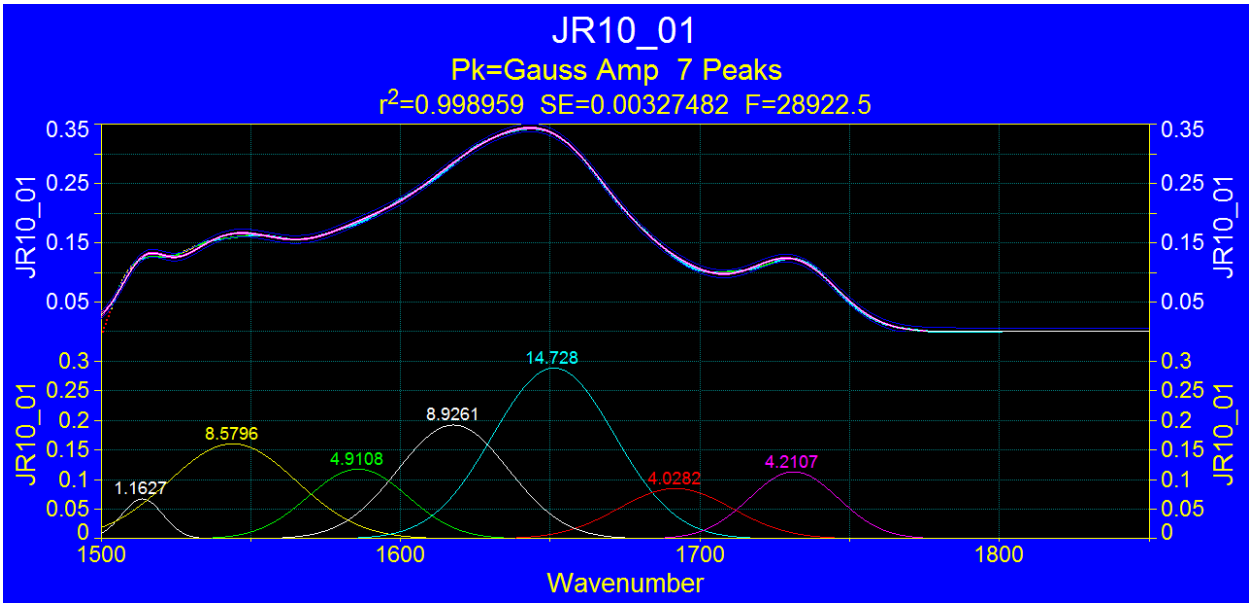

Figure 99 PeakFit model of stream bank grass sample JR10_01 from the Nicolet data in the 1,600 cm^{-1} region. Upper graph displays the input measured data in white with the 95% confidence interval of the model in pink that consists of the separated peaks shown in the bottom graph.

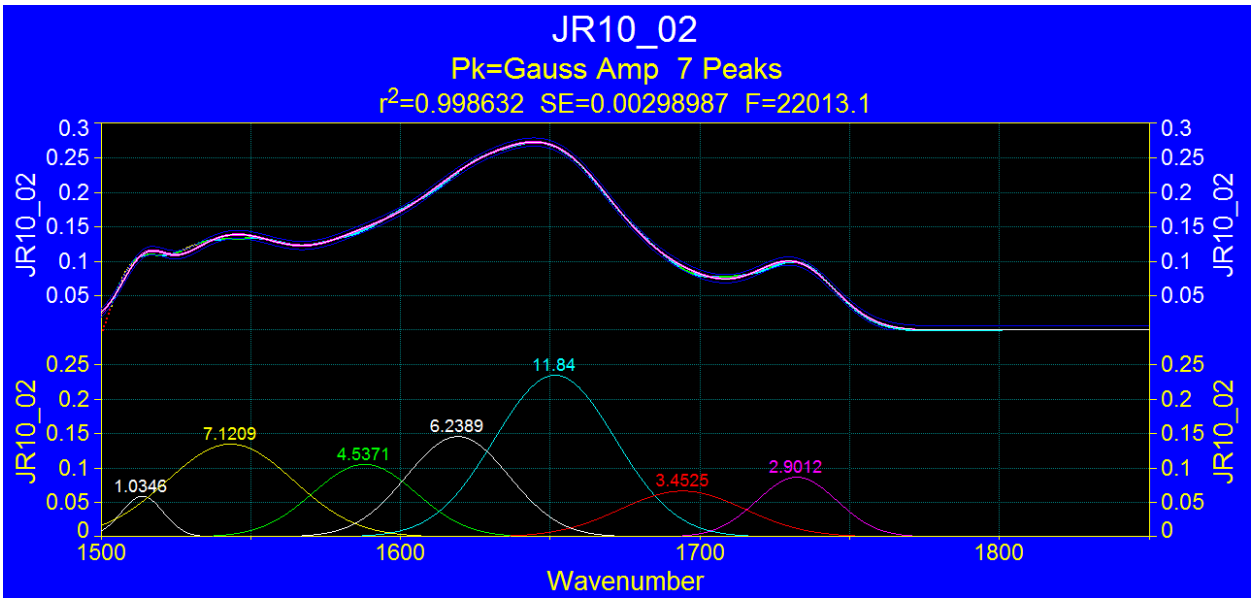

Figure 100 PeakFit model of stream bank grass sample JR10_02 from the Nicolet data in the 1,600 cm^{-1} region. Upper graph displays the input measured data in white with the 95% confidence interval of the model in pink that consists of the separated peaks shown in the bottom graph.

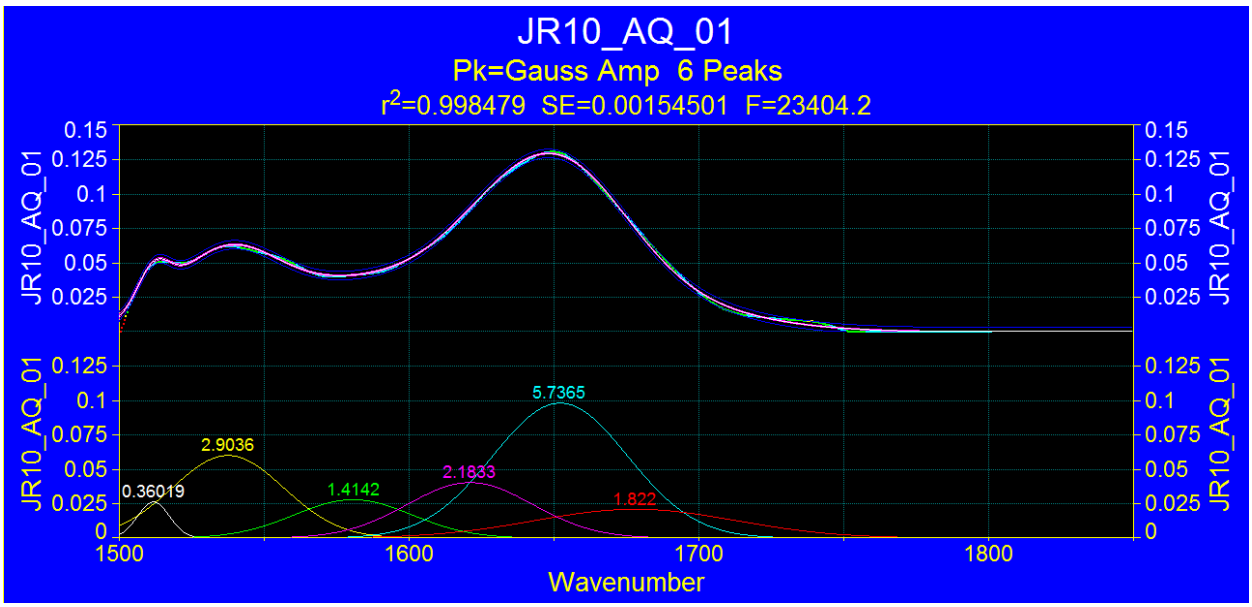

Figure 101 PeakFit model of stream bank grass sample JR10_AQ_01 from the Nicolet data in the 1,600 cm^{-1} region. Upper graph displays the input measured data in white with the 95% confidence interval of the model in pink that consists of the separated peaks shown in the bottom graph.

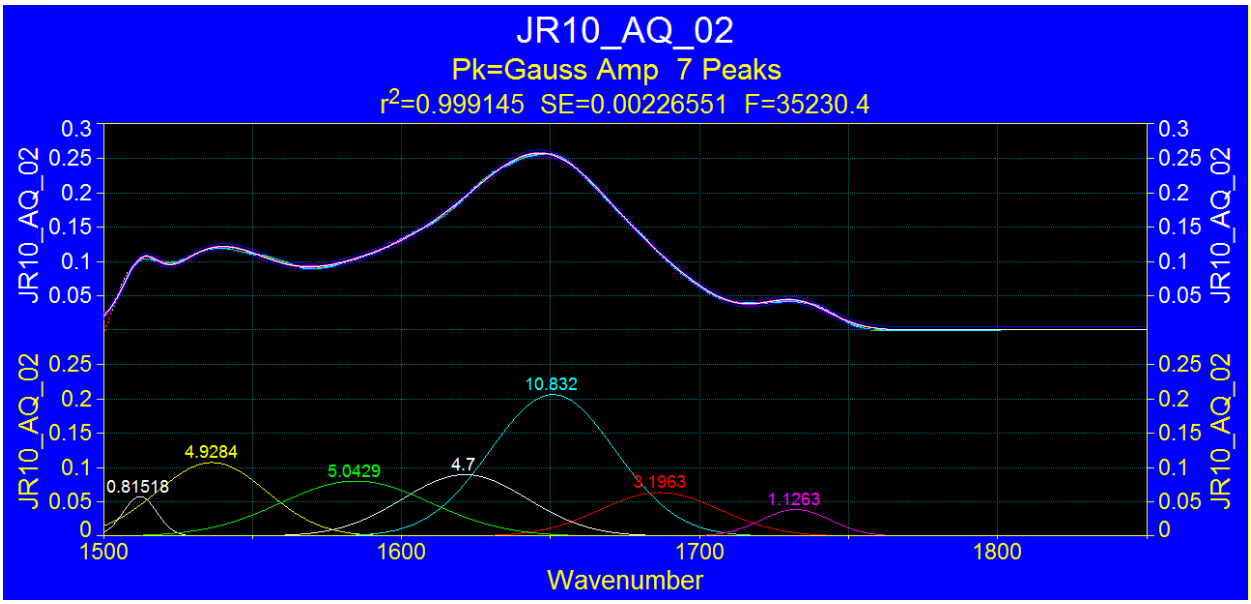

Figure 102 PeakFit model of stream bank grass sample JR10_AQ_02 from the Nicolet data in the 1,600 cm^{-1} region. Upper graph displays the input measured data in white with the 95% confidence interval of the model in pink that consists of the separated peaks shown in the bottom graph.

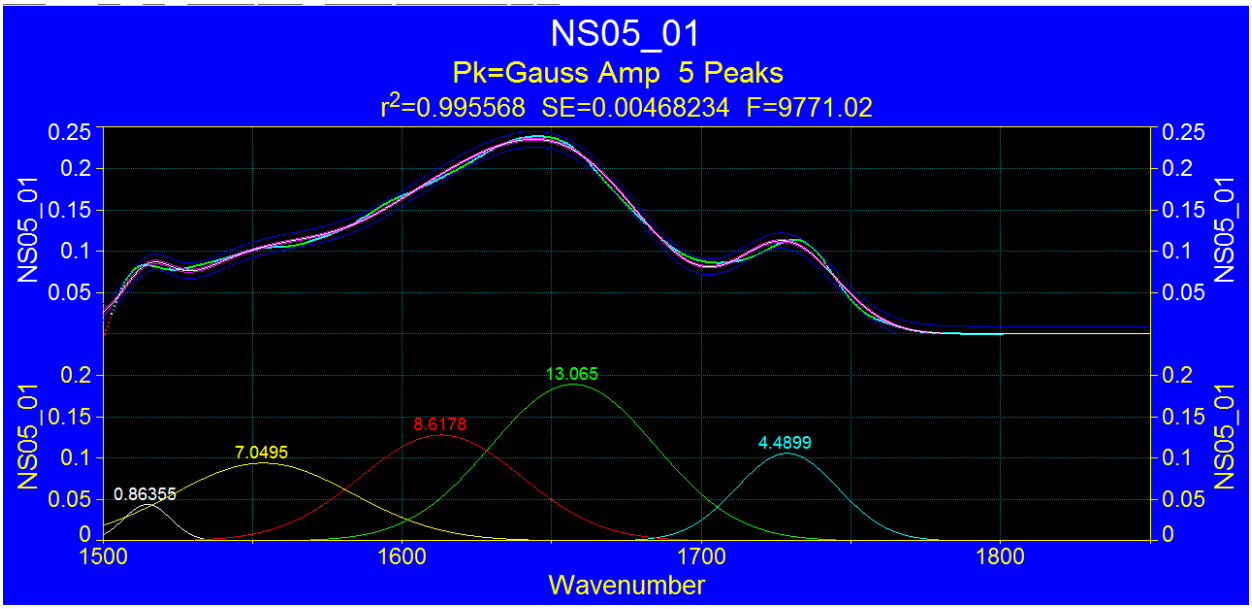

Figure 103 PeakFit model of stream bank grass sample NS05_01 from the Nicolet data in the 1,600 cm^{-1} region. Upper graph displays the input measured data in white with the 95% confidence interval of the model in pink that consists of the separated peaks shown in the bottom graph.

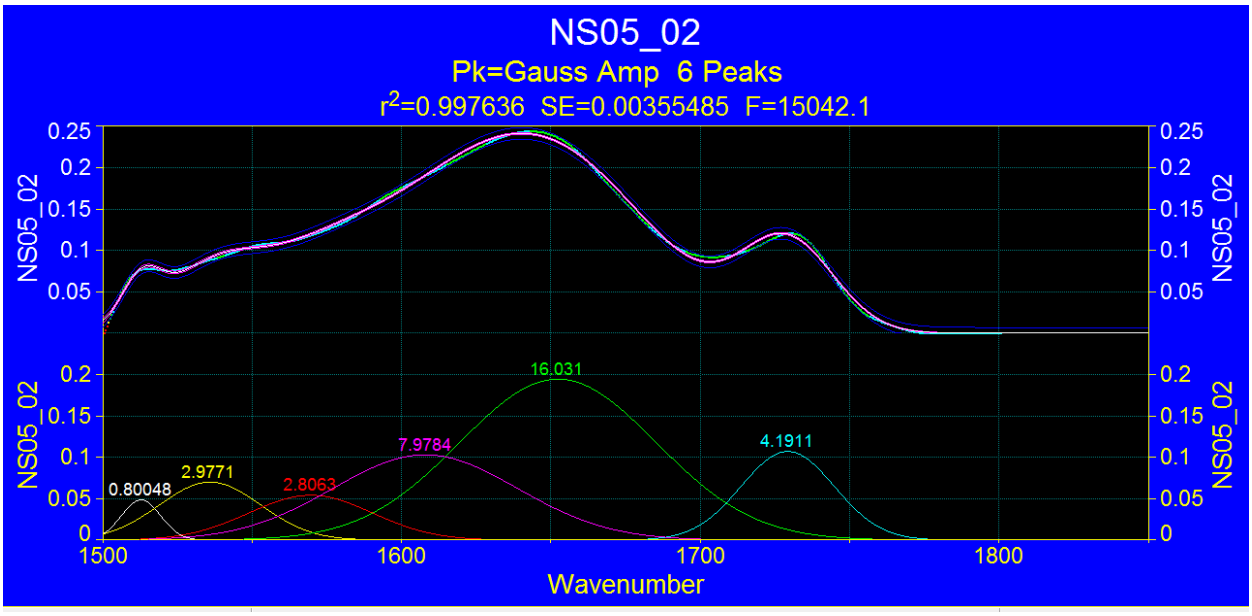

Figure 104 PeakFit model of stream bank grass sample NS05_02 from the Nicolet data in the 1,600 cm^{-1} region. Upper graph displays the input measured data in white with the 95% confidence interval of the model in pink that consists of the separated peaks shown in the bottom graph.

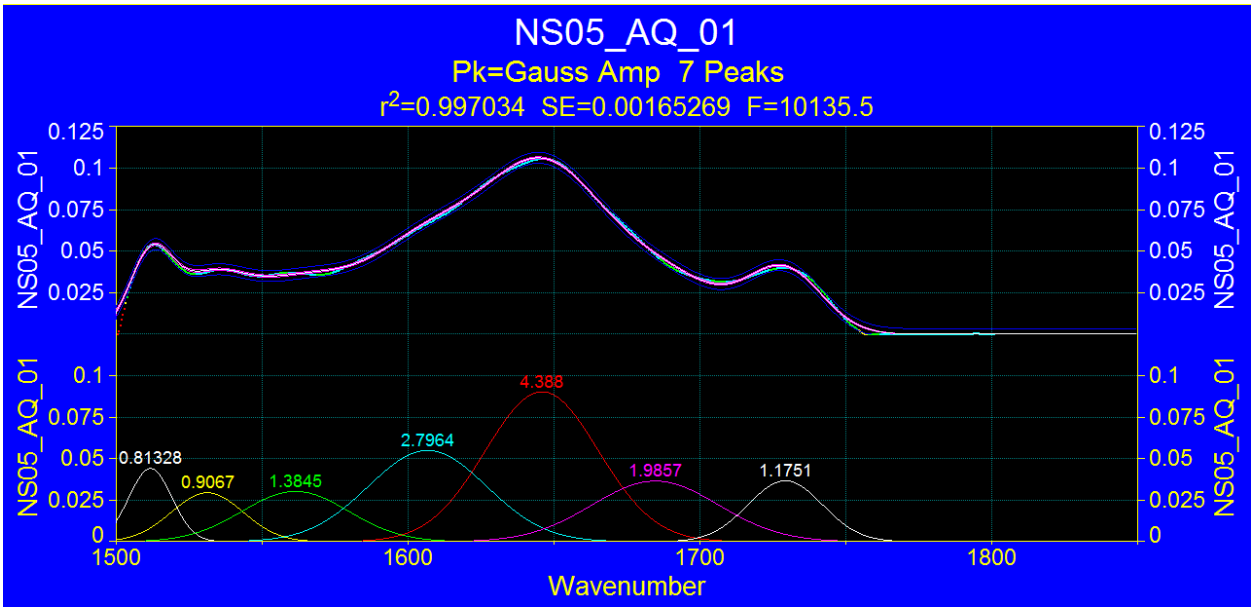

Figure 105 PeakFit model of stream bank grass sample NS05_AQ_01 from the Nicolet data in the 1,600 cm^{-1} region. Upper graph displays the input measured data in white with the 95% confidence interval of the model in pink that consists of the separated peaks shown in the bottom graph.

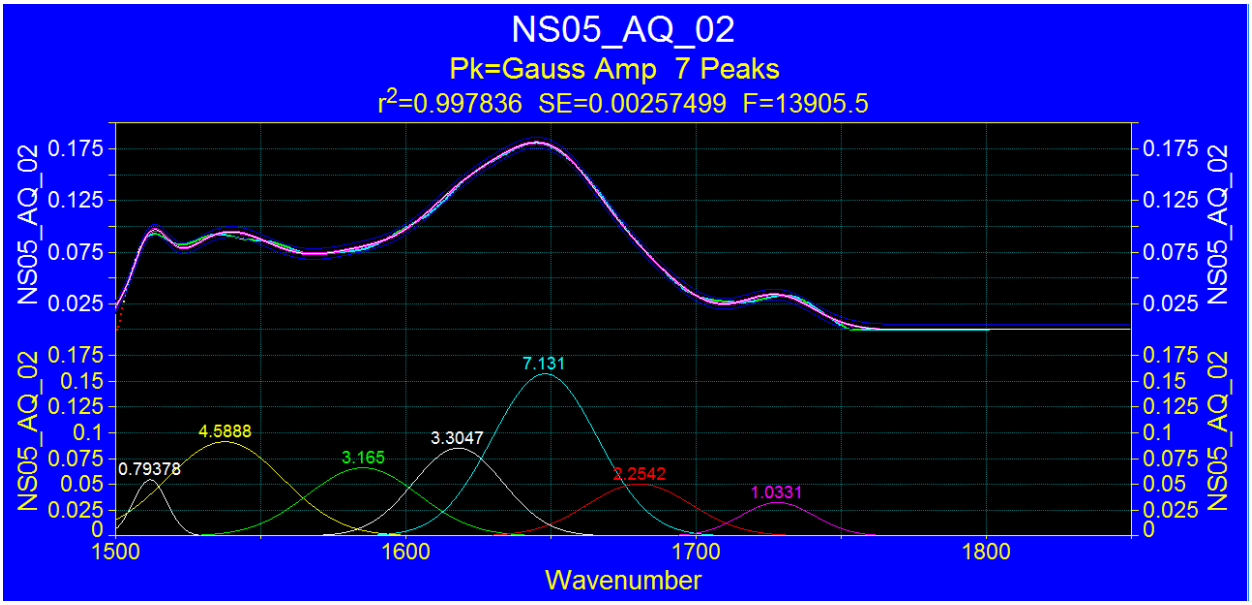

Figure 106 PeakFit model of stream bank grass sample NS05_AQ_02 from the Nicolet data in the 1,600 cm^{-1} region. Upper graph displays the input measured data in white with the 95% confidence interval of the model in pink that consists of the separated peaks shown in the bottom graph.

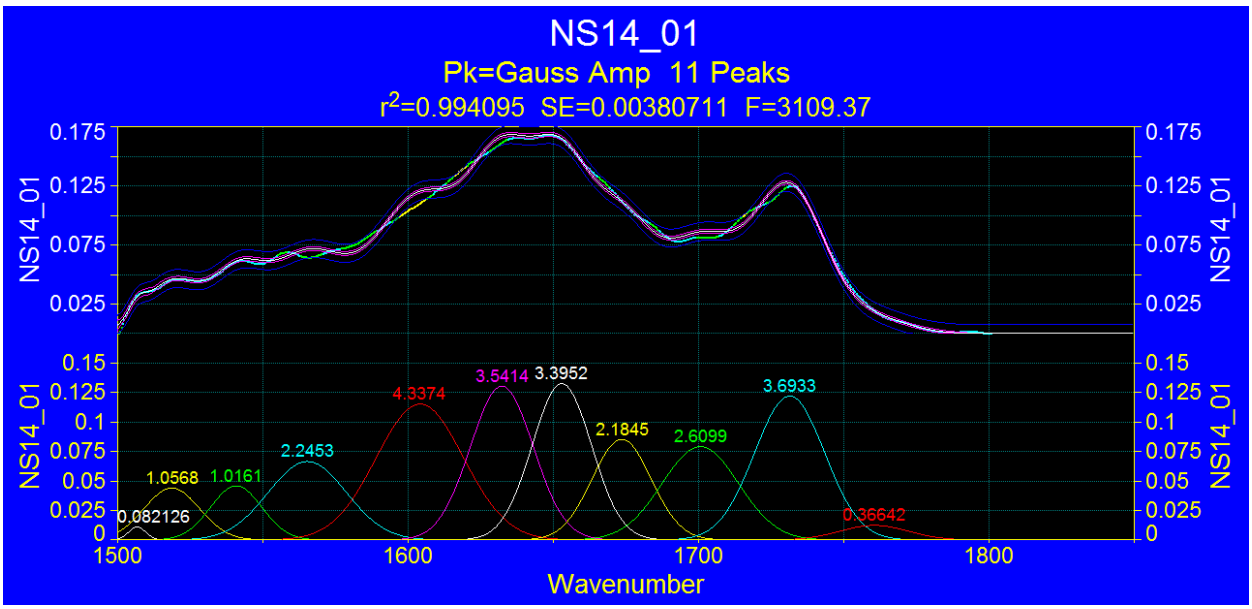

Figure 107 PeakFit model of stream bank grass sample NS14_01 from the Nicolet data in the 1,600 cm^{-1} region. Upper graph displays the input measured data in white with the 95% confidence interval of the model in pink that consists of the separated peaks shown in the bottom graph.

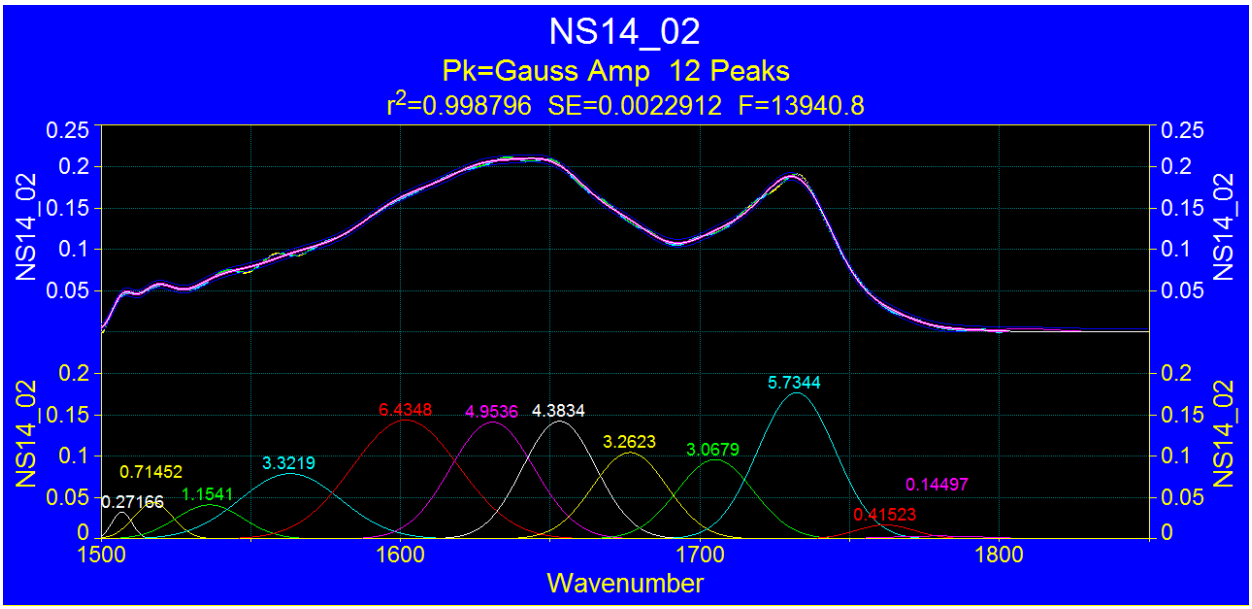

Figure 108 PeakFit model of stream bank grass sample NS14_02 from the Nicolet data in the 1,600 cm^{-1} region. Upper graph displays the input measured data in white with the 95% confidence interval of the model in pink that consists of the separated peaks shown in the bottom graph.

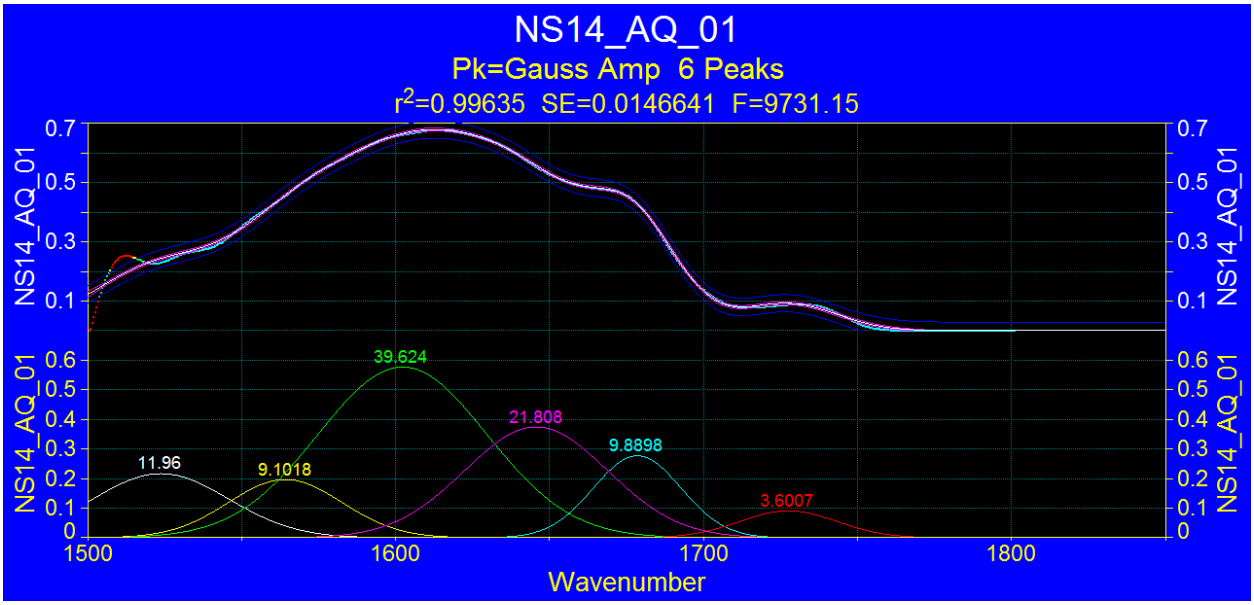

Figure 109 PeakFit model of stream bank grass sample NS14_AQ_01 from the Nicolet data in the 1,600 cm^{-1} region. Upper graph displays the input measured data in white with the 95% confidence interval of the model in pink that consists of the separated peaks shown in the bottom graph.

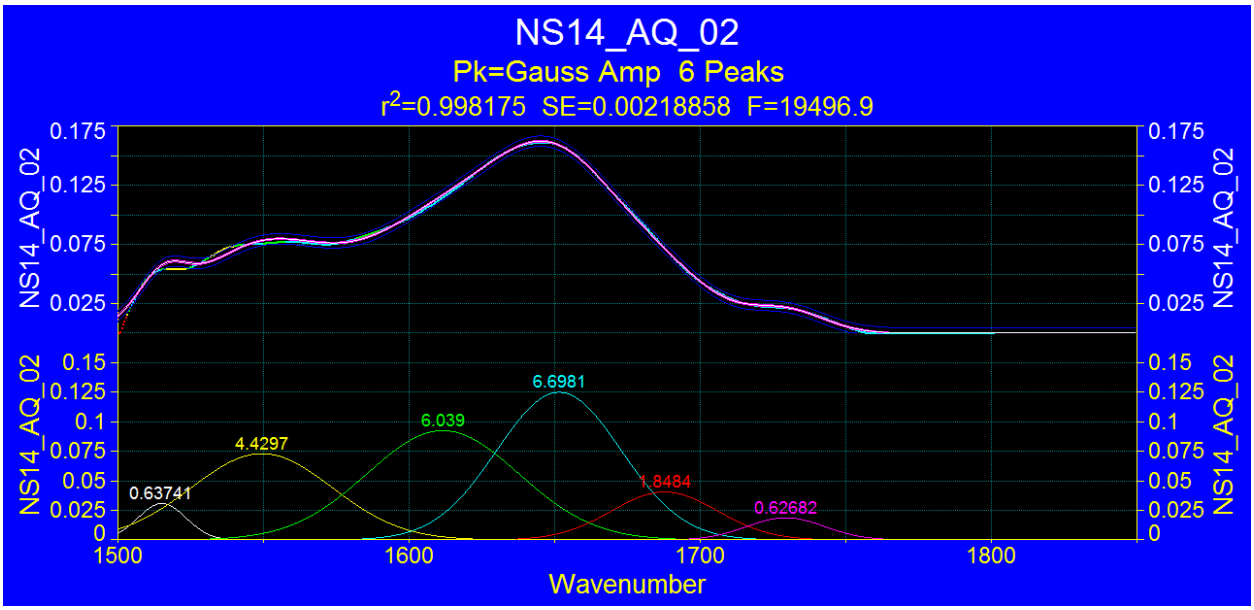

Figure 110 PeakFit model of stream bank grass sample NS14_AQ_02 from the Nicolet data in the 1,600 cm^{-1} region. Upper graph displays the input measured data in white with the 95% confidence interval of the model in pink that consists of the separated peaks shown in the bottom graph.

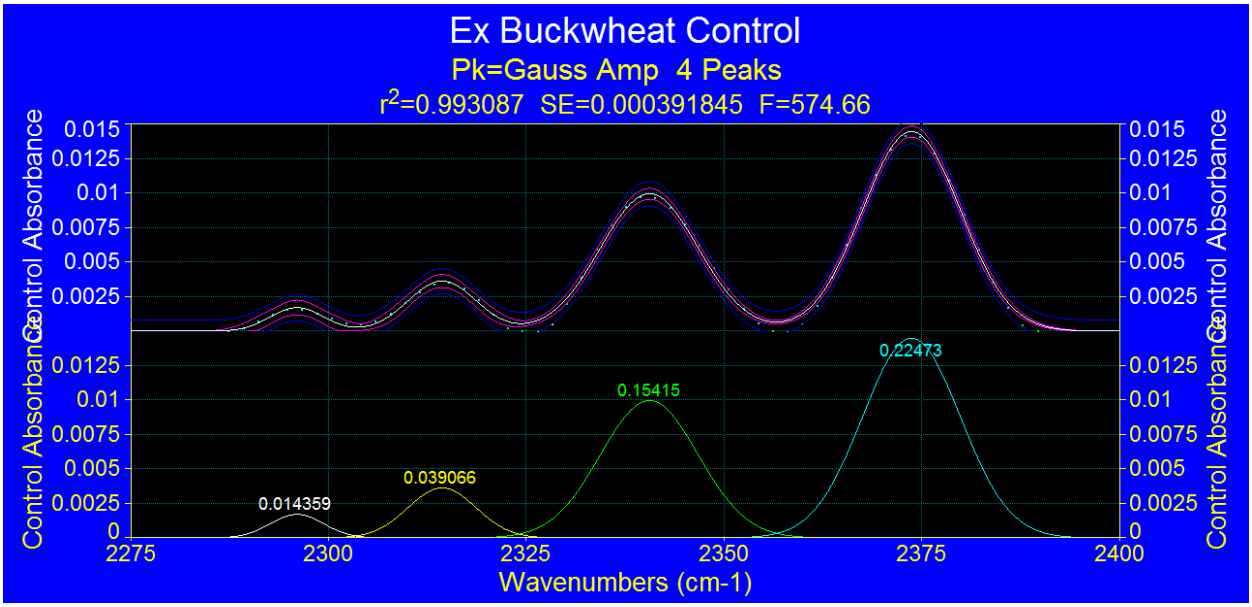

Figure 111 PeakFit model of buckwheat sample from the Exoscan data in the 2,300 cm^{-1} region. Upper graph displays the input measured data in white with the 95% confidence interval of the model in pink that consists of the separated peaks shown in the bottom graph.

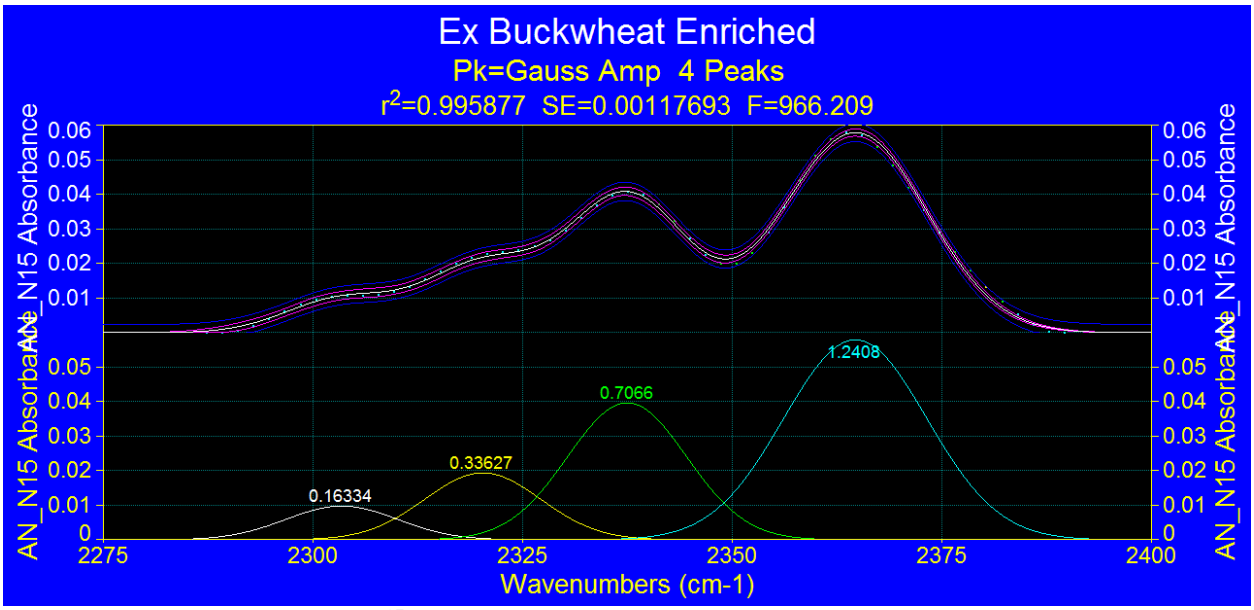

Figure 112 PeakFit model of ^{15}N enriched buckwheat sample from the Exoscan data in the 2,300 cm^{-1} region. Upper graph displays the input measured data in white with the 95% confidence interval of the model in pink that consists of the separated peaks shown in the bottom graph.

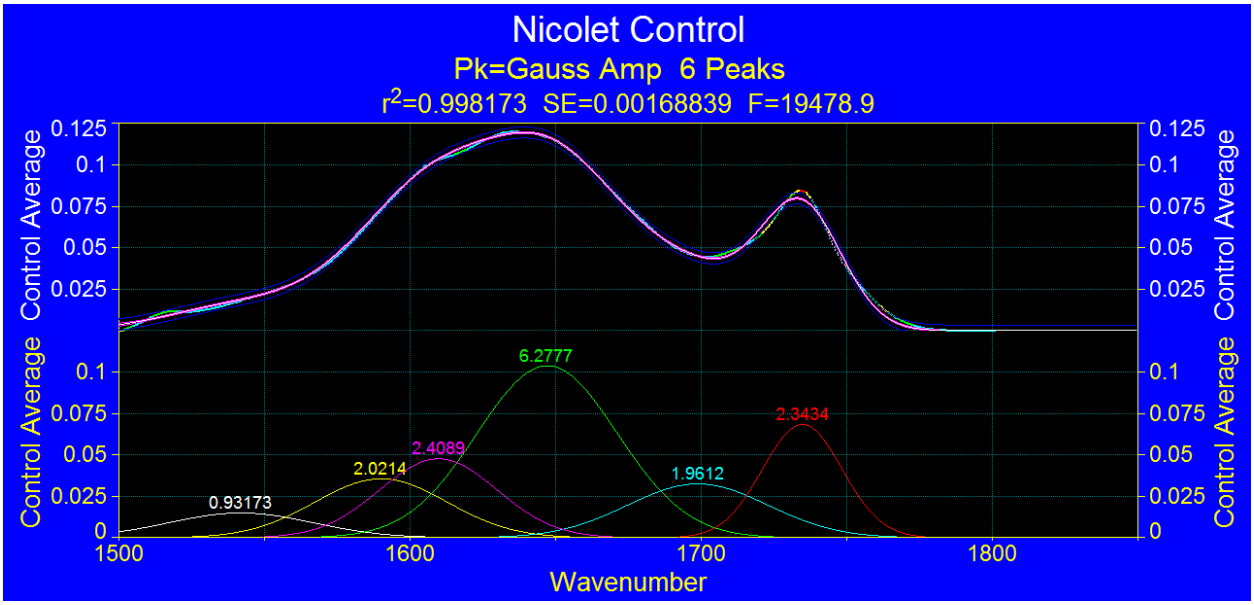

Figure 113 PeakFit model of buckwheat control sample from the Nicolet data in the 1,600 cm^{-1} region. Upper graph displays the input measured data in white with the 95% confidence interval of the model in pink that consists of the separated peaks shown in the bottom graph.

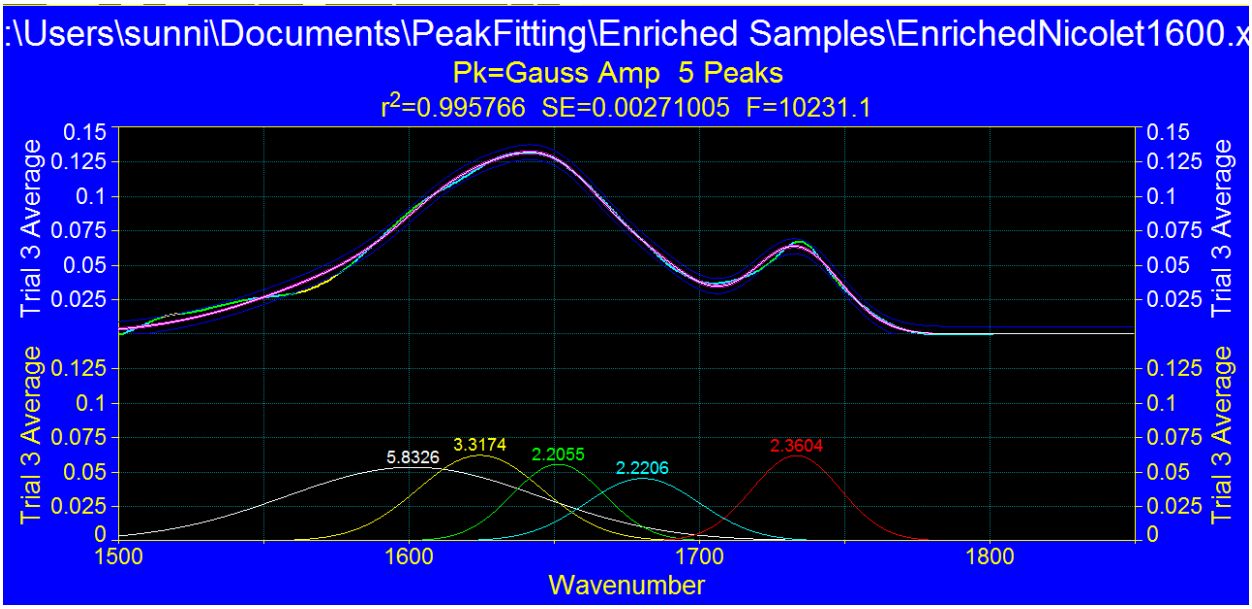

Figure 114 PeakFit model of enriched buckwheat sample from the Nicolet data in the 1,600 cm^{-1} region. Upper graph displays the input measured data in white with the 95% confidence interval of the model in pink that consists of the separated peaks shown in the bottom graph.

Each individual peak in the bottom portion of the PeakFit graphs make up the composite spectral signature in the upper portion of the graph that matches the original input spectrum with 95% confidence. Separating the peaks of the composite spectra enables attribution to isotope components. In the case of the Exoscan data, peaks were chosen for isotope analysis that matched the well-defined features in the spectral data where the ^{15}N enriched buckwheat spectra showed a downshift from 2,372 cm^{-1} and 2,363 cm^{-1}. For the Nicolet FTIR-ATR data, computational chemistry was performed previously to determine which nitrogen containing plant compounds vibrate in this portion of the spectrum that could cause the shifts observed in the collected data. Computations were run on nitrogen containing amino acids under conditions where the nitrogen present was ^{14}N or ^{15}N and showed that ammonium, a common plant nitrogen compound, vibrates at 1,643 cm^{-1} and shift to 1,635 cm^{-1} with the ^{15}N replacement. The PeakFit model peaks were attributed to ^{14}N or ^{15}N accordingly and used for stable isotope analysis. Additionally, each constituent peak automatically assigned by the Peak Fit model matched the wavenumber peak value within 1 or 2 wavenumbers. This is within the original sensor input data spectral resolution, meaning the peak position assignments are consistent with expected results.

Infrared Nitrogen Stable Isotope Analysis

PeakFit model peaks at the wavelengths associated to ^{14}N or ^{15}N were used to calculate the integrated peak area at each peak location. A simple ratio of the heavier to lighter isotope was calculated and the computed averages from each sample group (figures 115 and 116).

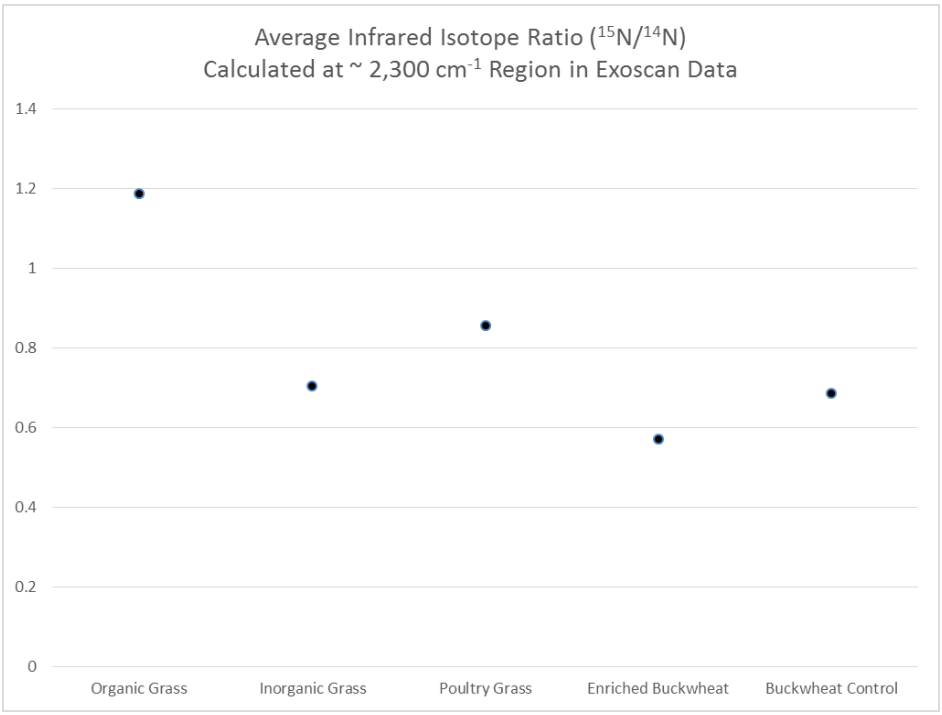

Figure 115 Average simple isotope ratio of the heavier to lighter nitrogen isotopes calculated from the peaks identified in the Exoscan data in the 2,300 cm^{-1} region.

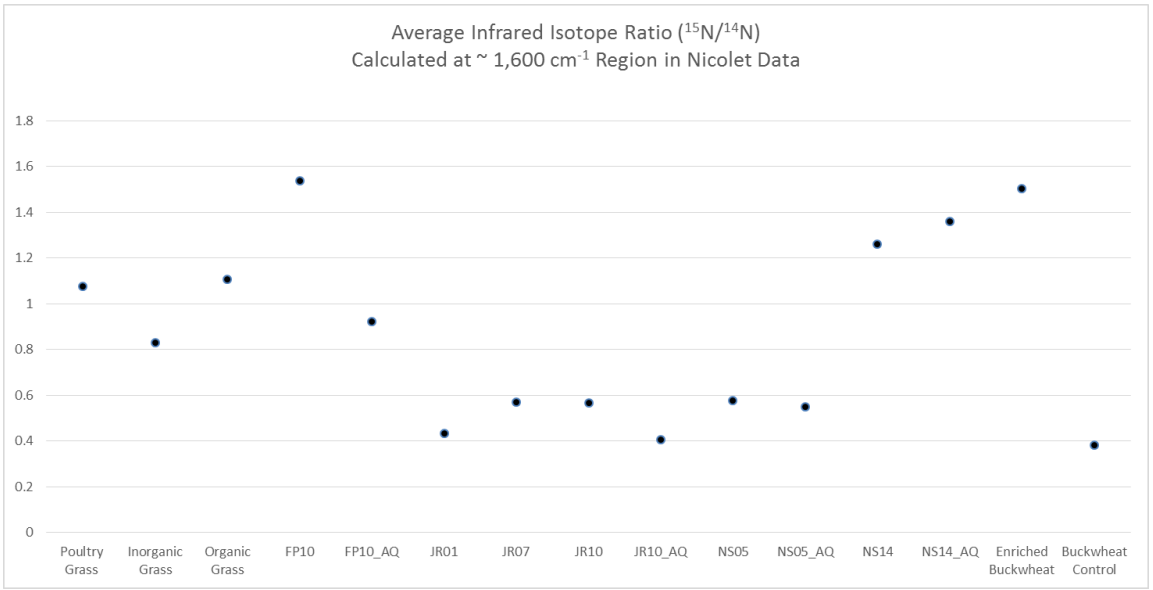

Figure 116 Average simple isotope ratio of the heavier to lighter nitrogen isotopes calculated from the peaks identified in the Nicolet FTIR-ATR data in the 1,600 cm^{-1} region.

A stable isotope ratio can be calculated using Equation 1. The resulting ratios were on a scale that does not compare to traditional isotope ratios, i.e 1,981 $\delta^{15}N$ for one of the grass samples growing in a poultry cage. Dividing the results by 100 scales the data to more expected values, i.e 19 $\delta^{15}N$ for the same sample. The resulting $\delta^{15}N$ values are shown in figures 117 and 118.

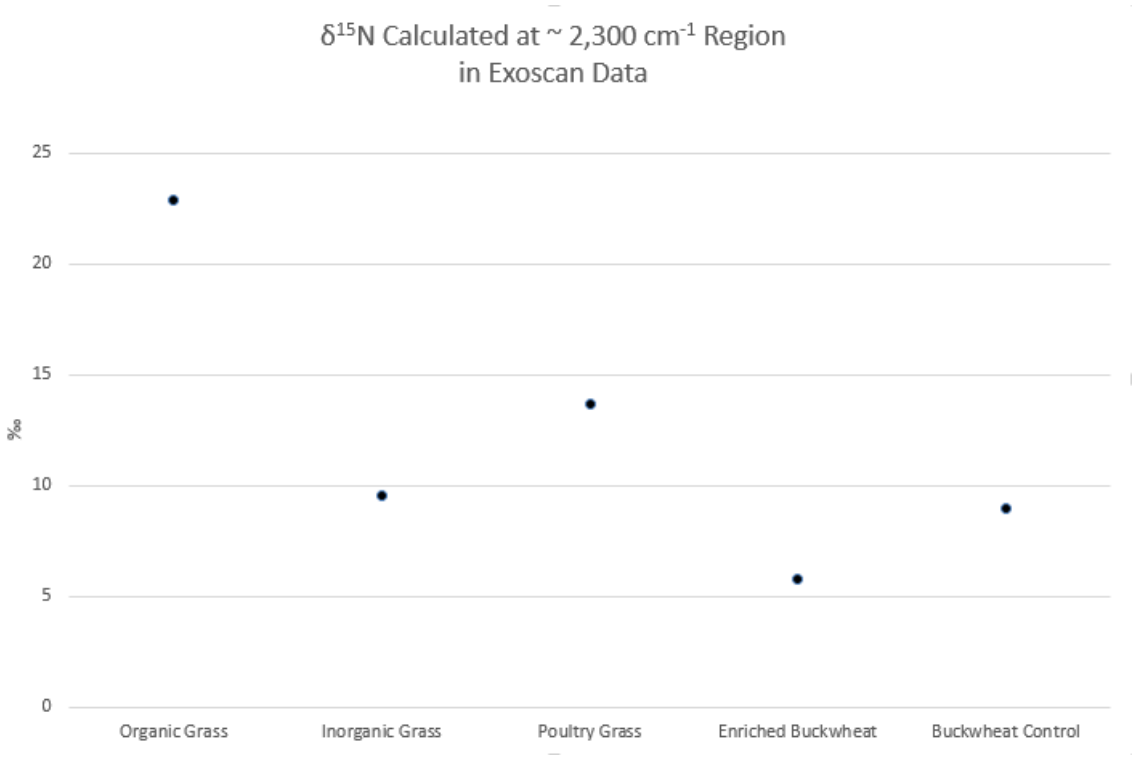

Figure 117 Average INSI $\delta^{15}N$ ratio of the heavier to lighter nitrogen isotopes calculated from the peaks identified in the Exoscan data in the 2,300 cm^{-1} region.

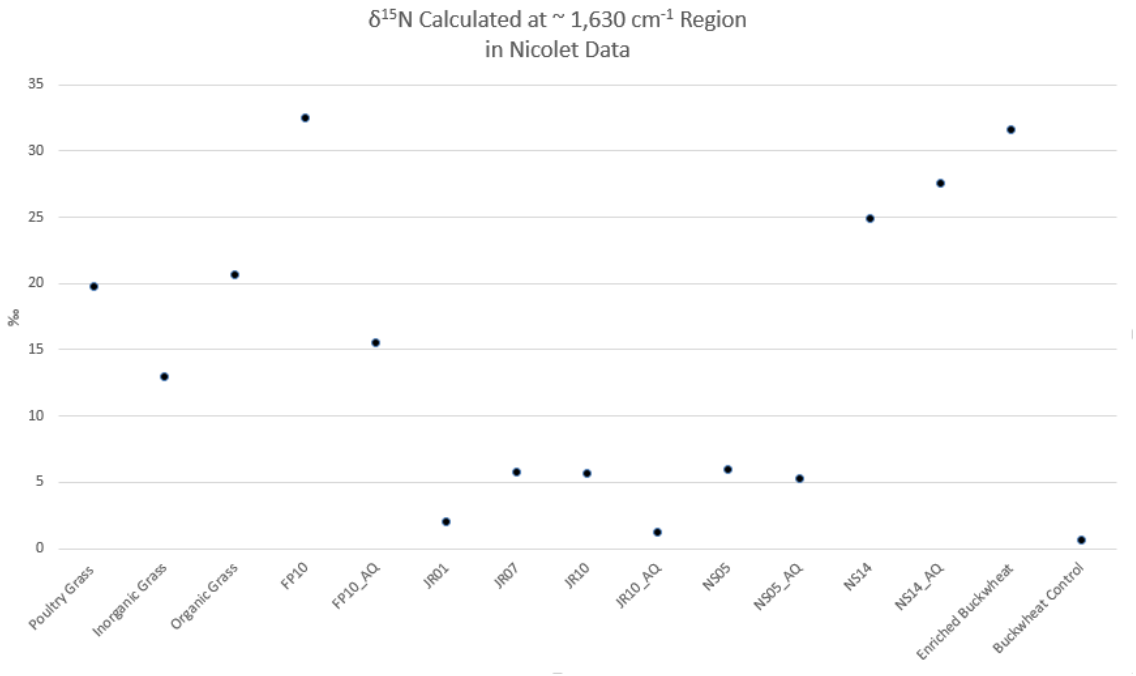

Figure 118 Average INSI $\delta^{15}N$ ratio of the heavier to lighter nitrogen isotopes calculated from the peaks identified in the Nicolet FTIR-ATR data in the 1,600 cm^{-1} region.

Discussion

Spectral Analysis

Without a concrete understanding of all plant compounds that have identifiable features along the entire spectrum, it is a speculation as to which peak or valley can be attributed to the presence of ^{15}N. For example, the identified wavelength shift that occurs at around 700 nm from the ASD spectrometer is within what is called the red-edge that is specific to vegetation. There is a clear peak shift in the derivative, but without specific compound analysis it is not certain to be caused by the differences in ^{15}N variation in each sample. The derivative shows a shift in the spectra of the enriched buckwheat plants, which is the change in the slope of the red edge between the sample groups measured.

This slope difference could be caused by numerous other factors besides just the presence of ^{15}N.

The features identified in the infrared regions from the Exoscan and Nicolet spectrometers are known to be related to specific molecular bonds with nitrogen giving a reasonable linkage to the presence of ^{15}N, particularly in the case of the enriched buckwheat spectra. Additionally, the computational modeling helps to narrow down not only the bonds that are attributable to the specific region, but to a specific molecule. The computational modeling of plant nitrogen compounds helps to understand what occurs in the infrared when a molecule contains ^{15}N instead of ^{14}N. The modeled spectra matched to the Nicolet data show that it is ammonium that causes spectral features identified in the 1,600 cm^{-1} region. These results show that stable isotope calculations in this infrared region might be possible given the attributions to the spectral features that have been performed in the computational modeling.

Infrared Nitrogen Stable Isotope Analysis

The calculated stable isotope ratios from infrared features identified in the Exoscan and Nicolet data are not precise measurements. However, comparisons can be made between the INIS ratios created from the samples collected. The results from the Nicolet FTIR-ATR 1,600 cm^{-1} region show two groupings of ratios, high and low, enriched or depleted. The samples with high infrared nitrogen stable isotope (INSI) ratios include the grass samples from the poultry cage (poultry grass), the grass from a cow pasture (organic grass), the grass from the FP10 and NS14 stream banks that were collected from both locations (FP10 and FP10_AQ), and also the enriched buckwheat

sample from previous growing experiment. These results suggest a level of positive validity of the methodology described herein. Both the poultry and organic grass samples should have higher levels of ^{15}N in the FP10 and NS14 streams. FP10 and NS14 are downstream from a wastewater treatment site and a chicken processing plant respectively. Additionally, traditional IRMS was performed on the samples. NS14 was computed to have $\delta^{15}N$ ratio of 7.72 and FP10 was shown to be much more depleted with a $\delta^{15}N$ ratio of -0.3. This results for FP10 was reassessed and the sample was determined to be contaminated with soil. The IRMS samples contained a high amount of dirt and soil that was not cleaned off in IRMS sample preparation. These comparisons between the INSI and IRMS ratios are an initial exploration between the two. Continued effort in this area should be performed.

The Exoscan data was only collected on the grass sample set collected and the results in this region and from this instrument are inconsistent with the expected results. The organic grass samples were calculated to have the highest INSI ratio instead of the expected poultry grass samples. Additionally, the enriched buckwheat sample had the lowest INSI ratio where it is instead expected to have the highest ratio due to its heavily enriched growth experiment where traditional isotope-ratio mass spectrometer ratios showed readings off the charts, on the order of 70,000 permil. These Exoscan results indicate this instrument or specific spectral region chosen are not able to produce infrared based isotope ratios.

Conclusions

With this study, in addition to traditional mass spectrometry, Nicolet FTIR-ATR measured data in the 1,600 cm^{-1} region has the potential to measure nitrogen stable isotope ratios in plant matter. These findings indicate that continued research should be performed with this methodology to refine the infrared nitrogen stable isotope (INSI) ratio developed in this research. The data measured by the Nicolet FTIR-ATR spectrometer was measured in 4 cm^{-1} wavenumber resolution, which is standard practice to balance signal to noise for this instrument. Increased spectral resolution through the application of ultraspectral technologies should be investigated. The INSI ratio requires continued research into its precision and accuracy that could be achieved with ultraspectral sensors yet to be developed.

The sample preparation for FTIR measurements is much faster than traditional IRMS instrumentation. Here, grass samples were collected and simply dried in the laboratory. The grass blades are simply then compressed to a known and standard compression onto the ATR sample port of the FTIR instrument. Scans are acquired in seconds without the need for tuning and calibration, significant and time consuming efforts required for IRMS measurements. The current limitation is the accuracy of the sample INSI ratios collected herein and requires continued investigation.

Future infrared sensors tuned to the absorption feature of ammonium at ~1,640 cm^{-1} in plants could be developed to operate in the field either by handheld, air or eventually space based sensors. This will allow researchers to better understand biogeochemical cycling on greater spatial scales and in a more rapid fashion. The INSI

ratio could be used actively in the field to aid researchers in refining field sampling locations where collection of samples for traditional IRMS measurements could occur, saving costs to research conducted in the field. It is unknown how precise and accurate the INSI ratio method could become with continued research. The foundational research conducted in this study should invigorate researchers to improve upon the methods developed herein.

References

Agilent 4100 exoscan FTIR operation manual. (2013).

Capelle, S. K., & Macko, S. A. (2016). Finding the spectral signature of ^{15}Nitrogen isotopes in plants by hyperspectral techniques. *Journal of Remote Sensing Technology, 4*(1), 115-120.

Coates, J. (2000). In Meyers R. A. (Ed.), *Interpretation of infrared spectra, a practical approach*. England: John Wiley & Sons Ltd.

Engel, M. H., Macko, S. A., & Leythaeuser, D. (1991). The potential application of stable isotopes for distinguishing indigenous versus migrated hydrocarbons in a mature shale/sandstone sequence. *Chemical Geology, 93*(1–2), 47-59.

FieldSpec(R) pro user's guide. (2002). Unpublished manuscript.

Friends of the Shenandoah River.Water window. Retrieved from http://www.fosr.org

Nicolet (TM) FT-IR user's guide. (2004). Unpublished manuscript.

Quillard, S., Louam, G., Buisson, J. P., Boyer, M., Lapkowski, M., Pron, A., & Lefrant, S. (1997). Vibrational spectroscopic studies of the isotope effects in polyaniline. *Synthetic Metals, 84*(1–3), 805-806.

Yun, S. I., Ro, H. M., Choi, W. J., & Chang, S. X. (2006). Interactive effects of N fertilizer source and timing of fertilization leave specific N isotopic signatures in Chinese cabbage and soil. *Soil Biology and Biochemistry, 38*, 1682-1689.

Chapter 5 – Conclusions

Stable isotopes have many applications in the study of the environment, in the investigation of chemical compounds and the investigation of natural processes to name a few. The sheer nature of isotope studies requires laboratory analysis and sample preparation. There currently is no capability to perform isotope studies and make direct isotope measurements in the field environment in a non-destructive way. Samples must be collected which have to be taken back to the laboratory for analysis. These samples represent discrete locations in the study area. Sampling large areas can be extremely exhaustive and requires long days in the laboratory to produce the results. These limitations have led to researchers seeking measurement alternatives (Wang *et al*., 2010). Specifically investigations have been made into understanding how the presence of stable isotopes interact with light energy differently and how these differences are measured in spectrometers. Most research thus far has focused on the change in a spectrometers response in reflectance values within the 0.3-2.5 μm region as measured by the field portable ASD spectrometer. The results are well correlated to the traditional IRMS measurements, but do not represent a direct measurement. The efforts so far are all proxies. This ASD instrument is a workhorse spectrometer for agriculture, environmental, and civil applications. It is well known and easy to use. This dissertation shows that the ASD might not be the correct choice for true stable isotope measurements. Instead, instrumentation in the mid-infrared produce better results and, with additional sensor development, could be used in the field.

This research suggests that spectrometers could be developed that are specifically tuned to a specific isotope in a particular substrate. The complexity of molecular interactions within an entire spectral region differ from sample to sample limiting the ability to develop a "one-size-fits-all" stable isotope spectrometer. The starting point of this investigation focused on the nitrogen stable isotope, ^{15}N. Nitrogen is a useful element to study in the geosphere particularly in the case of pollution and runoff. Nitrogen can be released into the environment above natural levels causing nutrient pollution in waterways, eutrophication and even anoxic conditions in water bodies. Understanding nitrogen stable isotope cycling can aid researchers with tracing the origins of samples. Until now, stable isotopes must be measured in the laboratory.

Initially, a thorough investigation was performed to understand how nitrogen stable isotopes in plant matter effect changes in reflective or Fourier transform infrared (FTIR) spectrometer measured data. First, a series of experiments were conducted in the laboratory. These experiments focused on heavily doping plants with 99.99% ^{15}N, which is far above natural stable isotope levels (~0.3%). After an initial few failed attempts, quick growing buckwheat was successfully grown aeroponically with a heavily enriched fertilizer solution. A similar aeroponic unit with standard natural abundance fertilizer was used as a control. Buckwheat leaves were collected and measured by three different spectrometers; the ASD field portable reflective spectrometer, the field portable Exoscan FTIR and the laboratory based Nicolet FTIR-attenuated total reflectance (ATR) spectrometers. The spectral data was analyzed to determine difference between the control and the enriched plants. Each instrument was shown to produce results indicating a

possible link to the unnaturally high level of ^{15}N in the enriched samples. Wavelength or wavenumber shifts in the spectral features in the enriched samples were observed in the ASD data near 700 nanometers (nm), the Exoscan data near 2,300 cm^{-1} and the Nicolet data near 3,300 cm^{-1} and 1,600 cm^{-1}. These results are expected shifts as the presence of a heavier isotope impacts the way in which the elemental bonds bend and rotate causing downshift in their vibrations.

Secondly, the identified shifts from the enrichment experiment were analyzed to assess what chemical functional groups have known vibrations that are related to nitrogen bonds. The ASD spectrometer does not have a library of known functional groups. The ASD data can be related to known spectral signatures published by organizations such as John's Hopkins Applied Physics Laboratory, the United Stated Geologic Survey, the Jet Propulsion Laboratory, and other signatures published in the literature. The ASD shift observed at 700 nm was located within the red-edge response of vegetation. The red-edge is associated with the health of vegetation. Specifically it is the sharp rise in reflectance values as chlorophyll absorptions transition into reflectance by plant cells. This region was determined to be less likely related to ^{15}N composition. The other regions in the infrared were determined to be related to nitrogen bonds such as NH (2,300 cm^{-1} and 3,300 cm^{-1}) and CN (1,600 cm^{-1}). Computational chemistry was performed in this research to aid in the understanding of the stable isotope in nitrogen containing plant compounds. Computational chemistry can model the infrared spectra of given molecules. The modeled infrared spectra of ammonium was shown to overlap with the spectral features observed experimentally in the 1,600 cm^{-1} region. This suggests an interplay between ammonium (NH_4) and CN bonds

existing in the plant structure. The experimental enrichment experiment showed a downshift from $1,642^{-1}$ to $1,637^{-1}$ and the modeled data showed a similar downshift from $1,643^{-1}$ to 1,635 cm^{-1} corroborating the FTIR-ATR measured data.

Finally, the same instruments were used to measure field samples of natural abundance stable isotope ratios to determine if the same features can be observed in the instrument data. Field samples were collected in fields and along stream banks with expected enriched levels of ^{15}N due to the fact that fractionation causes the heavier isotope to remain in the manure and organic wastes whereas inorganic fertilizer created using the Haber process, extracting nitrogen from the air, is depleted in the heavier isotope as atmospheric nitrogen is the standard for nitrogen stable isotope studies at 0 per mil ^{15}N ratio. Two of the four regions with isotope shifts were observed in the natural abundance samples 2,300 cm^{-1} and 1,600 cm^{-1} measured by the Exoscan and Nicolet spectrometers respectively. The peaks at these features were modeled to separate the peaks into their constituent peaks where it is expected that each isotope can be assigned to a peak at the specific wavenumbers identified. The models did show good peak separation enabling area measurements. These area measurements can then be used to derive infrared nitrogen stable isotope (INSI) ratios for the field samples. Interestingly, the INSI ratios in the 1,600 cm^{-1} showed enrichment for the samples where enrichment was expected; within fields where poultry and cows were raised and along streambanks downstream from a wastewater treatment site and a chicken processing plant. This research shows that the INSI ratio has the potential to calculate nitrogen stable isotope ratios with future sensor development and refinement of the methodology presented herein. .

The method developed in this research should be used to develop a new field based sensor tuned to the plant based nitrogen stable isotope features at 1,600 cm^{-1}. Increased spectral resolution through the application of ultraspectral technologies should be investigated. The INSI ratio requires continued research into its precision and accuracy that could be achieved with ultraspectral sensors yet to be developed.

Future infrared sensors tuned to the absorption feature of ammonium at ~1,640 cm^{-1} in plants could be developed to operate in the field either by handheld, air or eventually space based sensors. This will allow researchers to better understand biogeochemical cycling on greater spatial scales and in a more rapid fashion. The INSI ratio could be used real time in the field to aid researchers in understanding the spatial extent of the stable isotopes in their sample area. Real time measurements can help to fine tune specific field sampling locations for traditional IRMS measurements, saving costs to research conducted in the field. Air based sensors with this technology could be employed to rapidly measure large geospatial areas and create maps of nitrogen stable isotope content across the region, such as collecting along the entire Chesapeake Bay watershed. This future capability could be used to identify focus area where nutrient management plans will have the most impact on the water quality of the Bay. It is unknown how precise and accurate the INSI ratio method could become with continued research. The foundational research conducted in this study should invigorate researchers to improve upon the methods developed herein.

Appendix A: Enrichment Experiments Spectra

Initial Signature Variable Analysis

Overview

The signatures displayed in this section were collected by the Analytical Spectral Device's FieldSpec Pro (*FieldSpec(R) pro user's guide*, 2002). It collects data from 0.35 to 2.5 µm. It is also a portable spectrodiometer useful for field work. That data collected in this dissertation was collected indoors with ASD's High Intensity Reflectance Probe which mimics solar radiation but without atmospheric artifacts in the resulting data. The signatures are measured from the plants in the experiment described in chapter two. Each spectrum displayed in this research is made from three independent measurements of either three or ten different leaves from either one of ten different plants where each measurement is averaged together from three measurements each consisting of 30 scans of each sample.

Fresh vs. Dry Leaf Measurements

It was important to first capture any potential variability in the measurement of the leaves in either their freshly clipped or dried state to determine if the observation of wavelength shifts changes. This set the baseline practice for subsequent leaf measurement for this research. The signatures below show that the water content in the fresh leaves prevent some shifts from observation by the sensors. Therefore this technique with this instrument would be best performed during the dormant season or where vegetation has senesced.

In Figure 29 below, notice the large features near 1450 and 1920 nm and shallow features near 0.98 and 1175 nm in fresh leaf spectrum (in black) not present in dried leaf measurement. Those features are due to water content in the plant material (Thenkabail *et al*., 2012). The feature near 1920 nm is also due to plant cellulose and lignin explaining why that feature continues to exist in the dried leaf spectrum (in red). The features above 2000 nm also become more apparent in the dried leaf spectrum rather than the fresh spectrum. This also shows that measuring dry leaves is preferable for this research.

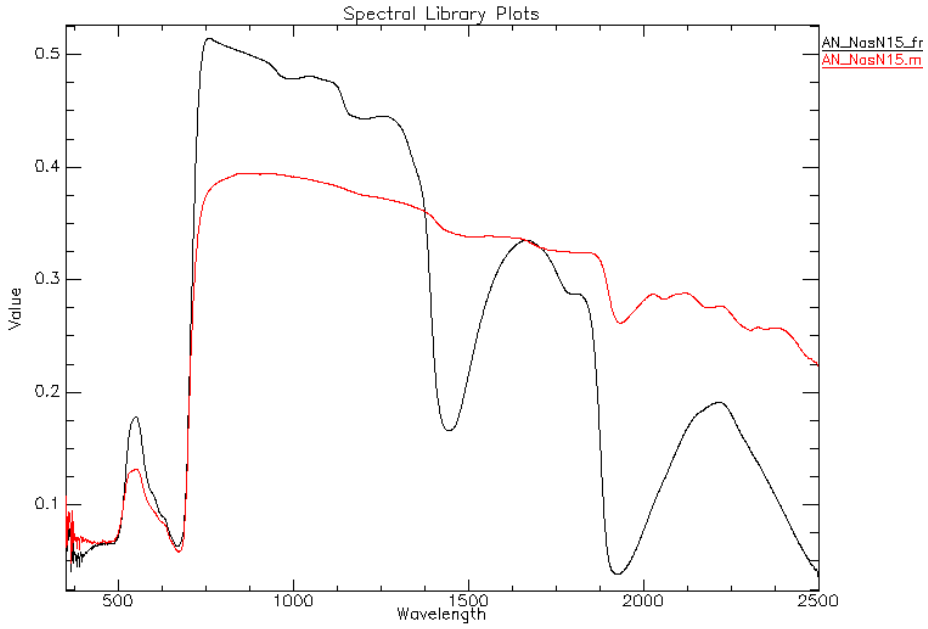

Figure 119 Fresh leaf measurement (Black) compared to dried leaf measurement (Red).

Uptake of Nitrogen Labels

A nitrogen label is a chemical where the nitrogen supplied is in the stable isotope (^{15}N) form and an abundance of 99.99%. The nitrogen labels use in the experimentation are commercially available in various compositions. An initial analysis was conducted to assess the performance on the plants using three different types of nitrogen labels; ammonium nitrate where ^{15}N was in the nitrate group (in red in figure 120), the ammonium group (in black in figure 120), or sodium nitrate (in dotted green in figure 120). Besides the measured spectra, plant health was also assessed. It is important for this research to have plants that grew enough leaves for measurement and also ones that grew long enough in order to uptake the supplied nitrogen labels.

The ammonium nitrate label where ^{15}N was in the nitrate group has a higher overall reflectance and some features are deeper showing that this label could be the better performer for these experiments. However, when looking at the overall health of the plant, the plants appeared stunted, yellow and produced smaller leaves than the other two options. This experiment only varied the label types. All other concentrations and variables were the same. These results show that the label to be used in subsequent experiments should be ammonium nitrate label where ^{15}N was in the nitrate group.

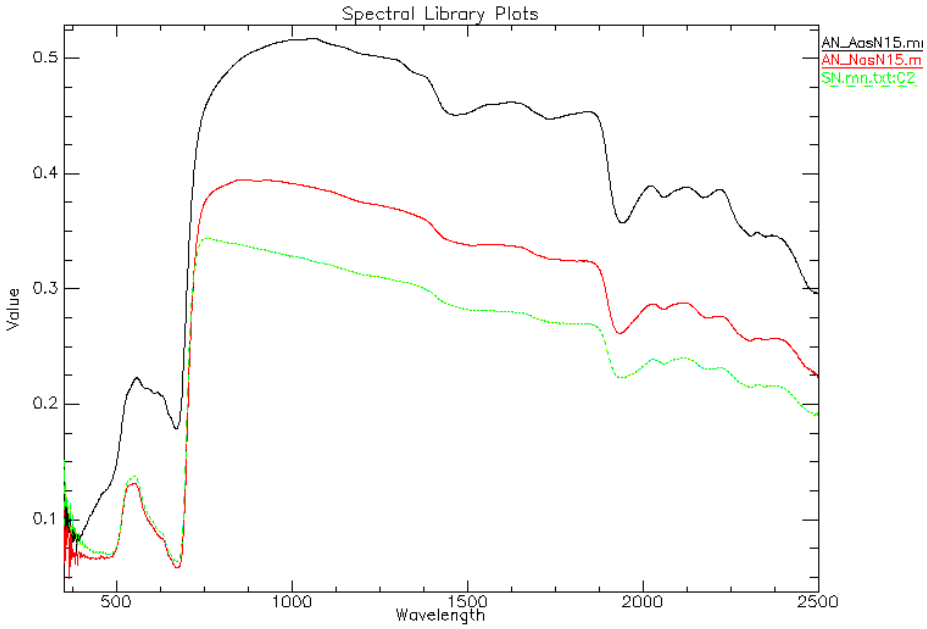

Figure 120 Plant spectra from each nitrogen label type.

VNIR/SWIR Signatures

Overview

The ASD signatures from the experiment discussed in chapter two are shown below for better visual clarity. Dried leaves were measured and ammonium nitrate label where ^{15}N was in the nitrate group was used.

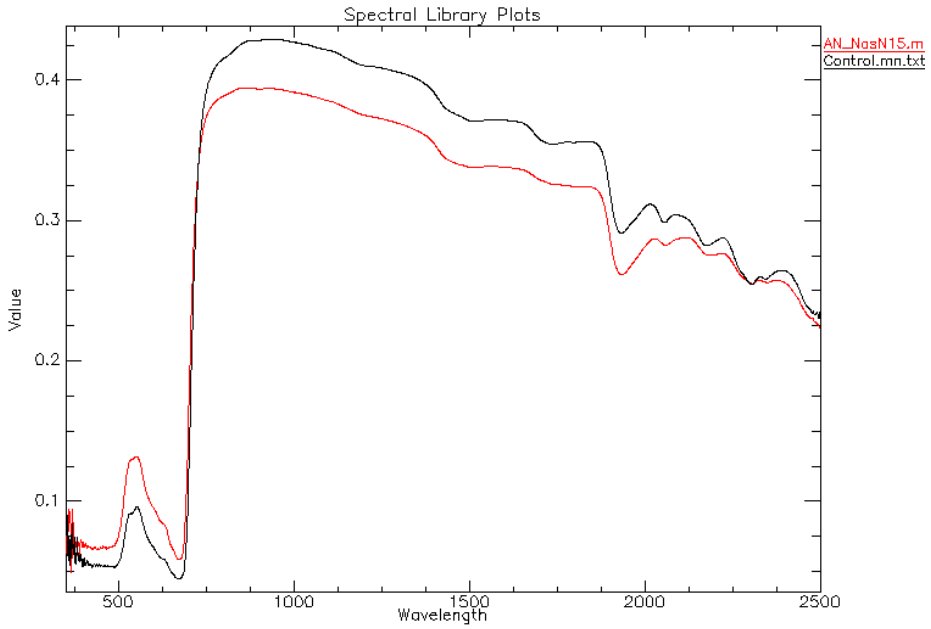

Figure 121 Full spectrum of labeled plant leaf (in red) and the control (in black).

Figure 121 shows the entire spectrum of the labeled leaf measurements (in red) versus to the control (in black). Clearly, the spectrum looks very similar. Spectral analysis of the first derivative of the same data helps to highlight the differences (figure 122).

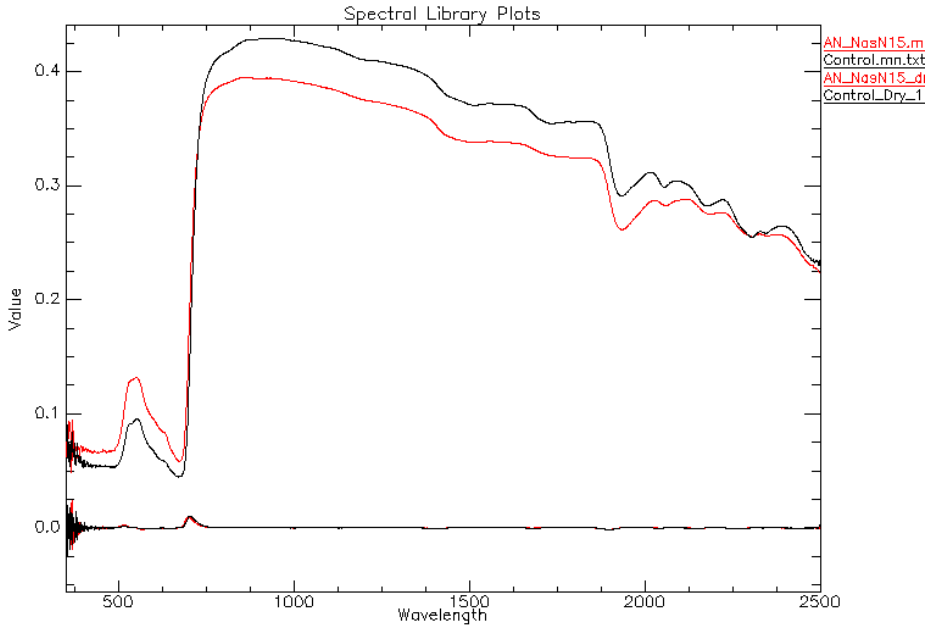

Figure 122 Reflectance spectra from Figure 14 shown in comparison to their first derivative spectra

The first derivative spectra shown in Figure 15 show places along the spectrum where differences occur. Removing the reflectance data and truncating the spectrum range to 480 to 2,350 nm to remove the sensor noise that occurs at the edge of the sensor detectors allows the derivative spectra to be observed. Figure 123 shows observable differences in this region between the control and the labeled plants that are not easily observed in the reflectance data.

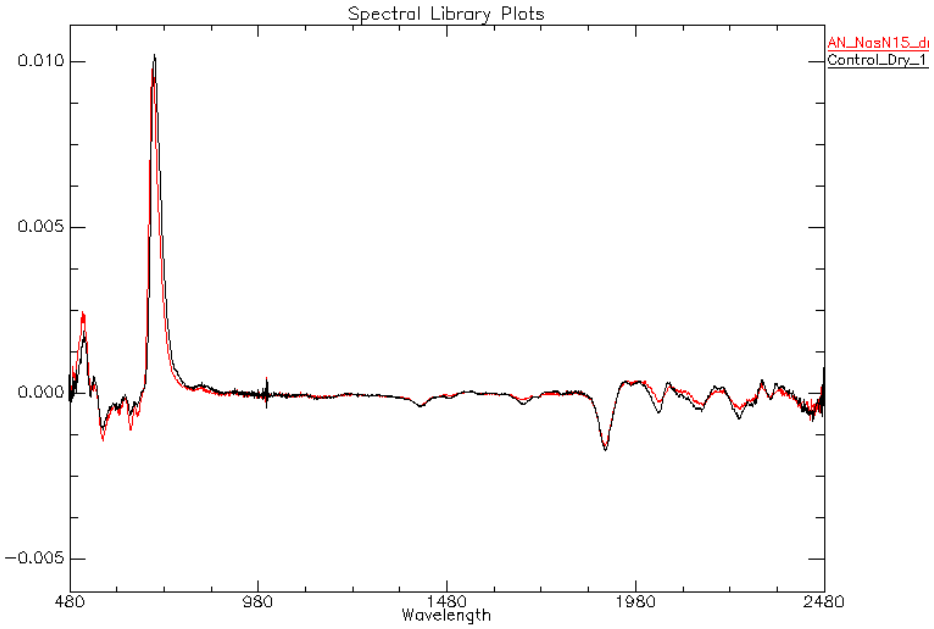

Figure 123 First derivative spectra of labeled (in red) and the control (in black) from 480 nm to 2480 nm.

Figures 124-127 display the shifts observed in the ASD derivative data across the full response of the instrument zoomed into to enable easier reading. The data shown is the raw derivative data, no smoothing is been applied. These figures show the many other sifts that occur between the labeled and control data and are summarized in table 8.

Region	Control Spectra Band Center (in nm)	^{15}N Labeled Spectra Band Center (in nm)
1	516	514
2	719	703
3	1485	1489
4	1901	1897
5	2040	2044
6	2254	2257

Table 8 List of regions where ^{15}N induces wavelength shifts are observed that are different from the control.

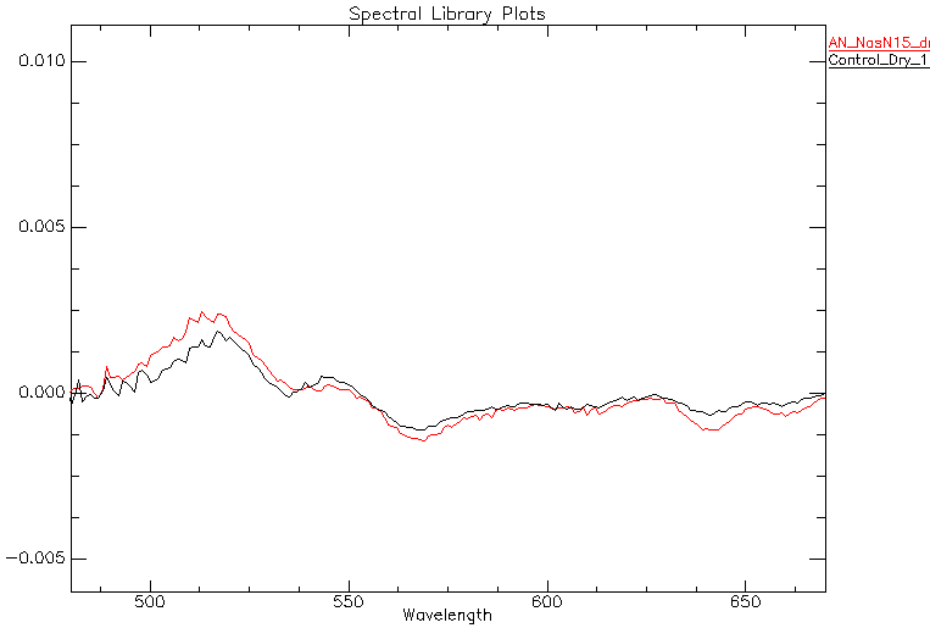

Figure 124 First derivative spectra of labeled (in red) and the control (in black) zoomed in to display the data from 480 nm to 670 nm.

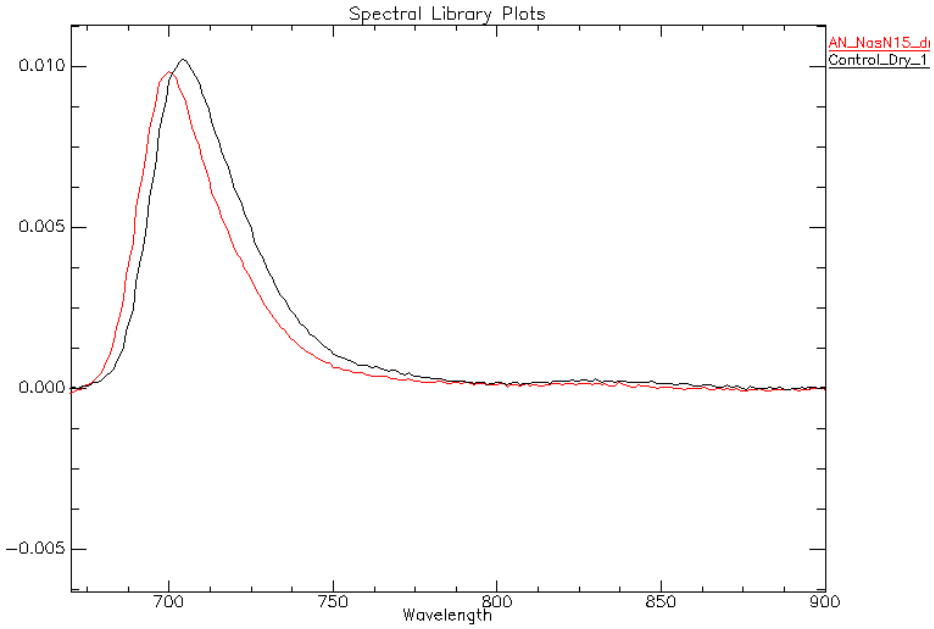

Figure 125 First derivative spectra of labeled (in red) and the control (in black) zoomed in to display the data from 670 nm to 900 nm.

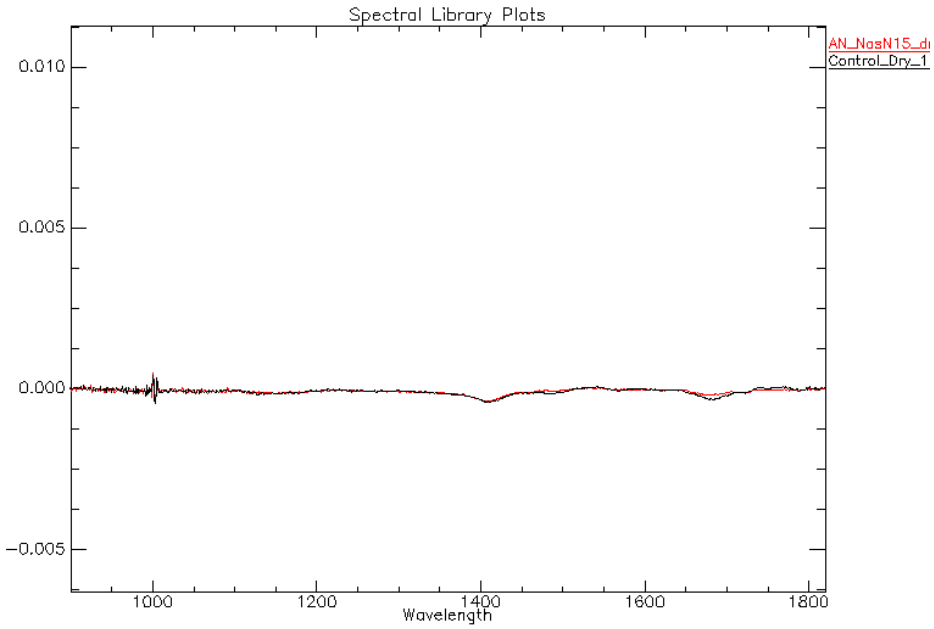

Figure 126 First derivative spectra of labeled (in red) and the control (in black) zoomed in to display the data from 900 nm to 1820 nm. (Feature at 1nm is cause by sensor detector, not from plant data)

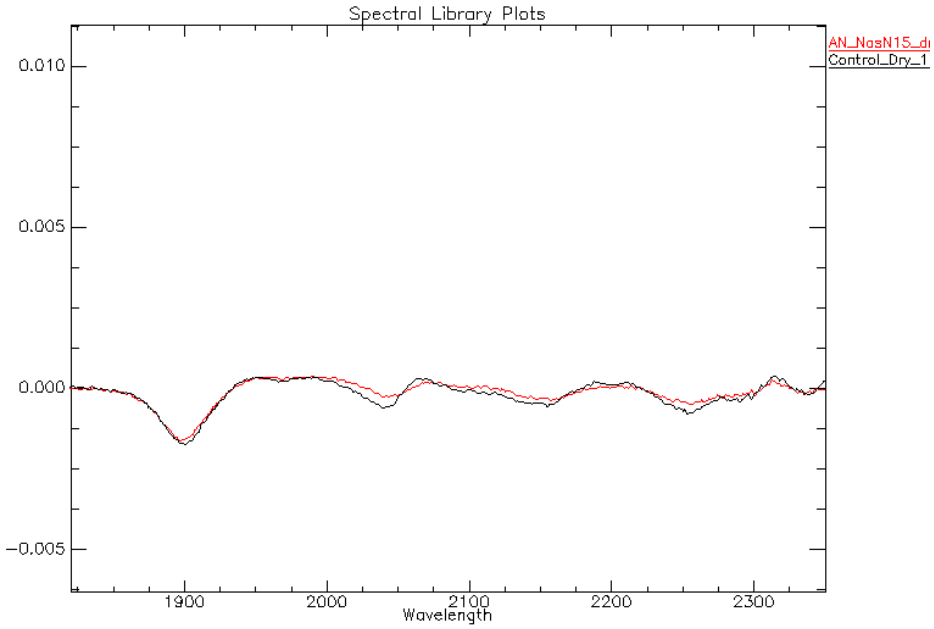

Figure 127 First derivative spectra of labeled (in red) and the control (in black) zoomed in to display the data from 1820 nm to 2350 nm.

MWIR/LWIR Signatures

Overview

The MWIR/LWIR signatures were collected from two different FTIR instruments; the Agilent 4100 Exoscan(*Agilent 4100 exoscan FTIR operation manual*, 2013) and the Thermo Scientific Nicolet 6700(*Nicolet (TM) FT-IR user's guide*, 2004) . These instruments measure data from 2.5 to 15 microns. The Exoscan is a field portable device whereas the Nicolet is a laboratory benchtop instrument. The Nicolet has increased sensitivity and the ability to measure samples with higher spectral resolution. All signatures reported below are measurements from ten leaves each from a different plant in the growing experiment. Each measurement is the average of 60 scans of each leaf. The Exoscan data was natively collected in absorbance but is displayed below as reflectance which is common practice for field instrumentation. The Nicolet data is

collected and reported in absorbance. Reflectance and absorbance are inversely related however the Exoscan FTIR spectrometer is a DRIFTS type FTIR spectrometer whereas the Nicolet FTIR was collected using the attenuated total reflectance (ATR) attachment. These differences, which are important to each for their designed utility, make their direct comparison of the resulting data impossible. Therefore, the data from each instrument will be reported independently.

Field Instrument Acquired

Figures 128-131 shows the data collected from the Exoscan for the ^{15}N labeled and control plants. Not only is the data reported in reflectance but also wavenumbers or inverse centimeters (cm^{-1}). As previously discussed in chapter two, wavenumbers and wavelength are inversely related. Figure 128 shows the data across the full measured region. The MWIR and LWIR regions allows for identification of specific chemical compound functional groups. There are noticeable differences between the control and the labeled plants particularly in the region near 2,200 cm^{-1}. In the control there is a broad peak near 2,200 cm^{-1} whereas in the control the peak begins to separate. Additionally at a slightly higher wavenumber there are specific absorption features that appear in the labeled spectra versus the control. In the control the broad peak is centered at 2,082 cm^{-1}, whereas the labeled plant spectra has two peaks at 1,980 cm^{-1} and 2,255 cm^{-1}. Function groups that vibrate in these region are C-N nitrile stretches (Coates, 2000). It is possible the increased ^{15}N present for the experimental plants has caused peak separation of the two nitrogen species.

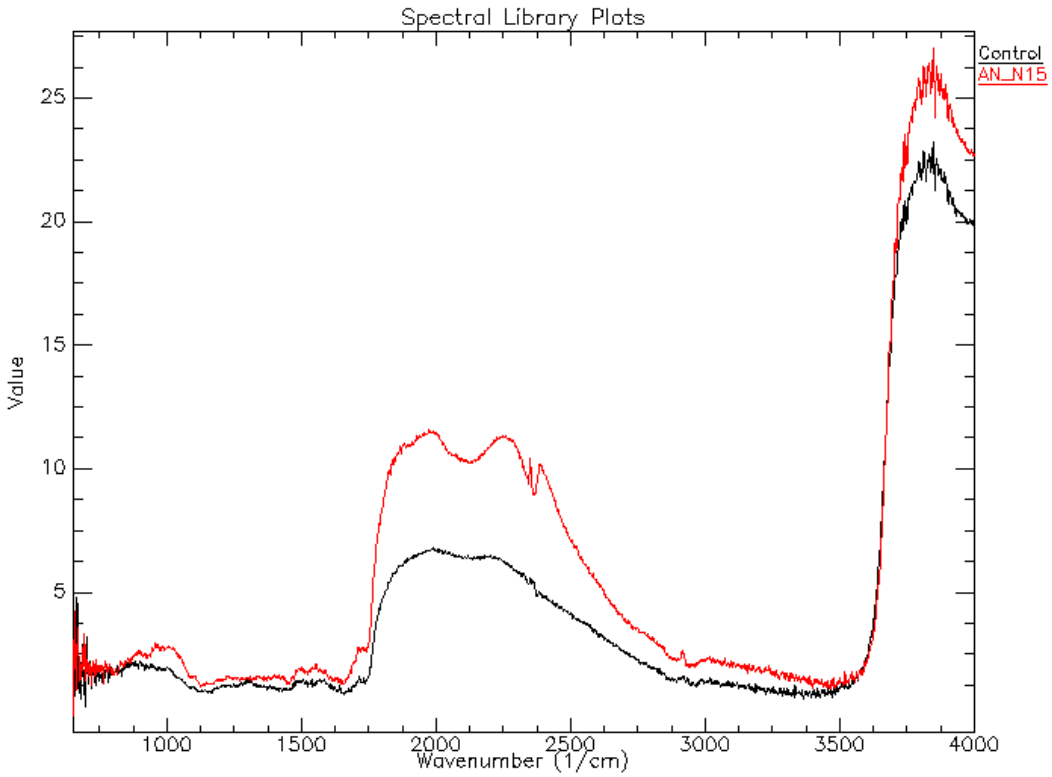

Figure 128 Spectra from Exoscan from 600 to 4000 wavenumbers

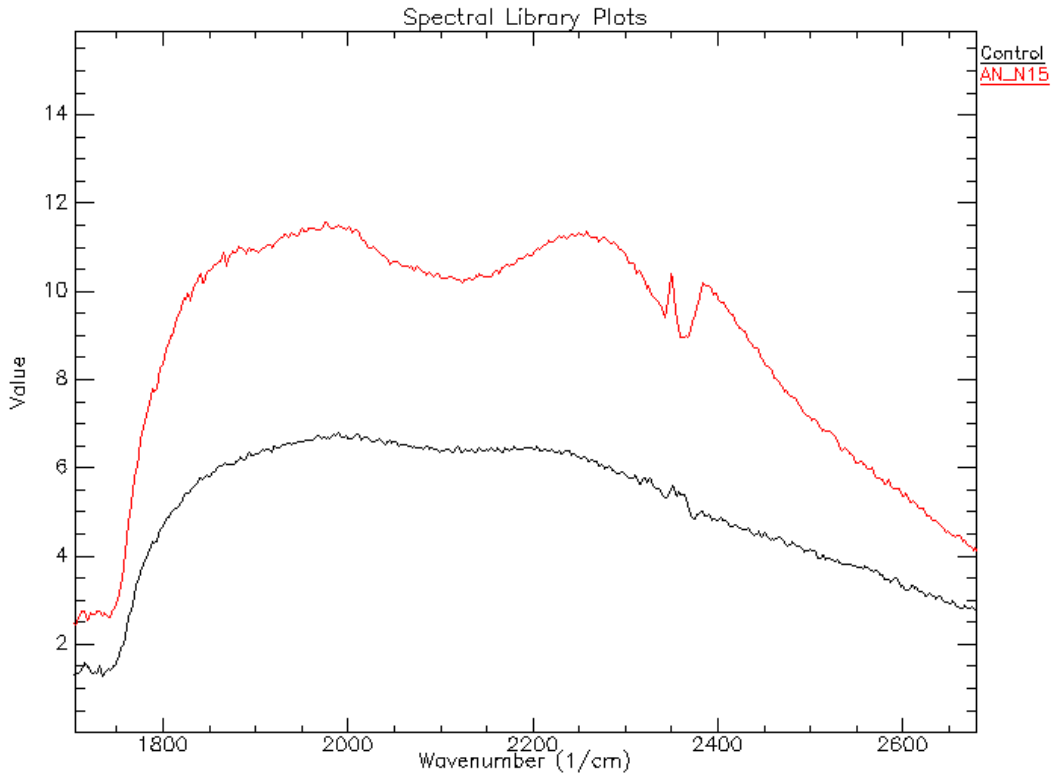

Figure 129 Exoscan data zoomed into peaks near 2,200 cm^{-1}

Figures 129 shows the peak separation near 2,200 cm^{-1} and the appearance of deeper features closer to 2,300 cm^{-1}. These features near 2,300 cm^{-1} are better displayed in figure 40. It is the deepest feature that displays a shift in the ^{15}N labeled plant versus the control and was reported on in chapter two. The control feature is centered at 2,372 cm^{-1} and the ^{15}N labeled plant is centered at 2,363 cm^{-1} and is shown in figure 41 with continuum removal applied to normalize the data to a common baseline due to the data sloping in this region. This is an important finding showing potential application for this technique using a field portable spectrometer.

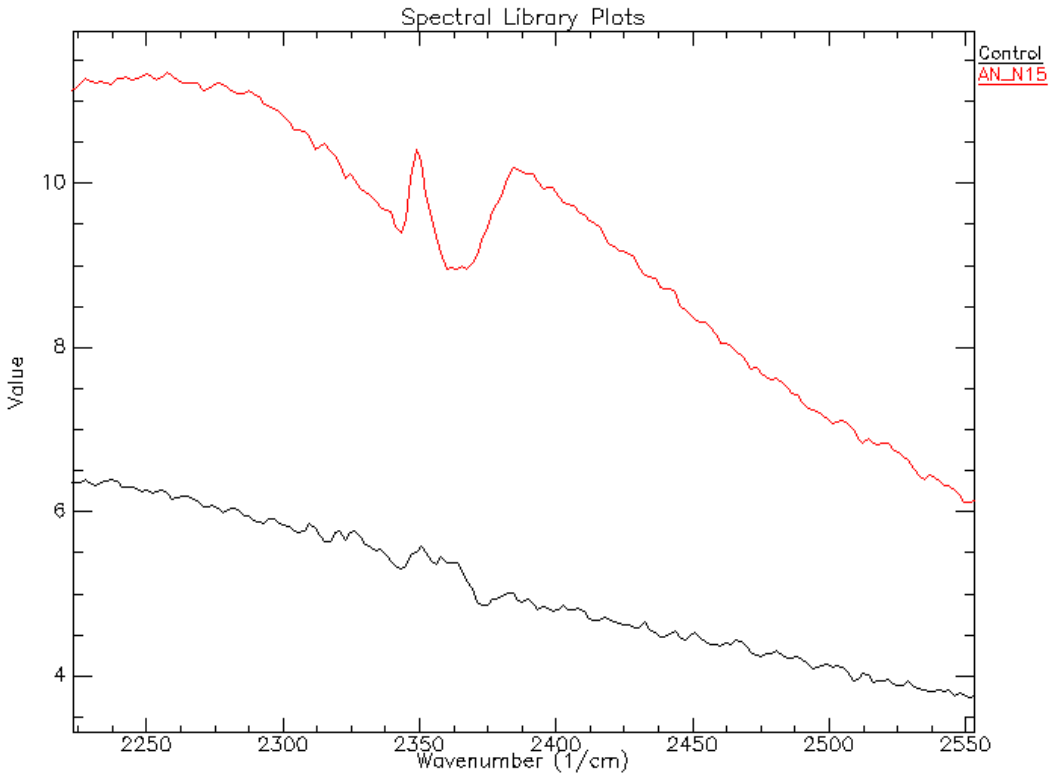

Figure 130 Exoscan data zoomed into features near 2,300 cm^{-1}

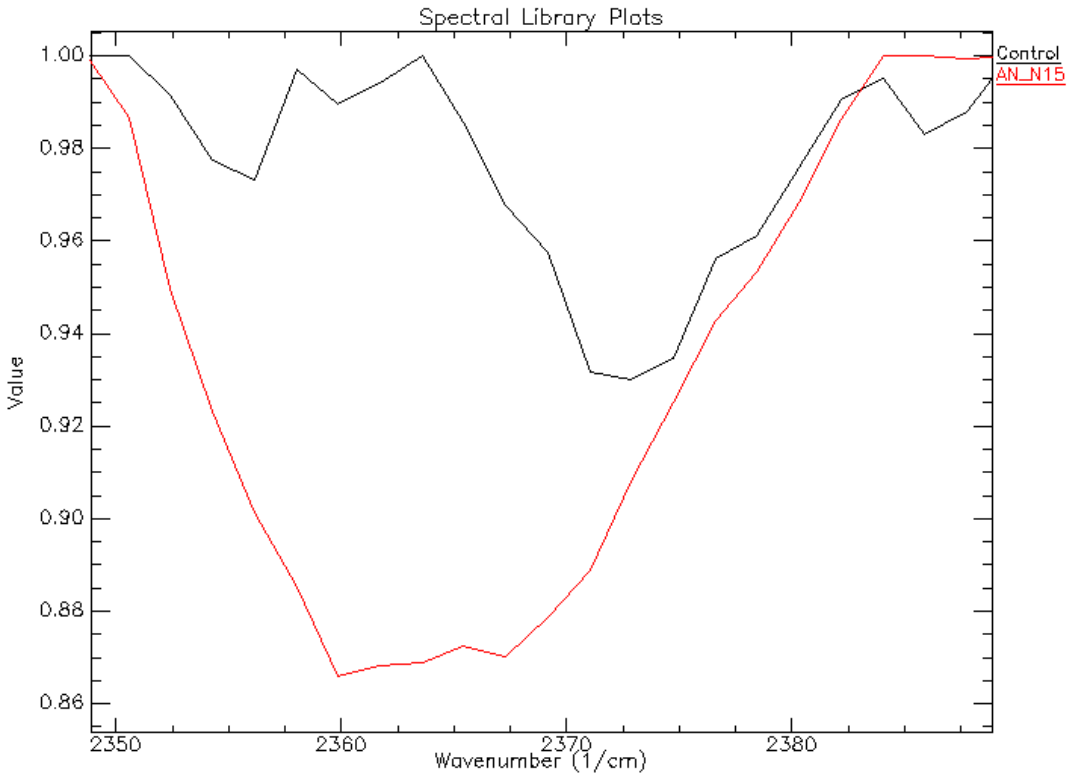

Figure 131 Exoscan continuum removed data zoomed into 2,360 cm^{-1} region.

Laboratory Instrument Acquired

The FTIR-ATR data was collected on two occasions from two different experiments that correspond to the data analyzed in chapters two and three respectively. The notable difference is the fertilizer composition between the two experiments. In chapter two, experiment one, the fertilizer was restricted to minimize any natural abundance ^{14}N available for uptake by the plants. In that data analyzed in chapter three, experiment two, the fertilizer composition varied in percentages of ^{14}N and ^{15}N across the three experimental trials. The FTIR-ATR data allows for more functional group analysis as it is a more sensitive instrument than the Exoscan described above as shown in Figure

132 to 134. For this reason there are more and different spectral features, peaks and valleys, in the spectra than that of the Exoscan.

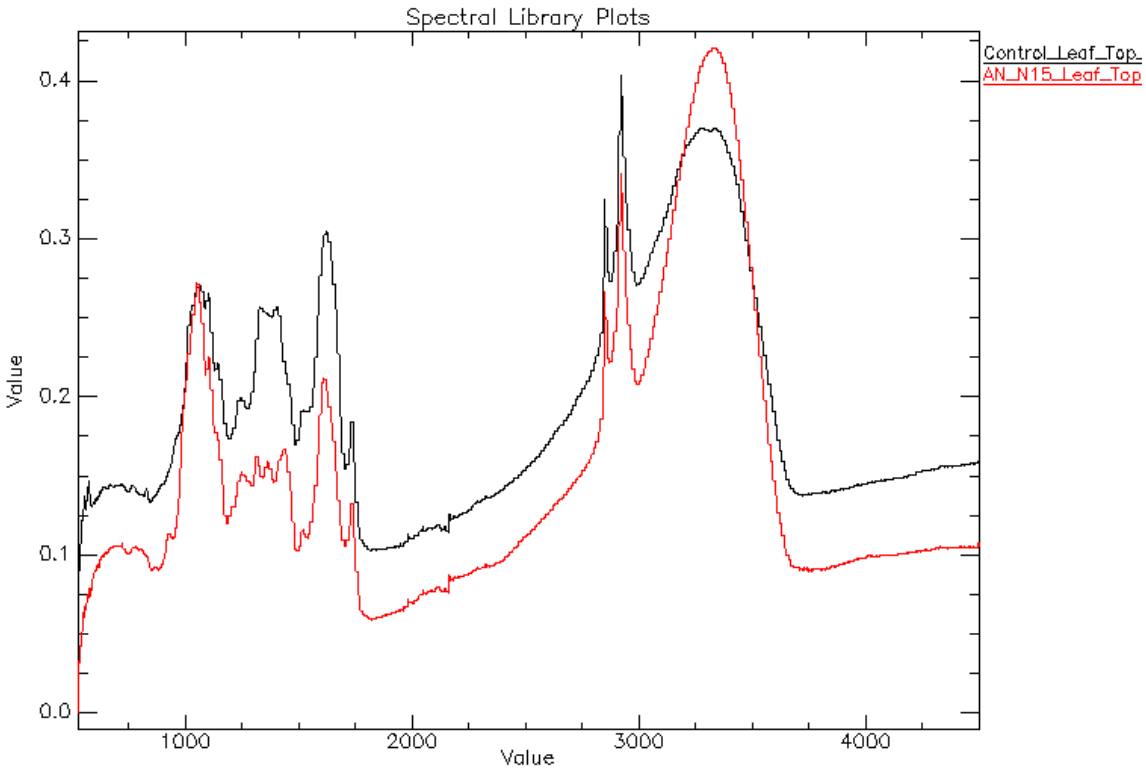

Figure 132 Nicolet spectra of the control plants and three experimental trials from Capelle and Macko (2016).

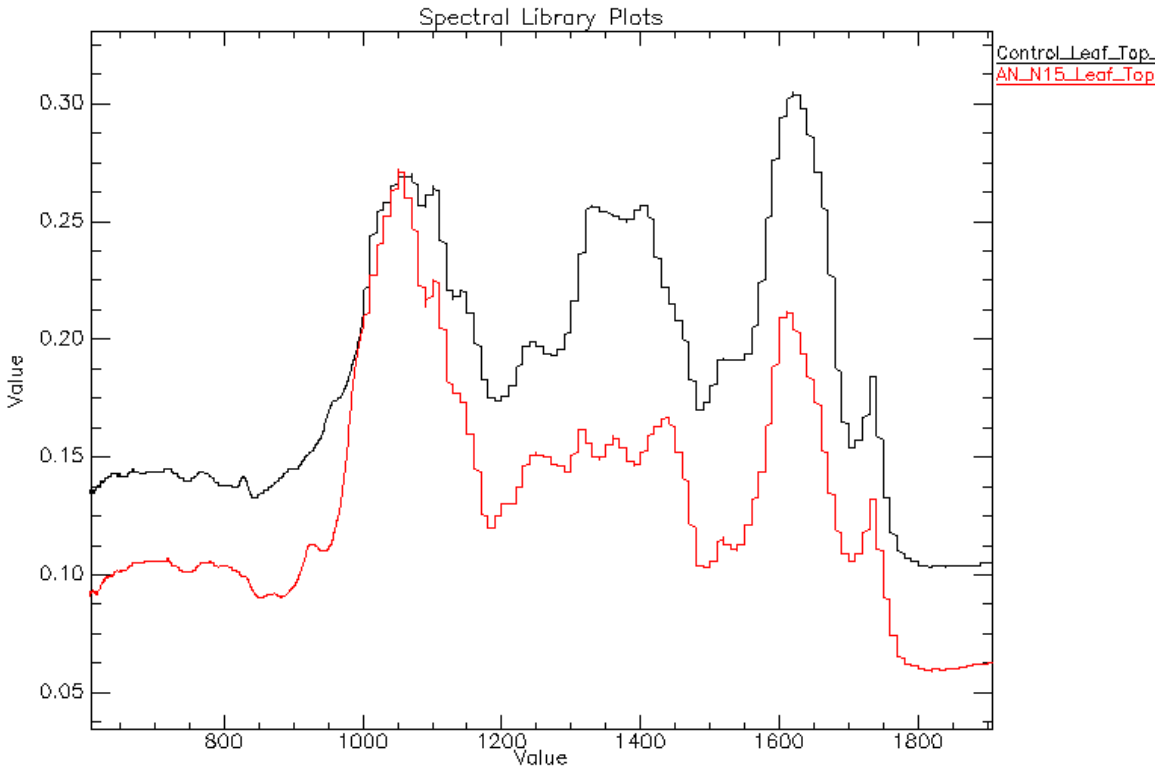

Figure 133 Zoomed in view of the Nicolet data near 1,200 cm^{-1} showing differences in the ^{15}N labaled plants versus the control.

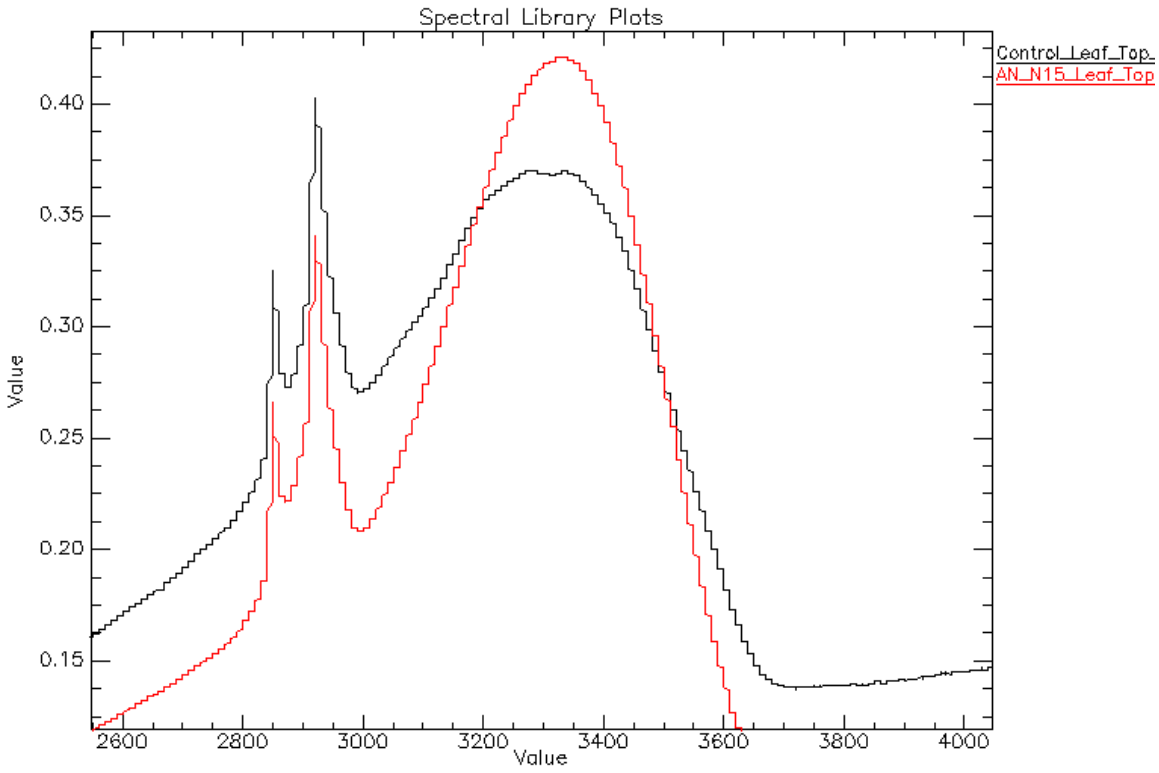

Figure 134 Zoomed in view of the Nicolet data near 3,300 cm^{-1} showing differences in the ^{15}N labaled plants versus the control.

Region	Control Spectra Band Center (in nm)	^{15}N Labeled Spectra Band Center (in nm)
1	1060	1050
2	1330	1315
3	1405	1365
4*	1620	1610
5*	3300	3330

Table 9 List of regions where ^{15}N induces wavelength shifts are observed from the control.

Top vs. Back of Leaves

The data in figure 135 show that the stomata structure difference between the top and back of deciduous plant leaves has no impact on the signature feature positions and overall signature shape. The change in absorbance percentage or amplitude is explained by sample positioning on the ATR crystal. Once the ATR crystal is compressed down onto the leaf it is impossible to flip it over and measure the same spot as it has been damaged by the compression.

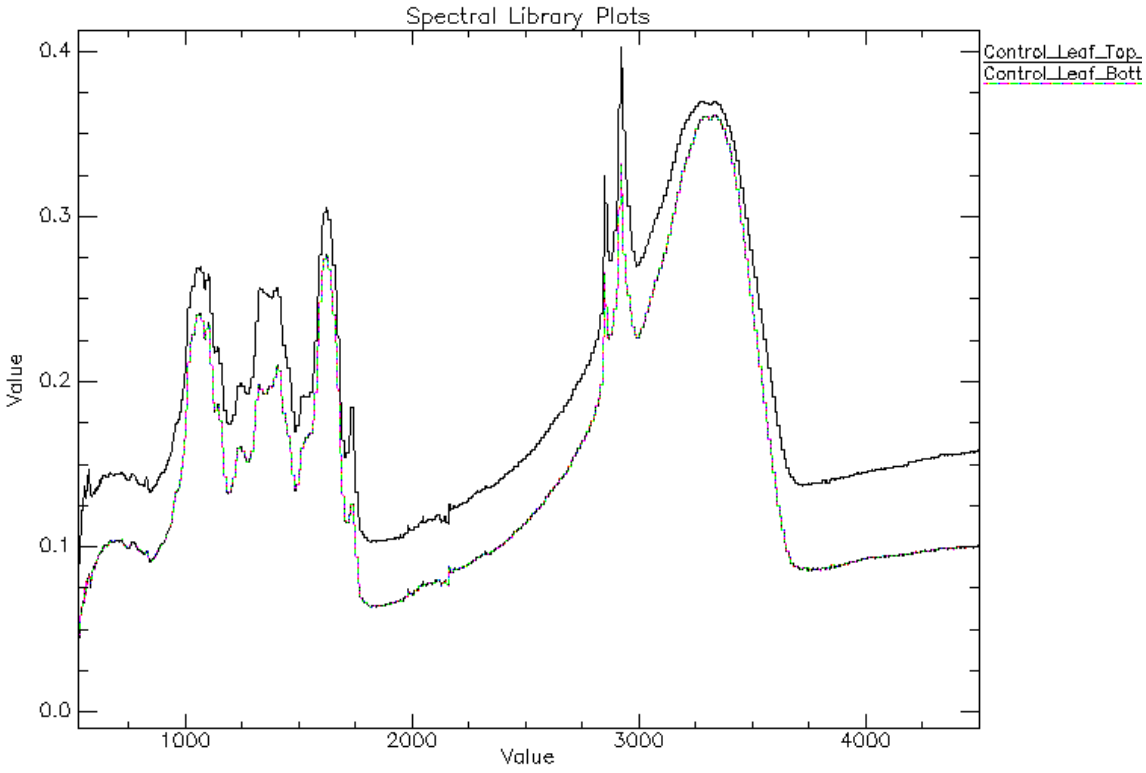

Figure 135 Nicolet data of the same leaf measured on the top (in solid black) and on the bottom (in dashed black).

Dried Whole Leaves vs. Ground Leaves

The raw data shown in figure 136 and with continuum removal in figure 137 show that there is no observable difference between dried ground leaves and direct measurement on the leaf surface. This is likely because the leaves are so thin that the light energy penetrates and reflects from the entire leaf. Drying and making the leaves homogenous though grinding with a mortar and pestle are not necessary for this technique.

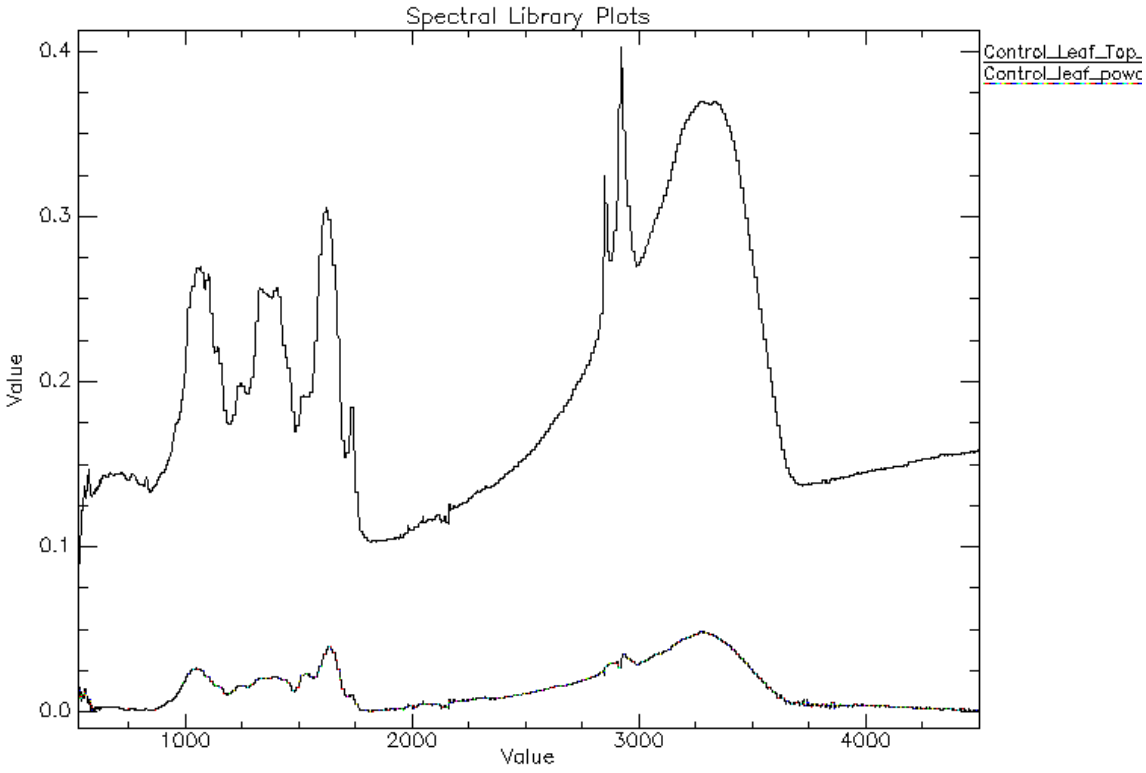

Figure 136 Nicolet data of the same leaf measured from the dry leaf top (in solid black) and once ground to a powder (in dotted and dashed black).

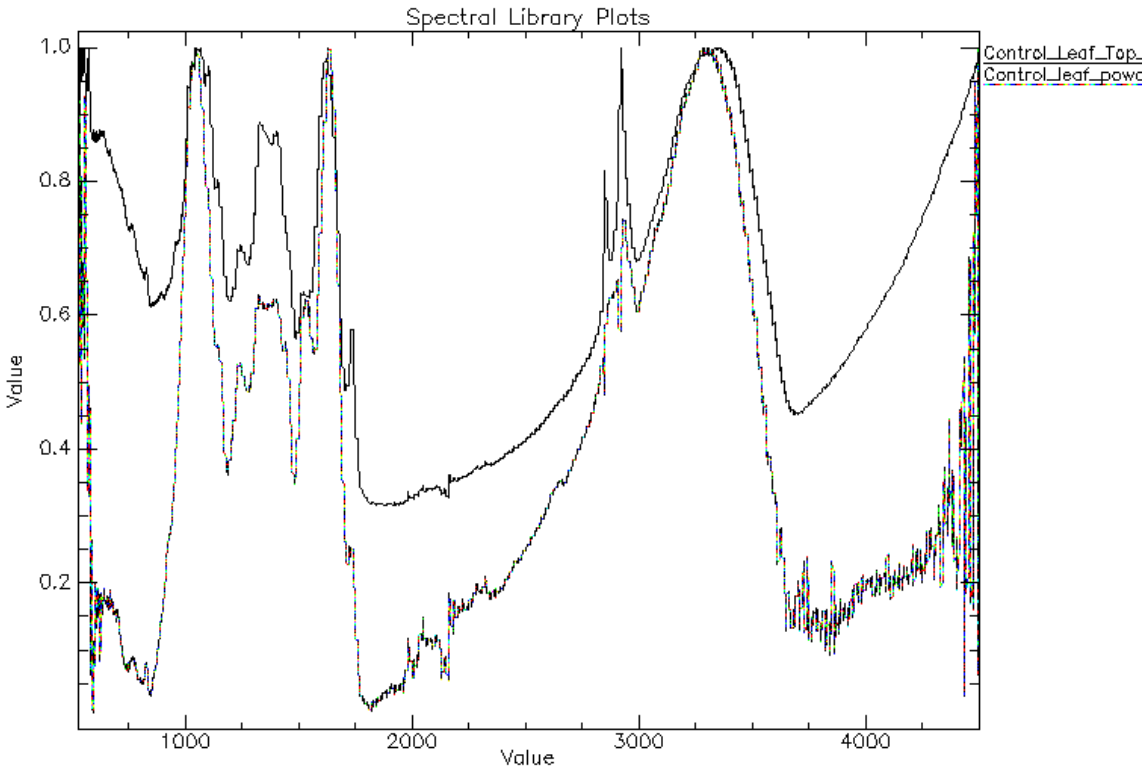

Figure 137 Nicolet data of the same leaf measured from the dry leaf top (in solid black) and once ground to a powder (in dotted and dashed black) with continuum removal applied.

Enriched Tomato Growth Experiment

Overview

A small scale exploratory kitchen experiment was conducted where two tomato plants were grown in similar soil based growing conditions except one plant was doped with a few sprinkles of ^{15}N ammonium nitrate label. The resulting spectra are included below. Performing continuum removal on the full scale plot begins to highlight regions of change. Zooming into the region around 1,000 cm-1 shows a few shifts more clearly. Specifically around 1,247 cm^{-1} where the labeled tomato peak shifts to a band center of 1,240 cm^{-1}. Additionally there is another peak that shifts from 1,157 cm^{-1} to 1,152 cm^{-1}

when labeled. This adhoc experiment continues to prove the detection of isotope induced shifts occur and are detectible by infrared spectrometers.

Tomato Leaf Spectra

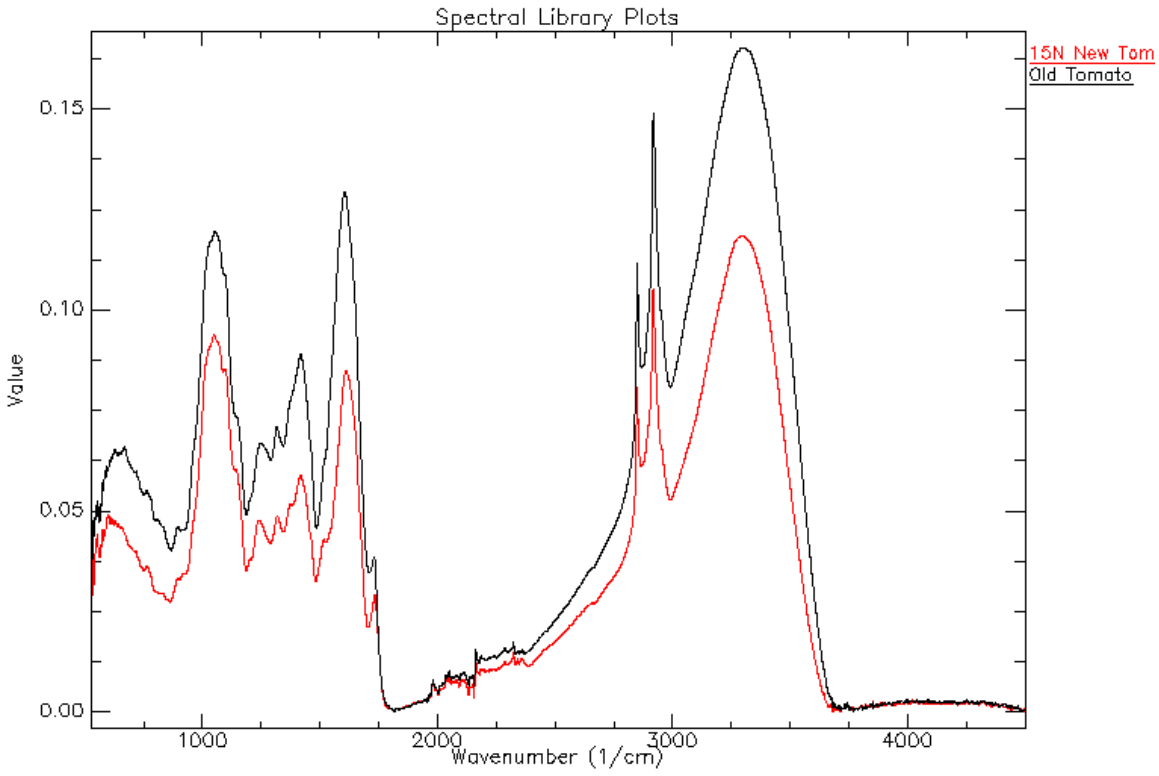

Figure 138 Full scale plot of ^{15}N labeled tomato leaf (in red) compared to natural abundance tomato leaf (in black).

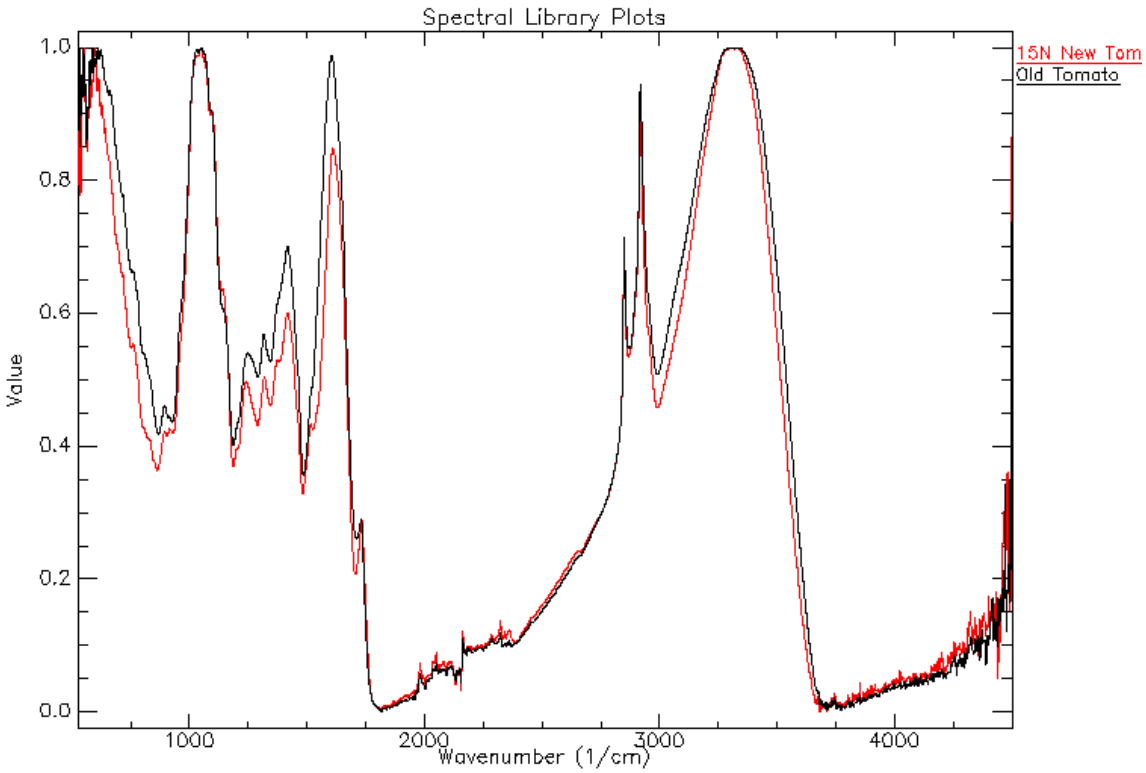

Figure 139 Tomato spectra with continuum removal applied to highlight differences

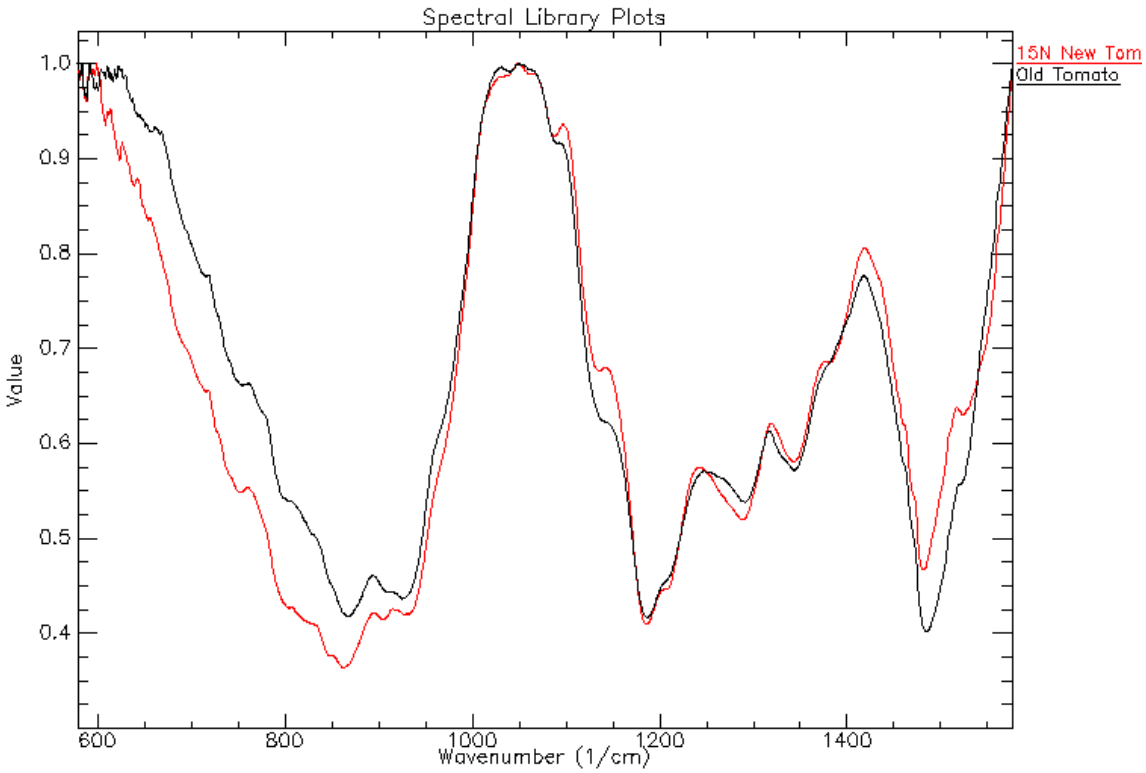

Figure 140 Continuum removal tomato spectra zoomed to 1000 cm^{-1}

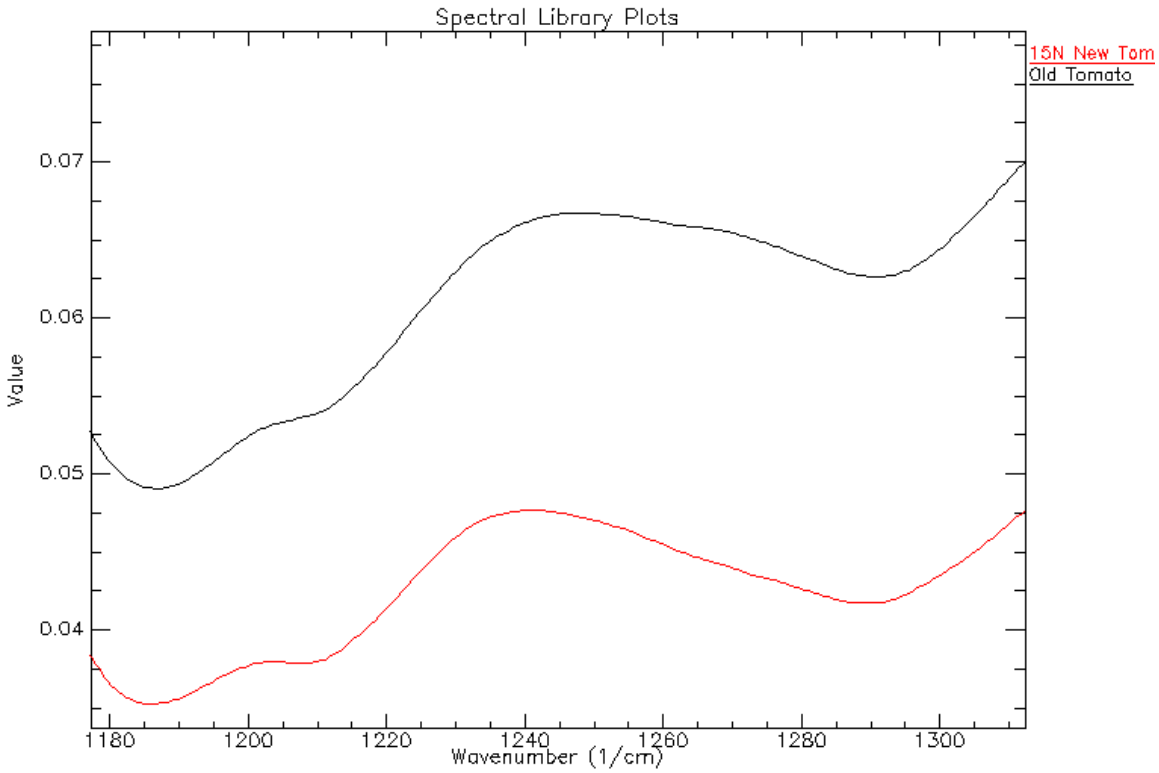

Figure 141 Tomato spectra region around 1,250 cm^{-1}

Appendix B: Monitoring Site Water Quality Data

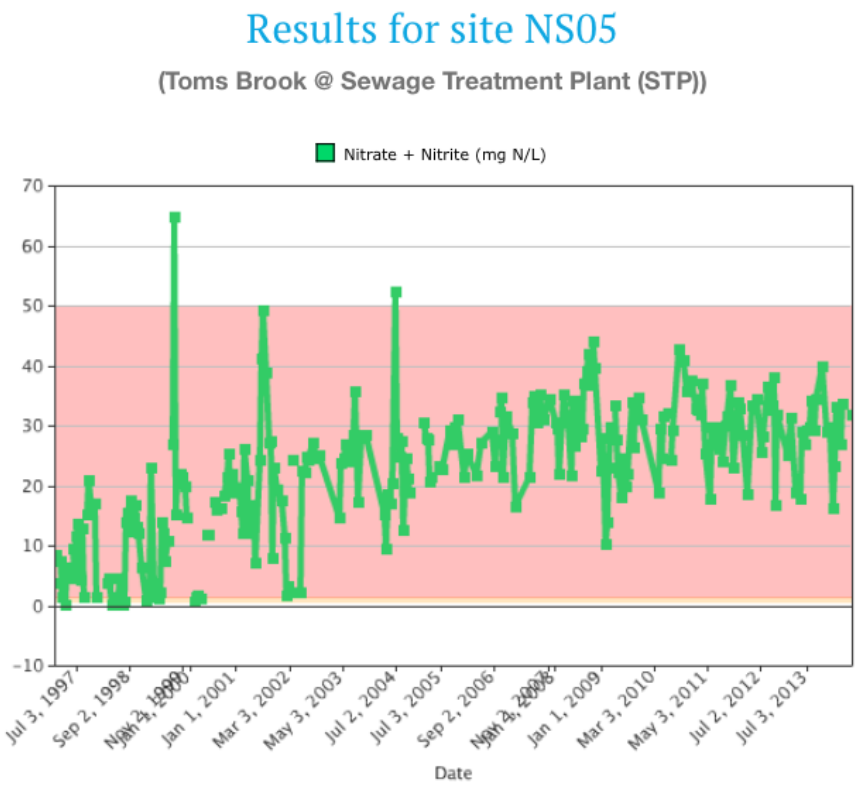

Results for site NS14

(Stoney Creek at George's Chicken Plant outfall)

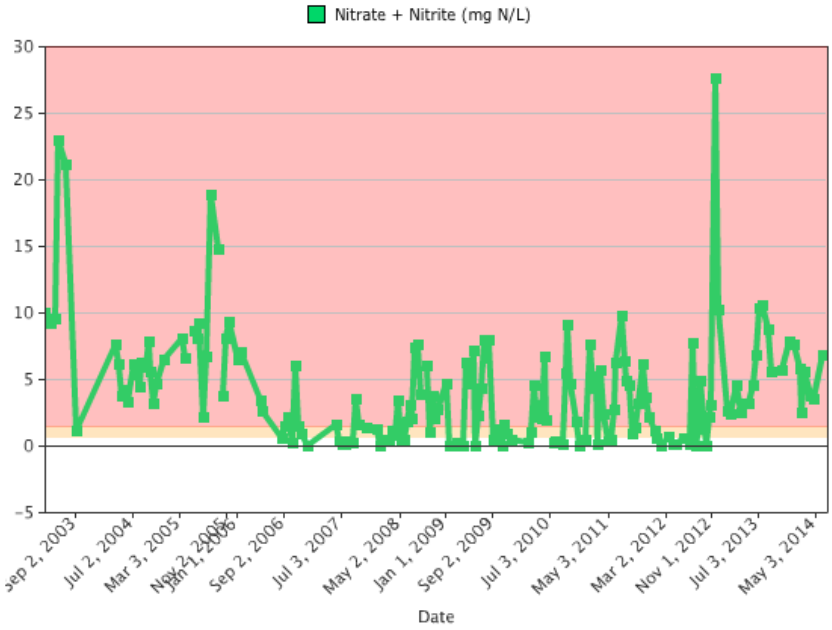

Results for site FP10

(Stanley Waste Water Plant)

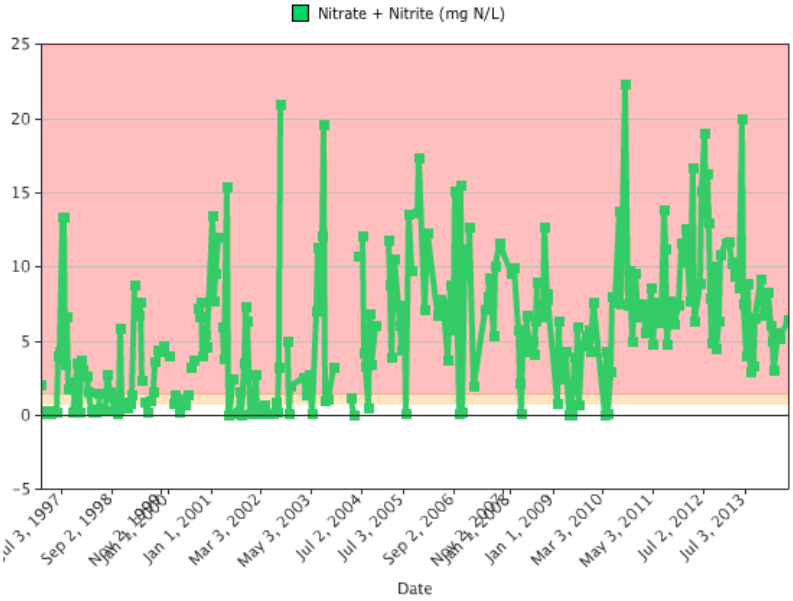

Results for site JR01

(Muddy Creek @ Rte 737 Rushville Rd)

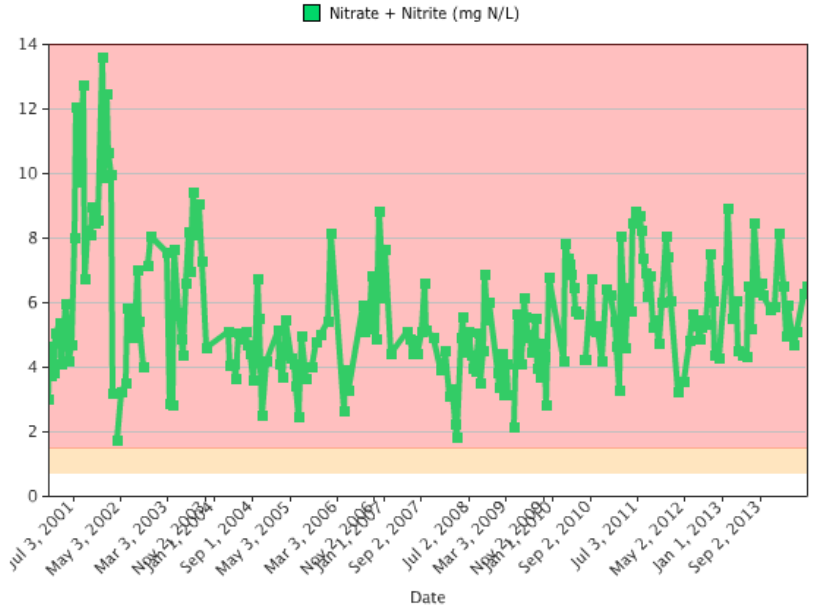

Results for site JR10

(Pleasant Run - North River watershed)

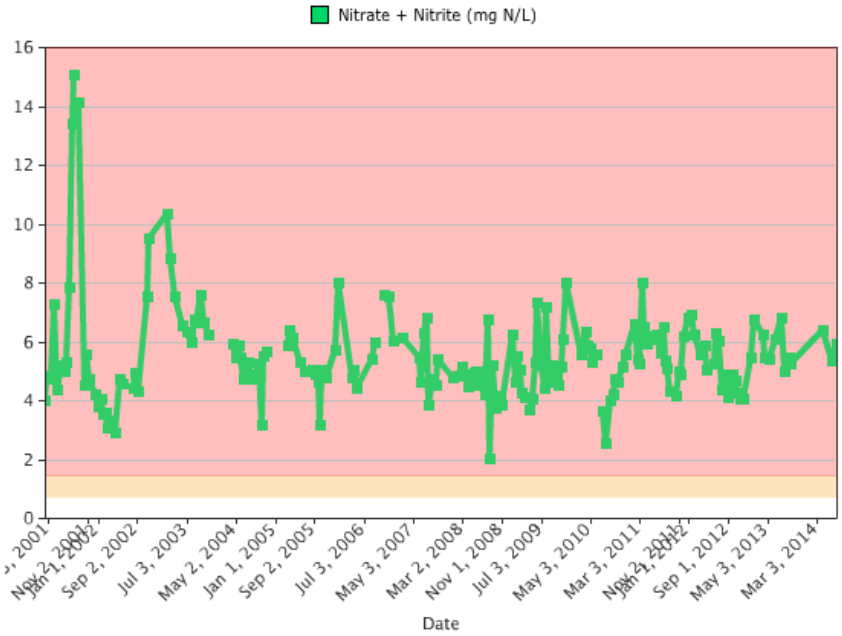

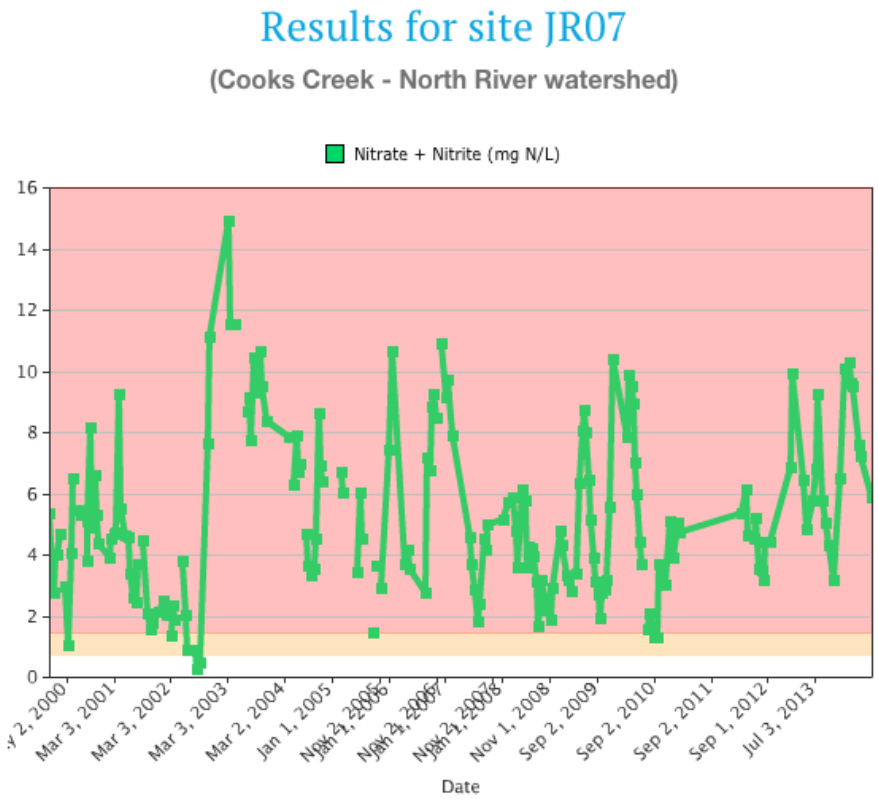
Results for site JR07
(Cooks Creek - North River watershed)
Nitrate + Nitrite (mg N/L)
16
14
12
10
8
6
4
2
0
Mar 3, 2001
Mar 3, 2002
Mar 3, 2003
Mar 2, 2004
Jan 1, 2005
Nov 1, 2008
Sep 2, 2009
Sep 2, 2010
Sep 2, 2011
Sep 1, 2012
Jul 3, 2013
Date